Telomere Dysfunction in Normal Human Epidermal Keratinocytes

Fay Minty, BSc (Hons)

This thesis is submitted to the University of Glasgow in accordance with the requirements for the degree of Doctor of Philosophy in the Faculty of Medicine

University of Glasgow

Beatson Institute for Cancer Research

February 2007

Abstract

TRF2 is one of the main telomere binding proteins and a key regulator in protecting the telomere, the end of a linear chromosome. The telomere can be artificially "uncapped" by expression of myc-TRF2$^{\Delta B \Delta M}$, a myc tagged dominant negative version of the protein. Both myc-TRF2 Full Length (FL) and myc-TRF2$^{\Delta B \Delta M}$ were retrovirally-infected into cells as part of an IRES-GFP construct. NHEK expressing GFP (and therefore either myc-TRF2 FL or myc-TRF2$^{\Delta B \Delta M}$) were selected at early time points using flow-sorting and this allowed either low or high expression levels to be isolated.

Low or high levels of expression of myc-TRF2$^{\Delta B \Delta M}$ altered colony morphology, reduced clonogenicity and almost completely prevented proliferation of NHEK. Several markers of DNA damage were investigated and a small amount of p53-phosphoS15 was detected 2 days after expressing myc-TRF2$^{\Delta B \Delta M}$ in NHEK. The number of small colonies containing senescent cells was increased in NHEK expressing myc-TRF2$^{\Delta B \Delta M}$ compared with Vector only controls. Induction of DNA damage responses is undoubtedly a contributing factor and senescence at least one cellular outcome of uncapped telomeres in NHEK.

Low levels of myc-TRF2 FL expression in NHEK also caused a reduction in cell proliferation, but not as severe as seen by expression of myc-TRF2$^{\Delta B \Delta M}$. High levels of myc-TRF2 FL demonstrated an even greater reduction in proliferation, equivalent to myc-TRF2$^{\Delta B \Delta M}$. Despite the reduced cell proliferation, NHEK expressing myc-TRF2 FL did not demonstrate any p53-phosphoS15. Excessive telomere processing may play a role in the dramatic effect seen in NHEK following expression of myc-TRF2 FL.

The majority of human cancers are of epithelial derivation. As a major focus of cancer therapy is centered on exploiting the properties of the telomere, a full understanding of it's properties in an epithelial context is warranted. This thesis examines the effects of uncapping telomeres in Normal Human Epidermal Keratinocytes (NHEK), the first time an investigation into telomere status has taken place with a primary epithelial cell system.

Table of Contents

List of Tables

List of Figures

Chapter 4: Characterising NHEK proliferation response to myc- TRF2 FL and myc- TRF2$^{\Delta B \Delta M}$

Chapter 5: Examining the mechanism to inhibit NHEK proliferation used by myc-TRF2 FL or myc-TRF2$^{\Delta B\Delta M}$

List of Accompanying Material

Appendix I	List of Suppliers and Manufacturers referred to in the material and methods.

Acknowledgements

Not only do I wish to acknowledge both my supervisors, Ken Parkinson and Paul Harrison, but I also would like to express my heart-felt gratitude for all their advice and patience with me throughout this PhD. I feel privileged to have worked with and learned so much from two individuals so dedicated to cancer research.

I would also like to acknowledge and thank Titia de Lange for providing constructs and antibody used in this thesis.

Not only do I acknowledge Tom Gilbey and Margaret O'Prey for all their hard work and help during this thesis I would also like to offer them my sincere thanks.

In addition to thanking the people in the groups I have worked within during this PhD (Katrina Gordon, June Munro, Nighean Barr, Hazel Ireland, Martha Wootton, Jim McCaul, Vivienne Morrison, Janis Fleming, Jo Thurlow and Paul Drake) I also thank the many other people within the Beatson who have shared lab space, coffee, lunch, wine, thoughts and trade secrets with me. Without everyone's generous spirit, the work presented in this thesis would not have been possible.

Finally, I would like to acknowledge the thousands of people who support the work of CRUK, who funded this research.

Author's declaration

I declare that I am the sole author of this thesis and that all of the work presented herein was performed by myself, unless otherwise stated. This thesis has not been submitted for consideration for any other degree in this or any other university.

Abbreviations

γ-IR	gamma-Ionising Radiation
AD	Autosomal Dominant
ALT	Alternative Lengthening of Telomeres
B/F/B	Breakage/Fusion/Bridge
BCA	Bicinchoninic Acid
BSA	Bovine Serum Albumin
B-gal	Beta-Galactosidase
Brd-U	5-Bromo-2'-deoxy-uridine
cAMP	cyclic Adenosine MonoPhosphate
cdk	cyclin dependent kinase
CO-FISH	Chromosome Orientation - Fluorescent In Situ Hybridization
Cyc	Cyclin
DC	Dyskeratosis Congenitia
DNA	Deoxy-riboNucleic Acid
DSB	Double Strand Breaks
EGF	Epidermal Growth Factor
FSC-H	Forward Scattered light
GFP	Green Fluorescent Protein
HI	Heat Inactivated
HMEC	Human Mammary Epithelial Cells
HPV	Human Papilloma Virus
HU	Hydroxyurea
IRES	Internal Ribosomal Entry Site
Kbp	Kilo base pairs
MEF	Mouse Embryo Fibroblasts
mM	milli Molar
mRNA	messenger RiboNucleic Acid
ng	nanograms
NHEJ	Non-Homologous End Joining
NHEK	Normal Human Epidermal Keratinocytes
PARP-2	Poly (ADP-Ribose) Polymerase 2
PBS	Phospho- Buffered Saline
PCR	Polymerase Chain Reaction
PD	Population Doubling
PE	PBS EDTA
PFA	ParaFormAldehyde
PI	Propidium Iodide
POT1	Protection of Telomeres 1
Rb	Retinoblastoma protein
RNAi	RiboNucleic Acid interference
SPB	Spindle Pole Body
SSC-H	Side Scattered light
T loop	Telomere Loop
TBS	Tris Buffered Saline
TBS-T	Tris Buffered Saline-Tween 20
TIFs	Telomere Induced dysfunctional Foci
TRAP	Telomerase Repeat Activation Protocol
TRF	Telomere Restriction Fragment
TRF1	Telomere Repeat Binding Factor 1

TRF2	Telomere Repeat Binding Factor 2
TRFH	Telomere Repeat binding Factor Homology
UV	Ultra Violet

Chapter 1: Introduction

1.1 Background

In the early 1930s, pioneering work with chromosomes was being performed in the maize plant by Barbara McClintock and in drosophila by Hermann Muller. Recounted in a historical perspective essay (McKnight and Shippen 2004), both scientists were investigating the consequences of broken chromosomes and recognised that the natural end of the chromosome was unique. Muller coined the term telomeres, from the Greek word "telos" meaning end, and "meros" meaning part.

Performing crosses between mutated and normal chromosomes, McClintock characterised the Breakage/Fusion/Bridge, B/F/B cycle, and described the formation of sister chromatid fusion and the formation of a di-centric chromosome. However, McClintock also found that dependent on what allele the zygote inherited after the unequal di-centric breakage, instead of proceeding through a B/F/B cycle, a ruptured end would 'heal' and therefore thought it likely that the healing process represented the formation of a new telomere where the chromosome had ruptured. McClintock recounted in her 1983 Nobel Prize seminar an observation that became the foundation in the study of the telomere; "A cell capable of repairing a ruptured end of a chromosome must sense the presence of this in the nucleus. This sensing activates a mechanism that is required for replacing the ruptured end with a functional telomere" (McClintock 1984). With the discovery of telomerase in 1985 (Greider and Blackburn 1985), and the recognition that a telomere actively communicates its status to the cell, a new field specifically investigating telomere biology emerged.

1.2 The Telomere

The telomere has been functionally defined as a region of DNA at the molecular end of a linear chromosome that is required for the replication and stability of the chromosome (Blackburn 1984). The exact sequence of non-coding repeats differs slightly between species; in humans the G rich strand sequence is $[TTAGGG]_n$ (Moyzis et al. 1988), and the complementary, C rich strand sequence

is $[CCCTAA]_n$. The integrity of this sequence is a requirement for the formation of a human telomere, as slightly altered sequences of telomeric DNA are not capable of seeding new telomeres (Hanish et al. 1994). The G rich strand overhangs the complementary strand in what is referred to as the G rich or 3'overhang. This single stranded DNA then folds back to invade the upstream telomeric sequence forming what is known as a T-loop, detailed in Section 1.10.

1.3 Telomeric Binding Proteins

A telomere is much more than just DNA. The length, 3'overhang, T-loop and correct binding proteins are all key elements of a functional, capped telomere.

Telomeres form nuclear matrix-associated, high order chromatin complexes at dispersed sites throughout the nuclear volume (Luderus et al. 1996). However, digestion of chromatin in cell lines with shorter telomeres revealed a pattern that suggests they have different nucleosomal packaging (Tommerup et al. 1994). One of the telomeric proteins about to be discussed below, TRF1, has recently been reported as specifically recognising and altering the nucleosomal structure, possibly allowing the nucleosomes to contribute to the function of telomere capping (Galati et al. 2006). In addition to associating with nucleosomal proteins, telomeres are bound by their own unique set of complex proteins.

Analogous to other chromosomal protein complexes, shelterin is a newly adopted term to refer to the 6 major telomeric binding proteins that shape and safeguard the telomere, (**Figure 1**). TRF1, TRF2 and POT1 all directly recognise and bind the telomeric repeat, whereas the other three components of shelterin, TIN2, TPP1 and hRap1, interconnect them. Despite inclusion of both TRF1 and TRF2 into the shelterin complex, they can be isolated separately and are therefore considered sub-complexes of shelterin. Not all proteins found at the telomere are part of shelterin, only the proteins that are abundant at the telomere and do not accumulate elsewhere in a cell under normal circumstances (de Lange 2005). Table 1 provides the details of the main human telomere binding proteins. It includes proteins which associate with the telomere through direct or indirect interaction, many of which are more traditionally associated with DNA damage repair. Characterisation of many of these proteins has been achieved through

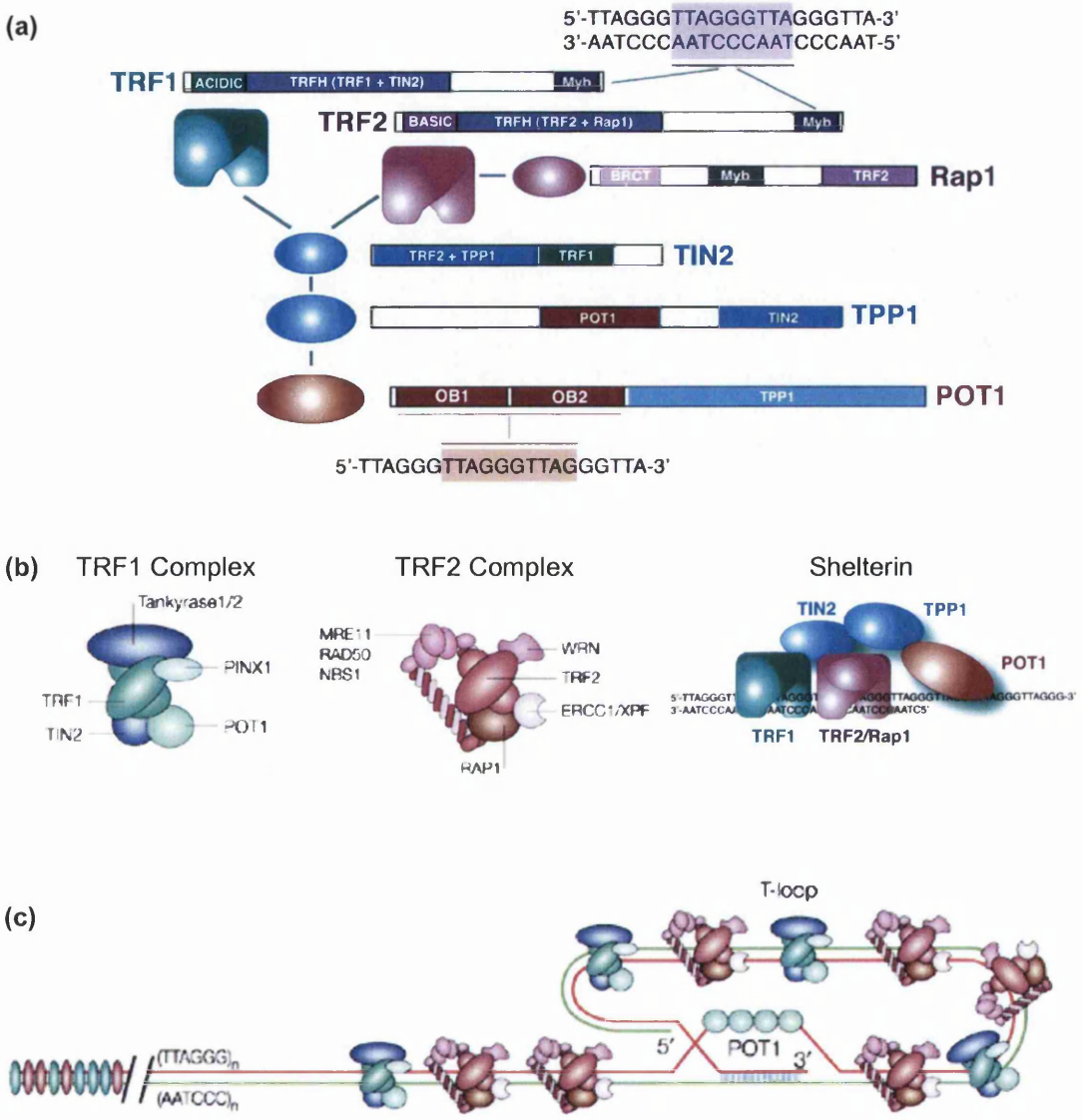

Figure 1. The telomere binding proteins and telomere structure.

The above illustrations were taken from:

de Lange, T. T-loops and the origin of telomeres. *Nat Rev Mol Cell Biol.* 2004 Apr;5(4):323-9.

de Lange, T. Shelterin: the protein complex that shapes and safeguards human telomeres. *Genes Dev.* 2005 Sep 15;19(18):2100-10.

(a) An illustration of the six main telomere binding proteins that are proposed to combine to form shelterin. Their characteristic domains and protein interaction sites are noted within the linear representations of the proteins.

(b) The telomere binding proteins in the different ways they are known to associate. A TRF1 and TRF2 complex have been established, however components from each are also known to associate and bind the telomere as shown in the shelterin model.

(c) Substantial evidence suggests that telomeres fold into a Telomere Loop, T-loop, largely aided by TRF2 which is seen in larger amounts where the 3'overhang strand invades the duplex telomeric DNA.

RNA interference, RNAi; the experimental manipulation of selectively removing one protein by designing a small RNA molecule complementary to the mRNA sequence of the protein to be "knocked down" such that it is degraded instead of being expressed.

Process the protein is traditionally associated with	**Table 1: Human Telomere Binding Proteins**
	Protein Name (first reference of protein in a telomere context)
Telomere binding	**TRF1** (Chong et al. 1995), **(Figure 1) (a).** Telomere Repeat binding Factor 1, TRF1, contains a large TRFH (TRF Homology) domain used for homo-dimerisation and an acidic domain at its N-terminus. Each TRF1 protein within the dimer contributes a myb domain which binds double stranded telomeric DNA and bends it to an angle of 120° (Bianchi et al. 1997). TRF1 controls telomere length in *cis* by inhibiting the action of telomerase at the ends of individual telomeres: over-expression of TRF1 results in progressive shorter telomeres whereas inhibition of TRF1 increases telomere length (van Steensel and de Lange 1997).
Telomere binding	**PIN2** (Shen et al. 1997) Pin2 is identical to TRF1 apart from an internal deletion of 20 amino acids generated by alternate splicing. Pin2 forms homo and hetero-dimers with TRF; both types of dimer are localised at telomeres. The level of Pin2 is strikingly increased in G2+M and decreased in G1 cells (Shen et al. 1997). Although Shen et al state that Pin2 is the major expressed product compared with TRF1, other groups do not differentiate between TRF1 and PIN2, referring to them both as TRF1 (Broccoli et al. 1997).

Telomere binding	**PINX1** (Zhou and Lu 2001) Experiments over-expressing PinX1 in HeLa cells demonstrate co-localisation with TRF1/PIN2 at the telomere. PINX1 also localised to the nucleolus. HT1080 (telomerase positive fibrosarcoma cell line) cells over-expressing PINX1 had shortened telomeres after 20-30 Population Doublings, PD, resulting in crisis and senescence (Zhou and Lu 2001).
Telomere binding	**TIN2** (Kim et al. 1999), **(Figure 1)(a)**. TIN2 binds the TRF1 homo-dimer forming a tertiary structure: this is speculated to aid the ability of TRF1 to induce pairing or higher order interactions between telomeric DNA tracts by causing conformational changes in TRF1 (Kim et al. 2003). As part of the TRF1 complex, TIN2 prevents Tankyrase from ADP-ribosylating TRF-1 which causes the complex to disassociate from the telomere (Ye and de Lange 2004), **(Figure 2)**. A mutant version of TIN2, lacking its amino-terminal sequences, allows elongation of human telomeres in a telomerase-dependent manner indicating that TRF1 alone is insufficient for control of telomere length in human cells and TIN2 is an essential mediator (Kim et al. 1999). TIN2 has also been shown to bind the TRF1 and TRF2 complexes simultaneously and stabilise the TRF2 complex on telomeres (Ye et al. 2004a).

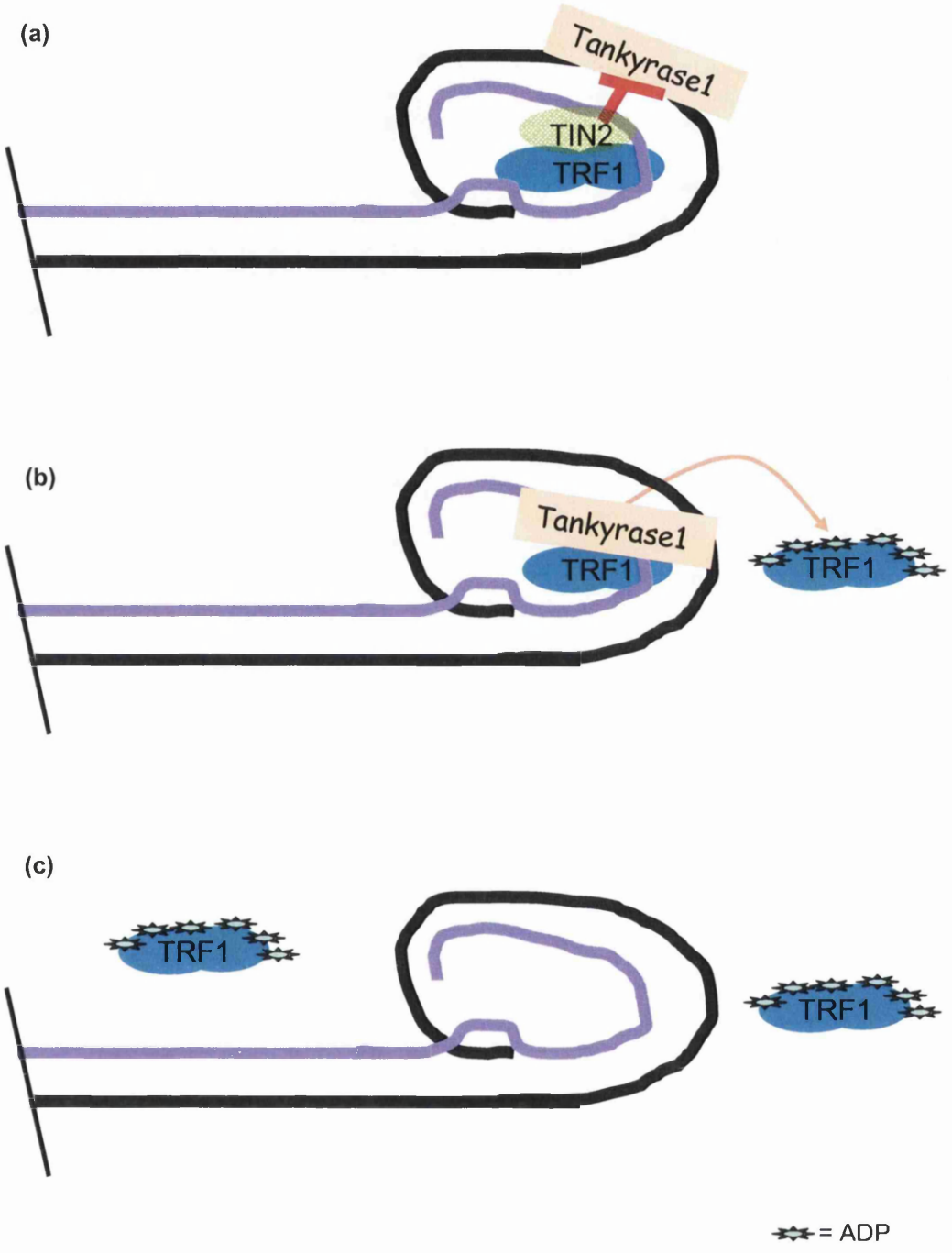

Figure 2. TIN2 and Tankyrase1 regulation of TRF1.

(a) When TIN2 is bound to TRF1 at the telomere, it prevents Tankyrase1 from catalysing the addition of ADP to TRF1.

(b) When TIN2 is deleted from cells, Tankyrase1 ADP-ribosylates TRF1. When bound by ADP, TRF1 is longer capable of binding the telomere (c).

Telomere binding	**POT1** (Loayza and De Lange 2003), **(Figure 1)(a).** Protection Of Telomeres, POT1, is a single stranded telomeric binding protein that interacts with the TRF1 complex in human cells to control telomerase-mediated telomere elongation (Loayza and De Lange 2003). $POT1^{\Delta OB}$ (lacking the oligo-nucleotide binding (OB) fold of POT1) is still capable of associating with the TRF1 complex, but is no longer capable of binding the 3'overhang; expression of this mutated protein results in elongation of the telomere (Loayza and De Lange 2003). *In vitro* binding experiments, determined the optimal substrate to be $[TTAGGG]_n$, ($n \geq 2$) and binding was enhanced by the proximity of a 3' end. However, POT1 was able to bind a $[TTAGGG]_5$ array when positioned internally, indicating that POT1 can bind both the 3'overhang and the displaced TTAGGG repeats at the base of the T-loop (Loayza et al. 2004). Two forms of human POT1 are generated by alternative splicing; POT1 and POT1-55. It is estimated that POT1 is approximately 10X more abundant than POT1-55. Using RNAi that targeted either both POT1 and POT1-55, or only POT1, in human cells (IMR90, BJ, BJ/hTERT, HeLa, HCT116, HTC75 - all defined in Table 2) the result was the same: the 3' overhang was decreased and telomeres elicited a transient DNA damage response, surprisingly without cell cycle arrest or telomere fusions. It was therefore concluded that the less abundant POT1-55 protein does not perform a distinct function within the cell. Random positioning of the 5' end that normally ends on the sequence ATC-5' resulted in a reduction in the amount of bound POT1 (Hockemeyer et al. 2005). It has also been reported that in fibroblasts, RNAi knockdown of POT1 resulted in apoptosis, chromosomal instability and senescence (Yang et al. 2005). This report also offered evidence that POT1 and TRF2 interacted, since expression of $TRF2^{\Delta B \Delta M}$ stripped the telomere of POT1 as well as endogenous TRF2 (Yang et al. 2005).

Telomere binding	**TPP1** Discovered simultaneously as PIP1 (Ye et al. 2004b), PTOP (Liu et al. 2004) and TINT1 (Houghtaling et al. 2004), this protein has now been renamed TPP1 (de Lange 2005). It tethers POT1 to TIN2 as part of the TRF1 complex. The knockdown of TPP1 results in telomere elongation thus mimicking the effect of POT1 deficiency.
Telomere binding	**Tankyrase1** (Smith et al. 1998), (**Figure 1**)(**a**). Tankyrase1 is a human telomeric poly(ADP-ribose) polymerase initially identified through its interaction with the telomeric protein TRF1 (Smith et al. 1998). ADP-ribosylation of TRF1 by tankyrase diminished its ability to bind telomeric DNA in vitro (Smith et al. 1998), (Ye et al. 2004a) (**Figure 2**). Long-term over-expression of Tankyrase1 in HeLa cells resulted in a gradual and progressive elongation of telomeres (Smith and de Lange 2000). The diminished level of TRF1 is thought to allow telomerase access to the telomere. During interphase, tankyrase1 is localised to the telomere, but in mitosis, tankyrase1 relocates to the periphery of the centrosome (Smith and de Lange 1999). Tankyrase1 lacks its own nuclear localisation sequence and there is evidence to support its reliance on TRF1 for nuclear import as well as telomere binding (Smith and de Lange 1999). Knockdown of Tankyrase1 caused mitotic arrest: sister chromatids separated at centromeres and arms, but remained associated at the telomere, possibly through a proteinaceous bridge (Dynek and Smith 2004; Chang et al. 2005).
Telomere binding	**Tankyrase2** Tankyrase 2 is a highly conserved version of Tankyrase1 which also interacts with TRF1 in vivo and in vitro, regulating it through ADP ribosylation (Cook et al. 2002). Both Tankyrase1 and 2 interact with TRF1 through its acidic domain (Cook et al. 2002).

Telomere binding	**TRF2** (Broccoli et al. 1997), (**Figure 1**)(**a**). This second telomere repeat protein, TRF2, also contains a large TRFH domain and a myb domain. TRF2 homo-dimer formation allows the two myb domains to bind the telomere (Broccoli et al. 1997). TRF2 differs from TRF1 in that its N terminus is basic rather then acidic. Despite investigation, no evidence has been found for hetero-dimerization of TRF1 and 2 (Broccoli et al. 1997). Crystal structures of the TRFH domain in TRF1 and 2 have revealed that the interfaces have unique interactions that prevent hetero-dimerization (Fairall et al. 2001). TRF2 is considered the protein responsible for protecting the telomere. As the work presented in this thesis all involves expression of TRF2 and its dominant negative form, $TRF2^{\Delta B \Delta M}$, a more detailed section on TRF2 and the consequences of its expression are in the text, Section 1.7 and 1.8.
Telomere binding	**hRap1** (Li et al. 2000), (**Figure 1**)(**a**). hRap1 is recruited to the telomere by TRF2 and affects telomere length (Li et al. 2000). Despite containing a myb domain, hRap1 cannot bind the telomere without TRF2 which it uses as a bridging protein. Cells over-expressing hRap1 in the HTC75 inducible system (derived from HT1080 fibrosarcoma cell line) elongated their telomeres over a period of 100 population doublings (PD) (Li et al. 2000). However, a further publication by the same author speculates that this finding might be an artefact of the excess hRAP1 sequestering other important telomerase suppressing proteins away from the telomere. Expression of a mutant version of hRAP1, lacking the RCT domain required for interaction with TRF2, also resulted in a longer, more homogeneous telomere population (Li and de Lange 2003). This suggests that hRAP1 suppresses telomerase activity at the telomere through its BRCT and myb domains.

Non- Homologous End Joining	**Ku** (Bianchi and de Lange 1999) The hetero-dimeric Ku (70 and 80/86 kDa), known for its role in Non Homologous End Joining, NHEJ, was shown to be capable of binding telomeric DNA in vitro (Bianchi and de Lange 1999). A 50% reduction of Ku86 levels using RNAi in HeLa, SAOS and U2OS cells results in a marked loss of telomere sequences, increased chromatid-type fusions by leading strand synthesis, an increase in apoptosis and a decrease in cell proliferation (Jaco et al. 2004). The colorectal carcinoma cell line HCT116, is heterozygous for Ku86. Functional inactivation of the remaining allele of Ku 86 resulted in profound telomeric shortening, longer 3'-overhangs, an increase in chromosome fusions, translocations and genomic instability resulting in the cells only being capable of limited proliferation prior to apoptosis (Li et al. 2002), (Myung et al. 2004).
Non- Homologous End Joining	**DNA-PK** (d'Adda di Fagagna et al. 2001) This interaction partner of Ku provides catalytic serine/threonine protein kinase activity (Collis et al. 2005) and has been found to associate in vivo with the telomere in human HeLa cells by Chromatin Immunoprecipitation, CHIP.
Non- Homologous End Joining	**Apollo** (also named hSnmB1(Freibaum and Counter 2006)) Localising to the telomere through its interaction with TRF2, Apollo, an Artemis-Related Nuclease, has 5'exonuclease activity (Lenain et al. 2006). Apollo is speculated to contribute to the resection of the C rich blunt end produced during DNA replication of the leading strand, see Section 1.10. RNAi directed against Apollo result in Telomere Induced dysfunction Foci, TIFs, (see Section 1.13) primarily during S phase, further implying that Apollo may have a role in telomere processing. Human fibroblasts senesce after 12 days without Apollo expression (van Overbeek and de Lange 2006).

Homologous Recombination	**RAD51D** (Tarsounas et al. 2004) RAD51D, one of the five RAD51 paralogs (RAD51B, RAD51C, RAD51D, XRCC2 and XRCC3) involved in genetic recombination, has been co-localised with TRF2 in both HeLa (cervical carcinoma) cells and WI-38 cells (fibroblasts that use Alternative Lengthening of Telomere, ALT, see Section 1.15.ii) (Tarsounas et al. 2004). Inhibition of RAD51D using RNAi in WI-38 cells results in telomere erosion and chromosome fusion (Tarsounas et al. 2004).
Homologous Recombination	**RAD50** (Zhu et al. 2000) RAD50 is stably associated with MRE11 and NBS1 in a complex that functions in response to double strand breaks (DSBs) in mammals (Carney et al. 1998). RAD50 is located at the telomere during interphase as indicated by indirect immunofluorescence. Evidence indicates that RAD50 binds the telomere through TRF2 as opposed to directly binding the telomeric DNA (Zhu et al. 2000).
Homologous Recombination	**MRE11** (Zhu et al. 2000) MRE11 is located at the telomere during interphase as indicated by immunofluorescence (Zhu et al. 2000). However, there is no evidence for direct interaction between MRE11 and TRF2, suggesting MRE11 is located to the telomere through a different telomeric protein.
Homologous Recombination	**Nbs1** (Zhu et al. 2000) Immunofluorescence and western blotting show Nbs1 is associated with TRF2 and telomeres in S phase, but not in G1 or G2 (Zhu et al. 2000). Nbs1 is capable of partially unwinding the DNA duplex and has an endonuclease specificity that allows Mre11/Rad50/Nbs1, the MRN complex, to cleave a 3'-protruding strand at a double-/single-strand transition (Paull and Gellert 1999). It is not understood exactly what function the MRN complex performs at the telomere.

Nucleotide Excision Repair	**ERCC1/XPF** (Zhu et al. 2003) ERCC1/XPF is a nucleotide excision repair endo-nuclease associated with TRF2 at the nucleus (Zhu et al. 2003). When TRF2 function is inhibited in immortalised normal fibroblasts, (using $TRF2^{\Delta B \Delta M}$, as discussed in Section 1.7) the cells show a reduction in their 3' overhang. In revealing contrast, inhibition of TRF2 in immortalised XPF deficient cells (cell lines derived from human XPF patients), does not cause a reduction of 3'overhang (Zhu et al. 2003), suggesting this is the endo-nuclease responsible for resecting the 3'overhang when telomeres are uncapped.
RecQ Helicase	**BLM** (Opresko et al. 2002) BLM, the gene defective in patients with Bloom's syndrome, co-localises and complexes with TRF2 in cells that employ the recombination-mediated mechanism of telomere lengthening known as ALT, see Section 1.15.ii (Lillard-Wetherell et al. 2004). The co-localisation increases in late S phase and G2/M (Lillard-Wetherell et al. 2004). TRF2 stimulates unwinding of telomere DNA and non-telomeric substrates by BLM, whereas TRF1 inhibits unwinding of telomere substrates by BLM (Lillard-Wetherell et al. 2004).
RecQ Helicase	**WRN** (Opresko et al. 2002) The Rec-Q family member, WRN, co-localises and physically interacts with TRF2, stimulating the 3'→ 5' helicase activity of WRN (Opresko et al. 2002), (Machwe et al. 2004). Cells lacking WRN, from Werner syndrome patients, exhibit deletion of telomeres from single sister chromatids on telomeres replicated by lagging strand synthesis (Crabbe et al. 2004).

DNA damage recognition	ATM (Karlseder et al. 2004) Ataxia telangiectasia is a disease characterised by characterized by chromosomal instability, cancer predisposition, radiation sensitivity, and cell cycle abnormalities. The gene mutated in this disorder has been named, Ataxia Telangiectasia Mutated, ATM (Savitsky et al. 1995), which is now known to play a very important role in recognising DNA double strand breaks and implementing their repair. TRF2 can directly interact with a region of ATM (containing S1981) and inhibit ATM's activation in response to DNA damage (Karlseder et al. 2004).

1.4 Telomere bouquet in meiosis

Although the function of some of the proteins bound to the telomere may not be immediately obvious, it is important to remember the context in which we observe them will affect our interpretation of their purpose. In addition to the important role the telomeres have in protecting the genome, they also serve in the early stages of meiosis, the process by which male and female -derived genomes are recombined and halved to form gametes (reviewed in (Scherthan 2001)). Before undergoing meiosis, telomeres attach to the nuclear envelope and gather near the centrosome (Tomita and Cooper 2006). In Maize plants during prophase of meiosis I, telomeres attach to the nuclear envelope and gather at one pole of the nucleus to form the 'bouquet' structure (Bass et al. 1997). Highly expressed in testis during meiotic prophase I, Tankyrase1, which associates with the centrosome, is suspected of playing a role in meiosis (Smith and de Lange 1999).

1.5 Other Proteins and factors that Influence the Telomere

The complex list of human telomere binding proteins in Table 1 is intended to be comprehensive; however it does not include all the proteins that regulate the human telomere. Proteins capable of regulating the telomere binding proteins in the table will also have considerable influence on the structure of the telomere. For example, over-expression of Fbx4 (a substrate-specific adaptor of ubiquitin ligase) promotes the ubiquitination and degradation of endogenous

Pin2/TRF1, resulting in progressive telomere elongation in human cells (Lee et al. 2006).

Another factor shown to affect the telomere is oxidative stress, which has been shown to increase the erosion and loss of telomeric DNA in human fibroblasts (von Zglinicki et al. 1995), (Tchirkov and Lansdorp 2003). Oxidative damage in telomere DNA, specifically a single 8-oxo-guanine lesion, has been shown to reduce the percentage of telomere bound TRF1 and TRF2 by at least 50%, compared with undamaged DNA. Multiple lesions to the DNA resulted in more dramatic effects of TRF1 and TRF2 binding (Opresko et al. 2005).

The DNA damage-dependent poly(ADP-ribose) polymerase 2, PARP-2, plays an active role in the base excision repair process and also associates through its N terminal domain with the myb domain of TRF2 (Dantzer et al. 2004). PARP-2 activity regulates the DNA binding activity of TRF2 via both a covalent hetero-modification of the dimerization domain of TRF2 and a non-covalent binding of poly-ADP ribose to the myb-domain of TRF2 (Dantzer et al. 2004).

1.6 Model systems

Model systems are an essential means for performing experiments that involve gene manipulation that are either very difficult or impossible to do in human cells. Experiments in less complicated organisms such as yeast allow a more straightforward evaluation of mechanisms altered as a result of the experimental manipulation, particularly as they minimise issues like redundancy which can complicate experimental interpretation in more evolved organisms. Once the function of a protein is established, protein homologues can then be assessed in more sophisticated organisms to see if they have a similar function.

1.6.i Yeast

In *S.pombe* (Fission yeast), telomere repeats are bound by Taz1, a regulator of diverse telomere functions considered to be the homologue of both human proteins TRF1 and TRF2 (Cooper et al. 1997). Taz1 is crucial for efficient replication fork progression, as loss of Taz1 leads to stalled replication forks at telomeres and internally placed telomere sequences, regardless of whether the DNA synthesis is leading or lagging strand (Miller et al. 2006).

Again using *S.pombe*, it has been shown that telomeres play an important role in meiosis: at early stages all the telomeres in the cell attach to the nuclear envelope and gather near the spindle pole body, SBP (centrosome in mammals), forming what is known as a 'bouquet (Chikashige et al. 1994). Expressed during meiosis, the recently discovered proteins, Bqt1 and Bqt2, are essential for connecting the telomeric protein Rap1 to the SPB (Chikashige et al. 2006).

Over the next several years, it will be interesting to see if any of the telomere binding proteins emerge as being associated with DNA replication and to determine what the mammalian homologues for Bqt 1 and 2 do within mammalian cells.

In *S.Cerevisiae* (budding yeast), studies of the replication intermediates of a linear plasmid in rad27delta cells are consistent with the idea that only one end of the plasmid acquires extensive G-tails, presumably the end made by lagging-strand synthesis (Parenteau and Wellinger 2002). How the 3'overhang on the lagging strand of telomeric DNA is generated in human cells has still not been fully elucidated (discussed in Section 1.10).

When deleted, Rap1, which binds the telomere directly in *S.cerevisiae* results in frequent fusion between telomeres of near wild type length by NHEJ (Pardo and Marcand 2005). Although still associated with the telomere in humans through TRF2, this protein has changed considerably during the evolution from yeast to human.

1.6.ii Rat

An interesting study examined the effects of the adenoviral infection of $TRF2^{\Delta B\Delta M}$ in proliferating and non-proliferating rat brain cells. In proliferating neural cells (primary astrocytes and neuroblastoma), $TRF2^{\Delta B\Delta M}$ triggered phosphorylation of H2AX, activated ATM and p53 and induced p21 as well as excess B-galactosidase staining (Zhang et al. 2006). In contrast, in non-proliferating neurons (primary embryonic hippocampal), $TRF2^{\Delta B\Delta M}$ triggered phosphorylation of H2AX, activated ATM, and an induced p21, but neither p53 nor senescence were induced and there was no evidence of apoptosis (Zhang et al. 2006). These results suggest that at least a certain amount of cell proliferation must occur before $TRF2^{\Delta B\Delta M}$ can induce the senescent phenotype (Zhang et al. 2006).

1.6.iii Mouse

Before the discovery of RNAi as a tool for knocking down a particular protein of interest, finding cells deficient in a particular protein was difficult. Through genetic engineering, mouse cells can be altered to lack a particular gene and is a common method that is still used to ask experimental questions. However, some major differences between the mouse and human must be considered when using mouse cells (or the whole animal) as a model for telomere alteration. Two strains of mice are commonly used for scientific study: Mus Musculus, an inbred mouse strain contains telomere lengths of up to several hundred kilobase pairs (Kipling and Cooke 1990). On the other hand, the outbred strain, Mus Spretus, contains telomere lengths more similar to those in humans, below 30 kbp (Prowse and Greider 1995). In contrast to human tissues, most mouse tissues have active telomerase at levels easily detected (Prowse and Greider 1995). Unfortunately, publications often fail to comment which mouse strains their cells are derived from.

The following experiment had to be performed in p53 null ($p53^{-/-}$) cells, otherwise the cells arrested before the difference in DNA ligase 4 expression could be evaluated. Mouse Embryo Fibroblasts, MEFs $p53^{-/-}$, either with DNA ligase IV ($Lig4^{+/+}$) or without ($Lig4^{-/-}$), were infected with $TRF2^{\Delta B \Delta M}$. $Lig4^{+/+}$ cells frequently contained telomere fusions, e.g. 51 telomeric fusions in 30 metaphases. In contrast, $Lig4^{-/-}$ cells contained 25 fold less telomere fusions (Smogorzewska et al. 2002). As DNA ligase IV is involved in NHEJ, this is likely to be the main mechanism by which telomeres are fused after TRF2 inhibition.

ERCC1/XPF is a nuclease that cleaves away sections of DNA damaged by UV light. Xeroderma pigmentosa, the human condition of ERCC1/XPF deficiency, is characterised by a propensity for skin cancer. MEFs deficient for ERCC1 contain circular extrachromosomal elements with telomeric DNA, termed double minute chromosomes and terminally short telomeres which fuse (Zhu et al. 2003). Based on this result, it seems clear that ERCC1/XPF plays a role in processing the telomere. It has been suggested that when the telomere is capped, ERCC1/XPF snips away inappropriate telomere loops and when the telomere is uncapped it is susceptible to being re-sected back by the nuclease (Zhu et al. 2003).

In $Ku70^{-/-}$ MEFs, in which the TRF2 gene can be deleted through the addition of Cre recombinase, telomeres had a normal DNA structure and did not activate a

DNA damage signal. However, on removal of TRF2, sister chromatid fusions occurred at approximately 15% of the chromosome ends (Celli et al. 2006). Combined deletion of TRF2 and another element of the NHEJ pathway, DNA ligase IV, did not elicit this phenotype, indicating that TRF2 and Ku70 act in conjunction to suppress homologous recombination at the telomere, at least in the mouse (Celli et al. 2006).

Conditional deletion of $TRF1^{-/-}$ from mouse embryonic stem cells, results in a growth defect and chromosomal instability. In addition to these changes, TIN2 is lost from the telomere and TRF2 showed decreased association (Iwano et al. 2004).

Despite the length of the mouse telomere, $TRF2^{\Delta B\Delta M}$ caused a growth arrest and senescent morphology in p53 proficient mouse cells. However, in contrast to human cells, loss of p53 alone is enough to circumvent the arrest of mouse cells indicating that the $p16^{INK4A}$ /RB response to telomere dysfunction is not active in mouse cells (Smogorzewska and de Lange 2002). Another investigation using $TRF2^{\Delta B\Delta M}$ in mouse liver cells established that low levels of telomere uncapping induced cell senescence and high levels of telomere uncapping caused apoptosis (Lechel et al. 2005).

MEFs triply deficient for RB1, RBL1 (RB Like 1) and RBL2 demonstrate decreased tri-methylation of histone H4 at Lysine 20 at both pericentric and telomeric chromatin, independent of the E2F family function (Gonzalo and Blasco 2005). This tri-methylation is consistent with compacted, repressed DNA and therefore alleviation of the compacted state by loss of RB allows a more open chromatin structure, making the telomeric DNA more permissive to sister chromatid exchanges and possibly also affect the ability of telomeric proteins to bind.

1.6.iv Mouse - Whole Animal

The generation of knockout mice lacking a particular gene can be created in 2 different ways. Mice either completely lack the gene or its removal can be controlled by a conditional circumstance.

TRF2 null mice are embryonic lethal before embryonic day 13.5 (E13.5) and could not be rescued by p53 deficiency (Celli and de Lange 2005). Mice lacking

TRF1 (Karlseder et al. 2003) or TIN2 (Chiang et al. 2004) were also embryonic lethal on days E5 - E6.

Tankyrase2 null mice were generated and surprisingly found to have normal telomere lengths and capping, but did exhibit reduced growth (Hsiao et al. 2006), (Chiang et al. 2006). The most likely explanation for this is redundancy of Tankyrase2 protein function with Tankyrase1.

Humans have one gene for POT1, that is alternatively spliced (See Table 1, POT1). In contrast, 2 POT1 paralogs have been found to bind to the mouse telomere. Single knockouts and complementation experiments show that POT1b has the ability to regulate the amount of single stranded DNA at the telomere terminus while POT1a is required to repress a DNA damage signal at the telomere (Hockemeyer et al. 2006). Another report demonstrates that Pot1a deficient cells exhibit an overall telomere length and 3'overhang elongation, as well as aberrant Homologous Recombination manifested in increased telomere sister chromatid exchanges and formation of telomere circles (Wu et al. 2006).

To generate mice with shorter telomeres, Mus Musculus engineered to lack the RNA component of telomerase, $mTR^{-/-}$, must be bred for four generations before chromosome ends lacking detectable telomere repeats, aneuploidy and chromosomal abnormalities including end-to-end functions are observed. A cross between $mTR^{-/-}$ Generation 6 mice, which have short telomeres, and $mTR^{+/-}$ mice which have long telomeres, results in some telomerase null offspring with half of their telomeres very short (Blasco et al. 1997). Loss of telomere function occurred preferentially on the critically short telomeres (Hemann et al. 2001). This indicates that it is the shortest telomeres that dictate the fate of the cell, and not the average telomere length. It has also been demonstrated that short telomeres even in the presence of telomerase limit tissue renewal capacity (Hao et al. 2005).

The absence of Ku86 and telomerase at the mouse telomere prevents end-to-end chromosome fusions that result from critical telomere shortening in telomerase deficient mice and apoptosis in the male early germ cell (Espejel et al. 2002). However, in cells where telomerase is present, Ku86 deficiency results in telomerase dependent telomere elongation and in fusion of random pairs of chromosomes (Espejel et al. 2002). Gene expression in the testis of 3-5 month

old mice were compared in the following phenotypes: $mTR^{-/-}$ Generation 3, $Ku86^{-/-}$, a combination of both knockouts or the wild type equivalents. This study established a change in the expression levels of genes involved in cell adhesion, cell-to-cell and cell-to-matrix communication as well as increased metabolic turnover and augmented anti-oxidant response (Franco et al. 2005). Transcriptional changes affecting chromatin remodelling such as retinoblastoma binding protein 7 (a histone deacetylase), the linker Histone 1 H2bc and the histone deacytlase 6, suggesting epigenetic remodelling associated with short and dysfunctional telomeres (Franco et al. 2005). Telomeres in mouse embryonic stem cells lacking DNA methyltransferases, such as DMNT1 or DMNT3a or 3b have dramatically elongated telomeres (Gonzalo et al. 2006).

Overexpression of TRF2 in the mouse epidermis results in telomere shortening, loss of the telomeric G-strand overhang and increased chromosomal instability. The epidermis suffered phenotypes resembling Xeroderma pigmentosum (human condition), and the telomere loss was mediated by XPF, the structure specific nuclease involved in UV-induced damage, nucleotide excision repair and mutated in individuals with Xeroderma pigmentosum (Munoz et al. 2005).

1.6.v Drosophila

Drosophila telomeres are unlike other eukaryotic telomeres in that they are made of repeats of Het-A and TERT retrotransposons that are maintained by transposition rather than telomerase activity and are protected by the binding of two proteins, heterochromatin protein 1 (HP1) and HP1 ORC2 associated proteins (HOAP) (Purdy and Su 2004). Despite the difference in mechanism for telomere length maintenance, Drosophila homologs defective for either ATM, Mre11 or Rad50 demonstrated increased telomere fusions (Bi et al. 2004) (Ciapponi et al. 2004).

1.6.vi Muntjac Deer

Chromosome fusions have had a dramatic effect of the karyotype of the muntjac deer. The Indian muntjac (2N= 6 chromosomes in female, 7 in male) has the lowest known chromosome number among mammals, the result of centric and tandem chromosome fusions. In contrast, the closely related Chinese muntjac still contains a higher number of chromosomes (2N = 46 chromosomes) (Wang and Lan 2000). Both species of muntjac deer still express both TRF1 and TRF2, ruling out the loss of either protein playing a role in the chromosome fusions

that occurred in the Indian muntjac (Hartmann and Scherthan 2005). Interestingly, TERT expression could not be detected in either muntjac species, yet the TRAP assay revealed functional telomerase in Chinese muntjac testis tissue, suggesting muntjacs harbour a diverged telomerase species (Hartmann and Scherthan 2005).

1.7 Uncapping the human telomere, experiments with TRF2$^{\Delta B \Delta M}$

In the de Lange lab, a dominant negative version of the TRF2 protein was created: TRF2$^{\Delta B \Delta M}$, missing both its basic and myb domain, (**Figure 1**). Another dominant negative version of TRF2, TRF2$^{\Delta B \Delta C}$ (lacks the N and C terminal domains which contain the basic and myb domains, respectively) has been used by another group. (Based on the molecular weight of it's product it is fair to speculate it actually is the same as the TRF2$^{\Delta B \Delta M}$ construct, however the authors do not define which amino acids are missing nor make reference to the other widely used construct.)

TRF2$^{\Delta B \Delta M}$ dimerises with endogenous TRF2, but because it is lacking a myb domain, the dimer is no longer capable of binding the telomere since a minimum of two myb domains are required for such an interaction. TRF2$^{\Delta B \Delta M}$ acts as a dominant negative and its expression is thought to mimic the uncapped telomere.

Table 2 lists the effects of expression of TRF2$^{\Delta B \Delta M}$, TRF2$^{\Delta B \Delta C}$ and TRF2$^{\Delta B}$ in various human cell types. Apoptosis is the result in 3 different immortal cancer cell lines, HeLa, MCF7 and JR5, none of which had functional p53 or p16^{INK4A}. In contrast, another p53 and p16^{INK4A} deficient, immortal cancer cell line; M14, did not result in apoptosis. Immortalised B cells with functional p53 and p16^{INK4A} underwent apoptosis, however B cells which also contained functional p53 and p16^{INK4A}, but lacked ATM did not apoptose. This illustrates the point that without functional proteins upstream or downstream of p53 or p16^{INK4A}, the status of these two tumour suppressor proteins may be irrelevant. Mortal primary CD4+ T cells also entered apoptosis, suggesting that the mortality status does not affect the cells decision to commit apoptosis or not. The other phenotype typically seen in human cells expressing TRF2$^{\Delta B \Delta M}$, e.g. HTC75 and IMR90, was chromosome end fusions and senescence. Apoptosis and senescence

Table 2: Experiments Involving Manipulation of TRF2 in Various Human Cell Types

Cell Line (site of derivation)	Mortality Im=Immortal M= Mortal	p53 status	$p16^{INK4A}$ status	TRF2 construct expressed	Result	Reference
HeLa (Cervical carcinoma)	Im	-ve (HPV18)	-ve (HPV18)	ΔBΔM	Apoptosis	(Karlseder et al. 1999)
MCF7 (breast carcinoma)	Im	+ve	-ve	ΔBΔM	Apoptosis	(Karlseder et al. 1999)
JR5 (melanoma) ~ 5kbp telomere length	Im	-ve	-ve	ΔBΔC	Apoptosis and reduced tumorgenicity	(Biroccio et al. 2006)
M14 (melanoma) ~ 9kbp telomere length	Im	-ve	-ve	ΔBΔC	No apoptosis and no reduced tumorgenicity (No comments regarding senescence or end-to-end ligations are made.)	(Biroccio et al. 2006)
B cells	Im	+ve	+ve	ΔBΔM	Apoptosis	(Karlseder et al. 1999)
B cells ($ATM^{-/-}$)	Im	+ve	+ve	ΔBΔM	No Apoptosis	(Karlseder et al. 1999)
BJ (foreskin fibroblast)	Im	-ve (SV40)	-ve (SV40)	ΔBΔM	Reduced cell proliferation and increased growth in soft agar, but not in nude mice.	(Brunori et al. 2006)
HTC75 (inducible cell line based fibrosarcoma HT1080 cells)	Im	+ve	-ve	ΔBΔM	Chromosome end fusions and involving ligation of telomeres that lost their 3'overhang.	(van Steensel et al. 1998) [HT1080 - p53/ $p16^{INK4A}$ status (Chang et al. 1999)]
Primary $CD4^+$ T cells	M	+ve	+ve	ΔBΔM	Apoptosis	(Karlseder et al. 1999)
IMR90 (embryo lung fibroblast)	M	+ve	+ve	ΔBΔM	Chromosome end fusions	(Smogorzewska and de Lange 2002)
IMR90 (embryo lung fibroblast)	M	+ve	+ve	ΔB	Dramatically shortened telomeres, T-loop sized telomeric circles, a DNA damage response and senescence.	(Wang et al. 2004)

are the common outcomes of uncapping the telomere in a range of human cells, however, neither a specific cell type, p53/ $p16^{INK4A}$ status, nor mortality can be associated with a particular cellular outcome.

Another method of experimentally creating an uncapped telomere within a cell is to introduce DNA oligonucleotides homologous to the telomere 3' overhang, T-oligos (Eller et al. 2002). One-week exposure to T-oligos resulted in a senescent phenotype in cultured human fibroblasts, mimicking both telomeres shortened through replication and the $TRF2^{\Delta B \Delta M}$ (Li et al. 2003).

1.8 How TRF2 Over-expression Regulates the Human Telomere

Other experiments have investigated the effects of over-expressing TRF2 in human derived cell lines. Over-expression of TRF2 is able to prevent the cell cycle arrest that would normally be induced following ionising radiation in fibroblasts (Karlseder et al. 2004). Typical post-translational modifications that should occur as a result of DNA damage such as the phosphorylation of ATM (at Serine1981), Nbs1, p53 and the up-regulation of p53 target genes were not seen in the TRF2 over-expressing cells, offering an explanation to the lack of cell cycle arrest (Karlseder et al. 2004).

Over-expression of TRF2 results in progressive telomere shortening similar to the phenotype observed with TRF1 over-expression (Smogorzewska et al. 2000). However, expression of exogenous TRF2 became extinguished in culture after 50 to 75 population doublings, despite continued selection pressure (Smogorzewska et al. 2000). This suggests that not only is increased telomere shortening an outcome, but also that there is a selective advantage to no longer over-expressing TRF2.

1.9 TRF2 involvement in the DNA damage response

It is likely that, in addition to its role at the telomere, TRF2 also plays a role at non-telomeric sites of DNA damage since TRF2 is rapidly phosphorylated in response to DNA damage. The phosphorylated form is not found bound to telomeric DNA, but is localised to sites of DNA damage (Tanaka et al. 2005). ATM is implicated in the phosphorylation of TRF2 which is largely dissipated

after two hours (Tanaka et al. 2005). In human fibroblasts, TRF2 protein has been shown to associate with DSB induced by pulsed laser microbeam irradiation within 2 seconds, as judged by co-localisation with γ-H2AX (Bradshaw et al. 2005). The response requires the basic domain of TRF2, but not its myb domain, and occurs in the absence of functional ATM, the MRN complex, Ku70, WRN and BLM repair proteins (Bradshaw et al. 2005). However, contrary evidence has also reported that TRF2 does not re-localise to sites of DNA damage as judged by co-localisation with MRN (Zhu et al. 2000). The authors of the latter paper do not indicate at what time they began to look for co-localisation, so it is possible they missed the early pattern of protein interaction.

1.10 The End replication problem and generation of the 3' overhang

The inability of the ends of linear chromosomes to be fully replicated during each round of replication was realised and first hypothesised as the cause of cell cycle arrest in senescent cells in a theoretical paper (Olovnikov 1971). DNA polymerases responsible for replicating genetic material require a RNA or DNA polynucleotide primer with a 3'hydroxyl (3'-OH) group, and are only capable of catalysing the addition of nucleotides to growing DNA strands in a 5'→3' direction, (**Figure 3**). When the primer is RNA, it is later removed once DNA synthesis has been primed. A consequence of this is a 3' overhang of telomeric DNA on the parental strand complementary to the newly formed lagging strand resulting in a small loss of telomeric DNA at each round of cell division. Telomeres have been shown to shorten by 50-200 bp per cell division (Cooke and Smith 1986), (Harley et al. 1990) (Allsopp et al. 1995) and this is known as the end replication problem, (**Figure 3**).

The 3'overhang folds back to invade the upstream telomeric sequence forming what is known as a Telomere loop, T loop, which have been found in cross-linked telomeric DNA purified from human (and mouse) cells when analysed by electron microscopy (Griffith et al. 1999), (**Figure 4**). Experiments investigating the role of telomeric binding proteins in the formation of the T-loops found that addition of TRF2 can remodel ~50% of a linear telomeric sequence DNA containing a 3'overhang into T loops. Where the linear DNA was remodelled, TRF2 was found at the tail loop junction, (**Figure 4**)(**b**). Without incubation of TRF2 protein,

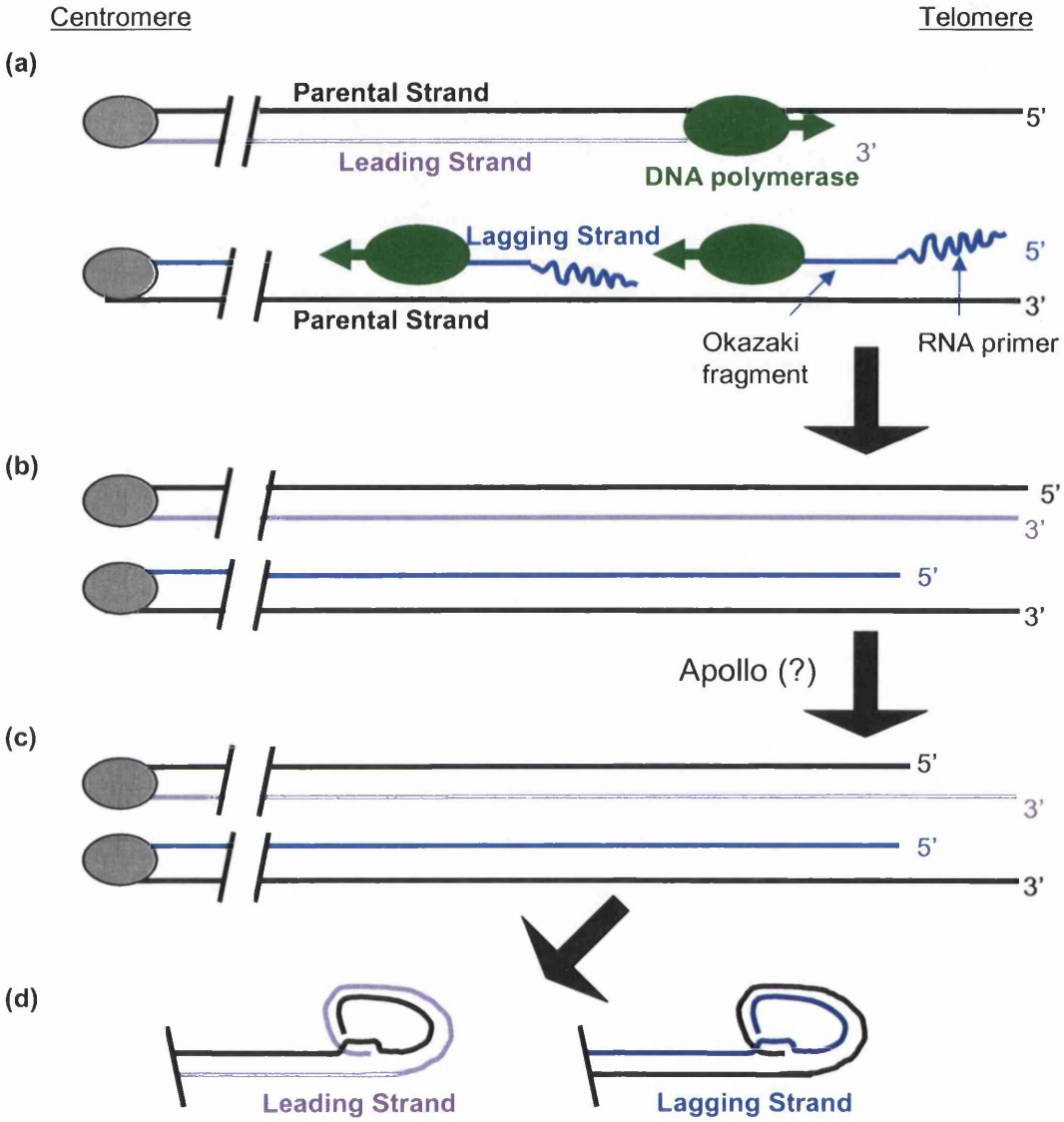

Figure 3. The end replication problem and generation of the 3'overhang.

(a) DNA polymerases only catalyse the addition of nucleotides in a 5'→ 3' direction, after being primed by a small RNA primer. During semi-conservative replication, on the lagging strand Okazaki fragments are joined by DNA polymerase acting on an upstream Okazaki fragment and the DNA replaces the interceding RNA primers, except at the telomere of the lagging strand.

(b) This results in a gradual shortening of telomeres and is referred to as the end replication problem.

(c) What is still not completely understood is how the blunt ended telomere from leading strand synthesis get resected to have a 3' overhang. Recent evidence now implicates the telomere binding/NHEJ protein Apollo in this role (See Table 1).

(d) The 3'overhang then invades the upstream telomeric DNA, a process thought to be largely aided by the binding of multiple components of the shelterin complex.

(a)

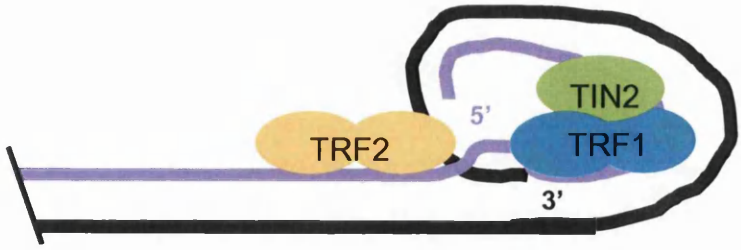

(b)

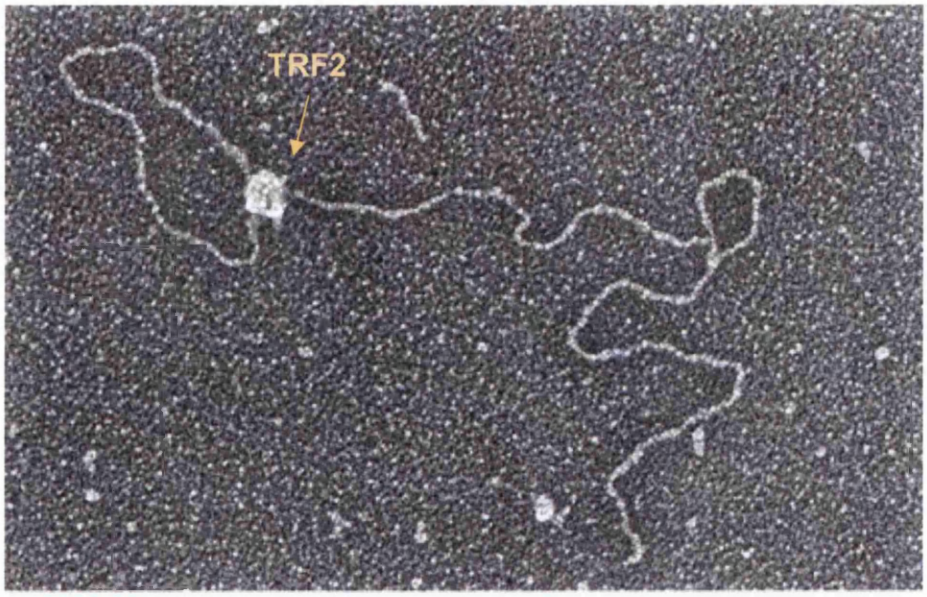

Figure 4. Telomere Loop Structure.

(a) Only the telomere binding proteins proposed to aide in the formation of the T loop by shaping the DNA into the correct formation are shown. TRF2 has been shown to increase the amount of T loops formed by 50% using linear telomere sequence DNA with a 3'overhang. In similar experiments, TRF1 on its own only can only remodel 2% of the DNA into T loops. However, it has recently been proposed that the ternary complex formed with TRF1 and TIN2 may aide in the folding the DNA back on itself.

(b) Taken from: Griffith JD, Comeau L, Rosenfield S, Stansel RM, Bianchi A, Moss H, de Lange T. *Cell.* 1999 May 14;97(4):503-14. Mammalian telomeres end in a large duplex loop.

This image demonstrates the scanning electron microscope image of piece of linear telomere DNA remodelled with the aid of TRF2. TRF2 is the large globular shaped structure at the site of the 3'overhang inversion and is thought to aide in this process.

only ~1% of the same DNA could be remodelled. Incubating the DNA with TRF1 resulted in formation of T loops in only ~2% of the population and TRF1 was never observed at the tail-loop junction. Formation of the T-loop in vitro was dependent upon the 3'overhang. A 3'overhang of at least 6 nucleotides is required for loop formation and termini with a 5' overhang, blunt end or a 3'overhang with non-telomeric sequence at the junction are not capable of forming a T-loop (Stansel et al. 2001). The ternary complex between TRF1 and TIN2 is suggested to aid in pairing of the duplex DNA and TRF2 is proposed to regulate the actual invasion of the 3' overhang. The T loop model puts forward an architectural solution to the end of the linear chromosome (Griffith et al. 1999).

The 3'overhang averages 130 - 210 bases in length in >80% of telomeres present in mortal primary fibroblasts, umbilical vein endothelial cells and leukocytes, as well as in immortalised fibroblasts (Makarov et al. 1997). The end replication problem is likely to be a contributing factor to generation of the 3' overhang. Exactly how the 3'overhang is generated during leading strand DNA synthesis in human cells is still unknown. It has been proposed that TRF2 enhances the 5' exonuceolytic processing of telomere ends, for instance by recruiting an exonuclease (Karlseder et al. 2002), possibly Apollo (Lenain et al. 2006). A recent report demonstrates that where MRN levels are reduced, a transient shortening of the 3' overhang is seen in telomerase positive cells, yet the terminal nucleotides of both the G-rich and the C-rich strands remain unaltered, indicating that MRN is not responsible for specifying the final end processing event (Chai et al. 2006b). Cultured normal human diploid cells have longer G overhangs at telomeres generated by lagging strand synthesis than at leading strand synthesis; whereas elongated overhangs are found in leading daughter telomeres in human cells expressing telomerase (Chai et al. 2006a).

In telomerase negative fibroblasts, Mre11, phosphorylated Nbs1 and ATM, are recruited to the telomere in every G2 of the cell cycle, an event that correlates with the partial release of POT1 (Verdun et al. 2005). Degradation of Mre11 using RNAi leads to increased accessibility to a terminal transferase, implying the MRN complex might regulate accessibility to the telomere during G2. Inhibiting ATM using caffeine in fibroblasts expressing HPV-E6 and E7, leads to telomere dysfunction. It has therefore been proposed that a localised DNA

damage response at telomeres during G2 involving both the MRN complex and ATM, is essential for recruiting the processing machinery that promotes formation of a capped telomere (Verdun et al. 2005).

Expression of $TRF2^{\Delta B \Delta M}$ results in at least a partial loss of the 3' overhang, whereas over-expression of TRF2 resulted in accelerated telomere shortening and a 15% increase in the 3' overhang (Karlseder et al. 2002). These results suggest that although TRF2 is not directly responsible for the end processing of the newly replicated telomere, it may be involved in recruiting the protein(s) that are.

1.11 The Double Strand Break (DSB) Repair Pathways

Many of the telomere binding proteins listed in Table 1 are more traditionally associated with DNA DSB repair. At first, the realisation DSB proteins were located at the telomere seemed counter intuitive since the entire purpose of the telomere is to prevent it from being recognised as a DNA double strand break. With the understanding that the telomeric DNA requires processing before it can fold into a capped form, the presence of the DNA damage proteins does not seem so illogical. Summarised below and in (**Figure 5**) are the two different pathways known to repair DSBs and the proteins involved in the process:

- Homologous Recombination, HR. During late S and G2, a cell can employ HR, a more accurate method of DNA repair. Activated ATM recognises the double strand break and then a series of proteins including the MRN complex, RPA, RAD51 family, RAD 52, BRCA1 and 2 initiate a single strand overhang that can invade the sister chromatid. DNA transcription then occurs by correctly replacing the DNA that was lost using the undamaged sister chromatid as a template (van Gent et al. 2001).

- Non-homologous end joining, NHEJ. During G1 and early S phase, NHEJ rejoins two broken chromosomes without checking the fidelity of the DNA sequence, typically resulting in a small deletion. The Ku heterodimer and DNA-PKs binds the DSB. The MRN complex is then recruited, and it is thought to use its helicase and endonuclease activity to create blunt ends

Figure 5. The two pathways of Double Strand Break (DSB) Repair.

These illustrations are taken from:

van Gent DC, Hoeijmakers JH, Kanaar R. Chromosomal stability and the DNA double-stranded break connection. *Nat Rev Genet*. 2001 Mar;2(3):196-206.

(a) Homologous Recombination

After the DSB is formed, ATM kinase is activated. Subsequent events include the recognition of DNA ends, which might include RAD52, and possibly then processing by the MRN complex. RAD51 polymerizes onto single stranded DNA to form a nucleoprotein filament with the aid of RPA and RAD52. Other proteins implicated in the response include BRCA1 and 2 and the RAD51 paralogues, XRCC2, XRCC3, RAD51B, RAD51C and RAD51D.

(b) Non-Homologous End Joining

Once the DSB is formed, the KU-DNA-PKs complex is probably involved in the initial recognition of the DSB and in the juxtaposition of the DNA ends. The ends might be processed, which results in the removal or addition of base pairs. The ends are then ligated by the DNA ligase IV-XRCC4 complex.

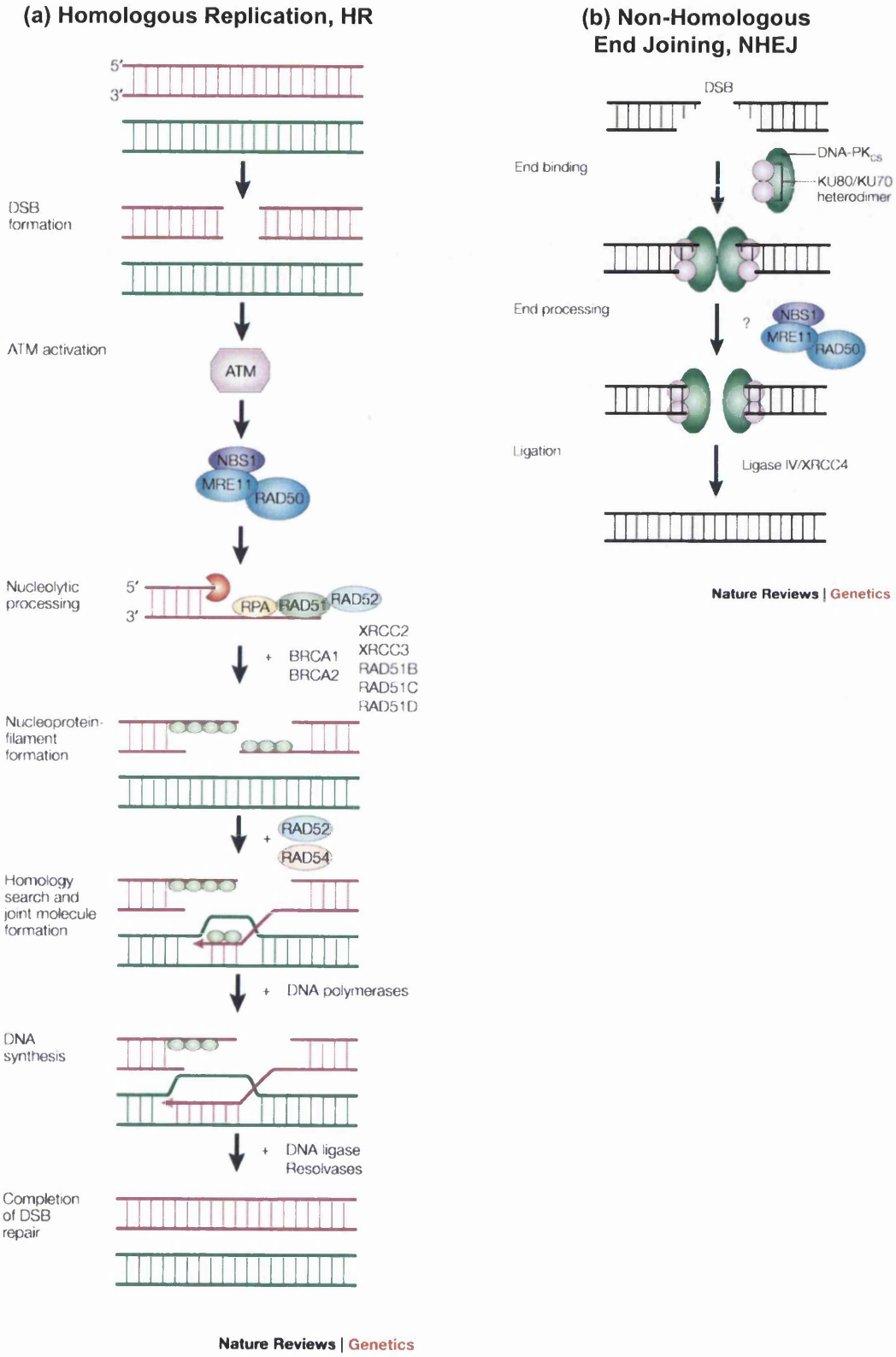

Figure 5. The Two Pathways of DSB Repair

suitable for ligation. XRCC4 and ligase IV are then (directly or indirectly) bound by the DNA-PK mediated phosphorylation (van Gent et al. 2001).

Although the exact logistics of what each of the DNA damage response proteins do during normal telomere processing has not yet been established, it is easy to imagine how the process may require helicases and endonucleases.

1.12 End-joining of uncapped telomeres

Although the properties of some of the proteins involved in NHEJ and HR are thought to be bound to the telomere for processing purposes, their exact role has not yet been fully determined. Unfortunately, these processing events can go wrong either when the proteins involved are de-regulated or when telomeres become critically short.

Telomere reduction occurs with aging and prior to crisis in human cancers (Hastie et al. 1990). Biopsies from ulcerative colitis patients (a chronic inflammatory disease of the colon associated with a high risk of developing into colorectal carcinoma), also reveal shorter telomeres than in control patients, presumably caused by a higher cell turnover. The study correlates short telomere length with chromosomal instability and a higher frequency of anaphase bridges (O'Sullivan et al. 2002).

Spontaneous telomere loss on a single chromosome in a human tumour cell line can result in sister chromatid fusion and prolonged periods of chromosome instability through breakage/fusion/bridge (B/F/B) cycles (Lo et al. 2002). Another study has shown that at the chromosome end missing a telomere, non-reciprocal translocation from one telomere to another resulted in telomere loss for the donor chromosome which consequently underwent additional translocations. In contrast, telomere donation through duplication, i.e. that did not involve telomere loss, stabilised the genome (Sabatier et al. 2005).

After expression of TRF2$^{\Delta B \Delta M}$ in HTC75 cells, under the control of a doxycycline-repressible promoter, telomere fusions were identified as anaphase bridges using the DNA intercalating dye; DAPI (van Steensel et al. 1998). Using the same inducible cell line, five days after expression of TRF2$^{\Delta B \Delta M}$, 44 out of 154 mitotic cells exhibiting end-to-end chromosomal fusions were detected using CO-FISH.

Figure 6. Mishaps during the cell cycle which lead to di-centric chromosomes.

(a) In S phase, each chromosome is duplicated during DNA replication. Each chromosome will contain one new strand (produced from leading or lagging strand synthesis) and one parental strand of DNA. The two chromosomes will be held together during throughout G2 at the centromere. During mitosis, microtubules align at the metaphase plate and are then pulled apart by microtubules that attach to the centromere.

During late S phase or G2, at least four different processes can occur that lead to the formation of di-centric chromosomes.

(b) If the telomeres are not processed properly, i.e. generation of the 3'overhang and correct coating of telomere binding proteins, it can be interpreted by the cell as a double strand break and hastily be "repaired" by Non-Homologous End Joining, NHEJ.

(c) As above, if the 2 telomeres were uncapped from different sister chromatid pairs, for example due to a problem with processing the leading strand synthesised during DNA replication, again improper NHEJ could occur resulting in a di-centric chromosome.

(d) Another process occurring at the telomere, possibly during the telomere lengthening mechanism used in ALT cells, is Homologous Recombination, HR. If the chromatid invasion, known as a holiday junction were not resolved, a di-centric chromosome would form.

(e) The Breakage/ Fusion /Bridge, (B/F/B) cycle, occurs when a DSB fuses with another chromosome and forms a bridge. The DSB could form at the telomere or arise elsewhere in the cell. The newly formed chromosome has two centromeres and will continue to form bridges and consequently break.

Telomeric DNA in incorrectly trapped between the 2 centromeres can lead to further HR events which again may not be resolved properly.

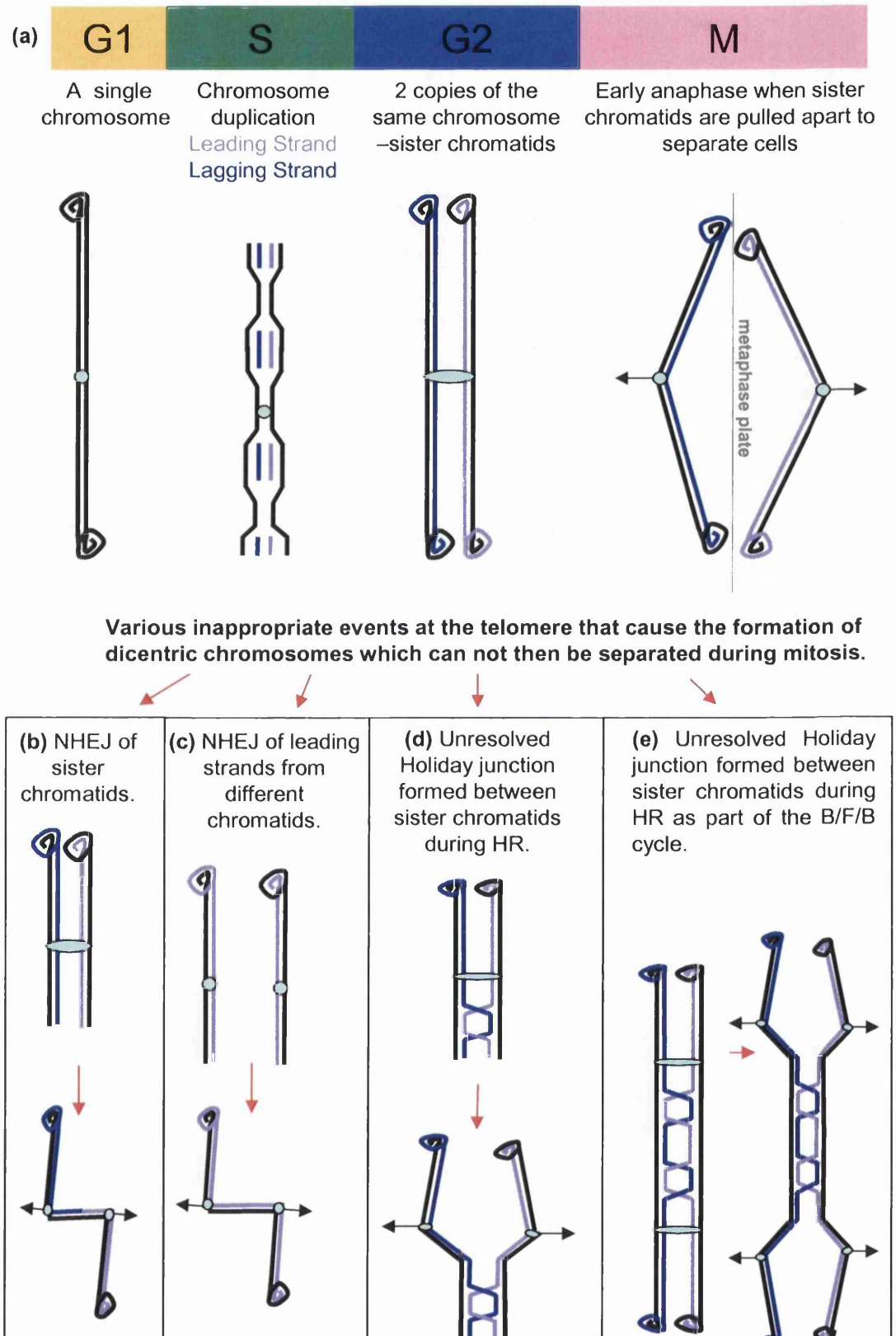

Figure 6. Mishaps during the cell cycle which lead to di-centric chromosomes.

After one round of replication in the presence of $TRF2^{\Delta B\Delta M}$, the telomere fusions were leading-to-leading strand (Bailey et al. 2001). Further work by another group established that TRF2 not only suppressed NHEJ of leading-to-leading strand, but also NHEJ of sister chromatids. Both types of end-joining were dependent upon DNA ligase IV (Smogorzewska et al. 2002) (**Figure 6**).

NHEJ of sister chromatids or different chromatids involving the lagging strands would require end resection of their 3'overhangs. When TRF2 function is inhibited in immortalised normal fibroblasts using $TRF2^{\Delta B\Delta M}$, the cells show a reduction in their 3'overhangs. In revealing contrast, inhibition of TRF2 in immortalised XPF deficient cells (cell lines derived from human patients), does not cause a reduction of 3'overhang (Zhu et al. 2003), suggesting this is the endo-nuclease responsible for resecting the 3'overhang when telomeres are uncapped.

In contrast, the mutant version of TRF2 that retained both its myb and TRFH domain, but no longer expressed the basic domain, $TRF2^{\Delta B}$, still repressed NHEJ (Wang et al. 2004). However, expression of $TRF2^{\Delta B}$ was not without consequence; Human cell lines IMR90, WI-38, HS68, BJ/hTERT, HT1080 and HeLa all demonstrated a reduction in mean telomere length. Both the C-rich and G-rich strands became shortened upon the expression of $TRF2^{\Delta B}$, but the 3'overhang remained unchanged (Wang et al. 2004). Using Chromosome Orientation Florescent in Situ Hybridization, CO-FISH, it was determined that the telomere deletion was shown to be preferentially generated in leading strand DNA synthesis and the deletions relied upon XRCC3 and NBS1. Relaxed, double-stranded DNA circles of telomeric DNA, called double minute chromosomes, were found in human cells expressing $TRF2^{\Delta B}$. Double minute chromosomes are also found in human cells that use ALT to maintain their telomeres and are known to contribute high-copy gene amplifications found in cancers (Hahn 1993).

1.13 Senescence

When placed in tissue culture, normal human cells can only undergo a limited amount of cell divisions, even under optimal conditions, before they stop proliferating. Cellular senescence was first defined by Leonard Hayflick as cell cycle arrest that accompanies the exhaustion of replicative potential in cultured

human fibroblasts (Hayflick and Moorhead 1961). Senescent cells are unable to respond to mitogenic signalling, which distinguishes them from quiescent cells (Dimri et al. 1996). Despite no longer proliferating, senescent cells remain metabolically active and display characteristic changes in cell morphology and gene expression. An up-regulation of the Beta-galactosidase gene is among these changes, resulting in senescent cells staining blue, after incubation with X-galactose at sub-optimal conditions (Dimri et al. 1995). Senescence is an extremely stable state, and this is thought to be attributed to formation of a distinct heterochromatin structure termed Senescence Associated Heterochromatin Foci, SAHF (Narita et al. 2003).

Senescence is the biological outcome of two different sets of circumstances:

(1) Oncogene Induced Senescence/ Premature Senescence/ Stasis -M0 - are all terms that refer to the same phenomena of cells entering a senescent state in response to: inappropriately activated oncogenes, DNA damage, oxidative stress or sub-optimal cell culture conditions (Serrano et al. 1997),(Campisi 2000)}. In addition to being shown in tissue culture, oncogene induced senescence has also been seen in vivo (Chen et al. 2005), (Braig et al. 2005). This type of senescence, typical of a naevi, is associated with increased $p16^{INK4A}$ levels, but not necessarily in every single cell (Michaloglou et al. 2005).

(2) Replicative Senescence - M1 - Replicative senescence is an established consequence of progressive telomere shortening, (Harley et al. 1990) (Counter et al. 1992). Tumour suppressor proteins p53 and $p16^{INK4A}$ act as Proliferative Lifespan Barriers, PLB, and regulate the onset of senescence (Wynford-Thomas 1999). Evidence has established both a p53 dependent (d'Adda di Fagagna et al. 2003), (von Zglinicki et al. 2005) and p53 independent (Jacobs and de Lange 2004) DNA damage responses in detecting the uncapped telomere(s) and instigating cell senescence in human fibroblasts (**Figure 7**).

Speculation that the DNA damage response pathway may mediate the effect of critically short telomeres has been a hypothesis for more than 10 years (Dulic et al. 1993). The over-expression of TRF2 increased the rate of telomeric shortening in primary cells without accelerating senescence, and reduced the

Figure 7. Proliferative Lifespan Barriers in primary human cells.

(a) "Mortality Stage 0 or 1 (M0/M1)" or "Senescence" is a viable proliferative arrest (at about 70 PD in human fibroblasts).

Senescence occurs when short telomeres are recognised by the p53 pathway. Rb remains hypo-phosphorylated preventing progression from G1 to S. p16 levels increase with passage in tissue culture and also increase in response to short telomeres. p16 prevents the phosphorylation of Rb, and can also cause senescence. Cells can escape from senescence through mis-regulation of both p53 and Rb (e.g. p53 mutation and p16 loss). M0 and M1 are biologically indistinguishable.

"Mortality Stage 2 (M2)" or "Crisis" is the result of critically short telomeres and causes cell death rather than growth arrest.

Cells within a human body are prevented from uncontrolled cell growth as they are regulated by these Proliferative Lifespan Barriers, PLBs, as are primary human cells (e.g. fibroblasts or epithelial cells) grown in tissue culture. Very rare cells which have lost p16, p53 and managed to activate either telomerase or the ALT pathway continue proliferating.

(b) This image is taken from the publication:

Preto A, Singhrao SK, Haughton MF, Kipling D, Wynford-Thomas D, Jones CJ. Telomere erosion triggers growth arrest but not cell death in human cancer cells retaining wild-type p53: implications for anti-telomerase therapy. *Oncogene.* 2004 May 20;23(23):4136-45.

K2 is a human thyroid cancer cell line that retains wt p53. Expression of a dominant negative version of hTERT inhibits telomerase activity and instigates a reduction in telomerase activity. Where cells express E6 (from HPV 16) their p53 is no longer functional and cells bypass senescence and proliferate until they reach crisis, demonstrated in panel * with a marker of apoptosis (TUNEL). In contrast, where p53 is still functional, the telomere shortening results in senescence and not apoptosis ◊.

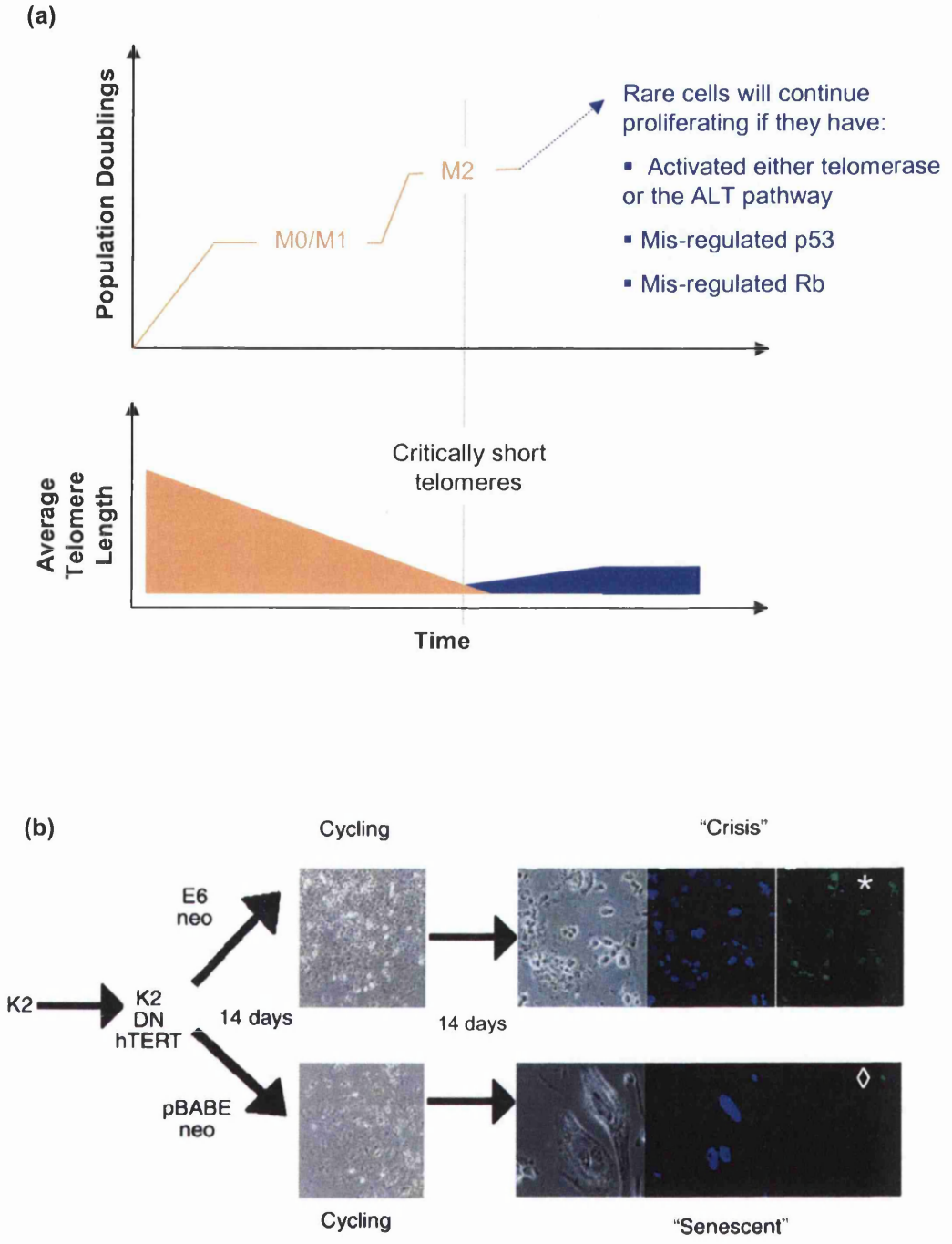

Figure 7. Proliferative lifespan barriers in primary human cells.

average telomere length at which point the cells start to senesce from 7 to 4 kbp (Karlseder et al. 2002). It was therefore hypothesised by Karlseder et al that replicative senescence is induced by a change in the protected status of shortened telomeres rather then by a complete loss of telomeric DNA. Uncapped telomeres in human fibroblasts were created using $TRF2^{\Delta B \Delta M}$ and then analysed for expression of DNA damage response factors. 53BP1, γ-H2AX, and activated. Rad17, ATM and Mre11 each co-localised with TRF1 signifying uncapped telomeres in what were branded Telomere-Induced dysfunctional Foci, TIF's (Takai et al. 2003). The presence of 53BP1 within a TIF was reduced by phosphatidylinositol 3-kinase inhibitors which affect ATM, ATR and DNA-PK. A cell line derived from an Ataxia Telangiectasia (AT) patient (a syndrome with mutations in the ATM protein) also demonstrated a diminished 53BP1 TIF response. However, these cells still senesced indicating an additional ATM independent pathway was also capable of recognising uncapped telomeres and instigating cell senescence. Phosphorylated H2AX, 53BP1, MDC1 and NBS1 are all proteins associated with the DNA damage response found activated in senescent human fibroblasts (d'Adda di Fagagna et al. 2003). It has also been established using Chromatin Immunoprecipitation or whole genome scanning approaches that the telomeres directly associate with some, but not all, DNA damage response proteins (Gire et al. 2004). Moreover, inactivation of DNA damage checkpoint kinases (pATM, pATR, pCHK1 and pCHK2- using microinjection of plasmids expressing kinase dead versions of protein) in senescent cells resulted in up to 20% of cells progressing to S phase (d'Adda di Fagagna et al. 2003). These publications were the first to provide evidence that critically short or uncapped telomeres were capable of initiating senescence through the DNA damage response pathway.

Not only are activated ATM and γ-H2AX readily observed in late-passage fibroblasts, but these signals can be abrogated with the addition of telomerase (Bakkenist et al. 2004), providing further evidence that it is the critically short telomere instigating the senescence. Once cells become fully senescent in the absence of telomerase, the activated ATM and γ-H2AX signals disappeared, indicating that their constitutive signalling is not required for the maintenance of senescence (Bakkenist et al. 2004). Although the signal for initiating senescence may not be required, the signals for maintaining it are. Micro-injecting p53 antibodies into human fibroblasts that had been senescent for at

least 19 days resulted in reversion to a much more compact morphology accompanied by a marked reduction in B-Gal and 14-17% of the cells incorporating BrdU (Gire and Wynford-Thomas 1998).

In naturally senescent human fibroblasts, loss of the 3' overhang has also been proposed as the altered telomere state that activates the cell senescence pathway (Stewart et al. 2003). However a conflicting report shows that normal human fibroblasts can maintain their 3'overhang at senescence and do not lose their overhangs when they bypass senescence after the inactivation of p53 and Rb (Chai et al. 2005).

1.14 Cell cycle regulating proteins associated with senescence

The progression from G1 to S phase during the cell cycle is controlled to a large extent by the Retinoblastoma protein, Rb. Hypo-phosphorylated Rb binds to the E2F proteins and prevents Polymerase II and other elements of the transcription machinery gaining access to the site. When hyper-phosphorylated, Rb is no longer capable of binding E2F and transcription of the genes required for progression to S phase takes place (**Figure 8**). Two well characterised cell cycle inhibitors known to work independentlyof one another are $p16^{INK4A}$ and p21. $p16^{INK4A}$ can prevent cell cycle progression from G1 to S by inhibiting CyclinD-Cdk4/6 from phosphorylating Rb. Likewise, directly downstream from activated p53, p21 prevents CyclinE-Cdk2 from further phosphorylating Rb (**Figure 8**).

The contribution of $p16^{INK4A}$ in response to uncapped telomeres in human cells has been a subject of great debate. As both fibroblasts (Morris et al. 2002) and human keratinocytes (grown with or without feeders, see Section 1.19) (Morris et al. 2002) age in culture, their protein levels of $p16^{INK4A}$ increase, resulting in growth arrest independent of telomere length. This has substantially complicated attempts to determine the interactions of the uncapped telomere and $p16^{INK4A}$.

In Herbig *et al*'s studies, they identified TIFs by co-localising γ-H2AX and a peptide nucleic acid labelled probe against the telomere in a process called immunoFISH; in addition to identifying TIFs, they also stained for p21, as a downstream marker of p53 activation. TIFs were found predominantly in either

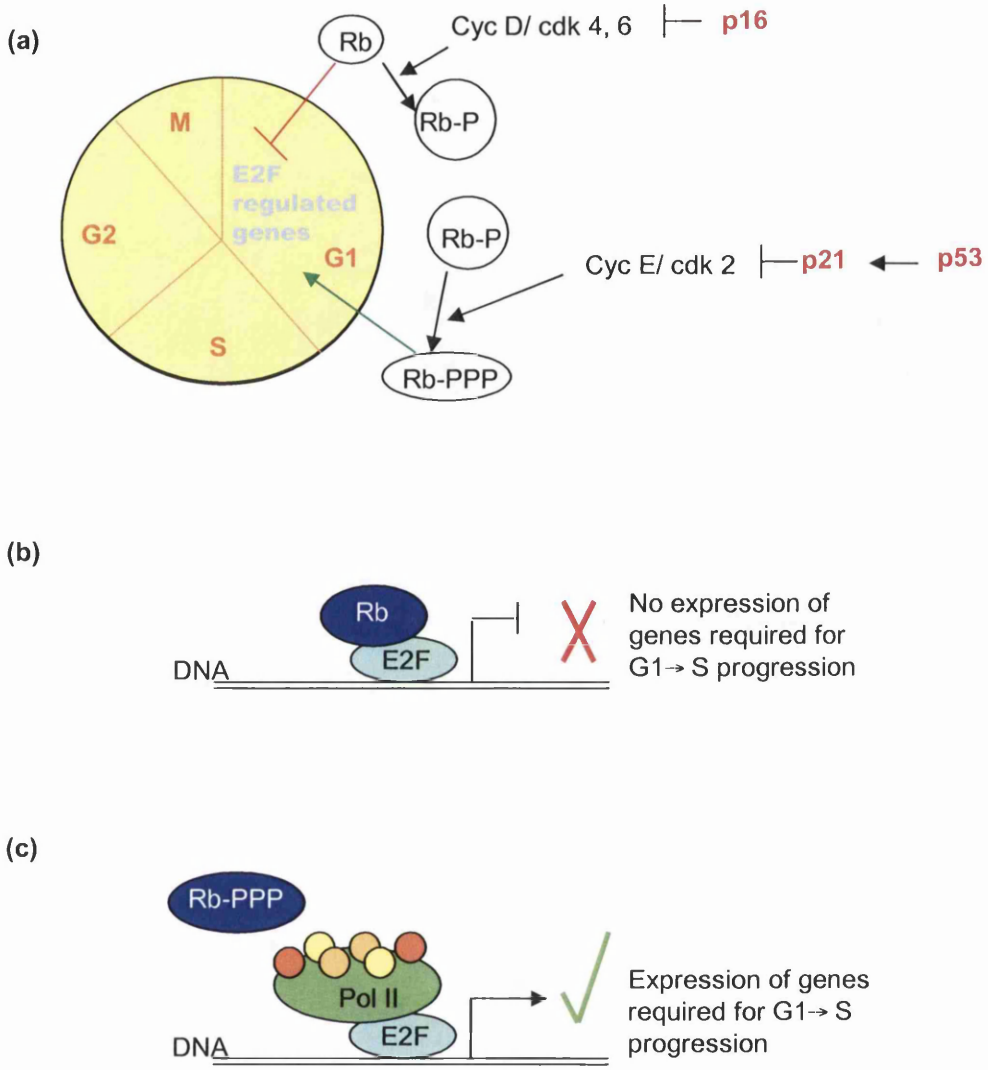

Figure 8. Cell cycle regulation by tumour suppressor proteins p16 and p21.

(a) Cell cycle progression from G1 to S phase is largely governed by the Retinoblastoma protein, Rb. It is phosphorylated by two separate Cyclin / Cyclin dependent kinase complexes: Cyc D/ cdk 4,6 and Cyc E/ cdk 2. The enzyme activity of both of these complexes can be inhibited by cyclin dependent kinase inhibitors, p16 and p21, respectively.

(b) When Rb is either not phosphorylated (Rb) or hypo-phosphorylated (Rb-P), it remains bound to the E2F transcription factor family proteins and prevents DNA transcription machinery from transcribing the G1 → S genes.

(c) When Rb is hyper-phosphorylated (Rb-PPP), it can no longer bind the E2F family proteins. E2F are then capable of recruiting the DNA transcription machinery (i.e. Pol II and associated proteins) and transcribing the genes required for progression from G1 to S phase.

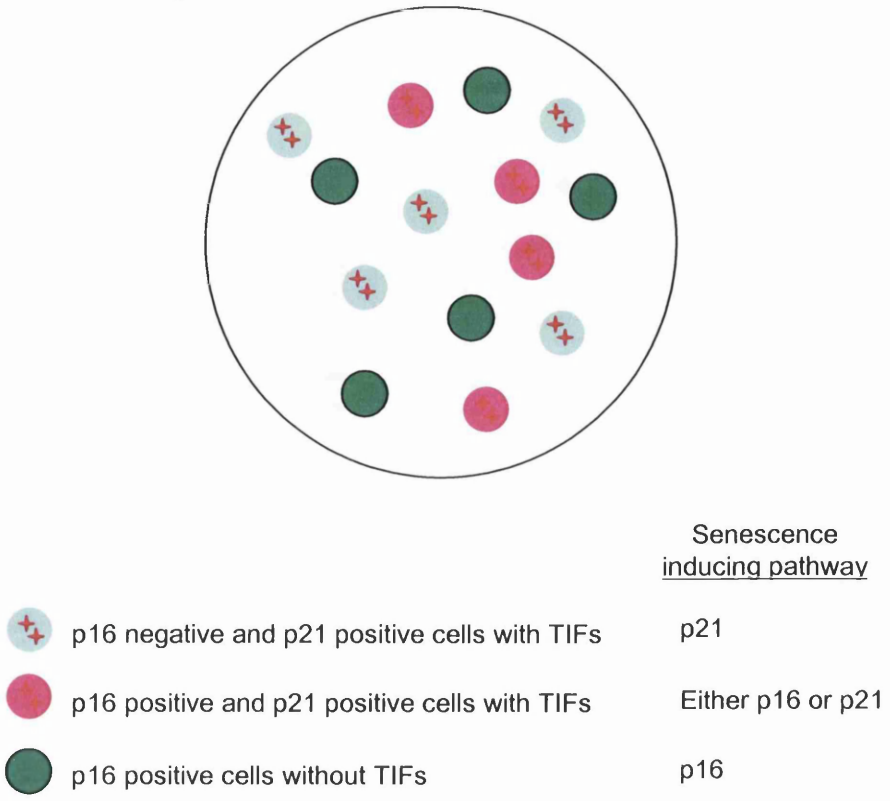

Figure 9. p16 and p21 response to critically short telomeres.
In both naturally senescent cells or cells artificially uncapped by TRF2$^{\Delta B \Delta M}$, TIFs are thought to form quickly after the telomere becomes uncapped, and then disappear. The above cartoon illustrates the results of Herbig et al (see text), who found that p21 positive cells with TIFs could either be p16 negative or positive.

p16 up-regulation is also thought to be a consequence of uncapped telomeres, but at a later time. It is possible that in p16 positive, TIF negative cells, the uncapped telomere had induced the senescence, but was no longer present in the senescent cell assayed for p16.

A further publication by Jacobs et al (see text) found that p16 was induced in most young fibroblasts as a result of expressing TRF2$^{\Delta B \Delta M}$. Cells deficient in p53 still exhibit a partial response to telomere uncapping and knocking down p16 ablates that partial response. Therefore, the p16 and p21 pathway responses to uncapped telomeres are capable of inducing senescence in conjunction and independently.

p21-positive or p21/ $p16^{INK4A}$ doubly positive cells, while $p16^{INK4A}$-positive (only) cells remained largely TIF free, illustrated in a cartoon (**Figure 9**). As the number of p21/ $p16^{INK4A}$ doubly positive cells with TIFs was roughly equal to the number of $p16^{INK4A}$ only cells without TIFs, they concluded that: (a) $p16^{INK4A}$ is regulated in a telomere independent manner; whereas p21 regulation is telomere dependent (b) both pathways could be up-regulated at the same time (Herbig et al. 2004). As further proof, it was shown that inhibition of ATM in senescent cells that contain TIFs results in cell cycle re-entry, indicating not only that stable arrest requires continuous signalling, but also that $p16^{INK4A}$ is not responding to the uncapped telomere(s) in these cells (Herbig et al. 2004).

The de Lange lab used the introduction of $TRF2^{\Delta B\Delta M}$ into fibroblasts to induce uncapped telomeres in 'young' human fibroblasts and found $p16^{INK4A}$ was induced in the majority of cells as detected by immunohistochemistry (Jacobs and de Lange 2004). They also established that fibroblasts deficient in p53 still demonstrated a partial response to telomere uncapping (Jacobs and de Lange 2004), and that inhibition of $p16^{INK4A}$ in the p53 deficient cells resulted in an almost complete bypass of telomere directed senescence (Jacobs and de Lange 2004). This led to the conclusion that, in addition to a p53 response, $p16^{INK4A}$ also plays a major role in telomere directed senescence. However, the induction of $p16^{INK4A}$ as a consequence of telomere dysfunction appears to be a very slow process, taking one to two weeks before $p16^{INK4A}$ is readily detectable (Jacobs and de Lange 2004). As Herbig *et al* used TIFs, an established early and transient mechanism of detecting telomere dysfunction it is not surprising that the $p16^{INK4A}$ staining they witnessed did not necessarily correlate with TIF detection (Jacobs and de Lange 2004).

ATR, an ATM-related DNA damage response protein more commonly associated with single DNA strand breaks, was also shown to play a minimal role in the response to the uncapped telomere. However, when the ATM response was removed, the ATR response became more prominent and the fibroblasts elicited a delayed G2 phase arrest (Herbig et al. 2004).

When neither the p53 nor Rb/$p16^{INK4A}$ proteins are functioning properly, human cells continue to proliferate, bypassing senescence. When an increased number of their telomeres become critically short, the cells will undergo crisis, large

scale apoptosis (Macera-Bloch et al. 2002), (Preto et al. 2004) (**Figure 9**). Only the very rare cell which has also managed to activate either telomerase or the ALT pathway is immortalised and capable of continued proliferation.

1.15 Telomere Elongation Mechanisms, ALT vs. Telomerase

As has already been established, proliferating cells experience telomere shortening and this ultimately leads to cell senescence or apoptosis. As mentioned in (**Figure 7**), rare cells down-regulate both p53 and $p16^{INK4A}$ in addition to up-regulating a telomere lengthening mechanism to achieve immortality. Two mechanisms have been characterised and account for nearly all the ways in which telomeres are extended: Telomerase activation and ALT.

1.15.i Telomerase activation

Telomerase is a large multimeric ribonucleotide protein whose core components are (1) hTR, an RNA template that associates with (2) hTERT, the reverse transcriptase that adds nucleotides to the end of the telomere (Nakamura et al. 1997). Telomerase is up-regulated in >85% of all human cancers (Kim et al. 1994), (Shay and Bacchetti 1997).

Short telomeres are preferentially elongated by telomerase and a low cellular concentration of telomerase is critical to achieve preferential elongation of short telomeres and telomere length homeostasis (Cristofari and Lingner 2006). Long telomeres do not permanently adopt a structural state that is non-extendable: when telomerase levels are increased in fibroblasts expressing hTERT, the level of telomere-bound TRF1 and TRF2 increase proportionally (Cristofari and Lingner 2006). In addition to binding the telomere, Ku70/80 associate physically with hTERT (Chai et al. 2002), suggesting this interaction might be part of the way telomerase gains access to the telomere.

Until 2003, telomerase was only considered to be active in germ cells, stem cells and cancer cells. However, that changed when evidence was published that hTERT is expressed during S phase of cycling primary pre-senescent human fibroblasts (Masutomi et al. 2003). The authors also established that disruption of telomerase activity in normal human cells slows cell proliferation, restricts cell lifespan and alters the maintenance of the 3' single stranded telomeric

overhang without changing the rate of overall telomere shortening (Masutomi et al. 2003).

Whether these effects are generated by telomerase per se or the telomere being elongated by telomerase is difficult to distinguish. Ectopic expression of hTERT leads to transcriptional alterations of a subset of genes and changes in the interaction of telomeres with the nuclear matrix, after telomerase has interacted with telomeres (Sharma et al. 2003). In addition to acting at the telomere, hTERT expression improves DNA damage repair at non-telomeric sites. Higher mRNA levels of some DNA repair genes were seen in cells expressing hTERT; thus a possible explanation for the increased DNA repair capacity is the increased level of nucleotides found in the ectopic hTERT expressing cells (Sharma et al. 2003). Suppression of hTERT using RNAi in human fibroblasts does not alter telomere integrity in the short term, but instead affects the overall configuration of chromatin. Cells lacking hTERT exhibit increased radio sensitivity, diminished capacity for DNA repair and fragmented chromosomes, demonstrating that loss of hTERT impairs the DNA damage response (Masutomi et al. 2005).

Finally, the telomere must be accessible to elongation by telomerase for active telomerase to have an effect. Both TRF1 and 2 have been shown to regulate such access (See Table 1). Drugs such as BRACO19 are capable of inducing the formation of G quadruplexes throughout the DNA, but particularly in the telomere, preventing active telomerase from interacting with and therefore elongating the telomere (Neidle and Parkinson 2002).

1.15.ii Alternative Lengthening of Telomeres, ALT

The presence of ALT is deduced from the combination of no detectable telomerase activity and telomeres that have a characteristic heterogeneity of length, ranging from short to abnormally long (Bryan et al. 1995). ALT accounts for ~10% of telomere maintenance in tumours and is commonly used by astrocytic brain tumours and osteosarcomas (reviewed by (Muntoni and Reddel 2005)). It has been suggested that, in human tumours where abundant amounts of extra-chromosomal telomeric repeats are found in linear and circular form, ALT is a deregulated version of an aspect of normal mammalian telomere homeostasis (Muntoni and Reddel 2005).

1.16 Dyskeratosis Congenita

Dyskeratosis Congenitia, DC, is the result of defective telomerase activity (reviewed in (Marrone et al. 2005)). Patients develop critically short telomeres characterised phenotypically by abnormal skin pigmentation, leukoplakia, nail dystrophy, an increased disposition to cancer and bone marrow failure.

Two types of mutation lead to DC:

In patients with an X-linked recessive version of the disease, mutations generate a defective form of dyskeratin, a protein known in other species to have a significant role in ribosomal RNA folding (Heiss et al. 1998), therefore effecting the ability of the RNA component of telomerase, hTR, to function properly.

An autosomal dominant (AD) mutation in the gene-encoding human telomerase RNA (TERC), results in telomere shortening. In one family carrying such a mutation, T cells were found to over-express senescence markers, including CD57 and Fas receptor and were moderately reduced in cell number. AD DC lymphocytes display a markedly reduced proliferative capacity, and an increased basal apoptotic rate (Knudson et al. 2005).

AD-DC has recently been associated with progressive telomere shortening. The disease becomes more severe in succeeding generations with a median age of diagnosis of 37 years in the parental generation and 14.5 years in the second generation (Vulliamy et al. 2004). Patients with more severe phenotype had shorter telomere lengths (Vulliamy et al. 2004).

1.17 Different cells respond differently to the same stimuli

Although model organisms are invaluable in providing information about the consequences of genetic manipulation in systems that can be both quicker and easier to manipulate, they do not always provide the most relevant information when treatment for a particular disease is being considered. For example, in contrast to human cells, loss of p53 alone is enough to abrogate the arrest of mouse cells indicating that the $p16^{INK4A}$ /RB response to telomere dysfunction is not active in mouse cells (Smogorzewska and de Lange 2002).

Even cells from different tissues of the same organism can respond differently to the same stimulus. For example, keratinocytes and fibroblasts were shown to respond differently to early Epstein Barr viral proteins; a G(1)/S block in cell cycle was seen in fibroblasts, but not in keratinocytes (Mauser et al. 2002).

Furthermore, expression of oncogenic Ras in human fibroblasts results in a permanent G1 arrest associated with accumulation of p53 and $p16^{INK4A}$ (Serrano et al. 1997). In contrast, Ras induces a proliferative phenotype in normal human thyroid epithelial cells (Gire and Wynford-Thomas 2000).

A final example of the different signalling pathways activated by different cell types is Smurf2, an E3 ubiquitin ligase thought to be up-regulated as a specific consequence of telomere attrition, in human fibroblasts. However, expression of $TRF2^{\Delta B \Delta M}$ in early pass fibroblasts did not result in an up-regulation of Smurf2, indicating that Smurf2 up-regulation is a specific consequence of short telomeres, not a dysfunctional telomere (Zhang et al. 2003). Expression of Smurf2 in early pass fibroblasts resulted in premature senescence (Zhang et al. 2003). However, Smurf2 levels have been shown to remain constant in populations of human mammary epithelial cells, HMECs, during their progression to replicative senescence (Zhang et al. 2003). A microarray study examining HMEC at senescence grown with either (1) a feeder layer, (2) on plastic alone in defined culture conditions or (3) senescent fibroblasts, showed surprisingly few expressed genes in common, even between the HMEC grown using 2 standard tissue culture methods (Zhang et al. 2004). These results indicate that replicative senescence is heterogeneous, rather then a unique process and also forewarns that use of the $TRF2^{\Delta B \Delta M}$ to mimic the uncapped telomere may not necessarily result in activating the same pathways that a senescent cell with reduced telomeres might.

1.18 The Epidermis

The largest organ in the human body, skin, consists of two layers: the dermis and the epidermis (**Figure 10**). The outer epidermis layer is composed of keratinized stratified squamous epithelium and contains 4 principal cell types:

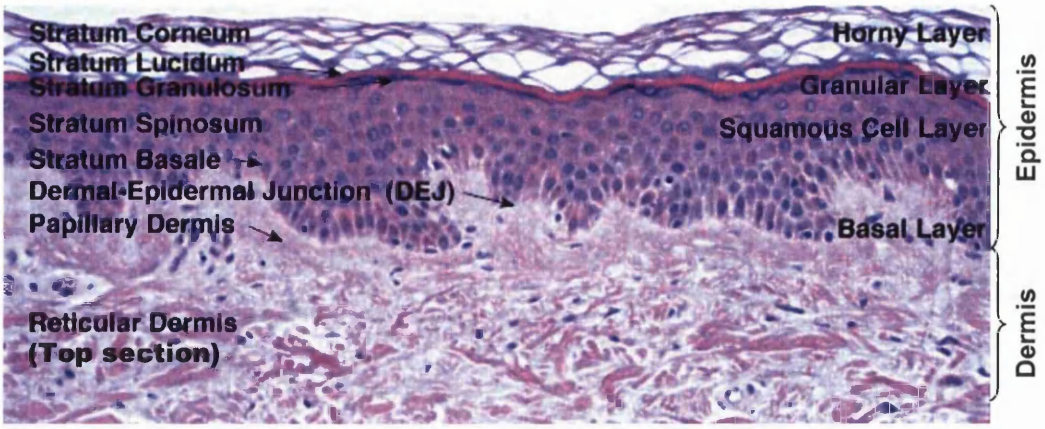

Figure 10. Haematoxylin and Eosin stained section of normal skin.

The above picture was taken from the Dept. of Dermatology - University of Iowa College of Medicine (M. S. Stone and T. L. Ray) http://tray.dermatology.uiowa.edu/DPT/Hist/Nrml-001.htm

The below text is taken from Principles of Human Anatomy, Eighth edition, Tortora, pg.90- 97.

Stratum corneum - the outer most level of the epidermis, contains in excess of 20 rows of dead, flattened keratinocytes which further add to the protective function of skin.

The **stratum granulosum** and **stratum lucidum** both contain flattened keratinocytes which produce granular proteins and lipids that serve in the epidermis' protective function.

Stratum spinosum – Layers of keratinocytes that fit closely together with long projections of melanocytes extending between them. In tissue culture, these would be referred to as the transit amplifying cells.

Stratum basale – a single row of cuboidal or columnar shaped keratinocytes (referred to in Chapters 3, 4 and 5 as basal cells), capable of continuous cell division. Melanocytes, merkel cells and langerhan cells are scattered among the keratinocytes of the basal layer.

Dermal-Epidermal Junction - Desmosomes bind basal cells to each other and to the adjacent epidermal layer. Desmosomes also bind to hemi-desmosomes, which bind the keratinocyte to the basement membrane which separates the epidermis from the dermis.

Papillary dermis – composing one fifth of the dermis and consisting of areolar connective tissue containing fine elastic fibres produced by fibroblasts within the region. Surface area of the dermis is increased by dermal papillae which project into the epidermis and contain many loops of capillaries and Meissner's corpuscles, tactile receptors sensitive to touch. The dermal papillae cause the ridges in the overlaying epidermis that cause fingerprints.

Reticular dermis – a dense, irregular connective tissue that contains interlacing bundles of collagen and elastic fibres interspersed by adipose tissue, hair follicles, nerves, oil glands and sweet gland ducts. Varying thickness of this region contribute to the different levels of thickness seen in skin.

Keratinocytes - these cells produce the protein keratin which helps to protect the skin and underlying tissues from light, heat, microbes and many chemicals and make up about 90% of the epidermis.

Melanocytes - produce the pigment melanin (brown-black pigment that contributes to skin colour and absorbs UV light) and constitute about 8% of the epidermal cells. Long slender projections extend between keratinocytes, transferring melanin granules to them.

Langerhan cells - arising from red bone marrow, these cells interact with helper T cells and are easily damaged by UV radiation.

Merkel cells - located in the stratum basal, these cells attach to keratinocytes (see below) by anchoring junctions and make contact with the flattened portion of the ending of a sensory neuron.

Keratinization is the accumulation of increasing amounts of keratin and loss of cytoplasm, nucleus and other organelles as the cells migrate and differentiate from the stratum basale to the stratum corneum. Undifferentiated keratinocytes contain numerous microtubules, which radiate out from a centrosomal organisation centre. Differentiating keratinocytes, which leave the basal layer begin to synthesise involucrin and display an altered cytoskeleton (Lewis et al. 1987).

1.19 Keratinocyte Growth in Tissue Culture

Keratinocytes isolated from human epidermis can be successfully grown in serial culture for 20-50 cell generations when grown with proliferation arrested fibroblasts, which are referred to as feeders (Rheinwald and Green 1975). Cells less then 11 μm in diameter form rapid growing colonies in culture whereas those larger then 12 μm are irreversibly committed to further enlargement and terminal differentiation (Barrandon and Green 1985).

Keratinocytes are heterogeneous in their proliferative potential. Three classifications have been established (Barrandon and Green 1987b):

(1) Holoclone - the greatest reproductive capacity, fewer then 5% of the colonies formed from the cells of a holoclone abort and terminally differentiate.

(2) Paraclone - cells with a short replicative lifespan (not more than 15 cell generations), after which they uniformly abort and terminally differentiate.

(3) Meroclone - a mixture of cells of different growth potential and is a transitional stage between the holoclone and the paraclone.

The incidence of the different clonal types is affected by aging, since cells originating from the epidermis of older donors give rise to a lower proportion of holoclones and a higher proportion of paraclones (Barrandon and Green 1987b).

Each keratinocyte colony ultimately forms a stratified squamous epithelium in which the dividing cells are restricted to the lower layer (Rheinwald and Green 1975). Hydrocortisone is added to the medium to make keratinocyte colony morphology more orderly and distinctive, particularly in secondary and subsequent cultures. This not only helps during subsequent feeder removal, but hydrocortisone also maintains proliferation at a slightly higher rate (Rheinwald and Green 1975). Increases in the cAMP levels (which can be achieved through the use of cholera toxin, dibutyryl cAMP, methyl isobutyryl cAMP or isoproterenol) increase the rate of proliferation of epidermal cells, including keratinocytes (Green 1978). The presence of cholera toxin increases the proportion of small cells which have a higher proliferation potential (Green 1978). The culture lifetime of epidermal cells of newborn humans is increased from 50 to 150 Population doublings by addition of Epidermal Growth Factor, EGF, to the medium (Rheinwald and Green 1977). Whereas cholera toxin increases the number of cells in growing colonies, EGF enlarges small colonies by flattening the cells (Green 1978). Intracellular adhesion of keratinocytes is mediated by desmosomes and non-disjunction cadherins which are dependent on calcium for their functions. Standard tissue culture concentrations of calcium range from 1.2 - 1.8 mM, and at these concentrations keratinocytes are capable of stratification. In limited concentrations of calcium, such as 0.05-0.10 mM; keratinocytes proliferate, but are unable to stratify and hence grow as a monolayer (Hennings et al. 1980).

Cell migration is essential for sustained growth of keratinocyte colonies, as they grow larger they increase in radius at a constant rate over time. The rate is increased 8-fold in the presence of epidermal growth factor (Barrandon and Green 1987a). Keratinocytes are able to migrate during wound healing and early neoplastic invasion (Natarajan et al. 2006). Plating keratinocytes on the γ-2 precursor form of laminin 5 immediately induces directional hypermotility followed by $p16^{INK4A}$ expression and growth arrest (Natarajan et al. 2006). Cells deficient in $p16^{INK4A}$ and either p14 or p53 become hypermotile, but do not growth arrest (Natarajan et al. 2006).

As human keratinocyte age in culture, protein levels of $p16^{INK4A}$ increase, resulting in growth arrest independent of telomere length, known as telomere independent senescence (Darbro et al. 2005). $p16^{INK4A}$ induction can be delayed and keratinocytes grown for longer in culture when grown with a post-mitotic fibroblast feeder cells (Darbro et al. 2005). Not only do feeder cells provide better growth conditions for normal human keratinocytes, they have also been established as a necessity in the culture of some Squamous Cell Carcinomas (Rheinwald and Beckett 1981). Two independent normal human keratinocyte cell strains expressing exogenous telomerase and co-cultured with feeder cells resulted in efficient extension of lifespan without an apperent crisis (Darbro et al. 2006). When the cells were transferred to plastic alone, they experienced a period of slow growth. Those that experienced $p16^{INK4A}$ promoter methylation achieved immortality and re-introduction of $p16^{INK4A}$ into those immortal cell lines resulted in rapid cell growth arrest (Darbro et al. 2006).

1.20 Keratinocyte DNA damage response

Epidermal keratinocytes specifically express genes that protect from UV light (Gazel et al. 2003). The response of the keratinocytes to UV irradiation has been better investigated than the response to γ-irradiation, which is not surprising as investigations into UV rays from the sun are a larger natural threat than γ-irradiation. UV irradiation is more likely to cause single strand DNA breaks which operate through different DNA damage response pathways, compared to double strand breaks that are induced by γ-irradiation or telomere

uncapping. This needs to be considered when making comparisons between the effects of DNA damage on keratinocytes.

UV-light induces DNA damage in keratinocytes in organotypic cultures of normal human skin. Activation of p53 triggered apoptosis, firstly in the basal layer within 2 hours and in the suprabasal layers after around 8 hours (Qin et al. 2002). The same publication also demonstrated that cultured keratinocytes undergoing spontaneous senescence constitutively contained low levels of p53 which were neither increased nor phosphorylated or acetylated after UV exposure.

In keratinocytes, UVB inhibits differentiation; but in HPV-16, E6/7-immortalized keratinocytes, UVB induces apoptosis (Simbulan-Rosenthal et al. 2005). Investigation into the differential effect found that Id2 expression was up-regulated in keratinocytes, but not in immortalized keratinocytes. It is possible that the up-regulation of Id2 by UVB might predispose keratinocytes to carcinogenesis by preventing their normal differentiation program (Simbulan-Rosenthal et al. 2005).

When wild type p53 is reintroduced into a Squamous Cell Carcinoma, SCC15, a transient G1/S arrest is seen. When these cells are irradiated, a G2/M arrest is seen (Niemantsverdriet et al. 2005). This study demonstrates that p53 is capable of causing two different types of arrest in the same cells in response to different types of stimuli.

1.21 PhD background

Cancer is a disease of uncontrolled cell proliferation, most commonly derived from human epithelial tissues. A Cancer Research UK 2002 study showed three epithelial tissues are the most prevalent sites of a primary tumour: breast, lung and colon. Interestingly, the ratio of mesenchymal to epithelial patients is 1:10 in the normal ageing population, compared to 1:1 in Werner's syndrome patients (Goto et al. 1996), further implicating the different cell proliferation control processes that become de-regulated in different cell types resulting in cancerous cells. Historically, genetically unaltered human epithelial cells have been harder to maintain in culture and perform experiments with, so with good justification laboratories have traditionally used fibroblasts. However, as

indicated above (Section 1.17) in any 2 given cell types, even from the same organism, cellular responses are still not necessarily the same, e.g. SMURF2 in fibroblasts vs. HMEC; or $TRF2^{\Delta B \Delta M}$ in fibroblasts vs. lymphocytes. Even the same cell type grown different ways, e.g. HMECs grown in serum-free medium without feeders or with feeders in medium with serum, can alter the transcriptome of the cells (Zhang et al. 2004).

Strategies to specifically inhibit cancer cell growth by targeting telomerase activity work on the premise that after a small period of proliferation (dependent upon telomere length of the tumour cells) telomeres will become critically short and thereby cause either cellular senescence or apoptosis. Senescent tumour cells are not necessarily a satisfactory cancer treatment outcome. Senescent cells are still viable and as such may continue to deregulate the organ they are invading. In addition to that, in unfavourable circumstance, senescence can be reversed through genetic alteration (Herbig et al. 2004). It is therefore a risky strategy, given the genetically unstable environment in which the tumour cells exist, to leave senescent tumour cells susceptible to mutation within the body. However, having stated that, although apoptosis of cancer cells is preferable to senescence, senescent tumour cells would still preferable to the uncontrolled cell growth which will result in patient death.

With a new found understanding of the importance not only in the length of the telomere, but also in the ability of the telomere binding proteins to regulate the telomeres structure; levels of telomere binding proteins are now being scrutinised in human cancers for evidence of mis-regulation. One study of POT1 mRNA levels in 51 gastric cancers found significantly higher levels of POT1 in later stage cancers (stage III/ IV) compared with tumours at an earlier stage (stage I/II) (Kondo et al. 2004). This result correlates with the telomere stabilisation seen during cancer development. Other studies have found TRF2 up-regulation in immortally transformed human mammary epithelial cells (HMECs), as well as in 11/15 breast tumour cell lines (Nijjar et al. 2005). The up-regulation of TRF2 is most likely due to differences in post-translational regulation, as mRNA levels were comparable in finite lifespan and immortal HMECs (Nijjar et al. 2005). An increase in levels of TRF2 has also been reported in some human skin basal or squamous cell carcinomas (Munoz et al. 2005).

1.22 Aim and Objectives

The effect of critically short telomeres has not been previously investigated in a normal human epithelial cell system. As such, we have chosen to examine the effect of uncapping the telomere in Normal Human Epidermal Keratinocytes, NHEK. As referred to earlier in this chapter, natural elevation of $p16^{INK4A}$ and p53 provide a barrier to long term culture of epithelial cells referred to as M0/M1. Although this can be overcome by knockdown using RNAi, we wanted to be able to assess the contribution of $p16^{INK4A}$ and p53 to the effect of an uncapped telomere. It is known that long term propagation of primary cells results in some genetic heterogeneity which can influence the cellular outcome. This was another drawback we hoped to avoid, by using NHEK.

The overall aim of this PhD has been to characterise the response of NHEK to uncapped telomeres using $TRF2^{\Delta B \Delta M}$. The specific objectives were as follows:

- Optimise a system to retrovirally infect NHEK allowing for selection of cells at early time points.

- Observe and characterise the effect of uncapped telomeres on colony morphology and proliferation.

- Determine if the DNA damage pathway is activated as a result of uncapping the telomere in NHEK as in fibroblasts.

Manufacturers' and Suppliers' details are listed in Appendix I.

2.1 Cells and Medium

Table 3: Cells and Medium

Cells	Catalogue Number	Supplier	Medium and *Culture Notes*
NHEK (Normal Human Epidermal Keratinocytes) are derived from a pool of a minimum of 3 neonatal foreskins and are prepared by digestion overnight at 4°C with dispase. The epidermis is then peeled from the dermis and the keratinocytes released from the epidermis by digestion with Trypsin-EDTA.	12332-011	Invitrogen	**FAD medium.** (Flavin Adenine Dinucleotide) medium supplemented with 10% (v/v) FBS, 2 mM L-Glutamine, 0.4 µg/mL hydrocortisone, 5 µg/mL insulin, 5 µg/mL transferrin, 10^{-10} M cholera toxin, 1.8 x 10^{-4} M adenine, and 10 ng/mL epidermal growth factor (added at the first medium change). **20% FAD** contained 20% (v/v) FBS and was used during infections.
3T3 Swiss Albino mouse fibroblasts 'Feeders'	CCL92	ATCC (Distributed by LGC)	**10C medium** supplemented with 10% (v/v) FBS, 2mM L-Glutamine and 20 mM Hepes.
Phoenix E (E, Ecotropic Receptor)	Beatson Institute Cell Stocks	Cells originate from: Dr G P Nolan	**10% medium** (v/v) FBS and 2mM L-Glutamine. Or during infections, **20% medium** (v/v) FBS and 2mM L-Glutamine.
Phoenix A (A, Amphotropic Receptor)	Beatson Institute Cell Stocks	Cells originate from: Dr G P Nolan	**10% medium** (v/v) FBS and 2mM L-Glutamine. Or during infections, **20% medium** (v/v) FBS and 2mM L-Glutamine.
PT67s (NIH-3T3 based retroviral packaging cell line with both Ecotropic and Amphotropic Receptors)	Beatson Institute Cell Stocks	Cells originate from: Becton Dickinson	**10% medium** (v/v) FBS and 2mM L-Glutamine. Or during infections, **20% medium** (v/v) FBS and 2mM L-Glutamine.

2.2 Routine Tissue Culture

In this thesis, NHEK are grown with lethally irradiated Swiss 3T3 feeders, referred to as feeders from here on in. (Later in the thesis, PT67s are also used as feeders during the NHEK infection process, but to clarify, they will be referred to as 'infectious PT67s.) All tissue culture was performed using aseptic technique inside a laminar flow hood. Retroviral infection of NHEK was performed in a category II containment suite, with safety precautions approved by the HSE and Beatson Institute Safety Committee. All cells were incubated at 37°C in a wet atmosphere containing 5% (v/v) CO_2, except when incubated at 32°C instead, in which case it is clearly denoted. Tissue culture plastics were supplied Falcon culture dishes (Becton Dickinson).

2.2.i Feeder Preparation

Between 2 to 20 flasks (T-75) of feeders were cultured every other week. The feeders were harvested and concentrated to a cell density between 1 - 4 $x10^6$/mL in a universal. Feeders were then kept either at 4°C or on ice until receiving 60Gy γ-IR, a lethal irradiation dose, the purpose of which was to prevent further replication during co-culture with NHEK. Although growth arrested, the cells are still capable of adhering to the tissue culture plate and produce extra cellular proteins which aid the growth and development of the NHEK. The feeder cell preparations were stored at 4°C and used for up to one week (at which point they were discarded and a fresh stock prepared). Every 3-4 months new vial of feeders were thawed from liquid nitrogen to replace the current stock.

2.2.ii Initial plating and continued culture of NHEK

Prior to an experiment, NHEK were resurrected from liquid nitrogen by being transferred from (liquid nitrogen) immediately into a 37°C water bath. The cells were then transferred to 9 mL of medium and centrifuged for 5 min at 4°C at 1000 RPM (to form a cell pellet). Re-suspended in fresh medium without the cryo-preservation agent DMSO, the NHEK were plated at an appropriate density with feeders in FAD medium, see Table 4. The following day, the medium was changed to include EGF, denoted FAD^+.

2.2.iii Feeder removal and trypsinisation

Feeders were removed prior to trypsinisation by directing a stream of PBS:0.02% EDTA, PE, (Provided by Central Services at the Beatson) against the plate with an element of force. Defining a certain point on the plate as 12 o'clock, the PE would firstly be directed around the edges of the plate, before concentrating on each quarter, e.g. 12 to 3 o'clock. The PE was then removed, and fresh PE applied before the plate was quickly scanned at low power at the light microscope for any remaining feeders. The cells were then washed with PBS and subjected to trypsinisation for 30 min at 37°C. (30 min is extremely long compared to normal tissue culture practices, however this length of time was required for the trypsin to get into the colonies to create the desired single cell suspension.) Worthington's Trypsin (Cat no. LS3703, distributed by Lorne Laboratories) was prepared in bulk, frozen into concentrated aliquots and used at a final concentration of 1 mg/mL, prepared in either PBS alone for feeders, or 0.01% PE for NHEK. After 30 min the trypsin was inhibited by the addition of FAD medium and the cells centrifuged for 5 min at 4°C, 1000 RPM. NHEK were then re-suspended and re-plated with an appropriate amount of feeders as listed in Table 4.

Table 4: **Plating densities of NHEK and Feeders**

Tissue Culture Dish/ Coverslip Diameter	Cell density of NHEK	Cell density of feeders
9 cm plate	$1 - 10 \times 10^5$	1×10^6
14 cm plate	$1 - 25 \times 10^5$	2.5×10^6
(3T3 conditioned) 15 mm coverslip	$0.5 - 1.0 \times 10^5$	1×10^4, for removal 2-3 days prior to NHEK plating

When required, population doublings, PD, were determined according to the equation: $PD = 3.32 [\log_{10} (\text{Cell Yield}) - \log_{10} (\text{Cell Input})]$.

2.2.iv 3T3 conditioning coverslips for NHEK

Swiss 3T3 fibrblasts were grown to confluence on Thermanox 15 mm plastic round coverslips (Cat no. L4353, Agar Scientific) in a 12 well dish. The Swiss 3T3 cells were then removed after 5 min of incubation with PE by pipetting the PE up and down with force. The PE washes were repeated and then the coverslips incubated in 5 mL of water for 30 min to lyse any Swiss 3T3 that may remain. The coverslips were then rinsed with PBS and the NHEK added (without feeders).

2.2.v Culturing retroviral packaging cell lines

Phoenix E and A were cultured in a standard 10% medium. As both cell lines adhered poorly to plates and single cell suspensions were not a necessity, neither were trypsinised. Instead, exhausted medium was removed and the cells were then sprayed off using fresh medium. Once suspended, the cells were pipetted up and down vigorously to break up as many cell clumps as possible before being re-plated. Cell splits of 1 in 10 were performed every 3-4 days to keep cells sub-confluent.

PT67s were also cultured in a standard 10% medium. However, these cells did require trypsinisation for re-plating. 1mg/mL trypsin (prepared in PBS) was used and inactivated by the addition of 10% medium. Cells were not centrifuged to remove trypsin prior to re-plating.

2.3 Telomerase Repeat Amplification Protocol, TRAP

Cell extracts were prepared by lysing NHEK in CHAPs buffer (supplied with TRAPeze kit, see below) at 200μL per 1 $x10^6$ cells for 30 min on ice. Lysates were separated from cell debris by centrifugation at 10,000 RPM for 20 min at 4°C. Bicinchoninic Acid, BCA, Protein Assay was used to determine the protein concentration of the lysates. A standard protein curve was prepared using 2 mg/mL Bovine Serum Albumin, BSA (Cat no. 23209, Pierce), and 10 μL samples of lysate were incubated with 200 μL of a BCA mix [BCA mix: 10mL Bicinchoninic Acid, (Cat no.B9643) + 200 μL $CuSO_4$ (Cat no.C2284), both supplied by Sigma] for 45 min at 37°C before being scanned for absorbance at 495nm in a plate reader.

Telomerase activity was determined using the TRAPeze Telomerase detection kit (Cat no. H08355, Flowgen Instruments), as per the manufacturer's recommendations. The PCR products were separated on a 12.5% polyacrylamide gel and visualised under UV light after 15 min incubation in 100 mL of 10mg/mL ethidium bromide, followed by 2x15 min washes with tap water.

2.4 Telomere Restriction Fragment, TRF, Assay

Cell pellets (1 $x10^6$) were lysed and digested overnight by 100 μg/mL Proteinase K (Cat no. BNO16333, Melford Labs) at 37°C in TESN buffer (0.1M TRIS pH8.8,

5mM EDTA pH7.5, 0.2% SDS and 0.2M NaCl) overnight with agitation at 37°C. An equal volume of ice cold isopropanol was added to the proteinase K cell solution and then the DNA spooled out as a white gelatinous precipitate using a flamed, sealed glass pipette. DNA was then dipped into 70% alcohol and allowed to air dry, before being dissolved in TE buffer pH 7.5 (0.1M TRIS, 1mM EDTA). 8 μg of genomic DNA was digested overnight at 37°C with restriction enzymes HinF1 and Rsa1, (Cat no. 1097067 and 1047671, respectively, Roche) in a One-Phor-all Buffer (Cat no. 27-0901-02, Amersham). The TRFs were then separated on a 1% agarose gel using pulse field electrophoresis (CHEF-DR II System; Bio-Rad) at 6 V/cm with an initial switch time of 1 s and a final switch time of 6 s for 16 h. The gel was transferred to Zeta-Probe GT membrane (Cat no. 162-0197, Bio-Rad) by capillary action in 0.4 N NaOH for 16 h. The membrane was rinsed in distilled water, and the DNA cross-linked to the membrane using a UV cross-linker (Stratagene) before being detected using the TeloTAGG kit (Cat no.2209136, Roche), as per the manufacturer's recommendations.

2.5 Sub-Cloning Vectors

Kindly donated by Titia de Lange (Rockfeller University, NYC, USA), pLPC-NMYCTRF2 (#2428) and pLPC-NMYCTRF2$^{\Delta B\Delta M}$ (#2431) were sub-cloned into the (IRES vector) pMIG (Van Parijs Lab, MIT Boston, Ma, USA), derived from pMSCVneo (**Figure 11**). pMIG was opened with restriction enzyme Bgl II (Cat no. 567639, Roche) and then blunt ended using DNA polymerase (Cat no. D0602H, Epicentre) prior to being cut with Xho I (Cat no. 899 194, Roche). Both TRF2 Vectors were opened with restriction enzyme Hind III (Cat no. 15207-020, Invitrogen) and then blunt ended using DNA polymerase (Cat no. D0602H, Epicentre) prior to be cut with Xho I (Cat no. 899 194, Roche). TRF2 coding DNA was then separated from its Vector backbone by running it out on an agarose gel, TRF2 and TRF2$^{\Delta B\Delta M}$ bands sized ~1500 bp were excised. Both TRF2 vectors were then phosphatased (Cat no. M820A, Promega).

pMIG and TRF2/TRF2$^{\Delta B\Delta M}$, were incubated overnight in ice water with agitation and ligated using the Rapid DNA ligation Kit (Cat no. 1 635 379, Roche). The newly cloned vectors were transformed into Max Efficiency Stbl2 Competent E.Coli Cells (Cat no. 10268-019, Invitrogen), spread onto ampicillian resistant plates and left at 30°C for 48 hours (no colonies had appeared after 24 hours, so

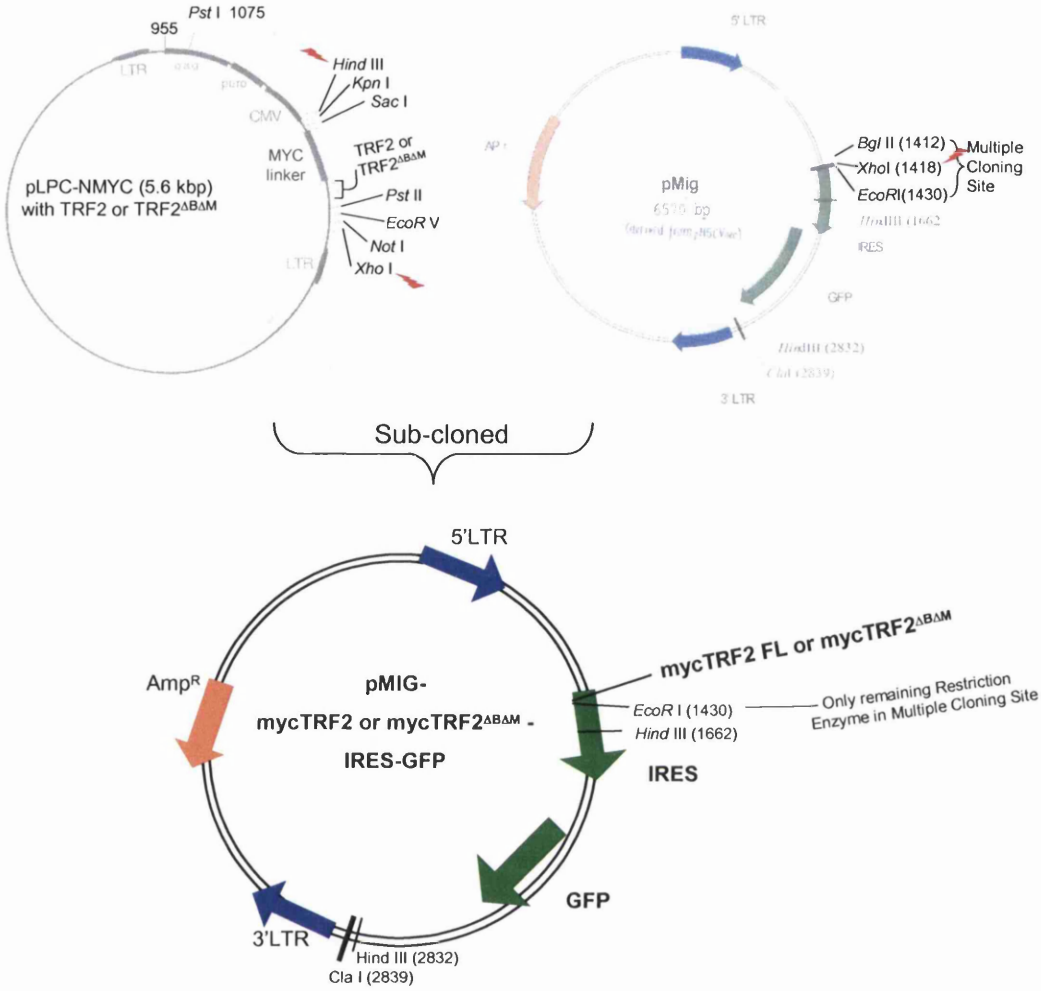

Figure 11 . Sub-cloning TRF2 and TRF2$^{\Delta B\Delta M}$ into pMIG.

The de Lange lab cloned TRF2 (amino acids 2-50) and TRF2$^{\Delta B\Delta M}$ (amino acids 45-453) into a pLPC-NMYC (5.6 kbp) Vector, such that it was preceded by a Kozak sequence and in frame with a N terminal Myc- tag. During the sub-cloning for this thesis, the pLPC-NMYCTRF2 and pLPC-NMYCTRF2$^{\Delta B\Delta M}$ were digested with Hind III (Kozak site retained), blunt ended with DNA polymerase and then cut with Xho I. pMIG was digested with Bgl II, blunt ended using DNA polymerase and then cut with Xho I. The pMIG vector backbone was then ligated to the myc-TRF2 and myc-TRF2$^{\Delta B\Delta M}$ inserts.

The sub-cloned:

pMIG-mycTRF2 -IRES-GFP is referred to as: myc-TRF2 FL

and

pMIG-mycTRF2$^{\Delta B\Delta M}$-IRES-GFP is referred to as :myc-TRF2$^{\Delta B\Delta M}$

for the duration of this thesis.

the plates were left a further 24 hours). Colonies were selected and cultures expanded. Glycerol stocks were prepared using 0.5 mL of newly created pMIG-TRF2-IRES-GFP Vectors and 0.5 mL of 80% glycerol and stored at -70°C in cryo-preserve tubes. The DNA was purified from the Stbl2 cells using Qiafilter Plasmid Midi Kit (Cat no.12162 , Qiagen).

The de Lange lab Vectors were not used again during this thesis. The sub-cloned pMIG-mycTRF2 FL-IRES-GFP and pMIG-myc-TRF2$^{\Delta B\Delta M}$-IRES-GFP are referred to as myc-TRF2 FL and myc-TRF2$^{\Delta B\Delta M}$ for the duration of this thesis.

2.6 Optimised Protocol of Retroviral Infection (with Variables) for NHEK Using a 3T3 Based Feeders System

High infection rates of keratinocytes are notoriously difficult to obtain. Following the work of Fiona Watt (Levy et al. 1998), a 2 step infection protocol was devised to obtain a high proportion of NHEK expressing either Vector only, myc-TRF2 FL or myc-TRF2$^{\Delta B\Delta M}$.

2.6.i Transfections

Phoenix E retroviral packaging cells were transfected with Vector only, myc-TRF2 FL or myc-TRF2$^{\Delta B\Delta M}$ Vectors. In a 9 cm dish, 15μg of DNA was prepared with 290 μL water and 500 μL HBS pH 6.9 (130 mM NaCl, 50 mM KCl, 5 mM Glucose, 21 mM Hepes and 2 mM $NaHPO_4.7H_2O$). $CaCl_2$ was added to 0.29M and the DNA solution then mixed briskly, before being incubated for 30 min at 37°C. 25 μM chloroquine was added to phoenix E cells, 5 min prior to the addition of the $CaCl_2$ precipitated DNA. Transfections were left overnight at 37°C. The DNA was washed from the plate and replaced with 20% medium. Phoenix E cells were stored at 32°C for duration of infection process.

2.6.ii Infection: Phoenix E → PT67

Routinely, the medium containing virus harvested from the phoenix E cells every 12 hours for a period of 36 hours was used to infect ~40% confluent PT67s. Alternatively, in some experiments a reduced time interval of every 4 hours for up to 12 hours was also used. The medium was passed through a 0.45 μM filter and then supplemented with 60 μg of polybrene (Cat no. H9268, Sigma).

2.6.iii Infection: PT67 → NHEK

Once confluent, the infectious PT67 cells were trypsined, resuspended in fresh 20% FAD medium and given a 60Gy γ-IR dose. The infectious PT67 were then re-plated at the same confluent density with NHEK (e.g. 1.0 x 10^6 NHEK/ entire plate of confluent irradiated infectious PT67/ 9cm dish), this point being defined as day -1. Medium was then replaced every 12 hours with 20% FAD^+, for a total co-culture time of 48 hours. Infectious PT67s were then removed from the plate in the same way as normal feeders would be (described in Section 2.2.iii). The medium was re-placed with FAD^+ and fresh feeders were applied.

2.7 Flow Sorting Cells

On the day of interest, the feeders were removed from the NHEK and trypsinised as described in Section 2.2.iii. To stop the trypsinisation, a 10% serum in Ca^{2+} and Mg^{2+} free-PBS solution was used. Cells were then centrifuged for 5 min at 4°C at 1000 RPM and re-suspended in PBS with 50 Units/mL penicillin, 1 mg/mL streptomycin and 50ng/mL gentomycin. All cells were stored on ice while a waiting flow sorting. Immediately prior to being placed in the flow sorting machine, the cells were passed through a 0.70 μM filter.

The flow sorting was done by either Tom Gilbey or Margaret O'Prey as an 'in-house' service provided at the Beatson Institute. Briefly, the cells were taken into the FACSVanatage™ SE (Becton Dickinson) at a flow rate of approximately 200 μL/min and were then stimulated with a 488 nm argon laser. Evaluations based on cell size (FSC-H) vs. GFP (FL2-H) were displayed. Low and high GFP expression was defined either side of the median GFP expression level (i.e. 10^2, (**Figure 19**) as it was the middle value of GFP expression for most infections.

2.8 Western Blotting

2.8.i Various Conditions for Controls

The γ-IR source was Cobalt. The adjusted dose rate at 0.8 m with a build-up plate and field size of 30x30 ranged from 2.05 Gy/min (Dec 04) to 1.65 Gy/min (Aug 2006). NHEK were subjected to varying doses of γ-IR and given varying recovery times, individual specifics are detailed in experimental results. NHEK were also treated for 24 hours with Cisplatin (Cat no. P4394, Sigma).

2.8.ii Whole Cell Extraction

Cell pellets were lysed by pipetting with cell lysis buffer (20 mM Hepes pH 7.0, 5 mM EDTA pH 8.0, 10 mM EGTA pH 8.0, 5 mM NaF, 100 ng/mL Okadaic acid, 1 mM DTT, 250 mM KCl, 0.4% Triton X-100, 1% Glycerol, 20 mg/mL pepstatin A, 20 mg/mL leupeptin, 300 nM PMSF, 1mM benzamidine and 50 mg/mL aprotinin A) for 30 min on ice. The extracts were cleared by centrifugation, and the supernatants stored at -70°C.

2.8.iii SDS-PAGE gels for Rb band shift

40% acrylamide (Cat no. 20-2000-05, Severn Biotech Ltd) and 2% w/v bis-acrylamide (Cat no. 20-2500-05, Severn Biotech Ltd) were used to make the following gels. The separating gel (0.24M TRIS pH 8.8, 7% (v/v) acrylamide, 0.1% (v/v) bis-acrylamide, 0.6% SDS, 0.8% ammonium persulfate and 0.1% Temed) was overlaid with water saturated butanol and allowed to polymerise. The butanol was then removed, the gel rinsed with water and overlaid with stacking gel (0.1M TRIS pH6.8, 3.6% acrylamide, 0.03% bis-acrylamide, 0.5% SDS, 0.8% ammonium persulfate and 0.1% Temed). Gels were run in buffer (25 mM TRIS, 0.1% (w/v) SDS, 0.19M glycine). Typically, cell lysate from 0.5-1.0 $x10^5$ cells were prepared using a 4X Sample Buffer (0.64M TRIS pH 6.8, 7% (w/v) SDS, 18% (v/v) glycerol, 35% (v/v) mercaptoethanol and 0.5% bromophenol blue (w/v)) and denatured in a hot block at 100°C for 5 min.

2.8.iv SDS-PAGE gels for analysis of all other proteins

Cell lysates were prepared as in the previous section and then separated on 12% (Cat no. 345-0118), 10% (Cat no. 345-0112) or 4-12% gradient (Cat no. 345-0124) SDS-PAGE gels (all supplied by BIO-RAD). XT-MOPS (Cat no. 161-0788) running buffer was diluted 1 in 20. The all blue marker (Cat no. 161-0373) and the dual colour marker (Cat no. 161-0374) were used.

2.8.v Western Blotting

The proteins in the gel were then transferred to a PVDF membrane (Immobilin P, Cat no. ipvh00010, Millipore) that had been wetted with neat methanol and then soaked in transfer buffer for >3min. Protein transfer took place at 100V and <0.7 Amps for 1 hour. The PVDF membrane was then blocked in 5% (w/v) skimmed milk powder prepared in TRIS Buffered Saline-Tween 20, TBS-T for 1 hour at RT. The membrane was then probed with the appropriate primary antibody overnight at 4°C, see Table 5. The following day the membrane was

washed, four times in one hour with TBS-T and then incubated with an appropriate secondary solution, see Table 6, prepared in 5% milk TBS-T, for 1 hour at 20°C. The membrane would be washed again for four times in one hour with TBS-T before being developed as described below.

2.8.vi Developing Western Blots

Three different strengths of solutions were used to develop western blots, see below. Membranes were dried and developed firstly with a diluted Femto Max sensitivity solution. If the signal was very weak and required >30 min development time it was washed briefly with TBS-T and then incubated with Femto Max. Conversely, if the initial signal was too strong the blot would be washed and incubated instead with ECL.

(1) For very weak strength signals: **Femto Max.** (Cat no. 34096, Perbio). Incubated for 5 min with a 1:1 mix of solutions 1 and 2 (as labelled by the supplier).

(2) For weak to medium strength signals: **Diluted Femto Max.** Incubated for 5 min in a 1 in 10 dilution of the above solution.

(3) For medium strength signals: **ECL** (Cat no. 32209, Perbio). Incubated for 1 min with a 1:1 mix of solutions 1 and 2.

2.8.vii Stripping Blots

If, and only if, a second protein of a similar molecular weight to the first protein was to be examined, the membrane was stripped using Stripping buffer (0.2M Glycine-HCl pH2.5, 1% (w/v) SDS) for 30 min at RT. The membrane was then washed three times in 30 min with TBS-T and re-incubated with the secondary antibody used (as above) to detect the first protein, before being washed and developed. If the first antibody had been satisfactorily stripped, the membrane was re-probed. If it had not been successfully stripped, the procedure was abandoned.

2.9 Primary and Secondary Antibodies

Table 5: Primary Antibodies			
Antibody raised against	**Catalogue Number**	**Supplier**	**Dilution for Application** WB = Western Blotting IF = Immunofluorescence FACS = FACS analysis
53BP1	05-726	Upstate	1:200 (IF)
Brd-U	M0744	DAKO Ltd.	1:50 (IF) prepared in PBS and 0.5% BSA
Brd-U	555627	Becton Dickinson	1:50 (FACS)
Chk1	sc-8408	Santa-Cruz	1:500 (WB)
Chk1-phosphoS345	2341	Cell Signalling (distributed by New England BioLabs)	1:500 (WB)
Chk2	2662	Cell Signalling (distributed by New England BioLabs)	1:1000 (WB)
Chk2-phosphoT68	2661	Cell Signalling (distributed by New England BioLabs)	1:750 (WB)
Cleaved Caspase 3	9661	Cell Signalling (distributed by New England BioLabs)	1:250 (WB)
Nbs1	A300-187A	Bethyl Laboratories	1:1000 (WB)
Nbs1-phosphoS343	A300-189A	Bethyl Laboratories	1:500 (WB)
p16	sc-9968	Santa Cruz	1:200 (WB)
p21	C24420	Transduction Laboratories	1:500 (WB)
p38	9212L	Cell Signalling (distributed by New England BioLabs)	1:1000(WB)
p53	sc-126	Santa Cruz	1:500 (WB)
p53-phospho15S	9284L	Cell Signalling (distributed by New England BioLabs)	1:500 (WB)
Rb- phospho608S	2181S	Cell Signalling (distributed by New England BioLabs)	1:500 (WB)
Rb- phospho780S	9307S	Cell Signalling (distributed by New England BioLabs)	1:500 (WB)
Rb- phospho795S	9301S	Cell Signalling (distributed by New England BioLabs)	1:500 (WB)
Rb- phospho807S/811S	9308P	Cell Signalling (distributed by New England BioLabs)	1:500 (WB)
SMC1	A300-055A	Bethyl Laboratories	1:1000 (WB)
SMC-1 phosphoS966	A300-050A	Bethyl Laboratories	1:500 (WB)
TRF1	-	kindly donated by T.d. Lange	1:3000 (IF)
TRF2	05-521	Upstate	1:1000 (WB) 1:3000 (IF)

Table 6: Secondary Antibodies			
Antibody raised against	**Catalogue Number**	**Supplier and Address**	**Dilution for Application** WB = Western Blotting IF = Immunofluorescence FACS = FACS analysis
Rhodamine Red Donkey anti Rabbit	711-295-152	Jackson Immuno Research (Distributed by Stratech Scientific)	1 in 250 (IF)
Cy5 Donkey anti Mouse	711-175-150	Jackson Immuno Research (Distributed by Stratech Scientific)	1 in 50 (IF)
Rhodamine Red Donkey anti Mouse	715-295-150	Jackson Immuno Research (Distributed by Stratech Scientific)	1 in 250 (IF)
Cy5 Donkey anti Rabbit	711-175-152	Jackson Immuno Research (Distributed by Stratech Scientific)	1 in 50 (IF)
FITC Goat anti Mouse	12064D	Pharmingen (distributed by Becton Dickinson)	1:50 (FACS)
HRP linked anti Rabbit	7074	Cell Signalling (distributed by New England BioLabs)	1 in 20,000 (WB)
HRP linked anti Mouse	7076	Cell Signalling (distributed by New England BioLabs)	1 in 20,000 (WB)

2.10 Proliferation Curves

On each day of interest, each NHEK variable was harvested in triplicate as detailed in Section 2.2.iii. The cells were re-suspended in 1 mL of medium and counted using a haemocytometer. Triplicates were then averaged and standard deviation calculated in Excel where the proliferation curves were plotted.

2.11 Clonogenicity Assay/ Rhodamine B Staining

After removing the feeders from the plate, NHEK were fixed for 10 min with 10% (v/v) Formaldehyde (Cat no. F/1500/PB15, Fischer) in PBS in a fumehood. All plates were then washed once with PBS prior to being overlaid with 1% Rhodamine B (Cat no. R6626, Sigma) prepared with water. Colonies were left to stain for 30 min in the fume hood. Plates were then washed with tap water and

left to drain and dry. Rhodamine B solution was retained after staining the plates and filtered immediately prior to subsequent use.

2.12 Colony Counting

Only GFP positive colonies were included during colony counting. Each plate was attached to a transparent grid of 40 different squares. [Prepared by Author by drawing a table in Windows Word program and printing to a transparency] of 40 different squares. Within each square, a field of view was assessed and the number of GFP positive colonies judged and placed into one of three categories: 0-5, 5-50 and >50 cells.

2.13 Brd-U Incubation (48 hour) for Immunofluorescent Analysis

On day 14 (12 days after being plated), the NHEK expressing Vector only, myc-TRF2 FL and myc-TRF2$^{\Delta B \Delta M}$ were fed FAD^{+} medium with 100μM 5-Bromo-2'-deoxy-uridine, Brd-U (Cat no. 550891, Becton Dickinson). The plates were left for 24 hours and then re-fed for a further 24 hours. Plates were washed with ice cold PBS and feeders removed with ice cold PE. A final wash in ice cold PBS was also performed. NHEK washed in a 1:1 mix of acetone:methanol and then fixed for 10 min using a fresh aliquot of acetone:methanol. Plates were air dried for 10 min and then permeabilised for 5 min at RT with 0.25% tween 20 (Cat no.P5927, Sigma) in PBS. Plates washed 3 times with PBS in 10 min, then incubated for 5 min with 1M HCl at 60°C, and finally they were washed for 30 min with 3 changes of PBS. At this point, the plates were processed as described in Section 2.14.ii.

2.14 Immunofluorescence Protocols

2.14.i Stringent Protocol

NHEK grown on coverslips (Section 2.2.iv and 2.14.iv, for coverslip details) were rinsed with PBS and then extracted with Triton X-100 buffer (0.5% Triton X-100, 20 mM Hepes-KOH (pH 7.9), 50 mM NaCl, 3 mM $MgCl_2$, 300 mM Sucrose) for 5 min on ice. Coverslips were then rinsed, twice in PBS and fixed using 3% paraformaldehyde (Cat no. P6148, Sigma)/2% sucrose prepared in PBS, for 10 min at room temperature. Coverslips were rinsed twice with PBS, re-permeabilised for 10 min at RT and again rinsed twice with PBS. Cells were then

blocked for 30 min with PBG [0.2% (w/v) cold water fish gelatine (Cat no. G7765, Sigma) and 0.5% (w/v) BSA (A2153, Sigma) prepared in PBS]. *2 Cells were then incubated for either 2 hours at 20°C or overnight at 4°C in the primary antibody solution at an appropriate dilution prepared in PBG. Cells were then washed 3 times in PBG for 15 min and incubated with a secondary antibody solution prepared using PBG for 30 min at 20OC. Cells were again washed twice with PBG and then washed twice with PBS*1 before being mounted as described below, Section 2.14.iv.

When NHEK were labelled with 2 different antibodies, the above protocol went directly from *1 back to *2, using the second set of antibody conditions before being mounted for immunofluorescent examination. Only primary antibodies raised in different species were used, e.g. mouse and rabbit.

Note: Because the GFP in the NHEK does not bind a particular cellular protein and the cells are not fixed prior to permeabilisation, GFP is lost from the cells using this immunofluorescence protocol.

2.14.ii Mild Protocol

NHEK were rinsed in PBS and then fixed in 2% paraformaldehyde (prepared in PBS) for 10 min at 20°C. Cells were rinsed again and then permeablised with a 0.5% NP-40 buffer for 10 min. Cells were then blocked for 30 min in 10% donkey serum prepared in 0.5% NP-40/PBS before being incubated with the primary antibody diluted in 10% donkey serum/0.5% NP-40, for either 2 hr or overnight at 4°C. Cells were washed three times for 5 min in 0.5% NP-40 prior to incubation with secondary antibody diluted in 10% donkey serum/0.5% NP-40/PBS for 45 min, and finally washed three times in 0.5% NP-40/PBS, 5 min each time, before being mounted as described in Section 2.14.iv.

2.14.iii Immunofluorescence on tissue culture plate

In the experiments (**Figures 23, 24, 25 and 26**) it was necessary to perform the immunofluorescence on the tissue culture plate. After fixation and at least one wash, an area of the plate larger than a coverslip was chosen for analysis and an area around it wiped dry. The dry circle would then be traced with a PAP pen (Cat no. S2002, Dako). The protocols were followed as described above. A drop of neat dapi vectashield (Cat no. H1200, Vector Laboratories, Peterborough) was added before the cells were sealed with a glass coverslip and nail polish. To

examine the processed cells under the microscope, the plate was then cut down to size in the fume hood, using a soldering iron. Samples were stored at 4°C until analysis.

2.14.iv Immunofluorescence on thermanox coverslip

Subjected to either the stringent or the mild immunofluorescent protocol, the coverslips were mounted as described (**Figure 12**). A diluted solution of dapi vectashield was used (1 dapi vectasheild: 1 normal vectashield (Cat no. H1000, Vector Laboratories) and sealed with nail polish. Samples were stored at 4°C until analysis.

2.14.v Confocal Image Analysis

Up to 4 channels of the Olympus Fluorview FV1000 confocal microscope were used per experiment for the following dyes and protein (Excitation/Emission): Dapi (405 nm/461 nm), Rhodamine Red-X (561 nm/ 591 nm), Cy-5 (633 nm/ 664 nm) and GFP (488 nm/ 510 nm). The sequential mode of scanning was line. Z-sections were stacked using Image J (Rasband, W.S., ImageJ, U. S. National Institutes of Health, Bethesda, Maryland, USA, http://rsb.info.nih.gov/ij/, 1997-2006.) and colours re-assigned for the best projection of the image.

2.15 Senescence Associated Beta Galactosidase Staining

After removing the feeders, NHEK were fixed for 5 min with 3% (v/v) formaldehyde (Cat no. F/1500/PB15, Fischer) in PBS. The cells were then washed twice with PBS and then incubated with 5 mL of X-Gal staining solution (50 mM MES, 150 mM NaCl, 2 mM $MgCl_2$, 5mM $K_4Fe(CN)_6.H_2O$ (potassium ferrocyanide), 5mM $K_3Fe(CN_6)$ (potassium ferricyanide) and 10 mg/mL X-gal (5-bromo-4 chloro-3 indolyl-β-D-galactoside (Cat no. B4252, Sigma) at pH 6.0. Plates were then incubated for 16 hours in a humid box at 37°C, washed with water, photographed and the number of senescent colonies counted as described in Section 2.12.

[Birds Eye View of] Coverslip Mounting Procedure:

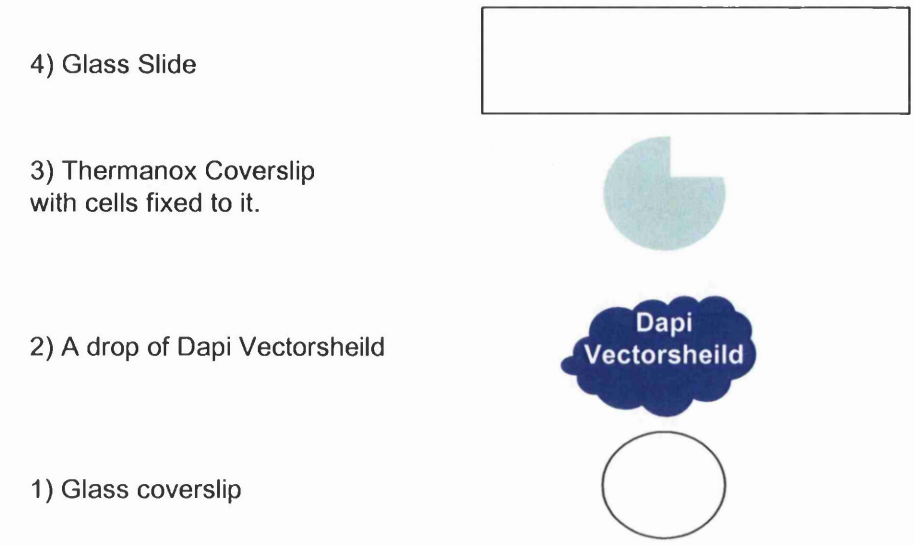

Side View of Mounted Coverslip:

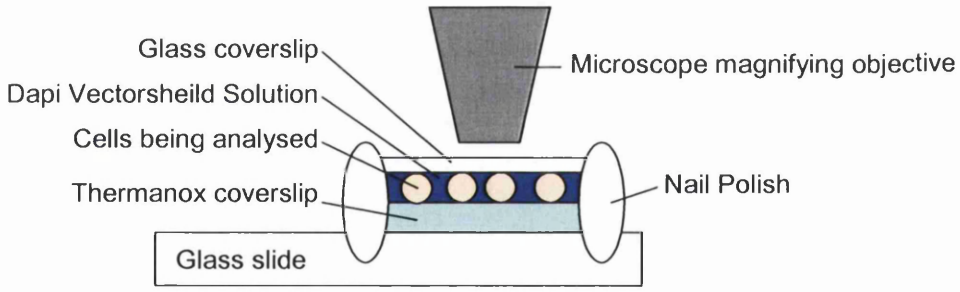

Figure 12. Procedure for Mounting Plastic Coverslips.

Prior to growing any cells on the thermanox coverslip, a small section was cut from it so that the 'cell side up' was always easily distinguished. Swiss 3T3 removal at the end of the conditioning process could result in the coverslip being flipped over.

A glass coverslip (of larger diameter then the plastic coverslip) is placed on a piece of tissue and a drop of Dapi Vectorsheild added to it. The thermanox coverslip is then added, cell side down, before being sandwiched by a glass slide. The excess dapi vectorsheild is then squeezed out by applying pressure as equally as possible to the glass slide and absorbed by the tissue. The slide and 2 coverslips are then turned over and sealed around the edge with nail polish.

The sideview demonstrates how the confocal microscope objective is then able to focus through the glass coverslip to the cells below.

2.16 Flow Cytometric Analysis (FACS)

2.16.i Treatment of Control Cells

NHEK were treated with varying concentrations of Hydroxyurea (Cat no. H8627, Sigma) to establish a G1 arrest FACS profile for NHEK. γ-IR source described in 2.8.i.

It is typical in FACS analysis to collect the dead cells floating in the medium and pellet them with the cells being analysed. Because the NHEK are grown with feeders, the cells floating in the medium were not collected as there would be no way to discern if they were NHEK or feeders.

2.16.ii With Propidium Iodide (PI)

The feeders were removed from NHEK and cells trypsinised as described in Section 2.2.iii. Trypsin was inhibited using 10% medium and the cells pelleted by centrifugation for 5 min at 4°C at 1000 RPM. About $5x10^5$cells were then re-suspended in 500 µL of PBS followed by 5 mL of ice cold methanol, allowed to fix for >30 min, pelleted again by centrifugation for 5 min at 4°C at 1000 RPM, and finally re-suspended in 400 µL of PI solution [50 µg/mL PI (Cat no. P3566, Molecular Probes) and 50 µg/mL RNaseA (Cat no.S23-24-26-36/37)] for a 30 min incubation in the dark at RT. A Becton-Dickinson FACS scan was used to analyse a minimum of 10,000 cells at 585 nm (PI).

2.16.iii FACS Analysis with PI and Brd-U

NHEK were pulsed with for 30 min with 10µM 5-Bromo-2'-deoxy-uridine, Brd-U (Cat no. 550891, Becton Dickinson). The feeders were removed from NHEK and cells trypsinised as described in Section 2.2.iii. Trypsin was inhibited using 10% medium and the cells pelleted by centrifugation for 5 min at 4°C, 1000 RPM. The ~$5x10^5$cells were then re-suspended in 100 µL of 70% ethanol for 30 min. 1 mL of a wash buffer (0.5% Bovine Serum Albumin, BSA (A2153, Sigma)) in PBS was used to wash the cells. Cells were pelleted again by centrifugation for 5 min at 4°C, 1000 RPM and re-suspended in 3N HCl solution and 0.5% Tween 20 (Cat no. P5927, Sigma). 1 mL of wash buffer was again added prior to centrifugation. The cells were re-suspended in 0.5 mL of 0.1M sodium borate pH 8.5 ($Na_2B_4O_7$, BORAX Cat no.S9640, Sigma) for a 2 min incubation at RT. Again, 1 mL of wash buffer was again added prior to centrifugation. 100 µL of anti-Brd-U

(Cat. No. 33281A, Pharmingen) was prepared at a dilution of 1:50 in 0.5% Tween 20/PBS. Cells were incubated for 20 min at RT before 1 mL of wash buffer was added prior to centrifugation. Cells were then re-suspended in FITC conjugated goat anti mouse IgG (Cat no. 12064D, Pharmingen) prepared at 1:50 and incubated for 30 min, in the dark. 1 mL of wash buffer was again added prior to centrifugation and the pellet resuspended in 0.5 mL of 10 μg/mL PI prepared in PBS. A Becton-Dickinson FACS scan was used to analyse a minimum of 10,000 cells at 585 nm (PI) and 530 nm (FITC).

Chapter 3:

Infecting NHEK with myc-TRF2 FL and myc-TRF2$^{\Delta B \Delta M}$

The aim of this thesis has been to characterise the cellular response to uncapped telomeres using myc-TRF2$^{\Delta B \Delta M}$ (a dominant negative form of the TRF2 protein) in a normal epithelial cell system for the first time. An IRES-GFP system was used so NHEK could be isolated as soon as they began to express the construct, thereby allowing evaluation of early time points. Not only did this allow examination of the effect of uncapping the telomere in NHEK, but also of the early downstream effects causing the cellular phenotype. Both the telomerase activity and the telomere lengths of the NHEK were established to determine the effects either may have on the experimental telomere manipulation.

3.1 Characterising telomerase activity in NHEK

Telomerase activity can be determined in vitro using a PCR based assay in which active telomerase from a cell extract extends a 50 base pair primer as if it were a telomere with the hexameric repeat: [TTAGGG]. When run out on a gel, the activity of telomerase can then be judged by how many hexameric repeats were added as indicated by the extent of the 6 bp ladder created within a set time and PCR cycle programme. To avoid saturating the assay, limited amounts of telomerase activity are used. Subjecting differently experimentally treated cells to the same TRAP conditions then allows comparisons of their relative telomerase activity to be drawn.

Telomerase activity can be found in the regenerative basal layer of the epidermis in human skin (Harle-Bachor and Boukamp 1996). As NHEK are a primary culture of the epidermis from newborn foreskin, it was determined if the cultures contained any telomerase activity (**Figure 13**). Very little telomerase activity was found in NHEK at 20 Population Doublings, (PD). Expressing an hTERT construct in NHEK (hTERT expression from 14 PD, harvested at 16 PD) demonstrated far more telomerase activity than that found in NHEK without exogenous hTERT expression; therefore telomerase activity in NHEK is limited by hTERT expression. Most likely, only cultured cells derived from the

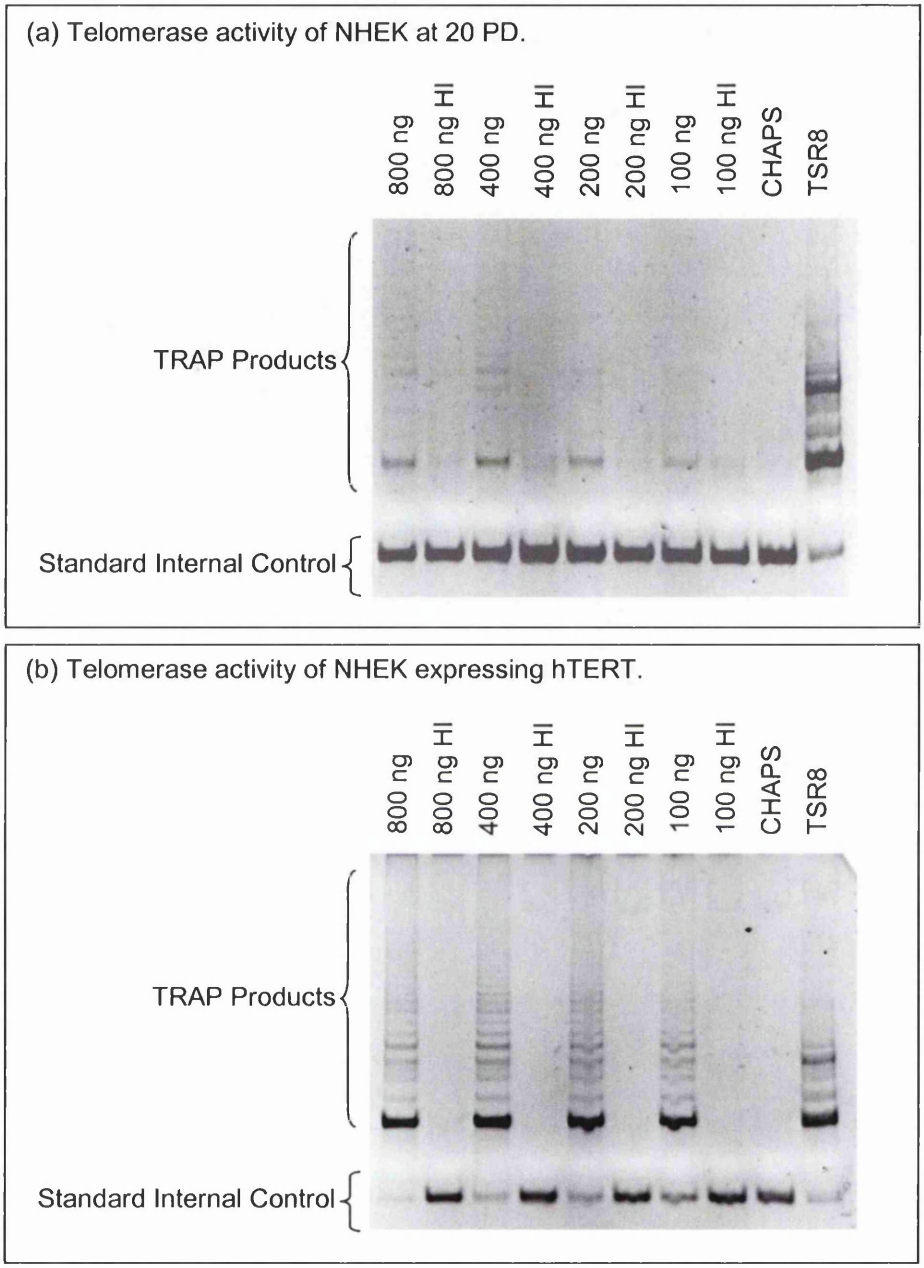

Figure 13. Telomerase Repeat Amplification Protocol (TRAP) analysis of telomerase levels in NHEK (a) before and (b) after infection with hTERT expressing retrovirus. Varying concentrations of cell lysate are used to determine a sensitive range of lysate concentration for measuring telomerase activity within a cell culture. As a negative control, an equivalent amount of sample is Heat Inactivated (HI) to show the telomerase activity measured in each lane is heat sensitive. Each sample also contains a standard internal control (SIC) that will amplify a PCR product of 36bp. The SIC and telomerase primers actively compete for reagents and therefore the amount of SIC is inversely proportional to the amount of TRAP product generated. The CHAPS lane is a negative control and contains buffer only, no sample. TSR8 contains the TSPrimer extended with 8 telomeric repeats acting as a quantitation control lane. **(a)** Decreasing concentrations of NHEK (20 PD) shows a decrease in their telomerase activity, demonstrating the assay is not saturated and the telomerase activity detected in this sample is very small. **(b)** NHEK expressing hTERT (infected at 14 PD) and harvested at 16 PD display considerably greater telomerase activity then NHEK not infected with hTERT retrovirus. The assay is saturated at 200 ng with these cell lysates.

basal cells in the epidermis are expressing active telomerase and the population is a mix of both basal and transit amplifying keratinocytes. By infecting the entire population with hTERT, even the transit amplifying cells are capable of producing an active form of the telomerase enzyme and therefore more telomerase activity is seen in the population.

3.2 Characterising telomere length in NHEK

Telomere length plays an integral role in determining the fate of a cell. Average telomere length can be determined for a cell system in a Telomere Restriction Fragment (TRF) blot in which genomic DNA is isolated and digested using restriction enzymes HinF1 and Rsa1 (Allshire et al. 1989). These restriction enzyme sites do not occur in the telomere or sub-telomeric sequence, so when the digest is run out on a gel, long tracts of telomeric and sub-telomeric DNA create a smear indicative of the range in length of all 92 telomeres within the cells harvested for analysis.

Being derived from newborn tissue, the NHEK have long telomeres (**Figure 14**). All NHEK have been co-cultured with a feeder layer (Swiss 3T3 cells) which have even longer telomeres, 9 to >23 kbp. Although the feeder layer is removed before NHEK are harvested, small levels of 3T3 contamination with the NHEK population may undoubtedly occur. For this reason, telomere lengths >9 kbp can not necessarily be attributed to the NHEK population. In (**Figure 14**), the telomere length of NHEK at 20 PD is between 8.5 and 10 kbp. As the NHEK undergo more PD, the lengths of the telomeres reduce as is expected in normal somatic cells without exogenous expression of hTERT (Bodnar et al. 1998). At 43 PD, telomeres as short as 3 kbp are seen. Interestingly, although telomeres within the population are clearly getting shorter, a subset of the 43 PD NHEK population still has telomeres as long as 8.5 kbp, the length of the telomere at 20 PD. It is possible that these are the telomeres from the telomerase positive basal layer keratinocytes.

Although NHEK at 20 PD have been shown to contain a trace of active telomerase, the reduction in telomere length during the growth of NHEK for 50 PD demonstrated that this limited amount of endogenous telomerase activity is

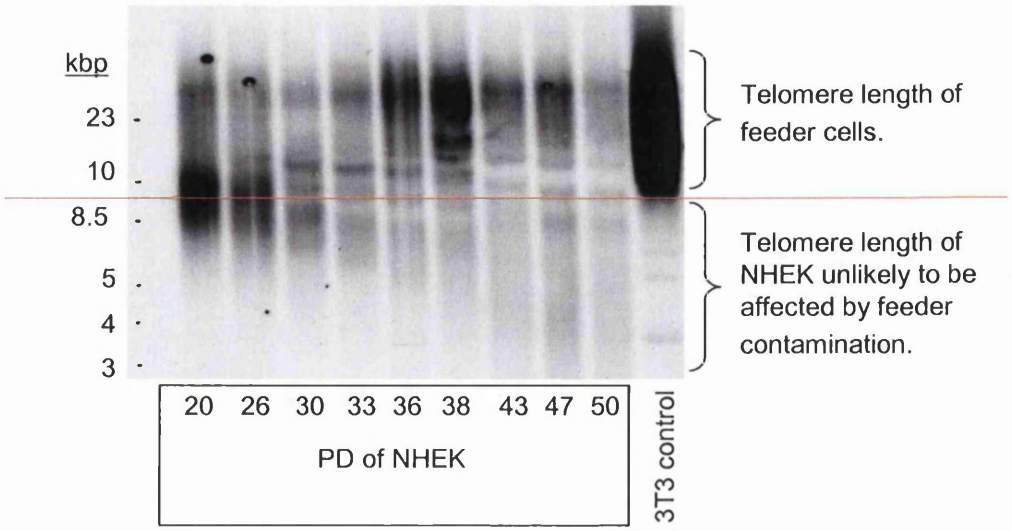

Figure 14. Telomere Restriction Fragment (TRF) blot of NHEK grown for 50 Population Doublings (PD). 8μg of genomic DNA were loaded per lane, except in the control lane (DNA from feeder cells) where only 4μg were loaded. Higher molecular weights of DNA fragments are condensed at the top of the blot. This causes a concentration of the molecular probe used to identify the telomeric DNA giving a false impression that proportionally there are more of the longer telomere fragments then shorter telomere fragments. Even though feeder contamination is only likely to be 0.5 – 5% of the total NHEK, telomeres from feeders are longer, 10- >23 kbp, and therefore give a stronger signal. As the NHEK in this work have all been grown with feeders, statements about telomere lengths greater then 10 kbp (i.e. above the orange line) can not necessarily be attributed to NHEK.

At 20 PD the average telomere length of the NHEK ranges from 8.5 - 10 kbp. A gradual reduction in telomere length is seen with increasing PD, as expected in cells with a limited amount of telomerase activity. By 43 PD, telomeres as short as 3 kbp are seen.

not enough to prevent telomere length shortening with increasing population doublings.

3.3 Optimising the process of infecting NHEK with TRF2 retroviral expression vectors

Titia de Lange's lab (Rockfeller University, NYC) used an adenoviral system to infect fibroblasts with a myc tagged TRF2$^{\Delta B\Delta M}$ or myc tagged TRF2 FL and looked at early time points. Close to 100% infection is assumed as adenoviral systems are so effective. However, we were advised by the de Lange lab and others that, if there was a choice, retroviral systems were preferable. Although easier to work with, a limitation of retroviral infection is that the percentage of cells infected is not as high as with adenoviral infection: therefore, traditionally drug selection is used (usually a minimum of 1 week) to ensure a pure population of cells expressing the gene of interest. As our interest is in early time points, to avoid this time-delay we sub-cloned myc-TRF2 FL and myc-TRF2$^{\Delta B\Delta M}$ retroviral constructs (generously donated to us by the de Lange lab) into the pMIG-IRES-GFP vector. As an Internal Ribosomal Entry Site (IRES) vector, pMIG is capable of translating both the gene of interest (i.e. myc-TRF2 FL or myc-TRF2$^{\Delta B\Delta M}$) and Green Fluorescent Protein (GFP) as separate proteins from the same transcript.

After being sub-cloned, sequencing of the myc-TRF2 FL and myc-TRF2$^{\Delta B\Delta M}$ vectors revealed a discrepancy with the NCBI sequence. The NCBI TRF2 cDNA encodes alanines in amino acid positions 434 and 435, whereas sequencing of our vectors indicated only one alanine in that position. The de Lange lab subsequently confirmed that other labs had also found this anomaly and [it has been concluded] that the NCBI site is incorrect. Satisfied that the sequences of the vectors were acceptable, we continued to use them for the project. Only the pMIG-myc-TRF2 FL - IRES - GFP and pMIG-myc-TRF2$^{\Delta B\Delta M}$- IRES - GFP vector were used for the rest of this thesis and will be denoted myc-TRF2 FL and myc-TRF2$^{\Delta B\Delta M}$ here after.

Prior to any experiments where NHEK are infected with myc-TRF2 FL and myc-TRF2$^{\Delta B\Delta M}$, a stock of primary NHEK was expanded and frozen down at 7 PD. The NHEK used in each experiment for the remainder of this thesis have not been infected with hTERT retrovirus. Each experiment used a fresh ampoule of NHEK

that was further expanded prior to infection with myc-TRF2$^{\Delta B\Delta M}$ or myc-TRF2 FL. At the point of infection, NHEK would have only undergone a total of between 10 and 14 PD, and therefore have a telomere length >8.5 kbp.

Infecting NHEK with retrovirus did not prove straightforward. Adding medium from amphotropic retroviral producing cell lines such as Phoenix A to NHEK resulted in very poor infection rates, less then 3%. The following protocol for infecting NHEK was established based on Fiona Watt's publications (Levy et al. 1998) and the optimised version used is outlined in (**Figure 15**). Each experiment described in this thesis starts on "day 0", when the expression of myc-TRF2$^{\Delta B\Delta M}$ or myc-TRF2 FL begins in the NHEK. Days prior to this point are negatively numbered.

The optimised process for infecting NHEK began with myc-TRF2 FL or myc-TRF2$^{\Delta B\Delta M}$ DNA being transfected into phoenix E, an ecotropic retroviral producing cell line using a $CaCl_2$ protocol. The phoenix E cells were left for 12 hours, before being washed and fed with medium. Once transfected, the phoenix E cells were maintained in a 32°C incubator as the half-life of a retrovirus is greater when stored at this lower temperature. Medium from phoenix E was harvested 3 times at 12 hours intervals, filter sterilised and used to infect PT67 cells, an amphotropic retrovirus producing NIH-3T3 cell line. Once the PT67s became confluent, they were trypsinised and given a lethal 60 Gy γ-IR dose (to prevent their further replication) before being re-plated with the NHEK at confluent levels. Retroviral infection is a more effective method of introducing genetic material into a cell line than transfection. By using phoenix E to retrovirally infect the PT67s, more PT67s produce the retrovirus than if PT67 were directly transfected themselves and this extra step ultimately leads to a greater infection rate of NHEK.

NHEK were co-cultured with lethally irradiated infectious PT67s in medium without Epidermal Growth Factor (EGF) for 12 hours at 37°C. The medium was then supplemented with EGF and refreshed every 12 hours for a minimum of 24 and maximum of 36 hours. EGF is not added until the cells have attached to the tissue culture plate as this aides cloning efficiency (Rheinwald and Green 1977). NHEK were co-cultured with infectious PT67 for a minimum of 36 hours and a maximum of 48 hours. Unless the NHEK were harvested immediately, as soon as

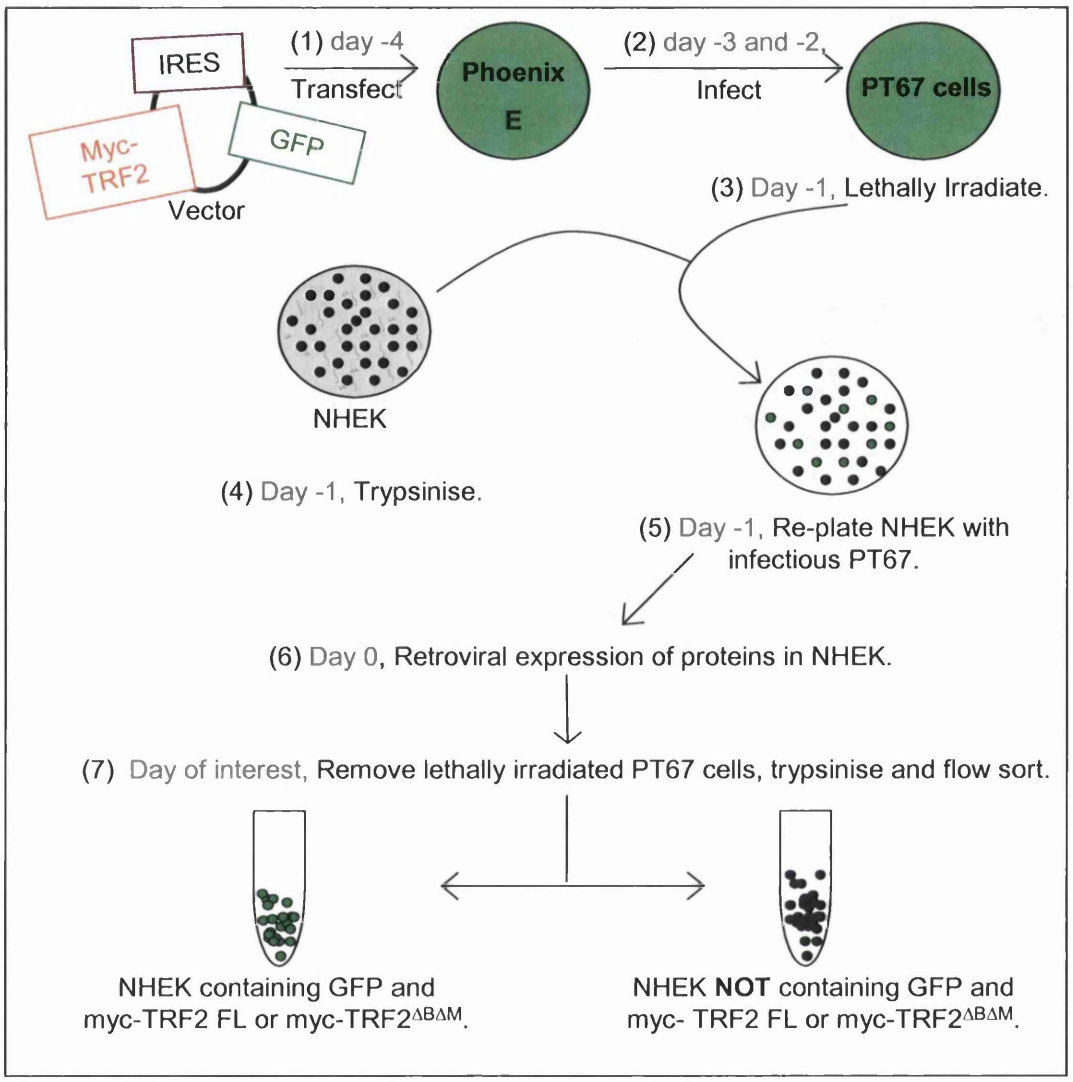

Figure 15. Retroviral Infection of NHEK with TRF2 Constructs. In each experiment:

(1) Vector only, myc-TRF2 FL and myc-TRF2$^{\Delta B\Delta M}$ were transfected into phoenix E retroviral packaging cells using $CaCl_2$.

(2) On each of the 2 subsequent days, medium containing retrovirus was then harvested from the phoenix E cells and used to infect PT67 cells, an NIH-3T3 amphotropic packaging cell line.

(3) Infectious PT67 cells were then harvested and lethally irradiated with 60 Gy of γ-IR.

(4) NHEK were trypsinised.

(5) NHEK re-plated using the lethally irradiated infectious PT67s as a feeder layer.

(6) Day 0 is designated the start point of each experiment, assuming one cell cycle is enough time for the retrovirus to be integrated and expressed.

(7) On the day of interest (different in each experiment) NHEK were flow sorted to isolate the GFP positive cells from the GFP negative cells. Day 2 was the most frequent day for flow sorting.

the infectious PT67s were removed, they were replaced with feeders. Co-culturing proved a highly effective way of introducing the TRF2 constructs into the NHEK: percentages of GFP positive cells ranged from 30 - 75%. The direct cell-to-cell contact between the PT67 and the NHEK allows the virus to pass straight from one cell to the other which is considered to be more efficient than retroviral infection of keratinocytes using viral supernatants.

As soon as NHEK began to express the GFP they could be isolated through flow sorting, allowing evaluation of the cells at early time points. However, despite these advantages there are some substantial drawbacks to flow sorting cells as a means of selection. The processing of flow sorting the cells leaves them vulnerable to bacterial contamination; therefore the cells are treated with antibiotics when plated after being flow sorted. Furthermore, a large percentage of cells are lost when flow sorted: on average, only 20% of GFP positive cells put through the flow sorter are returned. This is largely to do with the cells actually reaching the collection tube after being deflected by the laser.

3.4 Myc-TRF2 FL and myc-TRF2$^{\Delta B \Delta M}$ expression in NHEK

Western blotting allows assessment of the level of expression of proteins from a cell extract. Denatured cell lysates separated based on size on an acrylamide gel are transferred to a suitable membrane and then recognised with an appropriate antibody.

Both myc-TRF2$^{\Delta B \Delta M}$ and myc-TRF2 FL are expressed in NHEK as early as day 1, as shown by recognition with a TRF2 specific antibody (**Figure 16**). Myc-TRF2$^{\Delta B \Delta M}$ is missing both its basic ($^{\Delta B}$) and myb ($^{\Delta M}$) domain which is why it appears 12 kDa below myc-TRF2 FL. Endogenous levels of TRF2 are not seen on the western blots unless they are developed for a longer period of time, at which point the exogenously expressed TRF2 is so overexposed that it is impossible to decipher the signal contributed from each lane. The considerable over-expression of the constructs is an important aspect of how myc-TRF2$^{\Delta B \Delta M}$ is effective at creating a dysfunctional telomere. TRF2 binds the telomere as a homodimer, with each half of the dimer providing a myb domain to interact with the DNA. Myc-TRF2$^{\Delta B \Delta M}$ is proposed to reform the homodimer with endogenous TRF2 and therefore render endogenous TRF2 incapable of binding telomeric DNA. As this

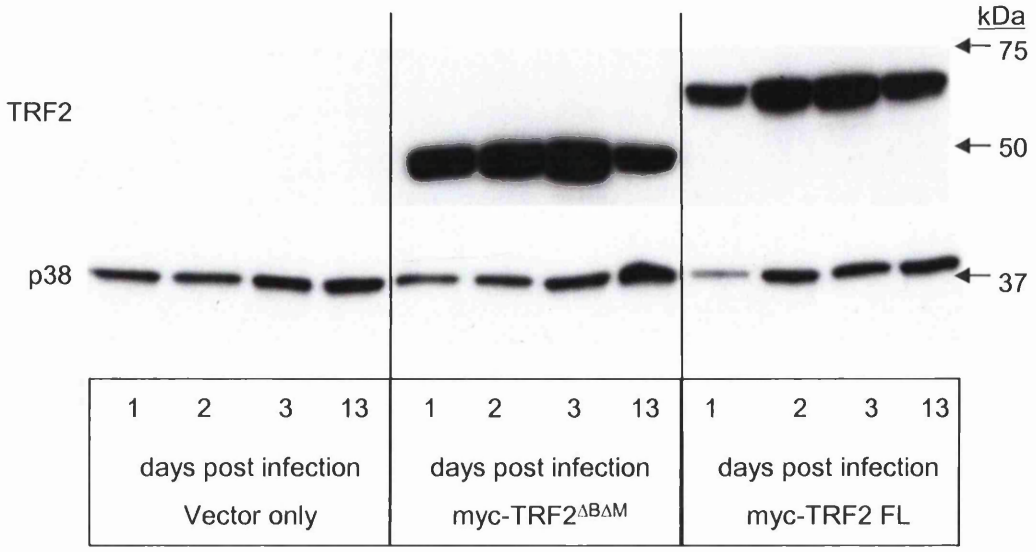

Figure 16. Detection of exogenous proteins myc-TRF2$^{\Delta B \Delta M}$ (50 kDa) and myc-TRF2 FL (62kDa) expressed in NHEK by western blot.

On days 1, 2 and 3, GFP positive cells were harvested immediately after flow sorting. On day 4, cells were flow sorted and GFP positive cells were re-plated with feeders. On day 13, these cells were harvested without further flow sorting.

The MAP kinase family member p38 is used as a loading control as it is a ubiquitously expressed protein that is regulated by phosphorylation, as opposed to up or down-regulation of its expression level.

is the mechanism, it is crucial that the myc-TRF2$^{\Delta B\Delta M}$ is expressed >1:1 with endogenous TRF2.

3.5 Assessing phenotypes of NHEK expressing TRF2 constructs

NHEK infected with Vector only, myc-TRF2 FL or myc-TRF2$^{\Delta B\Delta M}$ were flow sorted on day 2 and then plated with feeders. On day 10, expression of Vector only and myc-TRF2 FL had no obvious effect on the NHEK colony morphology when evaluated using a light microscope at 25X magnification (**Figure 17**). The GFP image in the right hand panel clearly demarks the NHEK cells from the feeders they are grown with. Differences in the appearance of the NHEK expressing myc-TRF2$^{\Delta B\Delta M}$ were obvious. A lot of the cells were more spread out, multi-nuclear and the colony sizes were a lot smaller. Although widespread, this phenotype was not absolute and there were also colonies present that did not differ at all from those expressing Vector only or myc-TRF2 FL.

3.6 Summary of Chapter 3

In order to evaluate the early downstream effects of a dysfunctional telomere in the epithelial cell system NHEK, TRF2 constructs were sub-cloned into an IRES-GFP vector. GFP expression signified the moment the TRF2 constructs were expressed and allowed for identification and isolation of NHEK expressing the TRF2 constructs using flow cytometry. The retroviral infection protocol was optimised and proved effective at infecting the NHEK, as myc-TRF2$^{\Delta B\Delta M}$ or myc-TRF2 FL were shown to be expressed by the NHEK as early as day 1.

A phenotype was clearly apparent in the morphology of the NHEK expressing myc-TRF2$^{\Delta B\Delta M}$ by day 10. Smaller colonies were seen indicating reduced proliferation and the cells in some colonies appeared more spread out, a characteristic indicative of senescence.

Telomerase activity was determined in NHEK and shown to be limited by insufficient hTERT expression. As will be discussed in chapter 6, the telomerase status of the NHEK is important in the context of evaluating if it is a contributing factor in the DNA damage response.

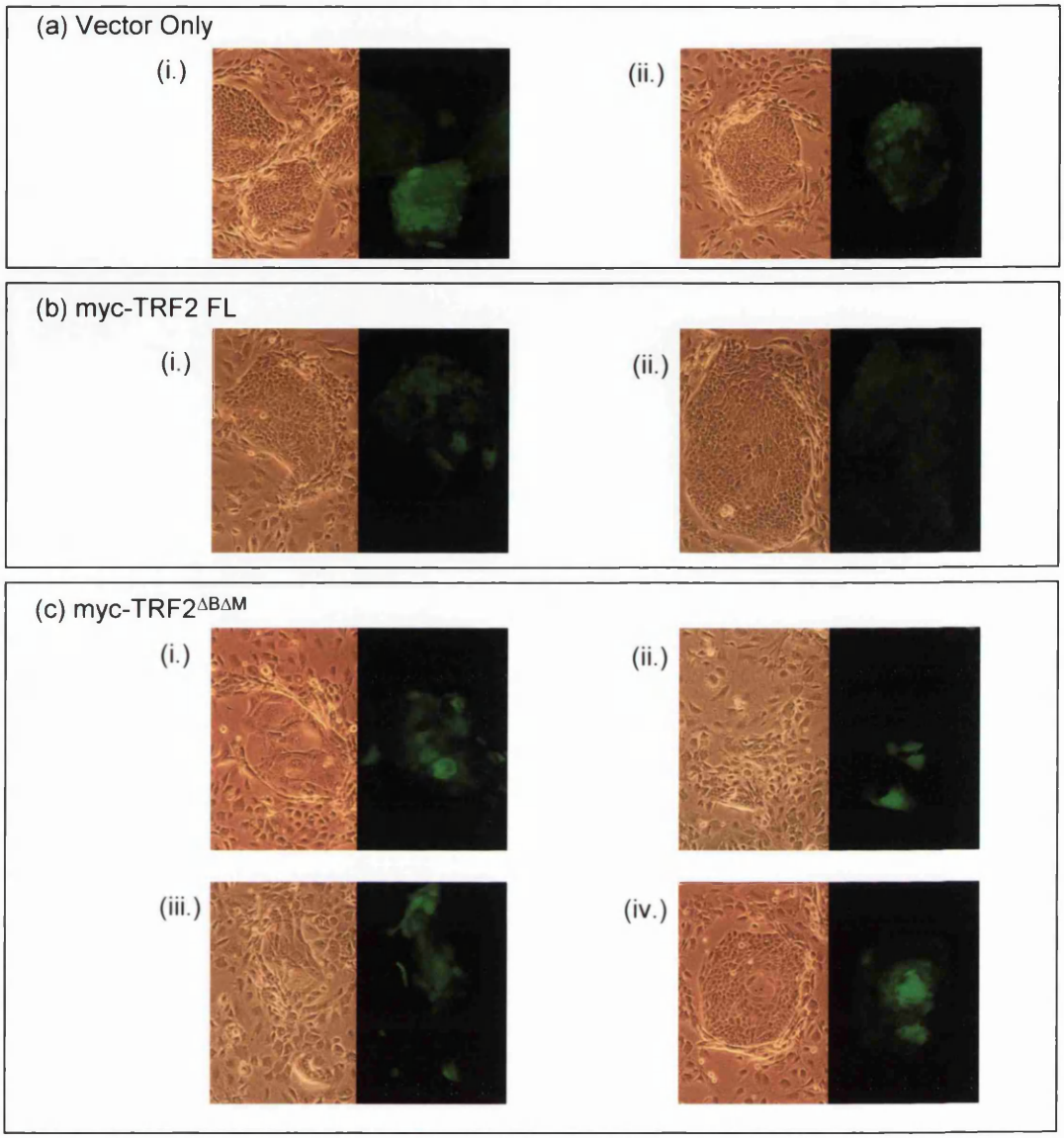

Figure 17. Representative colonies of NHEK expressing (a) Vector only, (b) myc-TRF2 FL and (c) myc-TRF2$^{\Delta B\Delta M}$ on day 10.

All images are shown at 25X magnification. Left panels are phase contrast images; right panels are photographs with longer exposure time under UV light illustrating their level of GFP expression. The feeders were not removed prior to the images being taken.

(a) Vector only (i.) 3 small adjoining colonies are shown, where the middle colony demonstrates more green fluorescence than the two either side. (ii.) 1 colony is shown. Both GFP positive Vector only colonies display the normal morphology seen in uninfected NHEK.

(b) myc-TRF2 FL. Again, (i.) and (ii.) both show colonies with morphology similar to uninfected NHEK.

(c) myc-TRF2$^{\Delta B\Delta M}$. (i.) Cells within the colony display a flattened spread out morphology typical of senescent cells. Colonies in (ii.) and (iii.) are both considerably smaller than colonies seen in NHEK infected with either vector only or myc-TRF2 FL. (iv.) The entire colony is GFP positive although the differentiated cells on top of the culture in the middle of the colony are more green then the cells surrounding it. The colony itself appears normal, no different to that seen in either vector only or myc-TRF2 FL.

The altered colony appearance of NHEK expressing myc- TRF2$^{\Delta B\Delta M}$ is evident in colonies (i.), (ii.) and (iii.) but not in (iv.).

When infected with the TRF2 constructs, the average telomere length of NHEK was shown to be greater then 8.5 kbp. Knowing this, there is confidence that the uncapped telomere phenotype being seen in the cells is created through the addition of myc-TRF2$^{\Delta B \Delta M}$ and not also being contributed to by critically short telomeres within the cell population.

Chapter 4:

Characterising NHEK proliferation response to myc-TRF2 FL and myc-TRF2$^{\Delta B \Delta M}$

Although the main objective of this project was to characterise the early downstream factors of dysfunctional telomeres, in order to establish the outcome for the cell, the effect of expressing myc-TRF2 FL and myc-TRF2$^{\Delta B \Delta M}$ was also examined over a period of 14 days.

4.1 Proliferation Curves of NHEK expressing myc-TRF2 FL or myc-TRF2$^{\Delta B \Delta M}$

NHEK were infected with the TRF2 constructs, flow sorted and plated so that they could be counted in triplicate on harvest days (**Figure 18**). NHEK expressing myc-TRF2 FL did not proliferate as well as NHEK expressing the Vector only. NHEK expressing myc-TRF2$^{\Delta B \Delta M}$ proliferated even less then myc-TRF2 FL and Vector only expressing cells. A lag in proliferation is seen in all cell variables from day 2 to day 8. This is inevitable as the NHEK will require time regain homeostasis before proliferation will begin. Also, it is inevitable that not all NHEK plated will attach to the tissue culture plate. In an attempt to account for this cell loss, the medium was harvested the next day (day 3). After reducing the volume, the non-adherent cell counts were found to be between 0.0- 1.0% of the NHEK plated. There was no obvious pattern of less cells adhering where Vector only, myc-TRF2 FL or myc-TRF2$^{\Delta B \Delta M}$ were expressed, so the most likely explanation for the lag seen in proliferation is the sluggish recovery of the cells after flow sorting and an equal loss of cells between variables when re-plating.

4.2 Effects of level of expression of TRF2 constructs on NHEK proliferation

Flow sorting showed a wide range in GFP expression level in NHEK infected with retroviral vectors, (**Figure 19)(a)**. As it is possible to collect 2 separate populations of cells at the Cell Sorter, low or high levels of GFP expression were

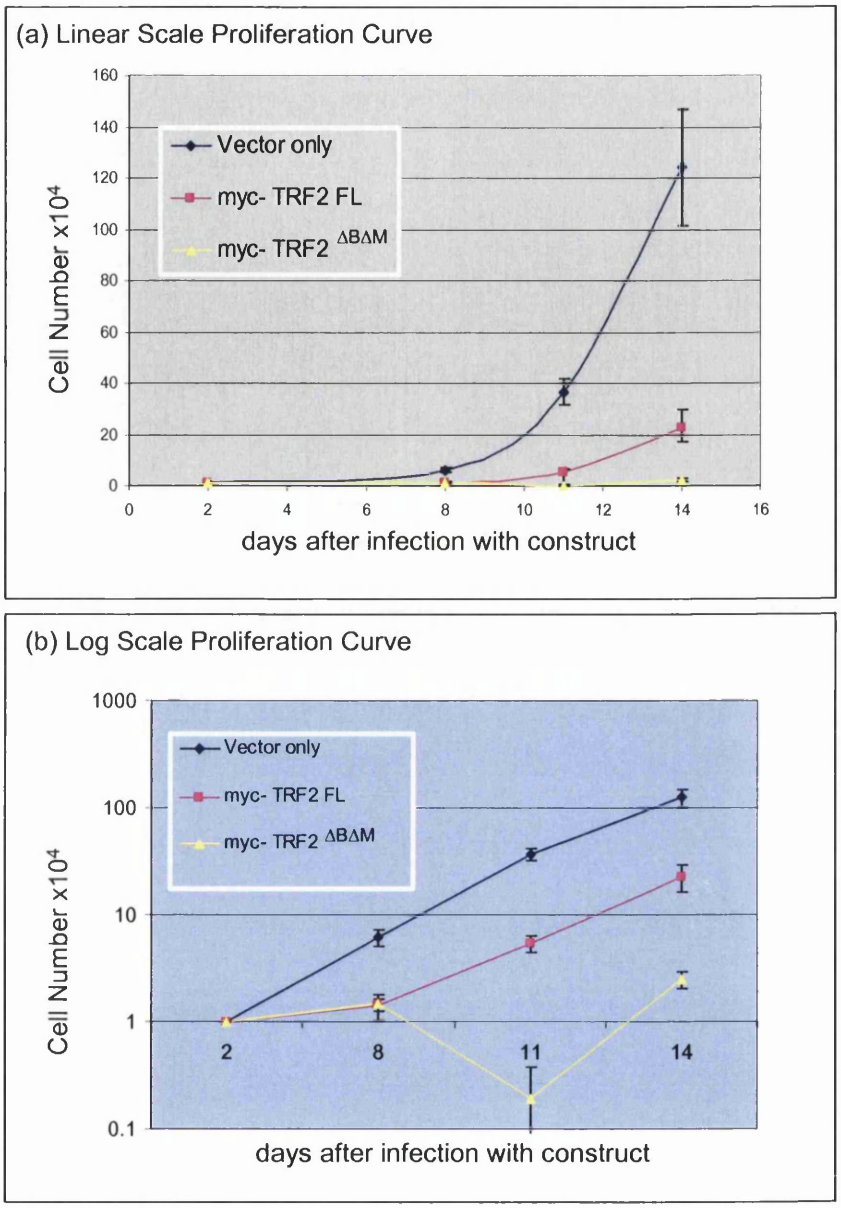

Figure 18. Proliferation curves of NHEK grown for 14 days with myc- TRF2 FL and myc- TRF2$^{\Delta B\Delta M}$.

Cells were flow sorted on day 2. GFP positive NHEK were then plated at 1x10^4 /plate (9 plates/ for each construct) with feeders. On each harvest day: 8, 11 and 14, the feeders were removed from 3 plates (per construct), the cells were trypsinised and the total number of NHEK counted using a haemocytometer. Error bars represent standard deviations.

(a) Typical exponential growth of NHEK is seen where Vector only is expressed. Expression of myc-TRF2 FL inhibits proliferation of the NHEK considerably and expression of myc-TRF2$^{\Delta B\Delta M}$ reduces further still the ability of the NHEK to replicate.

(b) The same data represented on a log scale.

(a) Cell Profile from Flow Sort of NHEK expressing Vector only

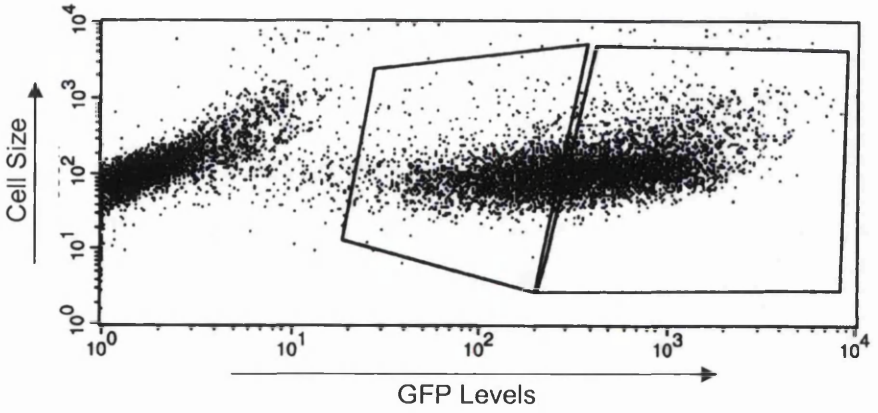

GFP Level:	low	high
Vector only	24%	34%
Myc-TRF2 FL	24%	50%
Myc-TRF2$^{\Delta B \Delta M}$	26%	38%

(b) Expression levels of myc-TRF2 FL and myc-TRF2$^{\Delta B \Delta M}$ isolated into low and high GFP expressing fractions

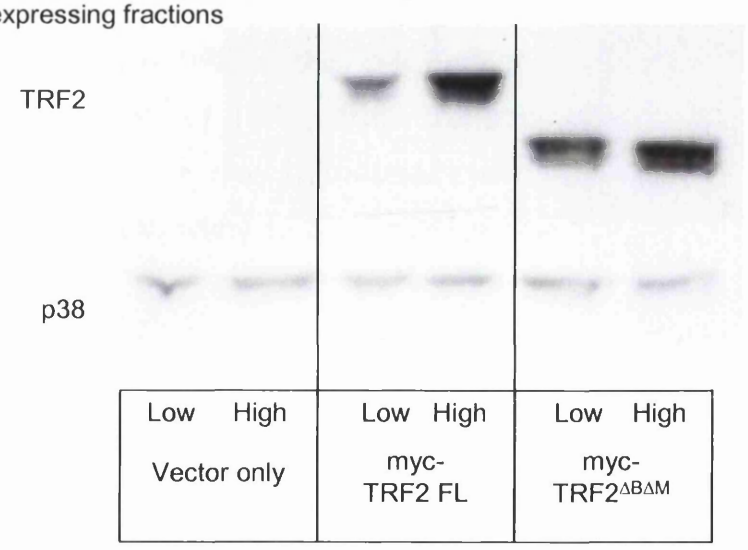

Figure 19. Isolating NHEK expressing low or high levels of GFP.

(a) A profile from a flow sort where a low and high GFP expressing population of NHEK population are isolated.

(b) Western blot analysis of NHEK isolated on day 4 (and plated with feeders) were then harvested on day 8. Cells sorted on the basis of low or high GFP expression express corresponding low or high levels of TRF2 constructs, even after 4 days in culture.

examined to see if this correlated with low or high expression of myc-TRF2 FL and myc-TRF2$^{\Delta B\Delta M}$ (**Figure 19**)(**b**). Cells sorted on day 4 and then plated with feeders were harvested on day 8 for western blot analysis. Correlation was seen, i.e. cells expressing low levels of GFP had low levels of myc-TRF2 FL expression.

The effects of low or high expression of myc-TRF2 FL and myc-TRF2$^{\Delta B\Delta M}$ on proliferation were then evaluated in NHEK (**Figure 20**). Again, the pattern was very similar to that seen in (**Figure 18**). Low or high levels of Vector alone did not cause much of a difference in the ability of the NHEK to proliferate. However, NHEK with low levels of myc-TRF2 FL were able to proliferate considerably more than cells expressing high levels of the same construct. This result could have three explanations. Higher levels of myc-TRF2 FL bound to the telomere may impede the cell's ability to separate the DNA at the telomere, thereby slowing down the rate the cells progress through DNA synthesis. Alternatively, as TRF2 has been shown to bind at non-telomeric DNA during the DNA damage response (Bradshaw et al. 2005), it is possible that very large amounts of TRF2 protein within the cell induce a DNA damage response. Thirdly, the large amounts of TRF2 within the cell which possibly don't have room to bind at the telomere, may still interact with other TRF2 binding proteins and prevent them from localising to the telomere and performing their function there.

Similarly, with myc-TRF2$^{\Delta B\Delta M}$, less proliferation is seen in cells expressing high levels of construct than in cells expressing low levels. The most likely explanation for this is that higher levels of myc-TRF2$^{\Delta B\Delta M}$ are more effective at stripping endogenous TRF2 from the telomere. However, it is also possible that higher levels of myc-TRF2$^{\Delta B\Delta M}$ induce apoptosis as witnessed by Lechel et al and discussed in Chapter 6 (Lechel et al. 2005). If so, since it is unlikely that a cell undergoing apoptosis will make it through the flow sorting process, apoptosis would need to be occurring after the NHEK are plated. Attempts at assessing cell death within the population subsequent to flow sorting and plating are described later.

As there is a differential effect in NHEK between low levels of myc-TRF2 FL vs. low levels of myc-TRF2$^{\Delta B\Delta M}$, the effects on cell proliferation are specifically

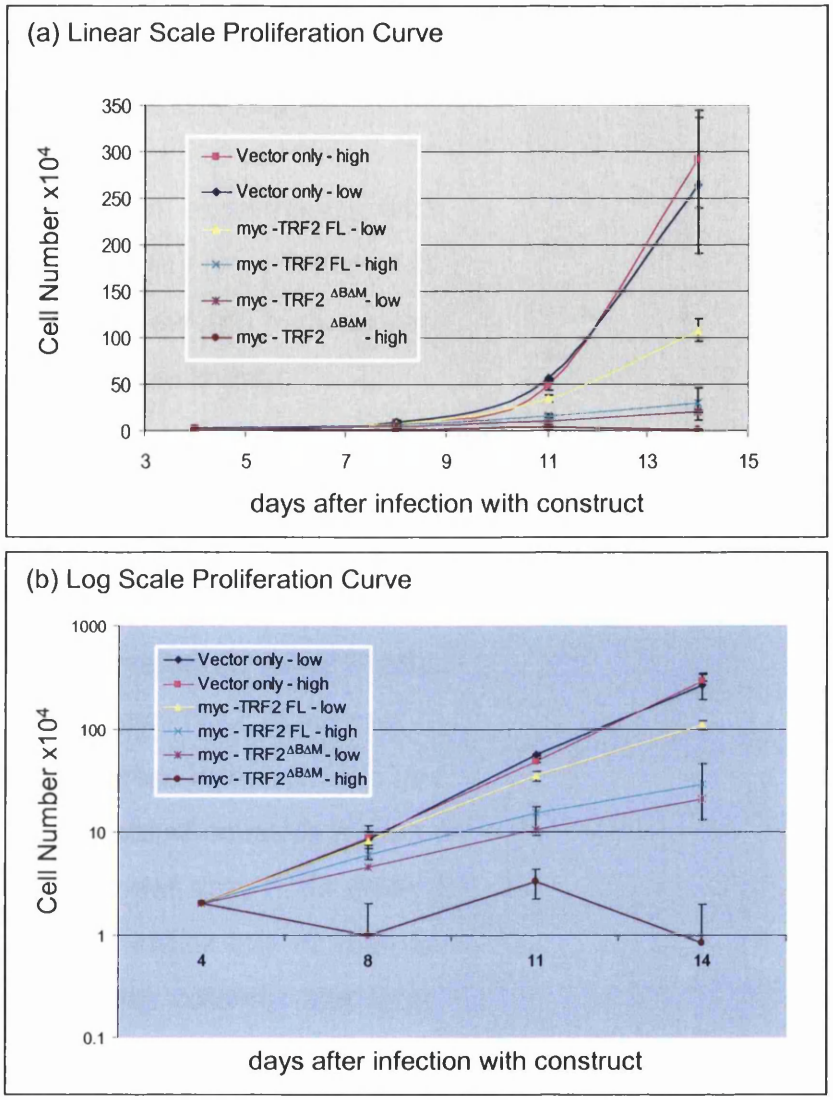

Figure 20. Proliferation curves of NHEK grown for 14 days with low or high levels of myc- TRF2 FL and myc- TRF2$^{\Delta B\Delta M}$.

Cells were flow sorted on day 2 and plated as described in Figure 19. Here the NHEK were plated at the higher density 2x10^4. Error bars represent standard deviations.

(a) The pattern of proliferation does not alter much when either low or high levels of GFP are expressed in the Vector only cells. Higher expression levels of myc-TRF2 FL prevent the NHEK from proliferating more then low levels of the same construct. In NHEK expressing myc-TRF2$^{\Delta B\Delta M}$, low expression levels drastically reduce their ability to replicate and high amounts prevent proliferation even more dramatically.

(b) The same data represented on a log scale.

being generated by the TRF2 construct rather than "non-specific effects" of protein over-expression. Where high levels of myc-TRF2 FL vs. high levels of myc-TRF2$^{\Delta B\Delta M}$ are being compared, it is more difficult to make the same claim as both variables have such a large effect on the cell proliferation; however, a differential effect was still seen.

In total, proliferation experiments with NHEK expressing TRF2 vectors were performed three times, once with total expression and twice where the cells were separated into low and high expressing fractions. Patterns of proliferation were similar in all experiments.

4.3 Clonogenicity of NHEK expressing low or high levels of myc-TRF2 FL or myc-TRF2$^{\Delta B\Delta M}$

Clonogenicity was evaluated using Rhodamine B staining in NHEK expressing low and high levels of myc-TRF2 FL or myc-TRF2$^{\Delta B\Delta M}$. Plates of colonies scanned as images on day 14 after infection and cell sorting are shown in (**Figure 21**) and the numbers and sizes of colonies from a separate experiment are quantitated in (**Figure 22**). There was very little difference in the number and size of colonies in NHEK expressing either low or high levels of Vector only. Both Vector only plates displayed more colonies and larger colonies than any of the four plates expressing TRF2 constructs. More colonies are seen where NHEK express low levels of myc-TRF2 FL than high levels; this was also the case with plates that expressed low or high levels of myc-TRF2$^{\Delta B\Delta M}$. All plates contained a proportion of small colonies of 1-5 cells, known as abortive colonies. The numbers of abortive colonies did not increase in NHEK expressing myc-TRF2 FL or myc-TRF2$^{\Delta B\Delta M}$ when compared to NHEK expressing high levels of Vector only as might have been expected. Instead, the expression of myc-TRF2$^{\Delta B\Delta M}$, and myc-TRF2 FL to a lesser extent, limits the colonies' ability to become larger than 6 cells.

Colony sizes were only quantitated in one experiment; however the clonogenicity pattern was determined in 4 separate experiments and found to be similar in all.

Figure 21. Clonogenicity of NHEK grown for 14 days with low and high levels of myc- TRF2 FL and myc- TRF2$^{\Delta B \Delta M}$.

Cells were flow sorted on day 2, those expressing low and high levels of GFP were collected separately and then plated at $1x10^4$ with feeders. Cells were grown until day 16, at which point the feeders were removed, the NHEK were fixed and stained with Rhodamine B.

Images outlined in red are enlarged insets from their associated pictures.

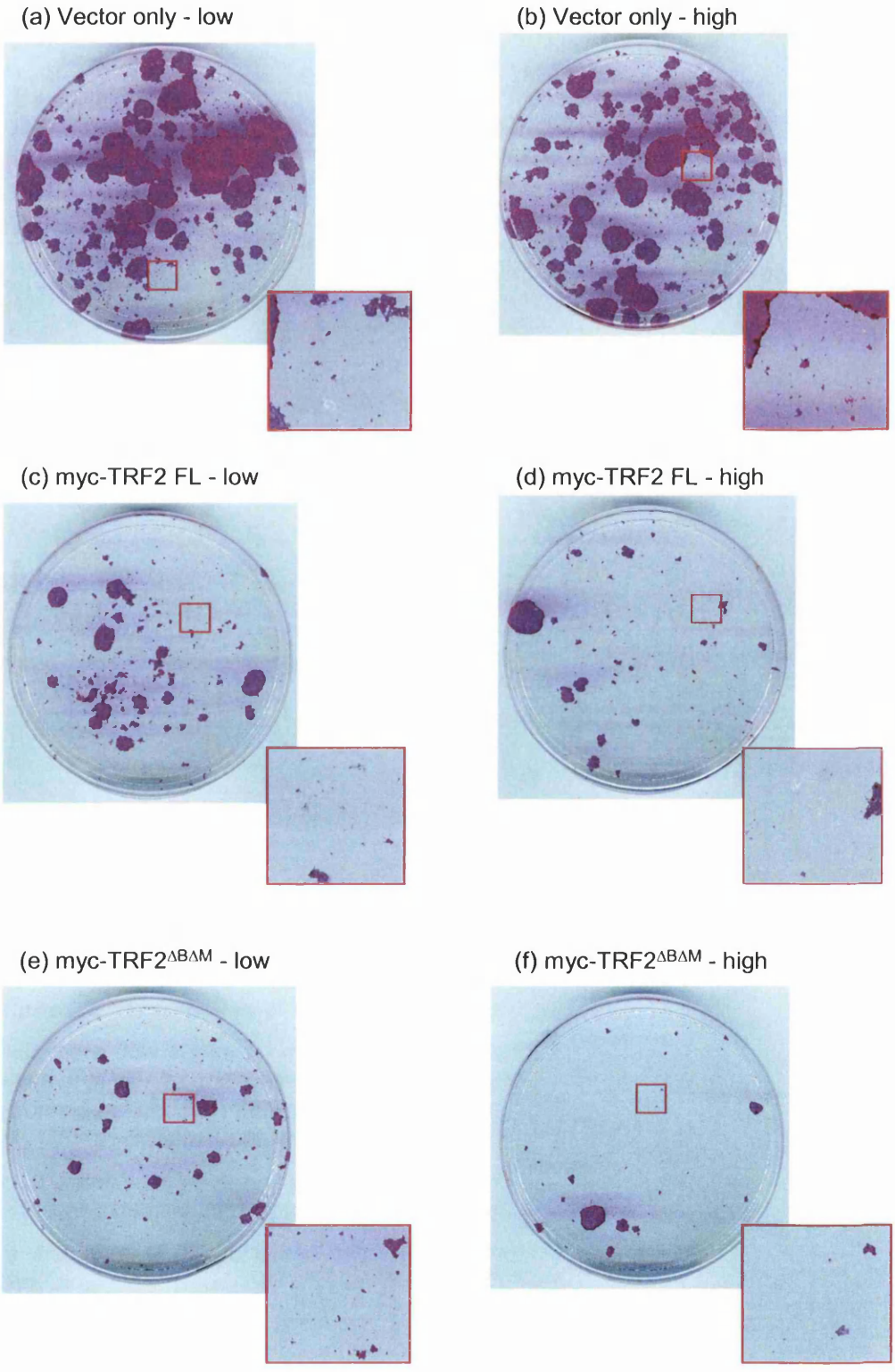

Figure 21. Clonogenicity of NHEK grown for 14 days with low and high levels of myc- TRF2 FL and myc- TRF2$^{\Delta B \Delta M}$.

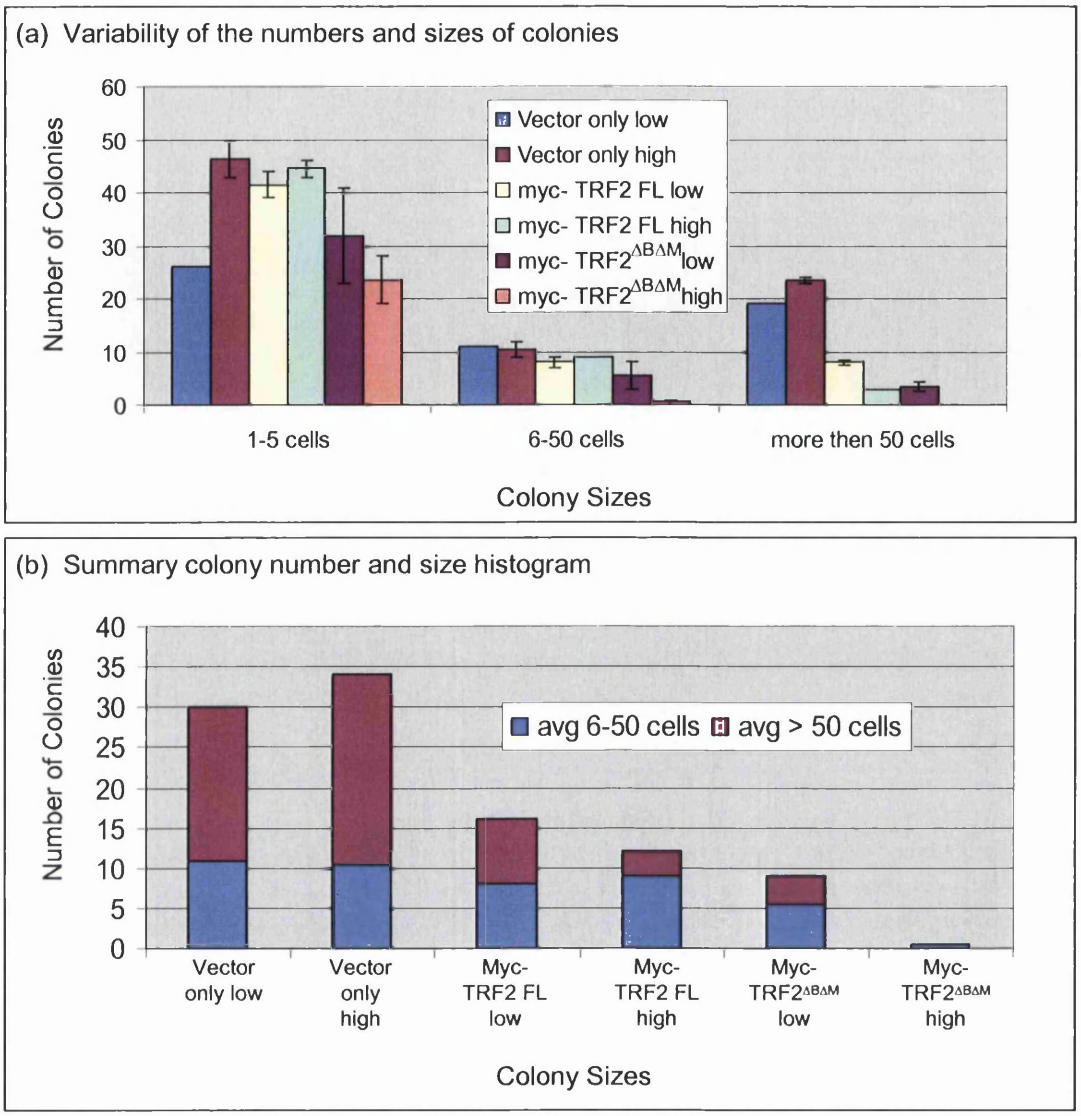

Figure 22. Quantitation of colony numbers and sizes.

Cells were flow sorted on day 2 and then plated at $1x10^4$ with feeders. Cells were grown until day 12 and then colony counts performed. Each 9cm plate was placed on a transparent grid with 40 boxes. A field of view was then assessed for each grid and only GFP positive colonies were scored.

(a) 2 plates were assessed per variable, except for Vector only low for which only one plate was available. The bars represent the individual values.

(b) Summary of the number of colonies with >6 cells for all variables using the same data.

4.4 DNA synthesis in NHEK expressing low or high levels of myc-TRF2 FL or myc-TRF2$^{\Delta B \Delta M}$

Brd-U is a nucleotide analogue that can be incorporated into DNA instead of thymidine during DNA synthesis. As NHEK expressing myc-TRF2 FL and myc-TRF2$^{\Delta B \Delta M}$ contained a mixture of colony sizes, the ability of these differently sized colonies to proliferate was determined by Brd-U incorporation. NHEK have a population doubling time of approximately 24 hours. To determine if the smaller colonies found on plates were replicating, they were incubated with medium containing 100μM Brd-U for 48 hours (**Figure 23**). As anticipated based on colony size, by day 16 all large colonies evaluated on all plates incorporated Brd-U, but small colonies did not. This shows that the small colonies were not undergoing DNA synthesis within a 48 hour period. As 48 hour Brd-U incubation confirmed the clonogenicity pattern seen on the plate where the cells had been cultured for 2 weeks, it was only performed once.

4.5 Understanding Colony Size Variation

These collective experiments show that expressing myc-TRF2 FL or myc-TRF2$^{\Delta B \Delta M}$ in NHEK reduces their ability to proliferate to varying degrees. However clonogenicity studies clearly demonstrate that some colonies on these plates are capable of continuing to proliferate, seemingly uninhibited.

The possibility that the colonies which are able to continue proliferating have managed to down regulate the myc-TRF2 FL or myc-TRF2$^{\Delta B \Delta M}$ was investigated using immunocytochemistry, (**Figures 24, 25, 26** and **27**). For these experiments, cells were fixed prior to being permeabilised as part of the mild immunofluorescence protocol. As a result, it is not possible to visualise endogenous punctate TRF2 staining and the exogenous expression of myc-TRF2 FL and myc-TRF2$^{\Delta B \Delta M}$ is dispersed throughout the nucleus. To try to investigate the differential effect of myc-TRF2 FL and myc-TRF2$^{\Delta B \Delta M}$, experiments using low levels of expression of constructs were evaluated. For each variable, 10 images were taken: 5 of small colonies and 5 of large colonies.

In the Vector only samples, (**Figure 24**), both small and large colonies display diffuse GFP expression throughout the cell.

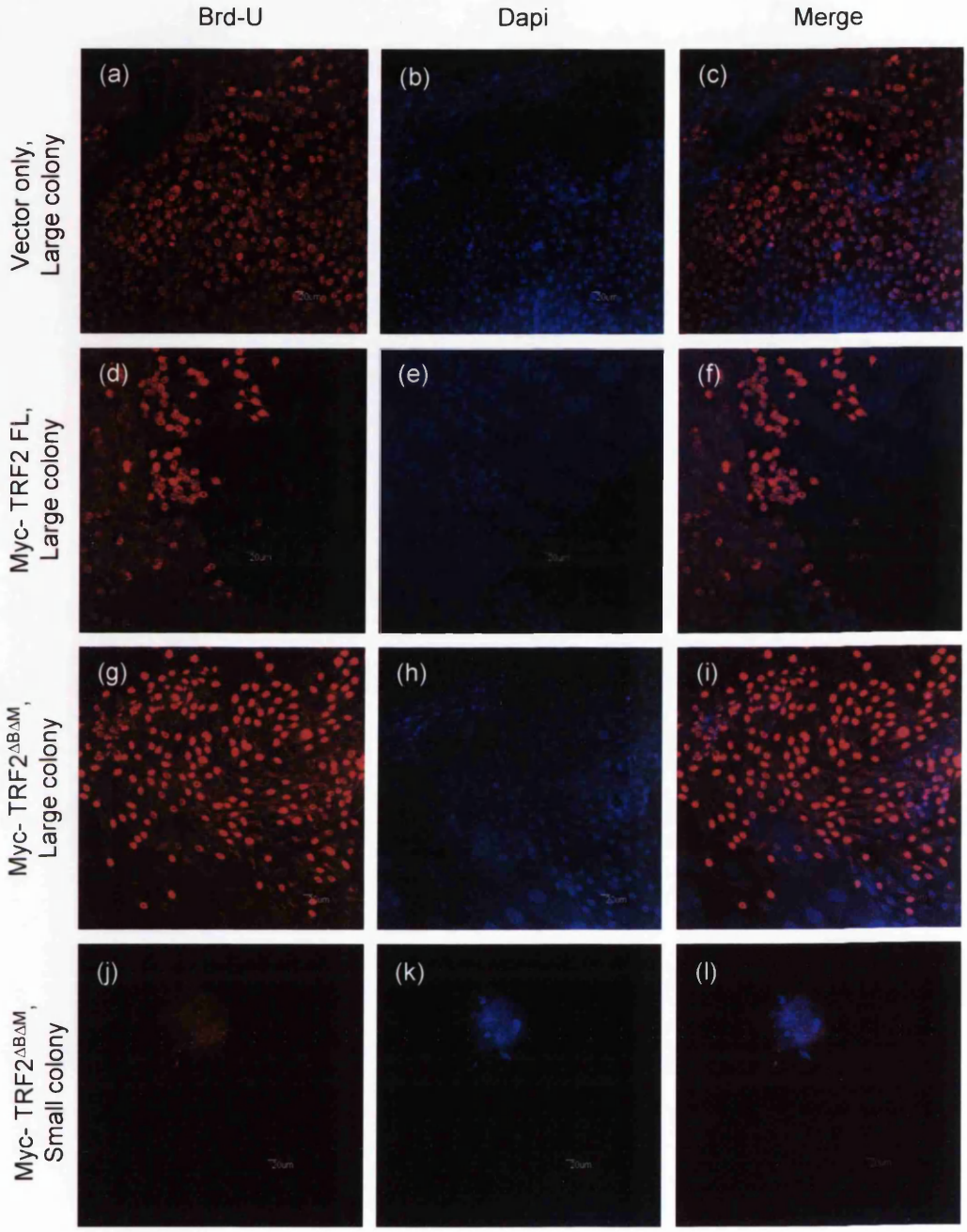

Figure 23. Brd-U incorporation into NHEK grown for 14 days with low levels of myc- TRF2 FL and myc- TRF2$^{\Delta B\Delta M}$.

Cells were flow sorted on day 2. Cells expressing low levels of GFP were collected, plated at 1x10^4 with feeders and grown until day 14 without Brd-U. On days 14 and 15, the medium was changed to include 100 μM Brd-U. Cells were fixed on day 16 and the Brd-U detected using immunofluorescence.

In the large colonies found on (a) Vector only plate, (d) myc-TRF2 FL plate and (g) myc- TRF2$^{\Delta B\Delta M}$ plate, Brd-U incorporation can clearly be seen. (b), (e) and (h) all show dapi staining, a DNA interacting molecule that fluoresces demarking the nucleus. (c), (f) and (i) show the overlay between Brd-U and dapi staining differentiating the cells that have incorporated the Brd-U from those which have not. (j), (k) and (l) show a small colony on the myc- TRF2$^{\Delta B\Delta M}$ plate that has not stained for Brd-U.

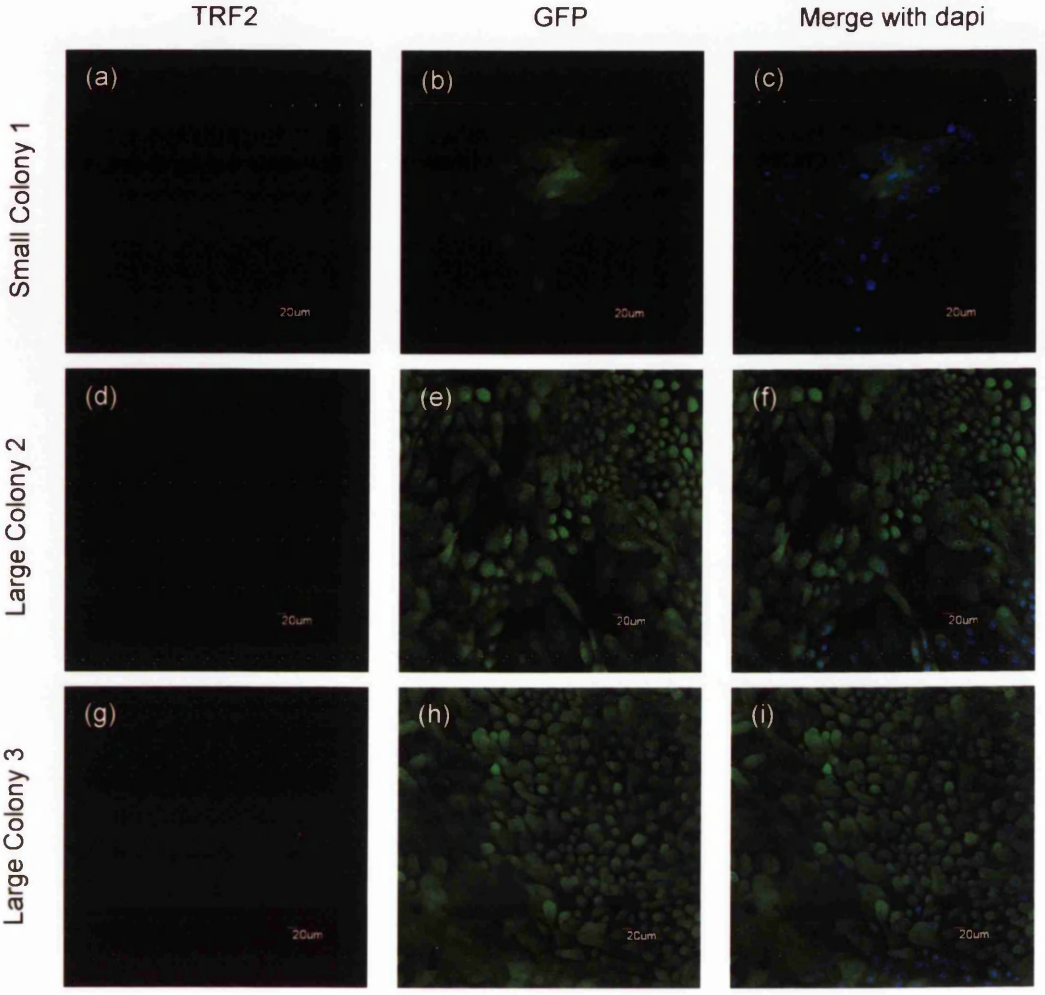

Figure 24. TRF2 levels in NHEK grown for 14 days with low levels of Vector only.

Cells were flow sorted on day 2. Cells expressing low levels of GFP were isolated and plated at $1x10^4$ with feeders, grown for 14 days and then fixed. Dapi staining was used to identify the top and bottom of the nucleus, defining a depth the confocal was to take images through. 1μm Z stacks were taken and merged using the image J program.

In (a), (d) and (g) no signal can be seen from the TRF2 staining, using this mild immunofluorescence staining protocol where cells are fixed prior to being permeabilised. In (b), (e) and (f) GFP present within the cells can easily be detected. (c), (f) and (i) all show the nuclei of each cell as marked by dapi staining nestled within the intensely GFP positive colony.

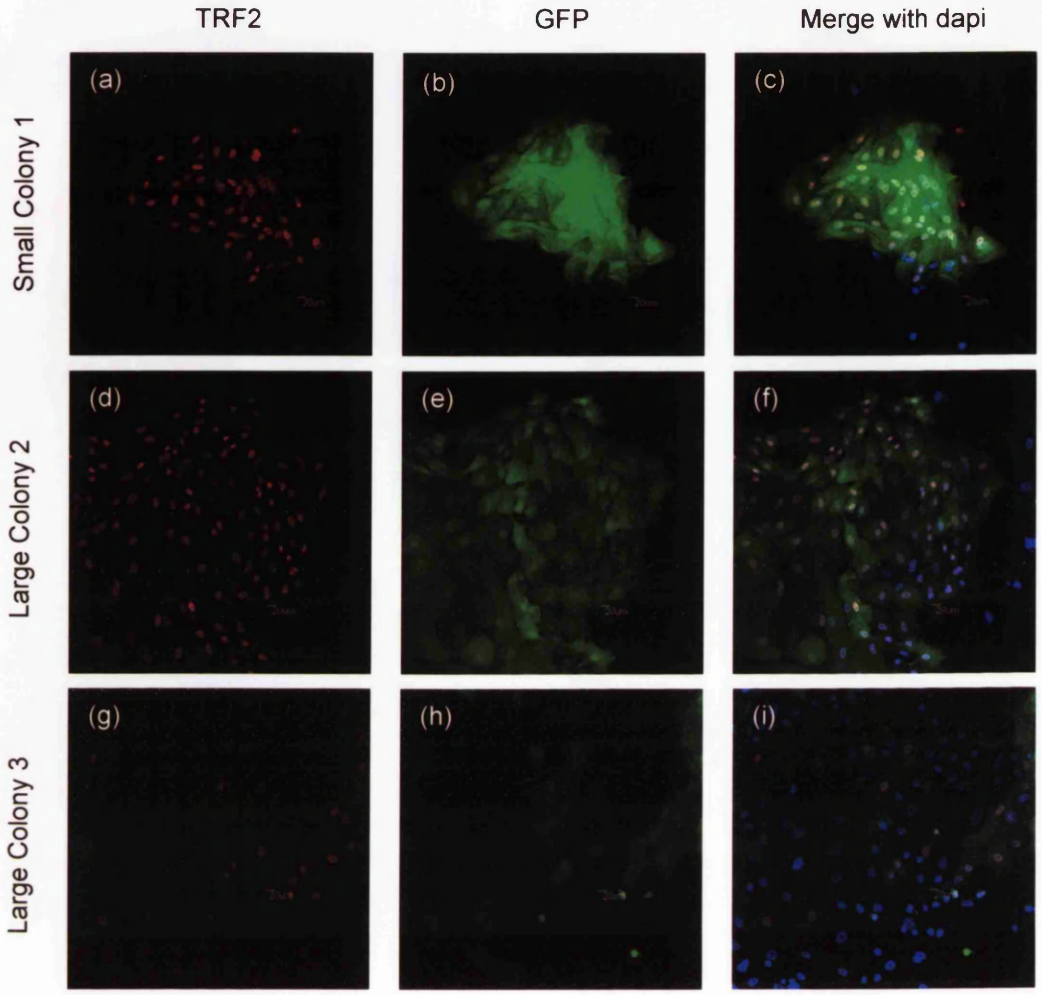

Figure 25. TRF2 Levels in NHEK grown for 14 days with low levels of myc-TRF2 FL. Cells processed as detailed in figure 24.

In (a)-(f) TRF2 staining can be clearly seen in all the GFP positive cells. The TRF2 staining co-localises with the dapi, illustrating it's nuclear localisation. In (g), (h) and (i), the TRF2 staining is not as strong and only the TRF2 positive cells are GFP positive. Dapi staining reveals TRF2 and GFP negative cells within the colony.

In (c) and (f) there are nuclei stained with dapi at the periphery of each colony that are neither TRF2 or GFP positive. Because of their distribution in relation to the TRF2/GFP positive colony it is likely that these are feeders that were not sufficiently removed from the plate.

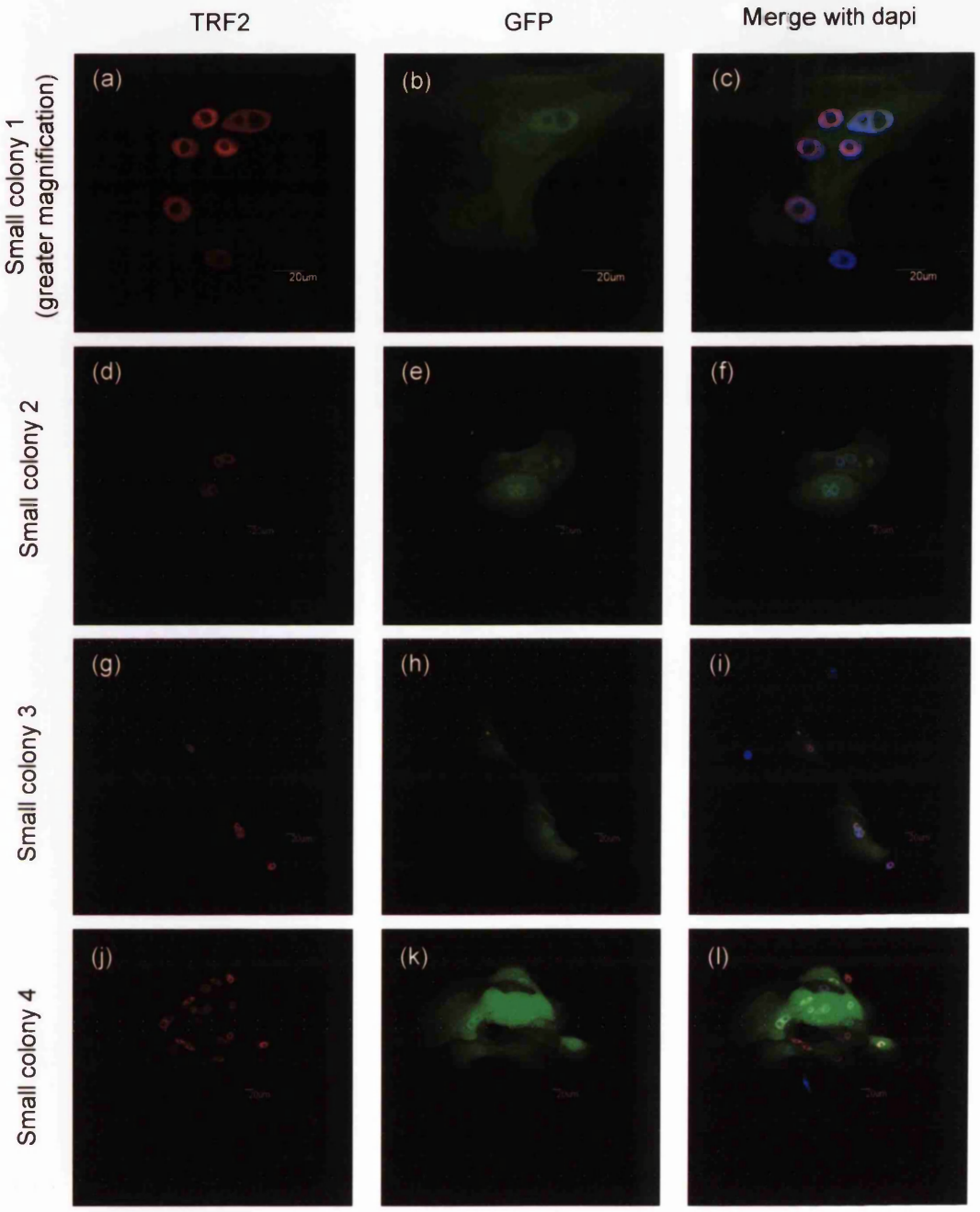

Figure 26. TRF2 Levels in small colonies of NHEK grown for 14 days with low levels of myc- TRF2$^{\Delta B \Delta M}$.

Cells were processed as detailed in Figure 24.

Note: The images in (a) – (c) are at a higher magnification then the other images taken.

In all images, TRF2 staining can be clearly seen in all the GFP positive cells. The merged images with dapi (c), (f), (i) and (l) show the TRF2 signal co-localising with the nucleus, detected using dapi. In both images (i) and (l) nuclei are seen that have not stained positive for TRF2. These cells might either be NHEK that have down-regulated both the TRF2 and the GFP or these are feeders that were not removed from the plate.

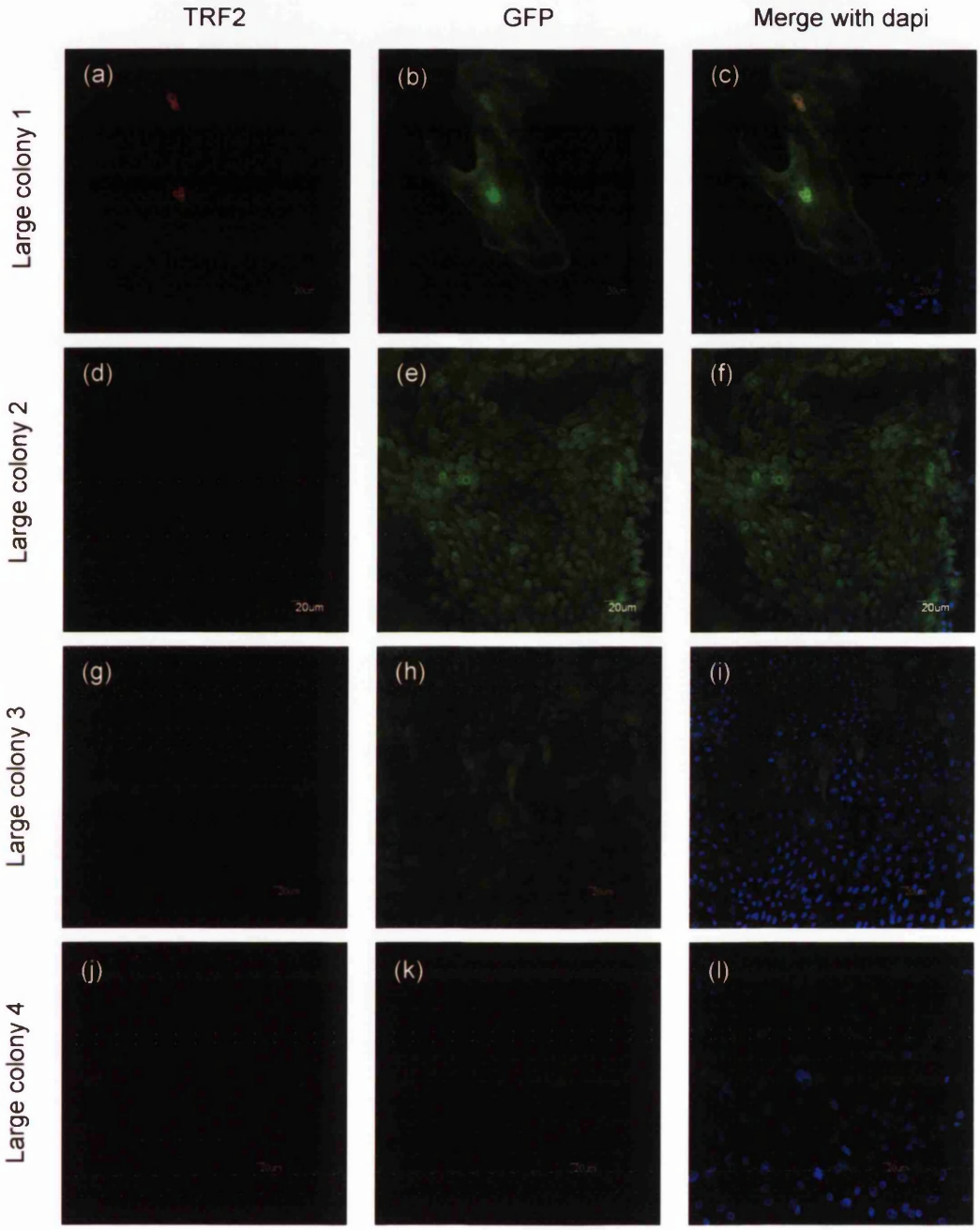

Figure 27. TRF2 levels in large colonies of NHEK grown for 14 days with low levels of myc- TRF2$^{\Delta B \Delta M}$. Cells were processed as detailed in Figure 24.

(a) – (c) In large colony 1, TRF2 staining can be seen in 5 cells (cluster of 3 and 2). The GFP distribution shows how their cytoplasm has spread out. The merged image reveals that these 5 cells are residing either on top or below a much larger colony that does not stain positive for GFP or TRF2.

(d) – (f) In large colony 2, TRF2 staining is extremely weak. The GFP staining remains quite bright. In the merged image, the weak TRF2 staining is not strong enough to contribute to the image.

(g) – (l) In large colonies 3 and 4 there is no TRF2 staining. Large colony 3 is still expressing GFP, however large colony 4 is not.

In NHEK expressing low levels of myc-TRF2 FL, (**Figure 25**), both small and large colonies still express both GFP and myc-TRF2 FL. However, a few large colonies (e.g. large colony 3) appear mosaic in that some cells express myc-TRF2 FL and GFP, but not all.

In NHEK with low levels of expression of myc-TRF2$^{\Delta B\Delta M}$, (**Figure 26**), all small colonies are both GFP and myc-TRF2 FL positive. In all images, but particularly well illustrated in the magnified small colony 1, (**Figure 26**)(**a**) - (**c**), it is possible that large nucleoli are present, however this would need to be confirmed with a nucleoli marker such as nucleophosmin. If the large non-dapi stained structure in the middle of the cell is the nucleolus it would indicate that the cells are arrested in either G1, S or G2, but not stuck in mitosis. In all images of small colonies expressing myc-TRF2$^{\Delta B\Delta M}$ there was no evidence of aberrant mitosis. This indicates that although dysfunctional, the telomeres are unlikely to be arresting the cell cycle in anaphase.

Large colonies found in NHEK expressing low levels of myc-TRF2$^{\Delta B\Delta M}$, (**Figure 27**), do not express myc-TRF2$^{\Delta B\Delta M}$ despite being GFP positive, thus explaining how these colonies are able to grow to such sizes. In large colony number 1, 5 cells stain positive for myc-TRF2$^{\Delta B\Delta M}$ and the GFP in their cytoplasm demonstrates how spread out the cells are. The rest of the colony has down-regulated both myc-TRF2$^{\Delta B\Delta M}$ and GFP. In large colony 2, the entire colony stains very weakly for myc-TRF2$^{\Delta B\Delta M}$, but positive for GFP. This indicates only very low expression of myc-TRF2$^{\Delta B\Delta M}$, which might possibly not be enough to strip the endogenous TRF2 away from the telomeres. In both large colonies 3 and 4, no myc-TRF2$^{\Delta B\Delta M}$ is seen. In large colony 3 GFP is still being expressed, however in large colony 4 even the GFP is no longer expressed. Large colony 4 was probably derived from a cell that had down-regulated the myc-TRF2$^{\Delta B\Delta M}$ construct; however it is possible that this was always a rare GFP/myc-TRF2$^{\Delta B\Delta M}$ negative cell that was not gated out of the cell population properly during cell sorting. Each of the 4 large colonies shown in (**Figure 27**) demonstrate that the large colonies on the myc-TRF2$^{\Delta B\Delta M}$ plate have only managed to grow to such proportions by down-regulating the myc-TRF2$^{\Delta B\Delta M}$ expression to either low levels or by completely turning it off. Undoubtedly, these cells that no longer represent an uncapped telomere population contribute a proportion of the cells counted in the proliferation curves in (**Figure 18**) and (**Figure 20**).

4.6 Identifying Senescent Colonies

Senescence Associated Beta-Galactosidase (B-Gal) activity has been used as an assay for determining senescent fibroblasts and keratinocytes since 1995 (Dimri et al. 1995). Normally contained in the lysosomal compartment and active at pH 4.0, in senescent cells excess amounts of B-Gal are produced resulting in activity in areas outside the lysosome at sub-optimal conditions, such as pH 6.0.

B-Gal activity was assessed in NHEK expressing the TRF2 constructs, (**Figure 28**). Naturally differentiated cells within the NHEK population also stain positive for B-gal. As the cells had been plated at very low density 14 days prior to being analysed, any colony larger then 50 cells was clearly proliferating and any B-gal staining it contained could be attributed to differentiation. In addition to that, almost every colony greater than 50 cells contained a "cuff" of displaced feeder layer (Rheinwald 1980) that also stained B-gal positive (e.g. **Figure 28(a)(ii)**).

For this reason a strict criteria had to be devised in order for B-gal quantitation to be meaningful. To be scored as a senescent colony, the colony had to (1) contain at least one B-Gal positive cell and (2) contain less then 50 cells. Although most of the NHEK that satisfied the criteria had a flattened, spread out morphology, it was not used as part of the criteria used to score the colonies as senescent.

The Beta-Gal staining was very difficult to reproduce. In total, 7 attempts were made in 3 separate experiments to visualise the Beta-Gal staining; however only two attempts proved successful. In both of these 2 experiments, X-galactose was used at 10 mg/mL, more concentrated than in the other 5 experiments where the X-galactose solution was 1 mg/mL, as per the original protocol published by Dimri et al (Dimri et al. 1995). As the integrity of this assay relies on sub-optimal conditions, it would be fair to criticise this modification. However, the clarity of B-gal retention in the lysosome of cells in colonies larger than 50 cells and in other small colonies indicates that excess levels of X-galactose is not giving false positives.

Images from the first experiment are shown in (**Figure 28**)(**a**)-(**c**). The second experiment was performed similarly except that the cells were plated at a higher density and were analysed on day 12, (**Figure 28**)(**d**). Vector only plates

Figure 28. Beta-Galactosidase staining of NHEK expressing low levels of myc-TRF2 FL and myc- TRF2$^{\Delta B \Delta M}$.

Cells were flow sorted on day 2 and those expressing low levels of GFP were isolated and plated at $1x10^4$ with feeders. On day 16, the cells were stained for senescence associated Beta-Galactosidase (B-gal). Images outlined in black are all at 25X magnification and those outlined in red are enlarged insets from within the images as marked.

(a) (i) and (ii) Vector only plates contained mostly large colonies that were not B-gal positive, although (iii) some naturally senescent colonies did occur.

(b) (i) and (ii) Myc-TRF2 FL plates also contained a mixture of B-gal negative and (iii) positive colonies.

(c) (i), (ii) and (iii) The myc-TRF2$^{\Delta B \Delta M}$ plates contained many B-gal positive colonies.

(d) In a different experiment, cells were flow sorted on day 2, but plated at the higher density of $2x10^4$ with feeders and harvested on day 12. B-gal positive colonies were scored looking at 40 separate fields of view on each plate as described in Chapter 2. Two plates were considered for each variable and the bars represent the numbers of positive colonies on duplicate plates.

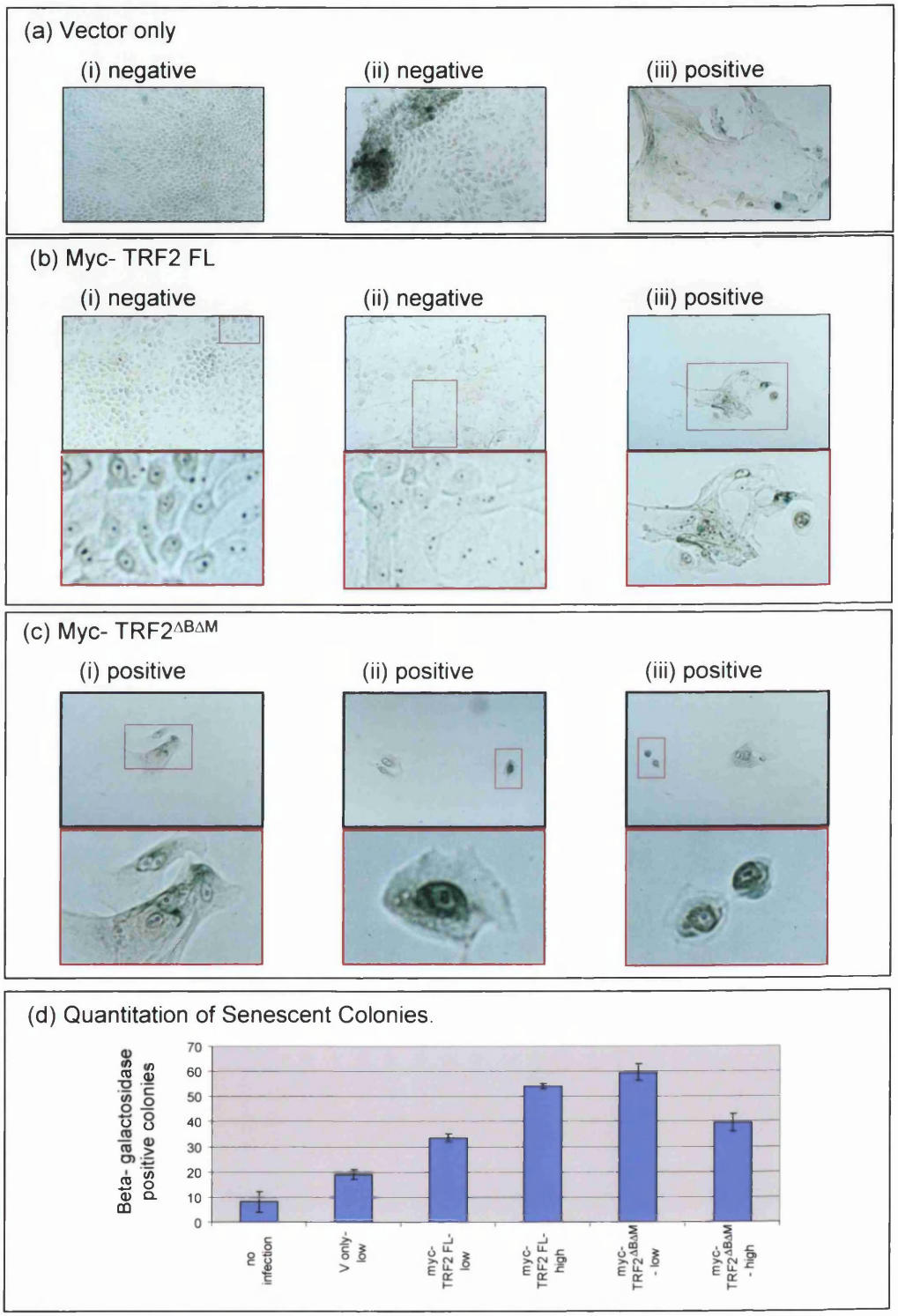

Figure 28. Beta-Galactosidase staining of NHEK expressing low levels of myc- TRF2 FL and myc- TRF2$^{\Delta B \Delta M}$.

contained mostly large colonies that were not B-gal positive, although some naturally senescent colonies did occur. Myc-TRF2 FL plates also contained a mixture of B-gal negative and positive colonies. In contrast, the myc- $TRF2^{\Delta B \Delta M}$ plates contained many B-gal positive colonies.

The relative numbers of senescent colonies were similar in each experiment with the exception that not as many senescent colonies were found in the NHEK expressing high levels of myc-TRF2 FL.

As senescent colonies are known to arrest with a G1 DNA content (Chen et al. 1998) the next investigation was to determine where in the cell cycle the non-proliferating NHEK were arrested, in order to confirm a G1 arrest.

4.7 Cell Cycle Analysis of Keratinocytes

Flow Assisted Cell Sorting (FACS) analysis of cells can determine the DNA content of individual cells within a population when they have been labelled with a DNA binding dye such as Propidium Iodide (PI). Cells in the G1 phase of the cell cycle are said to contain 2N DNA content, cells in G2 contain 4N DNA content and cells in S phase contain a DNA content in between 2N and 4N.

Before evaluating the DNA content of NHEK expressing the TRF2 constructs, control experiments were performed to establish cell cycle profiles of NHEK treated with different cell cycle inhibitors. Cells were either arrested using Hydroxyurea (HU) or subjected to low and high doses of γ-IR to assess where cells arrest in the cell cycle as a result of multiple double strand breaks (**Figure 29**). Treating NHEK with 1.0 mM HU for 24 hours was enough to growth arrest the cells at the G1/S boundary, (**Figure 29(a)**. This control was helpful in determining a profile of NHEK arrested with a 2N DNA content. Treating NHEK with a low, 2 Gy γ-IR dose, resulted in a small accumulation of cells in G2 at 6 hours and then a return to a "normal" (i.e. a cell cycle distribution as seen in untreated cells) cell cycle profile by 12 hours. NHEK subjected to a high, 20 Gy γ-IR dose resulted in a build-up of cells in G2, 18 hours after the γ-IR. What is not clear in this Figure is whether or not the cells in G1 are arrested in G1 or if these cells were repaired after the γ-IR dose was administered and these cells are cycling normally. It was unexpected to see normal cells with wild type p53

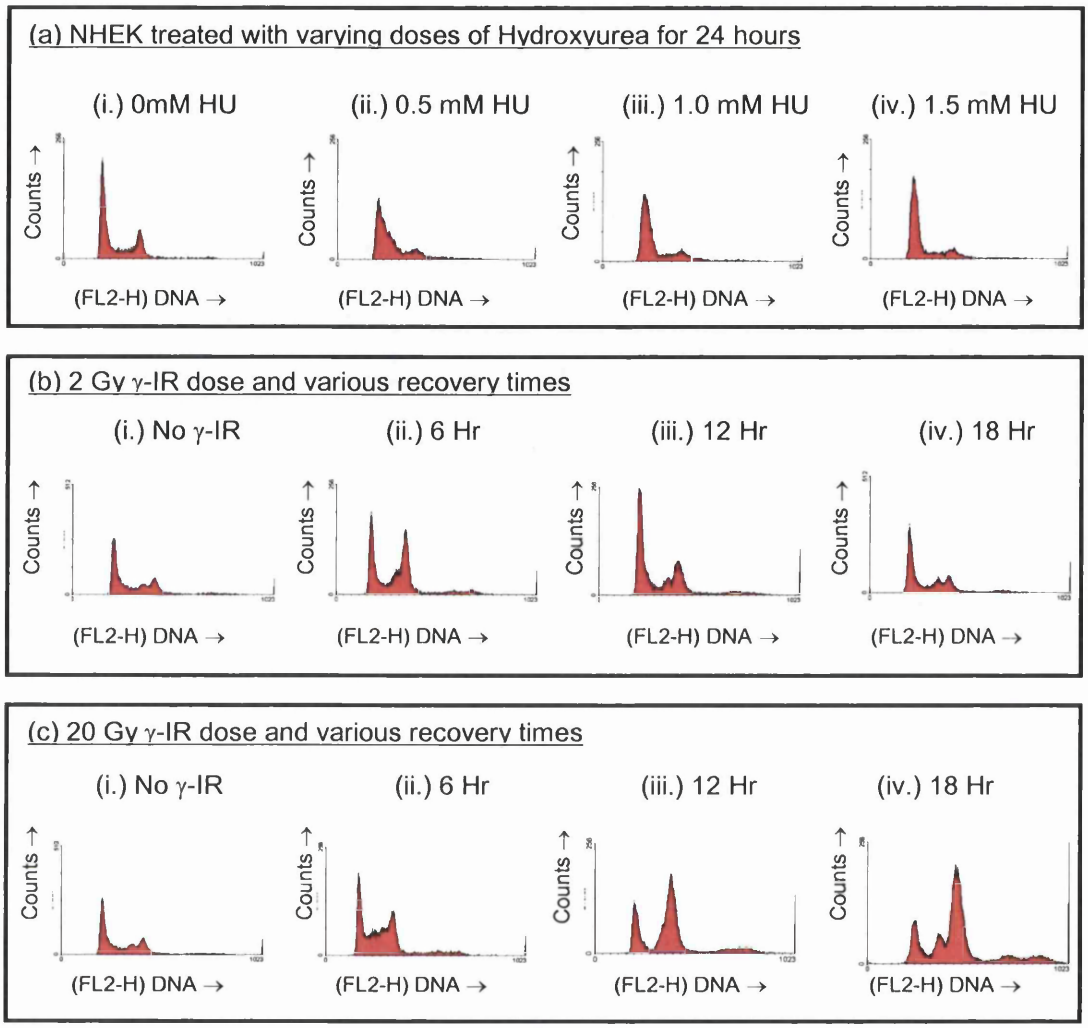

Figure 29. Cell cycle analysis profiles of NHEK treated with Hydroxyurea or γ-IR.

(a) (i.) Cell cycle profile determined by FACS in untreated NHEK. (ii.) 0.5 mM HU slows the cell cycle and prevents entry into S phase. (iii.) 1 mM and (iv.) 1.5 mM HU causes cell cycle arrest at the G1/S boundary.

(b) (ii.) 6 hours after 2 Gy of γ-IR a small accumulation of NHEK in G2 can be detected. (iii.) 12 and (iv.) 18 hours after 2 Gy of γ-IR, NHEK resume normal profiles.

(c) (ii.) 6 hours after 20 Gy of γ-IR an accumulation of NHEK in S phase is observed. (iii.) 12 hours later the majority of NHEK are either in G1 or G2 and (iv.) 18 hours later most of the NHEK are in G2.

arresting in G2 as opposed to G1 after γ-IR, however this is not unprecedented (Scott et al. 2004). It has been shown that the exposure of normal human fibroblasts to genotoxic agents provokes permanent cell cycle exit in the G2 phase of the cell cycle, whereas mouse embryo fibroblasts and transformed human cells progress through mitosis and arrest in G1 without intervening cytokinesis (Baus et al. 2003).

Current literature has established that naturally occurring (d'Adda di Fagagna et al. 2003) or experimentally created (Takai et al. 2003) dysfunctional telomeres are recognised as DNA double strand breaks, resulting in human fibroblasts arresting in G1. Given that the NHEK with double strand breaks caused by exposure to γ-IR arrest in G2, it was of interest to determine where in the cell cycle the NHEK arrest after the exogenous expression of myc-TRF2 FL or myc-TRF2$^{\Delta B\Delta M}$.

4.8 Cell Cycle Analysis of Keratinocytes expressing myc-TRF2 FL and myc-TRF2$^{\Delta B\Delta M}$

In addition to labelling cells with PI to determine their DNA content, the percentage of cells in S phase can be measured after a limited exposure to Brd-U (e.g. 30 min). By staining cells for Brd-U during FACS analysis it is then possible to better define the proportion of cells in S phase and obtain more accurate percentages of cells in G1 or G2.

10 days after infection with myc-TRF2 FL or myc-TRF2$^{\Delta B\Delta M}$, NHEK were given a 30 min Brd-U pulse immediately prior to being harvested for cell sorting. Being aware of the growth advantage shown by NHEK that have managed to either partially or completely down-regulate the myc-TRF2$^{\Delta B\Delta M}$/GFP expression on day 16, day 10 was chosen for this cell cycle analysis (**Figure 30**). The rationale was that the ratio of cells growth arrested by the myc-TRF2$^{\Delta B\Delta M}$ would still be high enough at this point to dominate the FACS analysis cell cycle profile. Labelling NHEK with Brd-U prior to FACS analysis provided good cell cycle analysis profiles, but unexpectedly did not provide evidence of a G1 or G2 cell cycle arrest (**Figure 30**). The variation in the cell cycle distribution was not considerably different in cells expressing Vector only, myc-TRF2 FL or myc-TRF2$^{\Delta B\Delta M}$.

Figure 30. Cell cycle profiling of NHEK 10 days after expression of (a) and (b) Vector only, (c) myc-TRF2 FL and (d) myc-TRF2$^{\Delta B \Delta M}$.
All GFP positive NHEK were seperated from GFP negative cells on day 10 immediately after Brd-U labelling of cells for 30 min [except in (a)]. The cells were then fixed and cell cycle profiling was performed by FACS analysis.
R1 = Whole cells are defined based on cell granularity vs. cell size.
R2 = Single cells are defined and cell doublets and triplicates are excluded.
R3 = NHEK with a G1 (or 2N) DNA content. (Except in (a) where no Brd-U is used.)
R4 = NHEK that stain positive for Brd-U and are therefore considered to be is S phase with a DNA content between 2N and 4N. (R4 was defined in (a)(iii) where the cells were not incubated with Brd-U and the region is therefore empty.)
R5 = NHEK with a G2 (or 4N) DNA content. (Except in (a) where no Brd-U is used.)

(a) Control sample in which Vector only cells were not labelled with Brd-U. (iv.) Cell cycle histogram shows a normal distribution.
(b) Vector only shows (iii.) a clear incorporation of Brd-U in R4 and cell cycle distribution percentages indicate a normal cell cycle profile (iv.).
(c) myc-TRF2 FL. The distribution of cells (iii.) and (iv.) is almost unchanged from NHEK containing Vector only.
(d) myc-TRF2$^{\Delta B \Delta M}$. The distribution of cells (iii.) and (iv.) is almost unchanged from NHEK containing Vector only or myc-TRF2 FL.

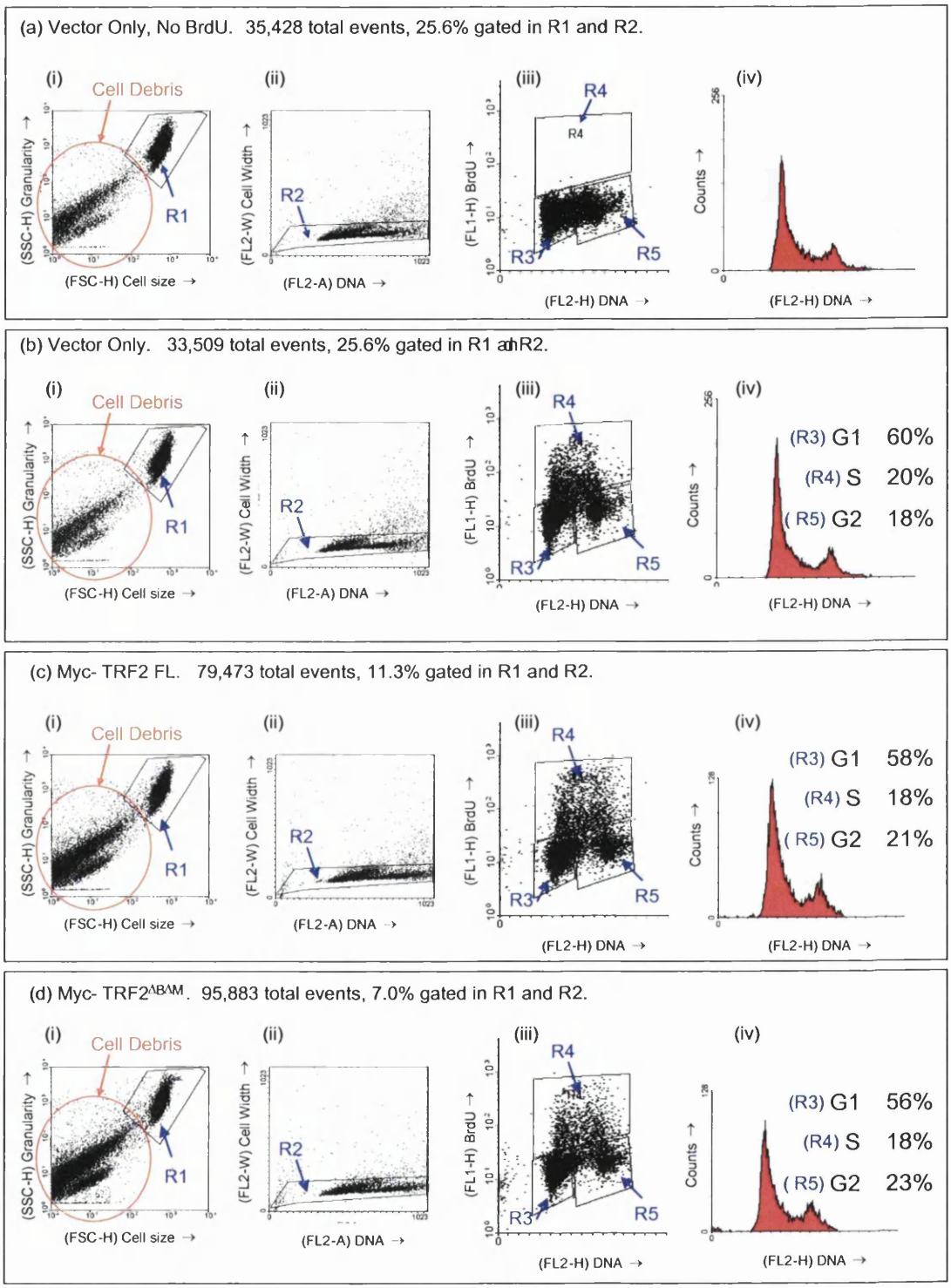

Figure 30. Cell cycle profiling of NHEK 10 days after expression of (a) and (b) Vector only, (c) myc-TRF2 FL and (d) myc-TRF2$^{\Delta B \Delta M}$.

One explanation for this might be that cell cycle arrested TRF2 construct expressing cells might be "lost" during cell cycle analysis. The fact that the percentage of cells being gated in TRF2 construct expressing cells is reduced suggests that this is the case. 25.6% of NHEK expressing Vector only, with or without Brd-U label were gated in R1 and R2. In NHEK expressing myc-TRF2 FL, that percentage decreased to 11.3% and in myc-TRF2$^{\Delta B\Delta M}$ it fell to 7%. The amount of cell debris clearly increases in both these samples, (**Figure 30**), indicating that the cells were not stable enough to remain intact for both the flow sorting and the FACS analysis. Based on the images obtained in (**Figure 27**), it appears that the only cells being assayed from the myc-TRF2$^{\Delta B\Delta M}$ population are those which are GFP positive and myc-TRF2$^{\Delta B\Delta M}$ negative. As part of the same experiment, NHEK were flow sorted and then harvested on days 8 and 12 for western blot analysis, (**Figure 31**). Myc-TRF2 FL is expressed on day 8, but considerably less is expressed on day 12, whereas a small amount of myc-TRF2$^{\Delta B\Delta M}$ expression is still seen on day 8, however by day 12 it has disappeared.

In another experiment (not shown), NHEK were flow sorted into low and high GFP expressing fractions and plated on day 2 and then analysed using FACS analysis on days 8, 12 and 15, i.e. without further flow sorting immediately prior to FACS analysis. Normal cell cycle profiles were seen in each sample; however the pattern of increased cell debris when progressing from cells expressing Vector only to myc-TRF2 FL to myc-TRF2$^{\Delta B\Delta M}$ also increased as described in (**Figure 30**).

It should be noted that there is an apparent contradiction between the expression levels of myc-TRF2$^{\Delta B\Delta M}$ in cells dependent on whether or not they were cell sorted 12 - 14 days after infection. A western blot in (**Figure 16**) demonstrates substantial expression of myc-TRF2$^{\Delta B\Delta M}$ at day 13 and (**Figure 31**) shows complete loss of myc-TRF2$^{\Delta B\Delta M}$ on day 12. This apparent anomaly is explained by the fact that in (**Figure 16**) the cells were not flow sorted immediately prior to harvest, whereas in (**Figure 31**) they were. (**Figure 26**) shows that on day 14 the small colonies were still expressing both GFP and myc-TRF2$^{\Delta B\Delta M}$: these cells were plated on day 2 and not flow sorted again before being fixed for the experiment. The conclusion that can be drawn from these experiments is that NHEK expressing myc-TRF2$^{\Delta B\Delta M}$ inhibited in mid-late stage

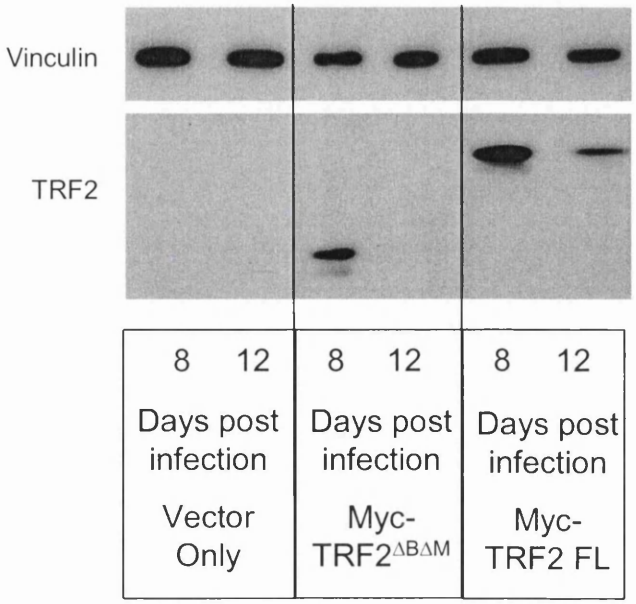

Figure 31. TRF2 expression in NHEK infected with myc-TRF2 FL and myc-TRF2$^{\Delta B\Delta M}$ on days 8 and 12 after flow sorting.

NHEK were flow sorted on day 8 or 12 and then immediately harvested for western blot analysis. Vinculin is used as a loading control in this western blot and shows even loading in all lanes. Between 8 and 12 days after infection, myc-TRF2$^{\Delta B\Delta M}$ expression is lost from NHEK despite the fact they are still expressing GFP. Some myc-TRF2 FL is still produced on day 12 although substantially less then that being expressed in day 8.

proliferation are not strong enough to withstand the rigour of flow sorting and FACS analysis.

4.9 Summary of Chapter 4

Expression of TRF2 constructs in NHEK results in reduced proliferation. High expression levels of myc-TRF2 FL cause a more drastic reduction in proliferation than low levels of expression, for reasons as yet undetermined. Expression of myc-TRF2$^{\Delta B \Delta M}$ resulted in an even more dramatic reduction of cell proliferation, again with higher levels of expression being more effective then lower levels.

NHEK expressing myc-TRF2$^{\Delta B \Delta M}$ were not capable of growing larger than 50 cells, however NHEK expressing myc-TRF2 FL were. Plates of NHEK expressing myc-TRF2$^{\Delta B \Delta M}$ stained with Rhodamine B also contain large colonies, however in this case immunofluorescence demonstrated that such large colonies no longer expressed the myc-TRF2$^{\Delta B \Delta M}$ construct. Plates of NHEK expressing myc-TRF2 FL stained with Rhodamine B show varying colony sizes and immunofluorescence demonstrates that some, but not all, large colonies are still expressing the construct.

Brd-U incorporation formally established that the only NHEK infected with either Vector only, myc-TRF2 FL or myc-TRF2$^{\Delta B \Delta M}$, and still proliferating on day 14 were those in the large colonies. Colonies of less then 50 cells did not incorporate Brd-U within a 48 hour time period.

Uncapped telomeres generated by myc-TRF2$^{\Delta B \Delta M}$ expression in NHEK induce senescence. Counting B-gal stained plates expressing Vector only, myc-TRF2 FL or myc-TRF2$^{\Delta B \Delta M}$ revealed a higher number of B-gal positive colonies in NHEK expressing myc-TRF2 FL, and even more so when myc-TRF2$^{\Delta B \Delta M}$ was expressed.

Paradoxically, NHEK expressing TRF2 constructs analysed by FACS analysis had normal cell cycle profiles similar to Vector only or uninfected cells. The most likely explanation is that the cells arrested as a consequence of expressing myc-TRF2 FL or myc-TRF2$^{\Delta B \Delta M}$ are lost during the FACS profiling.

Chapter 5:

Examining the mechanism to inhibit NHEK proliferation used by myc-TRF2 FL or myc-TRF2$^{\Delta B \Delta M}$

In NHEK, myc-TRF2 FL and myc-TRF2$^{\Delta B \Delta M}$ over-expression causes a reduction of cell proliferation to varying degrees. To evaluate how expression of the TRF2 constructs was actually causing this phenotype within the NHEK, the DNA damage response was investigated to assess if it was being elicited by the cells.

5.1 Immunofluorescence studies of the localisation of low and high levels of myc-TRF2 FL or myc-TRF2$^{\Delta B \Delta M}$ within NHEK

Using a protocol for immunofluorescence that permeabilises the NHEK before fixation, it was possible to detect punctate staining of both telomeric binding proteins TRF1 and TRF2, low expression levels - (**Figure 32**) and high expression levels - (**Figure 33**). In NHEK expressing the Vector only, punctuate spots of endogenous TRF1 and TRF2 were found to co-localise. As expected, much more TRF2 was detected in the cells expressing myc-TRF2 FL. The exogenous myc-TRF2 FL co-localised with TRF1 confirming its presence at the telomere. In NHEK expressing low levels of myc-TRF2$^{\Delta B \Delta M}$, far less punctate staining of TRF2 was seen, demonstrating the ability of the myc-TRF2$^{\Delta B \Delta M}$ to strip endogenous TRF2 from the telomere.

A differential effect was seen in the proliferation curves, particularly for cells expressing low vs. high levels of myc-TRF2 FL (Chapter 4 - **Figure 20**). Side by side comparison of different fields of view in this experiment demonstrate it is not possible to see more myc-TRF2 FL being bound where high levels are expressed as opposed to low levels, (**Figure 34**). Likewise, with myc-TRF2$^{\Delta B \Delta M}$, there is no evidence that more endogenous TRF2 is stripped from the telomere when high levels of the construct are expressed.

Intriguingly, endogenous levels of both TRF1 and TRF2 are better visualised in NHEK expressing high levels of Vector only (as opposed to low levels), it is not clear why this is.

Figure 32. Co-localisation of TRF1 and TRF2 in NHEK expressing low levels of myc-TRF2 FL and myc-TRF2$^{\Delta B \Delta M}$ on day 4.

Cells were flow sorted on day 2, and those expressing low levels of GFP were isolated and plated on 3T3 conditioned coverslips without feeders. Cells were grown for 2 days and permeabilised prior to being fixed using the stringent immunofluorescence protocol. The plane of focus was adjusted until the dapi stained nuclei were at their largest for as many cells as possible. 1 μm start and stop Z section positions were then defined either side of that middle point. The confocal (Olympus FV1000) was set to take 0.2μm Z stack images that were then merged using the NIH image J program.

(a) – (c) Vector only. Punctate staining of TRF1 and 2 is seen in individual panels and co-localisation is seen where the images are merged. (d) Merge inset.

(e) – (g) myc-TRF2 FL. Considerably more TRF2 is seen binding to the telomere then compared to vector only panel. The TRF1 and TRF2 staining still merges indicating the myc-TRF2 FL construct is binding to the telomere. (h) Merge inset.

(i) – (k) myc-TRF2$^{\Delta B \Delta M}$. Less TRF2 is seen in this sample then in Vector only. This is consistent with the proposed mechanism that myc-TRF2$^{\Delta B \Delta M}$ strips endogenous TRF2 from telomeres. (l) Merge inset.

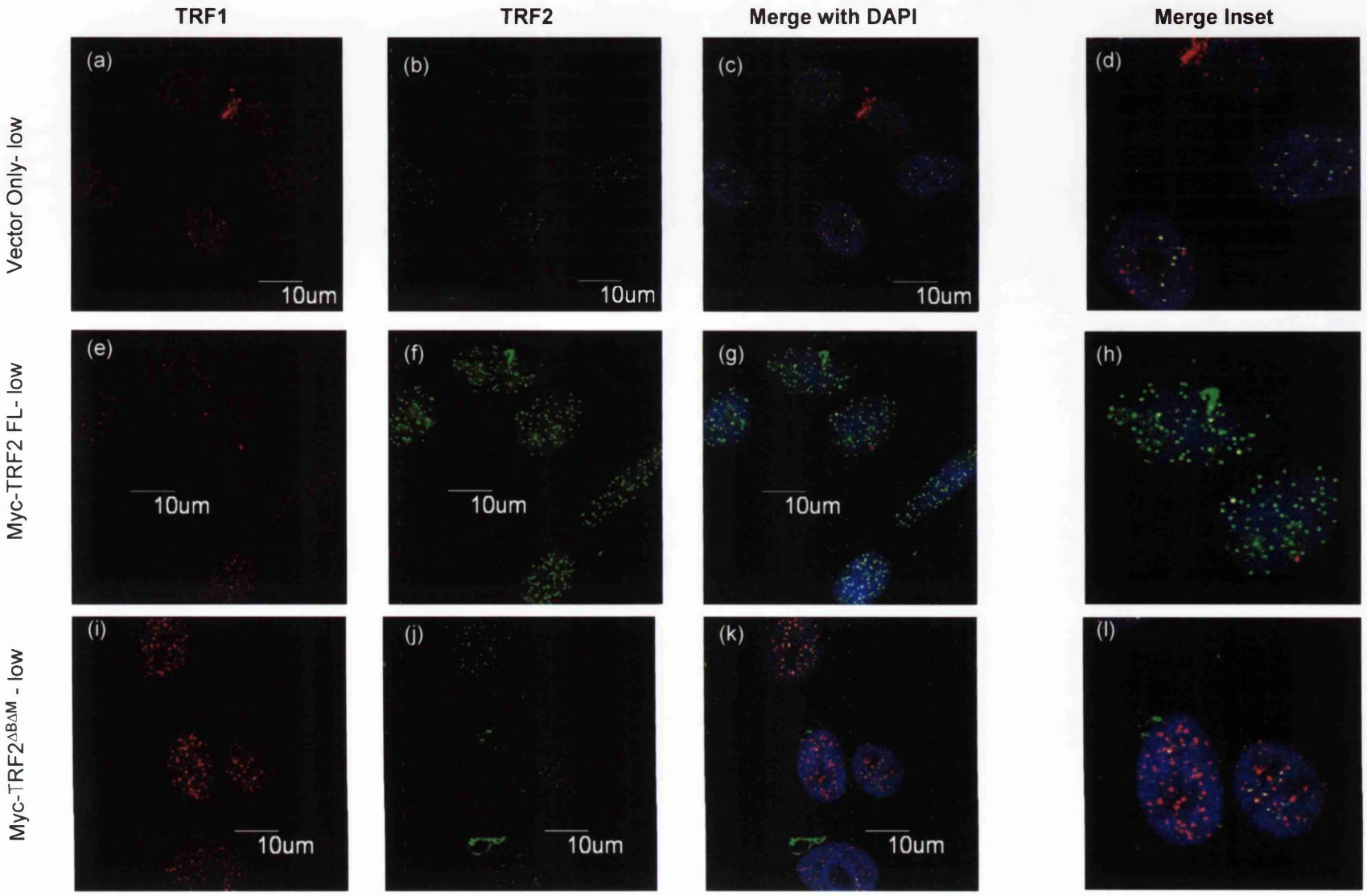
TRF1
TRF2
Merge with DAPI
Merge Inset
Vector Only- low
Myc-TRF2 FL- low
Myc-TRF2ΔBΔM - low
(a)
(b)
(c)
(d)
(e)
(f)
(g)
(h)
(i)
(j)
(k)
(l)
10um

Figure 33. Co-localisation of TRF1 and 2 in NHEK expressing high levels of myc-TRF2 FL and myc-TRF2$^{\Delta B \Delta M}$ on day 4. Images were obtained as detailed in Figure 32.

Over 70 nuclei per variable (NHEK expressing high levels of GFP) from 2 independent experiments were assessed and their foci scored as either (red) TRF1 or (green/ yellow) TRF2/merged foci.

(a) – (d) As in Figure 32, endogenous levels of TRF1 and 2 co-localise at telomeres in NHEK expressing high levels of Vector only. Endogenous levels of both TRF1 and TRF2 are brighter in this Figure then in Figure 32. Vector only demonstrates a large degree of TRF1 and TRF2 co-localisation. The percentage of (red) TRF1 foci is 32% of the total number of foci.
(e) – (h) High levels of myc-TRF2 FL can be seen in these images co-localising with TRF1. Localised over-expression of TRF2 is evident where myc-TRF2 FL is expressed and the percentage of (red) TRF1 foci is 29%.
(i) – (l) Substantially less TRF2 is found bound at the telomeres in these cells while TRF1 levels remain normal. The loss of TRF2 staining is apparent were myc-TRF2ΔBΔM is expressed and the % of TRF1 foci becomes 77%.

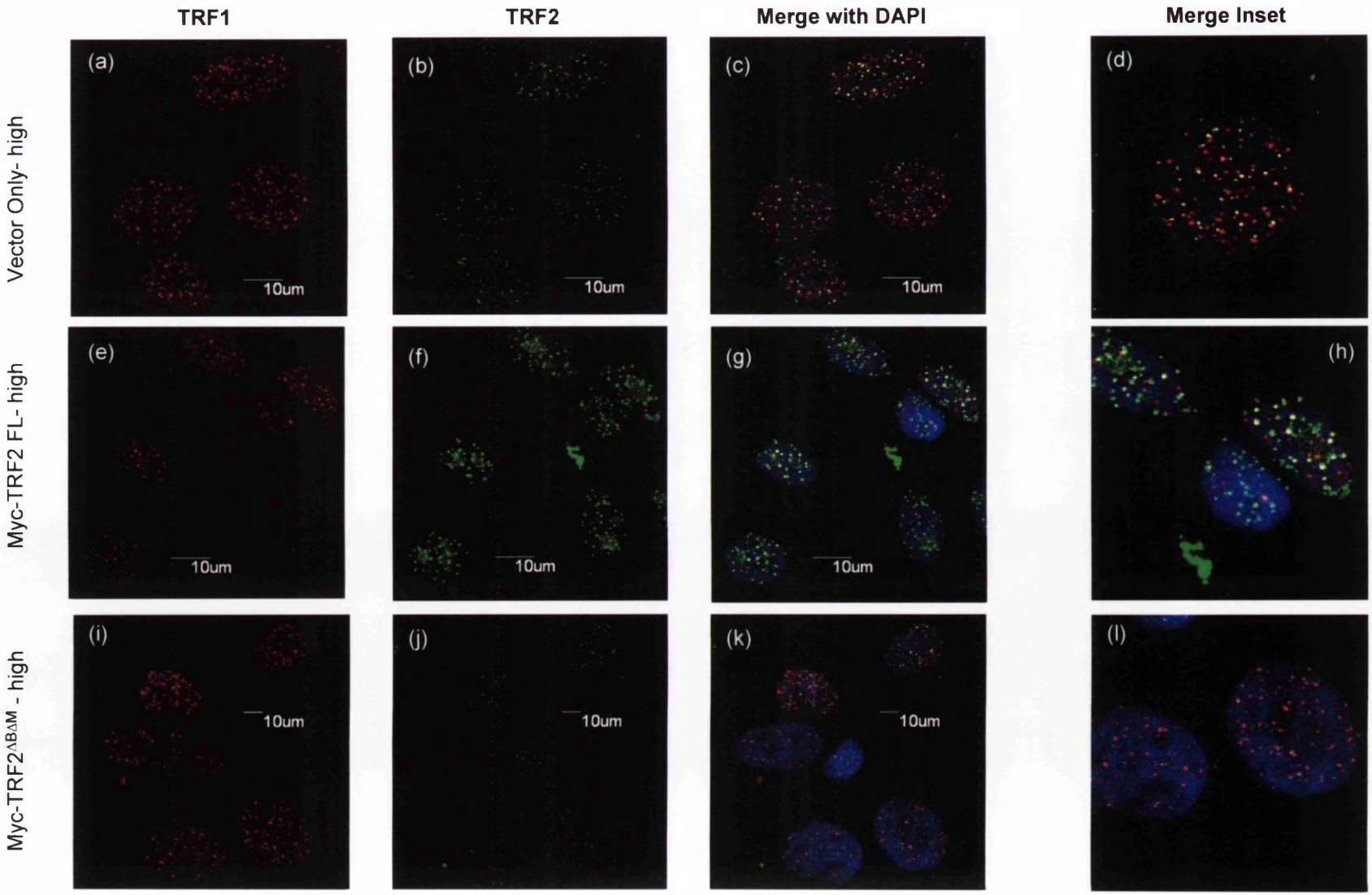
TRF1
TRF2
Merge with DAPI
Merge Inset
Vector Only- high
Myc-TRF2 FL- high
Myc-TRF2ΔBΔM - high
(a)
(b)
(c)
(d)
(e)
(f)
(g)
(h)
(i)
(j)
(k)
(l)
10um

Figure 34. Side by side comparison of low vs. high levels of myc-TRF2 FL and myc-TRF2$^{\Delta B \Delta M}$ in NHEK on day 4. These images were obtained as part of the same experiment as detailed in Figures 32 and 33. However, different fields of view are shown.

(a) – (f) Both low and high expressing Vector only cells show co-localisation of TRF1 and 2 again. Inexplicably, endogenous levels of TRF1 and TRF2 are higher in the Vector only high cells as opposed to Vector only low.
(g) – (l) Both low and high levels of myc-TRF2 FL display an increase in TRF2 staining compared to Vector only, however myc-TRF2 FL high does not show an increased amount of TRF2 bound to the telomere compared with myc-TRF2 low.
(m) – (r) Substantially less TRF2 staining occurs in NHEK expressing either low or high levels of myc-TRF2$^{\Delta B \Delta M}$. Less punctate staining of TRF2 is seen outside the dapi stained nucleus in both images (o) and (r). It is possible that this staining is either myc-TRF2$^{\Delta B \Delta M}$ being produced or degraded.

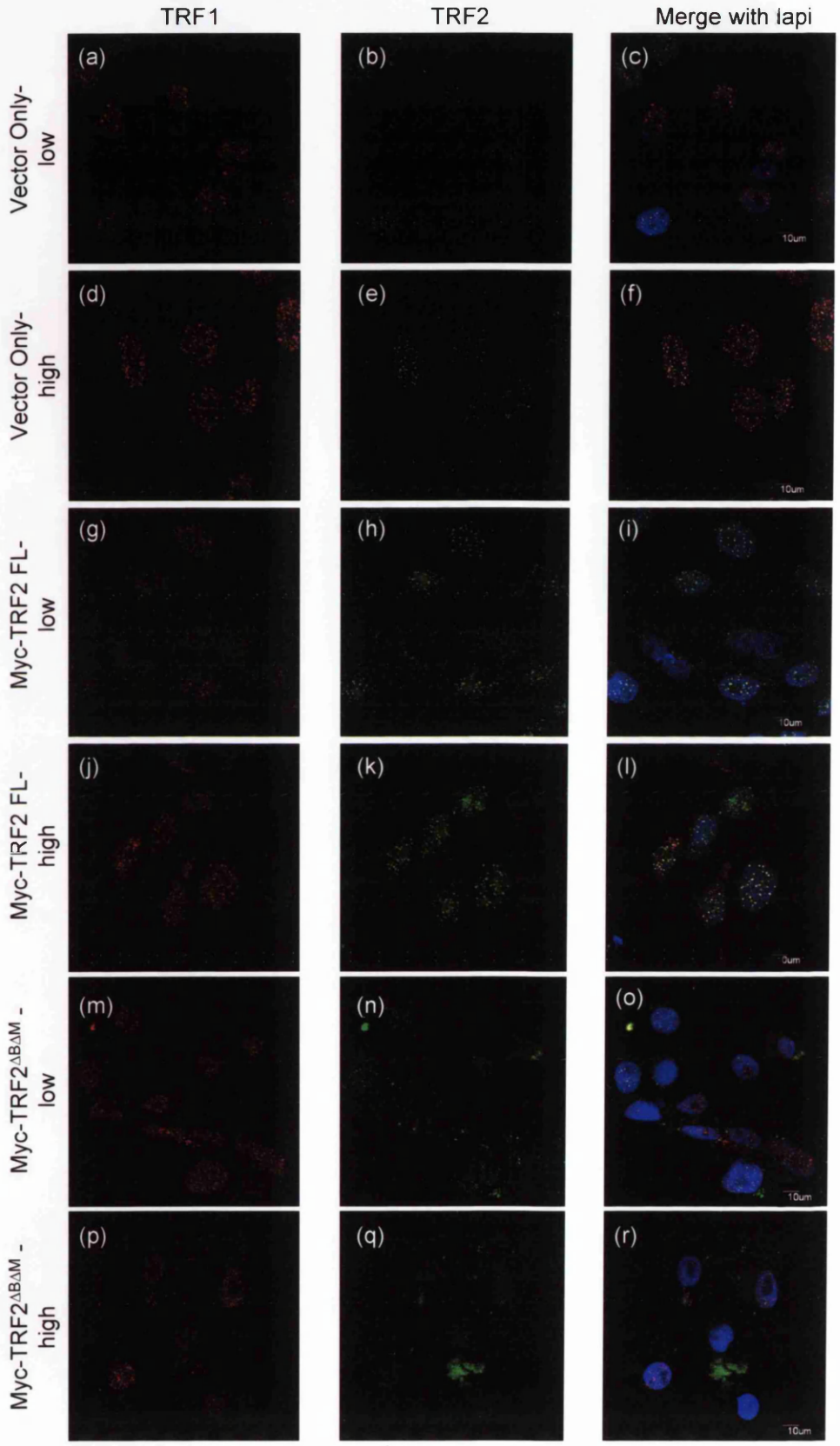

Figure 34. Co-localisation of TRF1 and 2 in NHEK expressing low and high levels of myc-TRF2 FL and myc-TRF2$^{\Delta B \Delta M}$ on day 4.

5.2 Evaluating DNA damage in NHEK using 53BP1 induction as a marker

In 2003, a DNA damage response was firmly established as part of the human fibroblast response to either naturally short telomeres (d'Adda di Fagagna et al. 2003) or dysfunctional telomeres created using myc-TRF2$^{\Delta B\Delta M}$ (Takai et al. 2003). In both publications, the DNA damage response proteins 53BP1 and γ-H2AX were shown to bind DNA and in one case these proteins were specifically shown to co-localise with TRF1 (Takai et al. 2003), indicating that the DNA damage response protein was binding at the telomere. These sites of co-localisation were denoted Telomere Induced dysfunctional Foci, (TIFs). Before trying to establish if TIFs were formed in NHEK, staining for 53BP1 was optimised after giving cells varying doses of γ-IR. 1 Gy induces about 25 double strand breaks (Lobrich et al. 1994). If the myc-TRF2$^{\Delta B\Delta M}$ was capable of removing the endogenous TRF2 from each telomere, then theoretically it would be reasonable to expect 92 DSB in each cell. However, it is unlikely that each telomere within a cell becomes dysfunctional as a result of expressing myc-TRF2$^{\Delta B\Delta M}$. Assuming 25-75% of telomeres become dysfunctional, a 1- 3 Gy γ-IR dose (25 - 75 DSBs) would induce a comparable amount of DNA damage.

Using the mild immunofluoresence protocol where cells were fixed before being permeabilised, punctuate 53BP1 staining was seen 15 mins after a 1 Gy γ-IR dose, (**Figure 35**). Untreated controls very infrequently demonstrated punctate 53BP1 staining, e.g. (**Figure 35**)(**a**)(**v.**), for reasons undetermined. It is possible that these are NHEK under going differentiation, premature chromatin condensation or some other process in which 53BP1 is perhaps involved, but not yet characterised. The majority of NHEK given either a 1 or 8 Gy γ-IR dose showed a punctate 53BP1 staining pattern, but not every single cell. Those that fail to respond may be in S phase and therefore not in a position to up-regulate production of 53BP1.

With a 15 min recovery time, the 53BP1 response after 1 Gy γ-IR was fairly robust. Escalating doses of γ-IR did not result in an obvious increase in the amount of 53BP1 localisation. For example, at the same time point, NHEK that

Figure 35. 53BP1 activation in NHEK exposed to increasing doses of γ-IR.

NHEK were subjected to various doses of γ-IR and given 15 min recovery time before being fixed in PFA prior to immunofluorescence.

(a) (i.), (ii.) and (iii.) Typically, either no 53BP1 or a single point of 53BP1 localisation is seen in cells that have not been given a γ-IR dose. (iv.), (v.) and (vi.) Very occasionally NHEK that have not been exposed to γ-IR express 53BP1.

(b) (i.), (ii.) and (iii.) More than 10 distinct foci of 53BP1 can be seen in cells after as little as 1Gy IR.

(c) (i.), (ii.) and (iii.) Exposure to 8 Gy γ-IR does not result in many more 53BP1 foci within a given cell.

(d) (i.) and (ii.) Staining NHEK for TRF1 was unsuccessful using the 2% PFA protocol which is optimal for 53BP1 staining.

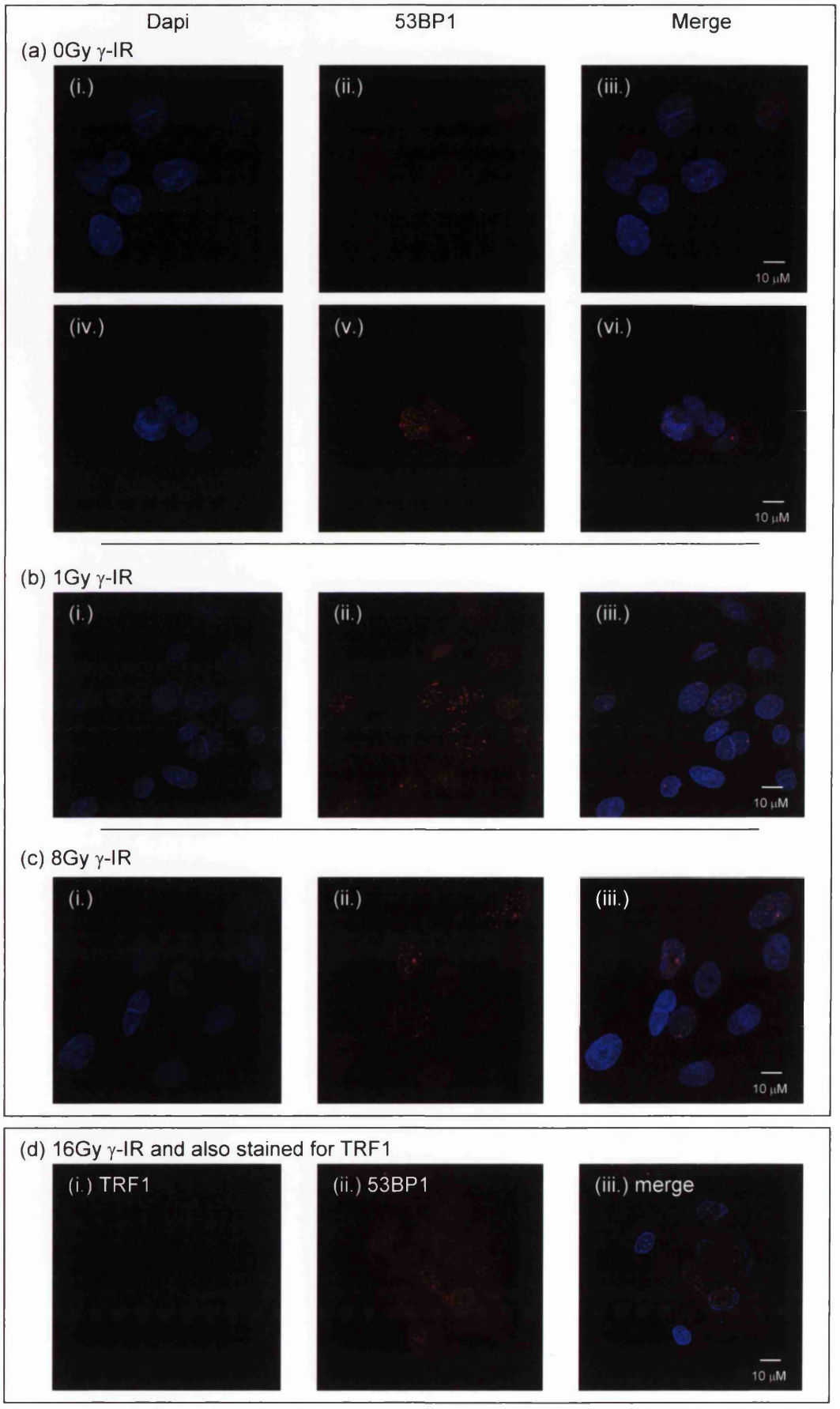

Figure 35. 53BP1 activation in NHEK exposed to increasing doses of γ-IR.

had received an 8 Gy γ-IR dose appeared very similar to NHEK that had received 1 Gy γ-IR dose. The lack of escalation in the amount of 53BP1 localisation with increasing IR dosage suggests that either more time is required to see a differential effect, that the reagents in the experiment were limiting or that after as little as 1 Gy γ-IR the maximum 53BP1 response had been achieved.

Attempts at visualising the endogenous levels of TRF1 using this immunofluorescence protocol were unsuccessful. As seen previously in (**Figure 24**), without permeabilising the NHEK prior to fixation, the TRF1 antibody failed to recognise the TRF1 protein.

5.3 Attempting to Identify TIFs in NHEK expressing myc-TRF2$^{\Delta B \Delta M}$

Using deconvolution microscopy Takai et al were able to observe TIFs 48 - 52 hours after G1/S synchronised cells were infected with adenoviral myc-TRF2$^{\Delta B \Delta M}$ (Takai et al. 2003). Given the different approach to infecting cells taken in this thesis, a slightly altered method was also taken in trying to identify TIFs, outlined in (**Figure 36**). Because the NHEK were not synchronised, a longer time window was evaluated for trying to identify TIFs.

Knowing that permeabilising the cells prior to fixation was necessary to visualise TRF1 protein, the stringent immunofluorescent protocol was used when trying to identify TIFs, (**Figure 37**). The 50 hour time point shown in (**Figure 37**) (**g**) - (**i**) demonstrates the best example of 53BP1 staining seen in NHEK expressing the myc-TRF2$^{\Delta B \Delta M}$. However, (**j**) - (**l**) is more representative of the 53BP1 staining commonly seen on the myc-TRF2$^{\Delta B \Delta M}$ plate.

A compromise must be made between the optimal techniques for detecting localisation of 53BP1 and TRF1 and therefore several issues exist that make it difficult to interpret this experiment: (1) Only large spots of 53BP1 can still be recognised using the stringent protocol, the finer spots seen when using the mild protocol where cells are fixed prior to permeabilisation are no longer seen. (2) The images for this experiment were performed relatively early in the course of this thesis and were taken using the Leica confocal which is not as sensitive for detecting small amounts of protein as the Olympus confocal which was acquired

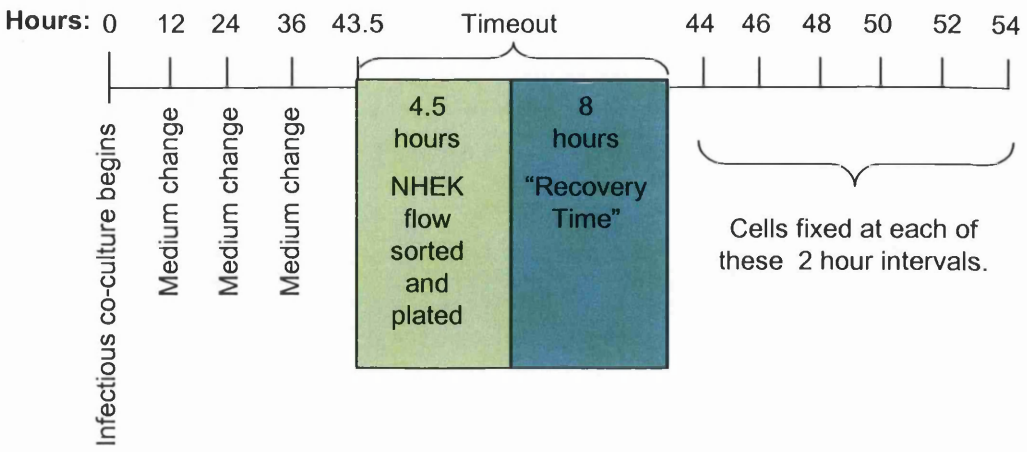

Figure 36. Timeline for TIF experiment.
The NHEK were co-cultured with the infectious PT67s for 43.5 hours at which point they were harvested for flow sorting. Flow sorting took 4.5 hours and then the GFP positive NHEK were plated onto 3T3 conditioned coverslips. 8 hours after being plated the cells had spread out and appeared "recovered" from the flow sorting. Not including within the timeline the 12.5 hours taken for both cell sorting and recovery, a set of Vector only, myc-TRF2 FL and myc-TRF2$^{\Delta B \Delta M}$ expressing NHEK were then harvested every 2 hours from 44 – 54 hours after infection.

Figure 37. Attempting to identify TIFs in NHEK expressing myc-TRF2 FL and myc-TRF2$^{\Delta B \Delta M}$. NHEK were flow sorted after 43.5 hours of co-culture with infectious PT67s (day 1) and plated onto 3T3 conditioned coverslips without feeders. Cells displayed in this Figure were grown until a 50 hour timepoint was reached (day 1) and permeabilised prior to being fixed using a stringent immunofluorescence protocol. Dapi staining was used to identify the middle of the nucleus, and 1 μm depths were defined either side of this point. The Leica confocal then took ten 0.2 μm Z sections through this region.

(a) – (c) In the Vector only, no 53BP1 staining is seen in this image, however spurious spots were seen in some cells indicating that 53BP1 will be activated at times in these cells. The TRF1 staining indicates telomeres.

(d) – (f) No 53BP1 staining can be seen in cells expressing myc-TRF2 FL, however the TRF1 staining is much stronger then in the Vector only image.

(g) – (i) These images display the best evidence of 53BP1 staining in the entire experiment.

(j) – (l) These images are more typical of the 53BP1 staining in the NHEK expressing myc-TRF2$^{\Delta B \Delta M}$.

(m) – (o) As a control, a set of vector only cells were given 4Gy γ-IR and 15 min recovery time. Again, some 53BP1 staining was seen.

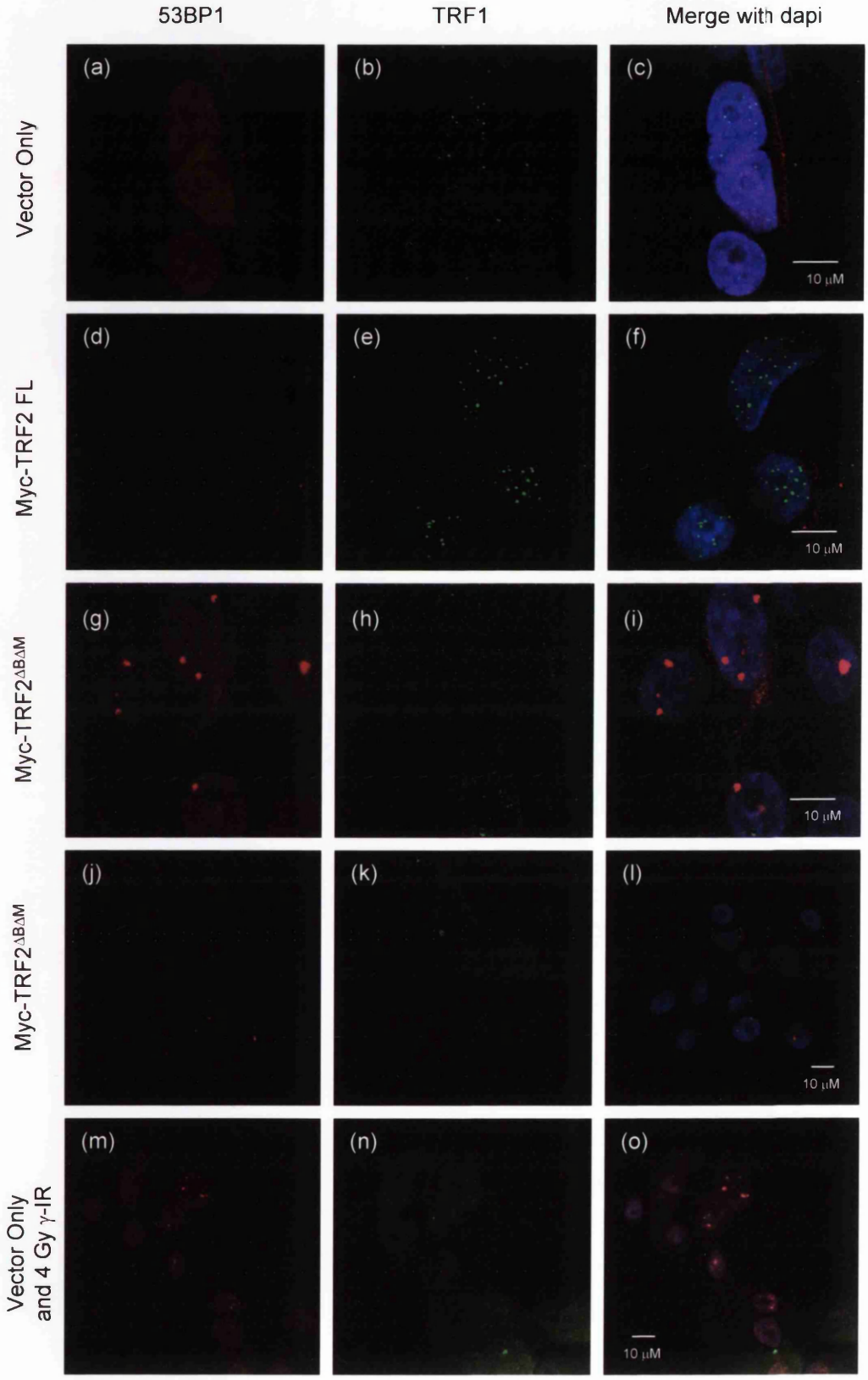

Figure 37. Co-localisation of TRF1 and 53BP1 in NHEK expressing myc-TRF2 FL and myc-TRF2$^{\Delta B\Delta M}$.

by the Beatson Institute towards the end of the thesis period. (3) Confocal microscopy had to be used instead of deconvolution microscopy, a technique that reduces background staining. Had deconvolution microscopy had been available it might have been possible to analyse the NHEK without permeabilising prior to fixation, thereby retaining the finer 53BP1 staining and visualising the TRF1 staining in the same sample.

5.4 Using γ-IR to evaluate the DNA response to DSBs in NHEK

As DNA damage detection using immunofluorescence was restricted, proteins induced in a DNA damage response were evaluated at a molecular level using western blotting. After consulting several publications (d'Adda di Fagagna et al. 2003), (Takai et al. 2003) and (Yoon and Smart 2004) antibodies recognising the proteins, Table 7, were tested using NHEK that had been subjected to varying doses of γ-IR and given varying recovery times.

Table 7: Commercially available antibodies that recognise proteins specifically involved in the DNA damage response evaluated using NHEK treated with γ-IR

Antibody
53BP1
53BP1(clone BP13)
C/EBP α (Keratinocyte specific DNA damage response downstream of p53)
Chk 1
Chk 2
Chk1-phosphoS345
Chk2-phosphoT68
H2AX- phosphoS139
Histone H2A.X
NBS1
NBS1-phosphoS343
p53
p53-phosphoS15
RAD17
RAD17-phosphoS645
SMC1
SMC1-phosphoS966

The purpose of these experiments was to find the most sensitive marker of DNA damage in NHEK detectable in western blotting. The assays that worked the best are shown in (**Figure 38**). Antibodies that recognised SMC1- phosphoS966, Nbs1- phosphoS343, Chk1-phosphoS345 and Chk2-phosphoT68 showed that activation of these proteins occurred when NHEK were treated with 8 or 16 Gy γ-

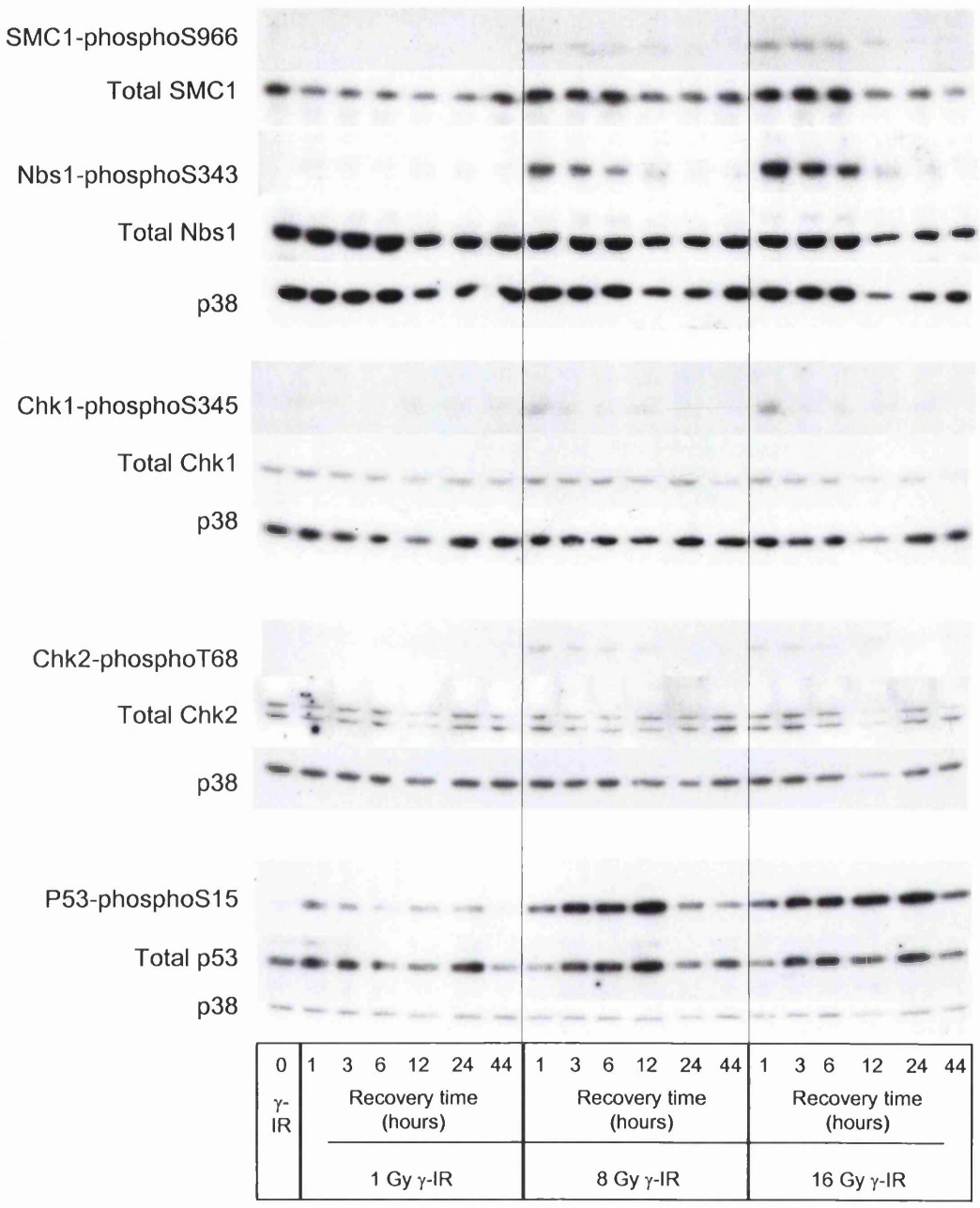

Figure 38. NHEK response to γ-IR induced DNA damage.

The activation of DNA damage response proteins was analysed after 1, 8 or 16 Gy γ-IR doses. The best commercially available antibodies (listed in Table 7) at detecting DNA damage, are shown above. The antibody against p53 phosphoS15 was clearly the most sensitive capable of detecting DNA damage, recognising the damage generated after as little as 1Gy. A p38 loading control was used on each separate blot.

IR. However, they were not sensitive enough to detect the DNA damage generated after 1 Gy γ-IR. Since the DNA damage response generated by myc-TRF2$^{\Delta B \Delta M}$ is expected to be more subtle then that triggered by an 8 or 16 Gy γ-IR dose, attention focused on p53-phosphoS15. This was the only antibody capable of recognising a member of the DNA damage response pathway at doses of γ-IR as low as 1 Gy.

5.5 p53-phosphoS15 levels in NHEK expressing myc-TRF2 FL and myc-TRF2$^{\Delta B \Delta M}$

Knowing from previous work in the literature that p53 activation is likely to occur soon after the expression of myc-TRF2$^{\Delta B \Delta M}$, we examined NHEK on days 1 and 2 after infection with TRF2 constructs, (**Figure 39**). NHEK expressing TRF2 constructs were harvested immediately after flow sorting GFP positive cells. In control lanes, an incremental increase was seen in p53-phosphoS15 signal intensity 6 hours after 1 - 16 Gy of γ-IR. However, there was a very slight, barely detectable increase in the amount of p53-phosphoS15 on day 2 in NHEK expressing myc-TRF2$^{\Delta B \Delta M}$.

The expression levels of p53-phosphoS15 in NHEK expressing the TRF2 constructs were also examined in two additional experiments, (**Figure 40**). Again, the intensity of the p53-phosphoS15 signals were marginally elevated on day 2 in myc-TRF2$^{\Delta B \Delta M}$ in comparison to equivalent cultures expressing Vector only or myc-TRF2 FL. An increase in total p53 has often been reported in cells responding to DNA damage. However, this stabilisation of p53 was not seen here.

These 3 separate experiments all provided evidence of minor elevation of p53-phosphoS15 on day 2 after infection with myc-TRF2$^{\Delta B \Delta M}$, however the evidence remains very subtle. In each experiment, the intensity of this signal is not even as strong as the signal in the control NHEK that received 1Gy γ-IR.

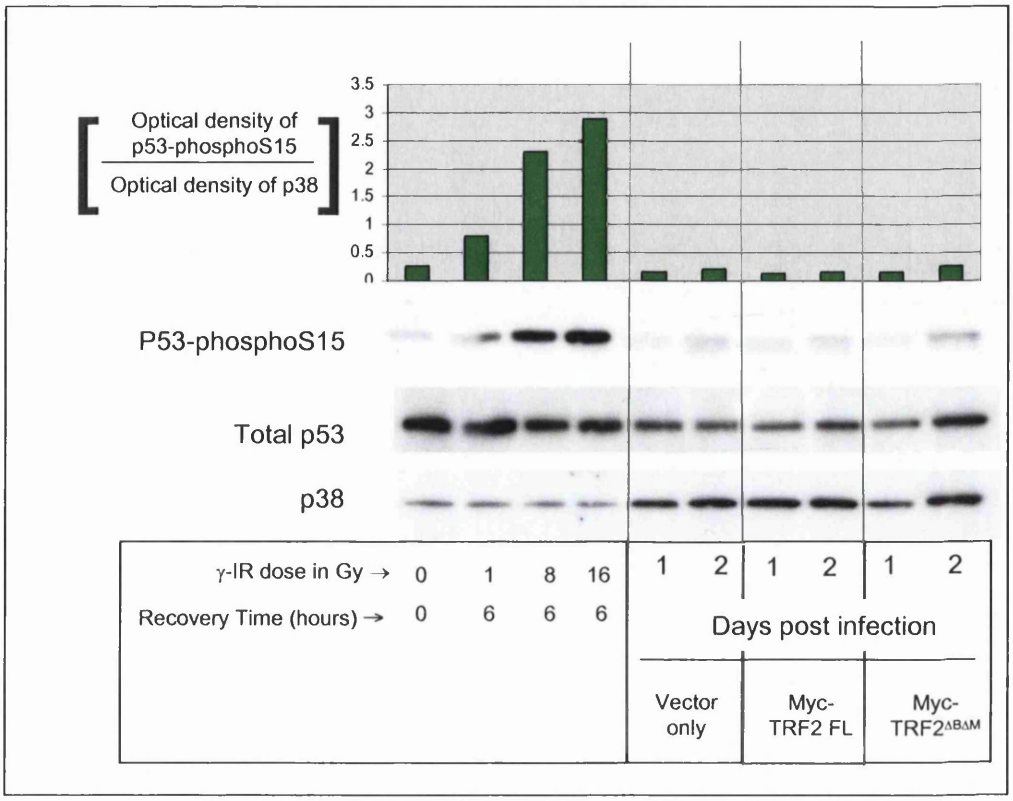

Figure 39. p53-phosphoS15 levels in NHEK on days 1 and 2 with myc-TRF2 FL and myc-TRF2$^{\Delta B \Delta M}$.

NHEK were harvested immediately after flow sorting and their p53-phosphoS15 levels evaluated. S15 phosphorylation is seen in γ-IR controls after 1, 8 and 16 Gy. In the western blot, the p53-phosphosS15 band in myc- TRF2$^{\Delta B \Delta M}$ infected on day 2 appears slightly more intense then in any of the bands in the vector only or the myc-TRF2 FL. Quantitation confirms this slight increase, but it is less then is found in the 1 Gy control lane.

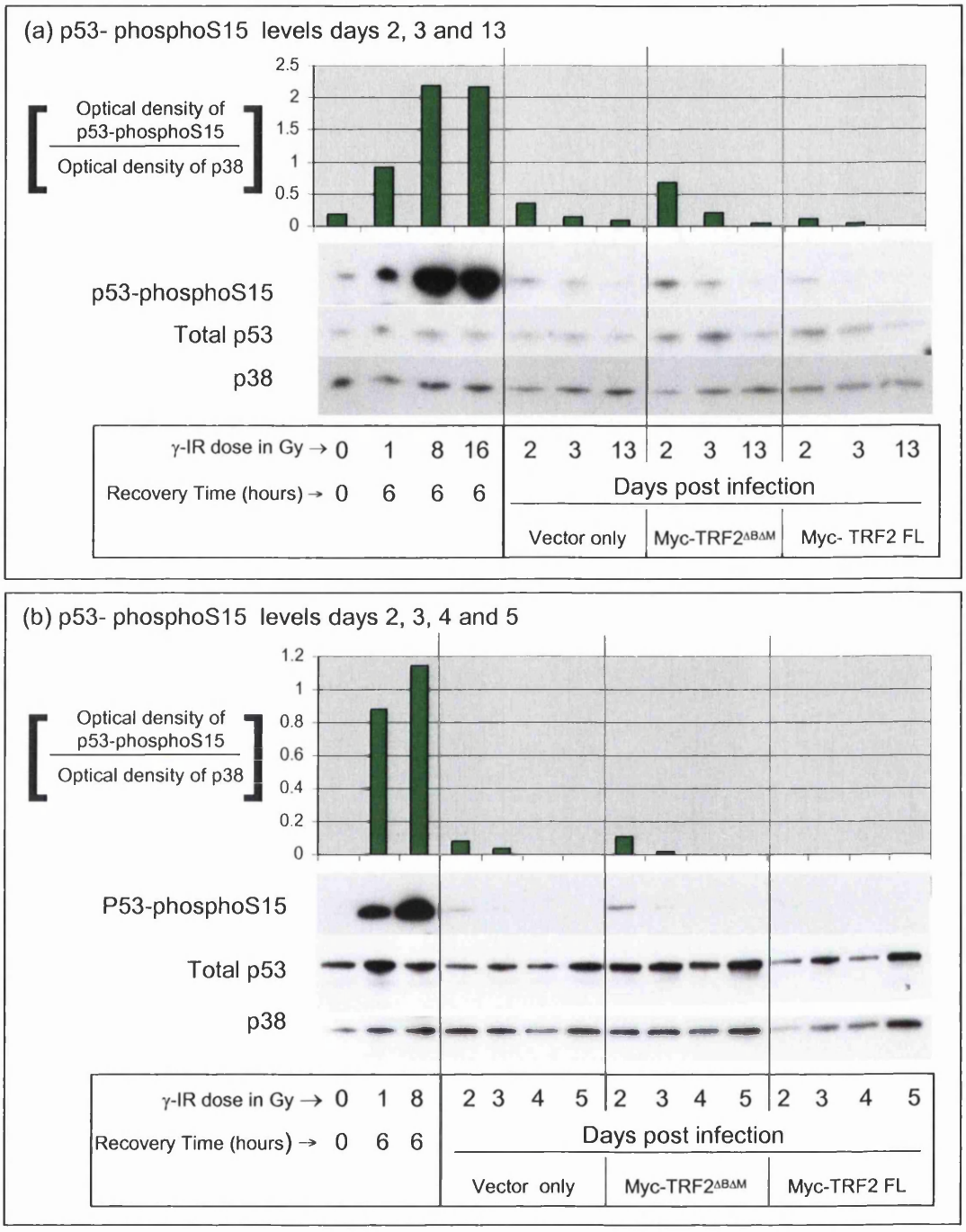

Figure 40. p53- phosphoS15 levels in NHEK at various time points after infection with myc-TRF2 FL and myc-TRF2$^{\Delta B\Delta M}$.

(a) NHEK were harvested immediately after flow sorting on days 2 and 3, whereas cells harvested on day 13 were flow sorted on day 4 and grown for a further 9 days before being harvested. On day 2, in NHEK expressing myc-TRF2$^{\Delta B\Delta M}$ the level of p53 –phosphoS15 is greater than in untreated cells or in cells that are expressing vector only. However, it is not as high as in cells that have received 1Gy γ-IR.

(b) NHEK were harvested immediately after flow sorting on days 2, 3, 4 and 5. Again, on day 2 the p53-phosphoS15 level in the NHEK expressing myc-TRF2$^{\Delta B\Delta M}$ is higher than that seen in either the untreated cells, but not higher than in cells that received 1 Gy γ-IR.

5.6 Levels of DNA damage in NHEK expressing myc-TRF2$^{\Delta B\Delta M}$ or myc-TRF2 FL without cell sorting

The cell cycle analysis and TRF2 expression data at late timepoints after infection with myc-TRF2 FL and particularly myc-TRF2$^{\Delta B\Delta M}$ suggest that the NHEK experiencing the most telomere induced DNA-damage maybe too unstable to survive the flow sorting process (Chapter 4). Therefore, in one experiment,

NHEK were infected with TRF2 constructs and then harvested on days 1 or 2 without any flow sorting, (**Figure 41**). On day 2, parallel cultures revealed that only approximately 30% of cells were GFP positive after infection with each of the three vectors (Vector only, myc-TRF2 FL and myc-TRF2$^{\Delta B\Delta M}$). As in the previous Figure, low levels of p53-phosphoS15 are seen in all NHEK expressing a TRF2 construct, but this level is less than that seen in cells given a 1 Gy γ-IR dose. On day 2, the p53-phosphoS15 signal in the NHEK expressing myc-TRF2$^{\Delta B\Delta M}$ cells is almost as strong as cells that received 8 Gy γ-IR dose. As only ~30% of the NHEK harvested were expressing the construct, this is the strongest evidence obtained for DNA damage induced by myc-TRF2$^{\Delta B\Delta M}$.

5.7 Flow sorting as a means of selection in later time points

Comparing the signals of p53-phophoS15 in (**Figure 40**) to those in (**Figure 41**) suggests that some myc-TRF2$^{\Delta B\Delta M}$ DNA damaged cells may be lost during the flow sorting process. It was shown in Chapter 4 that on day 10 the most likely reason for not detecting where in the cell cycle the NHEK had proliferation arrested was the low proportion of GFP cells still expressing the myc-TRF2$^{\Delta B\Delta M}$. The difficult decision that needed to be made regarding how to harvest the cells while trying to establish if the p53-phosphoS15 signal seen on day 2 could be further validated is summarised in (**Figure 42**).

5.8 p21 levels in NHEK expressing myc-TRF2 FL and myc-TRF2$^{\Delta B\Delta M}$

When activated, p53 forms a tetramer capable of acting as a transcription factor. One gene tightly controlled by activated p53 is p21, a protein that

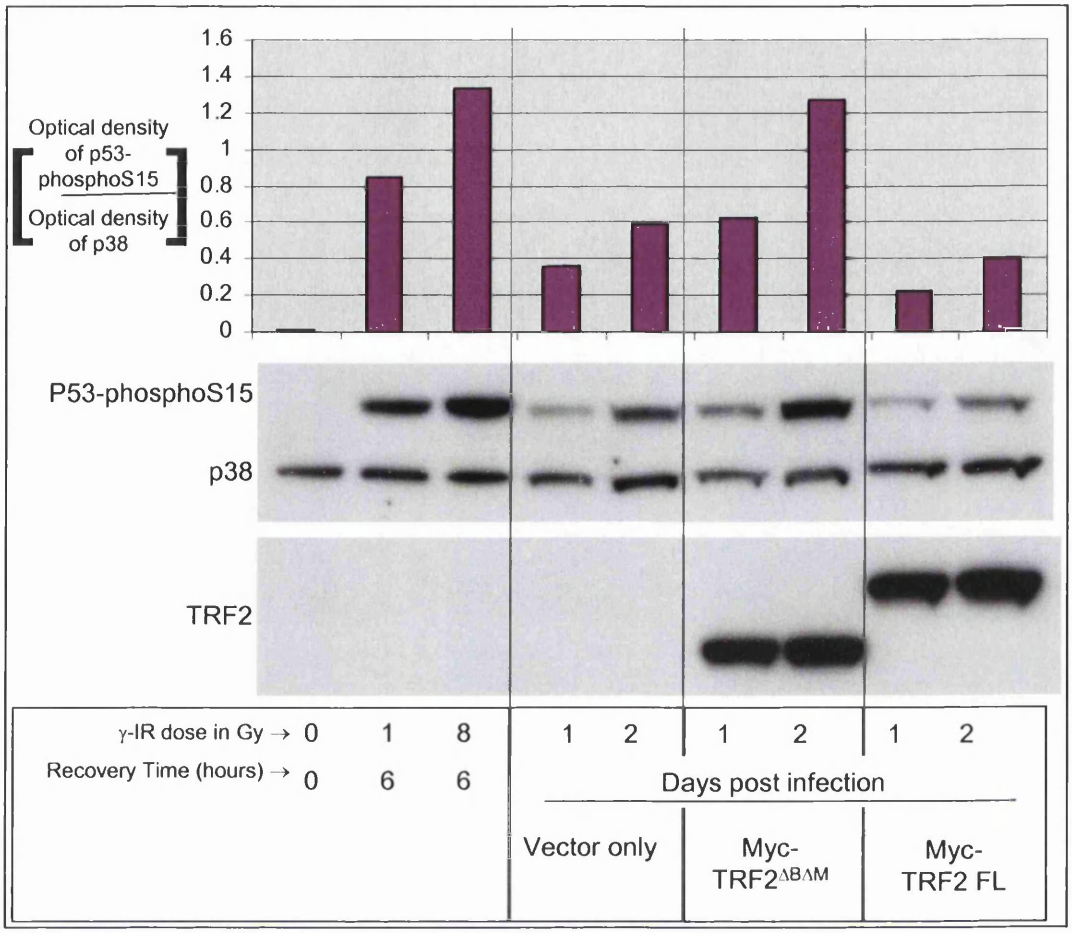

Figure 41. p53-phosphoS15 levels in NHEK expressing myc-TRF2 FL and myc-TRF2$^{\Delta B \Delta M}$ on days 1 and 2 without flow sorting.

Feeders were removed from NHEK and cells harvested without being flow sorted. Parallel cultures that were flow sorted (on day 2) were 30% GFP positive on average. An increase in the level of p53-phosphoS15 is seen on day 2 in NHEK expressing myc-TRF2$^{\Delta B \Delta M}$ almost as high as the level seen after NHEK receive 8Gy IR. P53-phosphoS15 levels in Vector only day 1 and 2, myc-TRF2$^{\Delta B \Delta M}$ day 1 and myc-TRF2 FL day 1 and 2 remain less then those seen in NHEK that received 1 Gy IR.

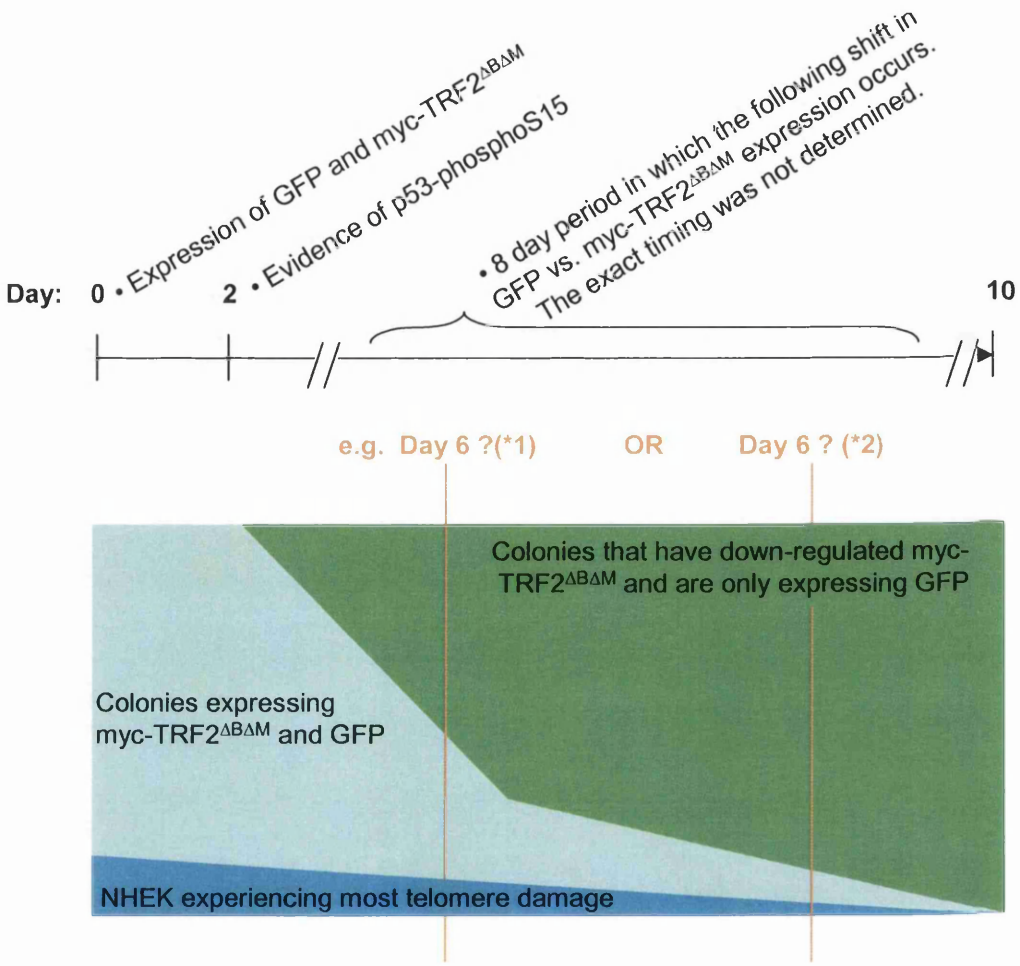

Figure 42. The possible dynamics of the relationship between myc-TRF2$^{\Delta B\Delta M}$ and GFP expression.

On day 0, expression of both myc-TRF2$^{\Delta B\Delta M}$ and GFP is most likely occurring in all cells infected with the myc-TRF2$^{\Delta B\Delta M}$ construct. Around day 2, as soon as effect of expressing myc-TRF2$^{\Delta B\Delta M}$ is realised by the NHEK, it applies a negative selection to those colonies. The cells that continue to express myc-TRF2$^{\Delta B\Delta M}$ and GFP stop proliferating, whereas the revertant cells that are not expressing myc-TRF2$^{\Delta B\Delta M}$, but are still expressing GFP begin to grow without growth inhibition, at an exponential rate. When the GFP positive cells are harvested at later time points, this causes a diluting effect on the extract of the cells that are still expressing the myc-TRF2$^{\Delta B\Delta M}$. As the time frame in which this shift takes place is unknown, day 6 could either have a profile as shown in (*1) where the ratio of cells still expressing myc-TRF2$^{\Delta B\Delta M}$ is still high enough that the proteins instigating the effect could be seen or day 6 could also be taking place at position (*2) where the ratio would not be high enough for an effect to be seen.

In addition to the diluting effect, there was evidence that the cells undergoing the most telomeric damage were lost during the flow sorting process.

inhibits the activity of cyclin-CDK2 or -CDK4 complexes thereby preventing cells from exiting G1. If the activation of p53 seen on day 2 (albeit very weak) in NHEK expressing myc-TRF2$^{\Delta B\Delta M}$ was driving a DNA damage response, an increase in p21 in those cells by day 3 would be expected as a consequence.

(**Figure 43**) (**a**) looks at the p21 levels in which NHEK have not been flow sorted immediately prior to harvesting. No increase in p21 is seen on days 7, 11 or 14. Unfortunately it is not possible to comment if this is because there definitely is not an increase in p21 or if an increase is not seen because of the diluting effect of the NHEK which are no longer expressing the myc-TRF2$^{\Delta B\Delta M}$.

Using extracts from an experiment where an increase in p53-phosphoS15 on day 2 in the myc-TRF2$^{\Delta B\Delta M}$ expressing cells had been demonstrated, we examined the p21 levels, (**Figure 43**) (**b**). Basal levels of p21 were easily detected in the NHEK and an increase in p21 levels was seen in control NHEK that had been treated with increasing doses of γ-IR and given 6 hours recovery time. No increase of p21 was seen in the NHEK on days 1, 2, 3 or 13 after infection with myc-TRF2$^{\Delta B\Delta M}$.

In contrast, a third experiment, (**Figure 43**)(**c**), clearly showed an increase in p21 expression in both myc-TRF2$^{\Delta B\Delta M}$ and myc-TRF2 FL expressing cells on days 5, 6, 7 and 8 after infection compared with Vector only cells. The result shown here and in (**Figure 43**)(**b**) together might suggest that p21 is activated by the uncapped telomere, but not until 5 days after infection. However, it seems unlikely that there should be a 3 day delay from p53-S15 phosphorylation on day 2 and p21 up-regulation at 5-8 days. In addition to this point, the following issues also arise from (**Figure 43**)(**c**).

- The levels of myc-TRF2$^{\Delta B\Delta M}$, and to a lesser extent, myc-TRF2 FL, decreased at later time points after infection. Despite the decrease, the p21 expression remained the same. One possible explanation is that the TRF2 constructs are being down-regulated and the initial expression of myc-TRF2$^{\Delta B\Delta M}$ already triggered a DNA damage response that continues to prevent cell proliferation. However, the FACS analysis in (**Figure 30**) (Chapter 4) provides evidence to the contrary.

- In Chapter 4, (**Figure 18**) and (**Figure 20**), demonstrate that NHEK expressing myc-TRF2 FL proliferate more then those expressing myc-TRF2$^{\Delta B \Delta M}$. If this differential affect is caused by the p53 activation on day 2 in the myc-TRF2$^{\Delta B \Delta M}$ expressing cells, then a higher level of p21 would be expected in these cells compared to the NHEK expressing myc-TRF2 FL.

As these points do not support the apparent up-regulation of p21 seen in (**Figure 43**)(**c**) it can not be considered authentic.

While not providing evidence in support of a p53 response, the difficulty in obtaining evidence of p21 up-regulation also fails to provide evidence against a p53 response. The most likely explanation from the data gathered regarding p21 is, akin to Section 4.8, any cells in the midst of a DNA damage response are too fragile to survive the flow sorting process. Unfortunately, an up-regulation of p21 was not seen in NHEK expressing myc-TRF2$^{\Delta B \Delta M}$ that had not been flow sorted, but this could be due to the diluting effect of cells no longer expressing the myc-TRF2$^{\Delta B \Delta M}$.

5.9 Assessing the phosphorylation status of Rb in NHEK expressing myc-TRF2 FL and myc-TRF2$^{\Delta B \Delta M}$

Although it was deemed likely that growth arrested NHEK expressing myc-TRF2$^{\Delta B \Delta M}$ had not survived the flow sorting process based on their p21 status, it was decided that another marker of cell cycle status should also be examined.

Ultimately, the main downstream affect of the activation of p53 is controlled through the phosphorylation status of the Retinoblastoma (Rb) protein. When hyper-phosphorylated, Rb does not bind to E2F, a transcription factor that controls the expression of many genes that allow entry into the S phase of the cell cycle. Conversely, hypo-phosphorylated Rb remains bound to E2F, thereby repressing it and preventing cells from progressing from the G1 to the S phase of the cell cycle.

- Control experiments were first designed to evaluate the reliability of the antibodies against several phosphorylation sites known to be involved in Rb regulation. NHEK grown to either 50% or 80% confluence all showed

Figure 43. p21 levels in NHEK at various time points after infection with myc-TRF2 FL and myc-TRF2$^{\Delta B \Delta M}$.

(a) NHEK were flow sorted and plated on day 2 and then harvested on days 7, 11 and 14 after infection without subsequent flow sorting. No increase is seen in p21 in any of the cells.

(b) NHEK were harvested immediately after flow sorting on days 1, 2 and 3 whereas cells harvested on day 13 were flow sorted on day 4 and grown for a further 9 days before being harvested. In the controls, an increase in p21 levels is seen after 1, 8 or 16 Gy γ-IR compared with cells that were not given any IR.

(c) NHEK were harvested immediately after flow sorting on days 5, 6, 7 and 8. At these time points p21 levels appear to increase in NHEK expressing myc-TRF2$^{\Delta B \Delta M}$ and myc-TRF2 FL compared with those expressing Vector only.

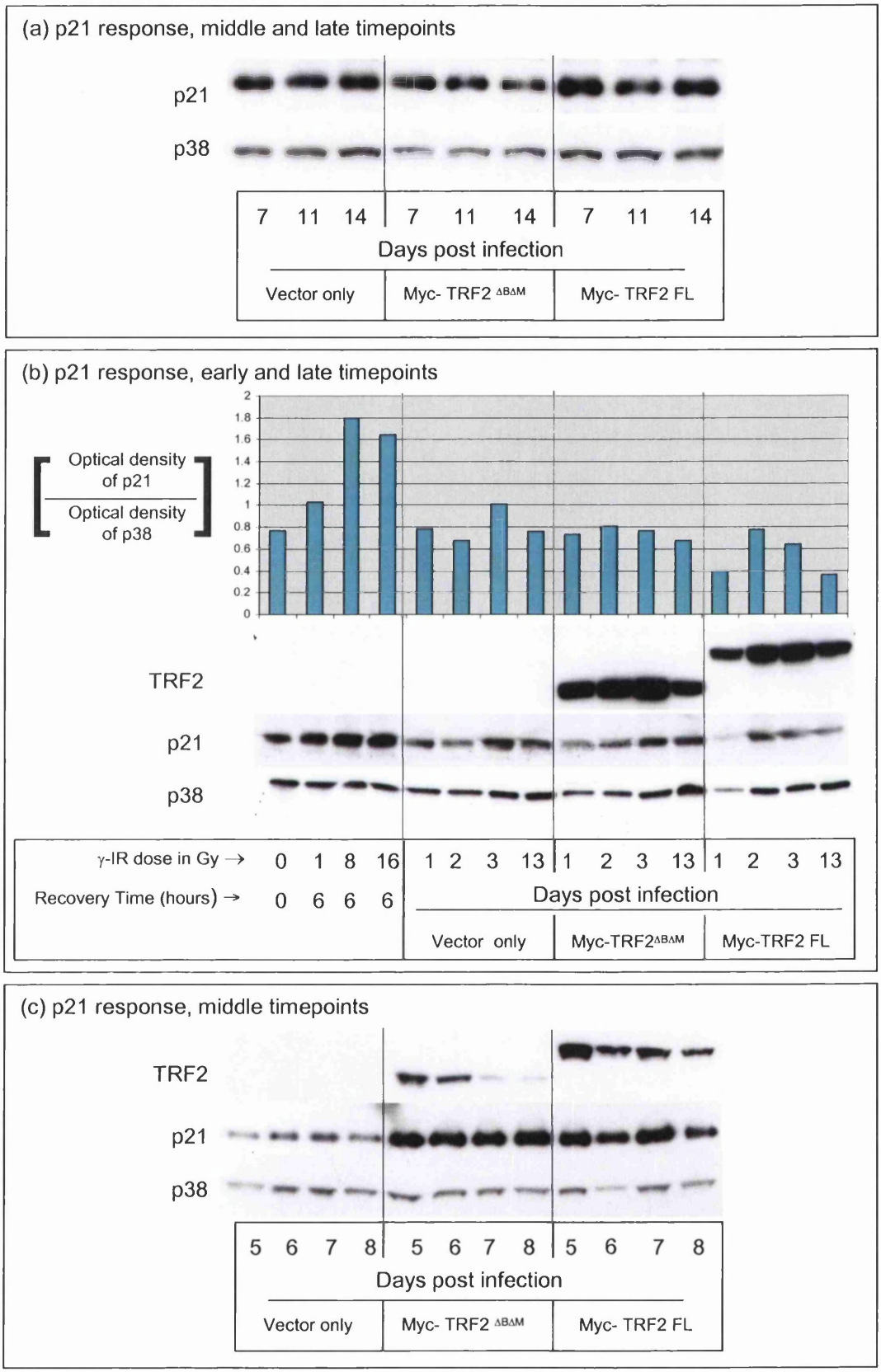

Figure 43. p21 levels in NHEK at various time points after infection with myc-TRF2$^{\Delta B\Delta M}$ and myc-TRF2 FL retroviruses.

Figure 44. Phosphorylation status of Rb in NHEK expressing myc-TRF2 FL and myc-TRF2$^{\Delta B\Delta M}$ at middle time points.

This Figure uses material from the same experiment as (Figure 43)(b).

Control NHEK were grown to either 50% or 80% confluence or held at confluence for 3 days. Sub-confluent NHEK all show the phosphorylated form of Rb as opposed to the confluent NHEK which do not show phosphorylated Rb at any of the 4 specific sites tested or in the supershifted positions in the total Rb lane.

GFP positive cells were flow sorted 5, 6, 7 and 8 days after infection with retroviral vectors and immediately harvested for western blotting. Myc-TRF2$^{\Delta B\Delta M}$ expressing NHEK show less phosphorylation in the total Rb lanes compared with Vector only or myc-TRF2 FL and less phosphorylation on day 8 at all 4 specific Rb phosphorylation sites tested. In samples harvested from day 5 to day 8, the amount of myc-TRF2$^{\Delta B\Delta M}$ is dramatically reduced. The amount of myc-TRF2 FL also reduced, but not by as much.

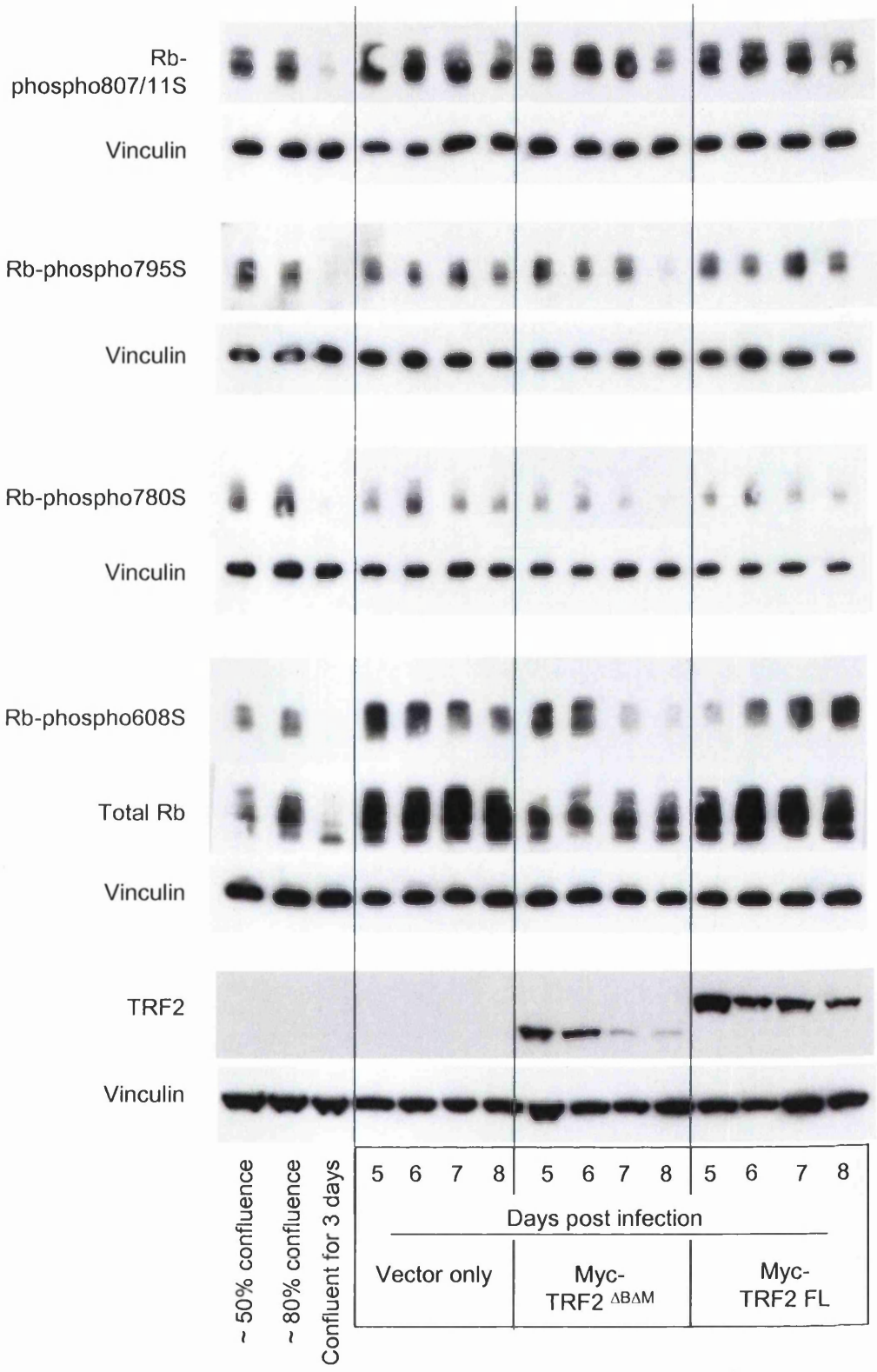

Figure 44. Phosphorylation status of Rb in NHEK expressing myc-TRF2 FL and myc-TRF2$^{\Delta B \Delta M}$ at middle timepoints.

phosphorylation of Rb at Serine sites 807/11, 795, 780 and 608 using phospho-specific antibodies, (**Figure 44**). NHEK held at confluence for 3 days did not show Rb phosphorylation using phospho-specific Rb antibodies. Antibodies against total Rb detected both the hyper- and the hypo-phosphorylated forms of Rb in sub-confluent cells as judged by their different electrophoretic mobility's, whereas in confluent cells was Rb was hypo-phosphorylated. As demonstrated by these controls, the level of confluence has a dramatic affect on the level of Rb phosphorylation. Extreme care was taken in all experimental conditions that the NHEK were not confluent prior to harvest. Using the same cell extracts from the previous (**Figure 43**), NHEK expressing myc-TRF2$^{\Delta B\Delta M}$ and myc-TRF2 FL demonstrated a reduction in the amount of phospho-Rb at sites 795S, 780S and 608S in myc-TRF2$^{\Delta B\Delta M}$ cells on day 8, (**Figure 44**). However, these changes in Rb phosphorylation are not evident from the blots using the total Rb antibody, (**Figure 44**). Again, it seems unlikely that the hypo-phosphorylation would not take place until day 8, a delay of 6 days from the activation of p53.

In another experiment the level of Rb-phospho780S were assessed on days 8 and 12 after infection with myc-TRF2 FL and myc-TRF2$^{\Delta B\Delta M}$, (**Figure 45**). Again, the cells were flow sorted immediately prior to harvesting. In contrast with (**Figure 44**), Rb-phospho780S was not reduced on day 8 in myc-TRF2$^{\Delta B\Delta M}$ compared to controls, however a large reduction was seen in day 12. Again, the levels of myc-TRF2$^{\Delta B\Delta M}$, and to a lesser extent, myc-TRF2 FL, decreased at later time points after infection.

5.10 Evaluating other markers of DNA damage in NHEK expressing myc-TRF2 FL and myc-TRF2$^{\Delta B\Delta M}$

Although p53-phosphoS15 was shown to be the most sensitive marker of DNA damage following γ-IR we decided to also investigate SMC1 and Nbs1 in case these proteins proved to be better than p53-phosphoS15 at recognising telomere specific, as opposed to radiation induced, DNA damage, (**Figure 46**). However, neither of these DNA damage response proteins were activated in cells expressing myc-TRF2$^{\Delta B\Delta M}$ as judged by SMC1-phosphoS966 and Nbs1-phosphoS343 antibodies.

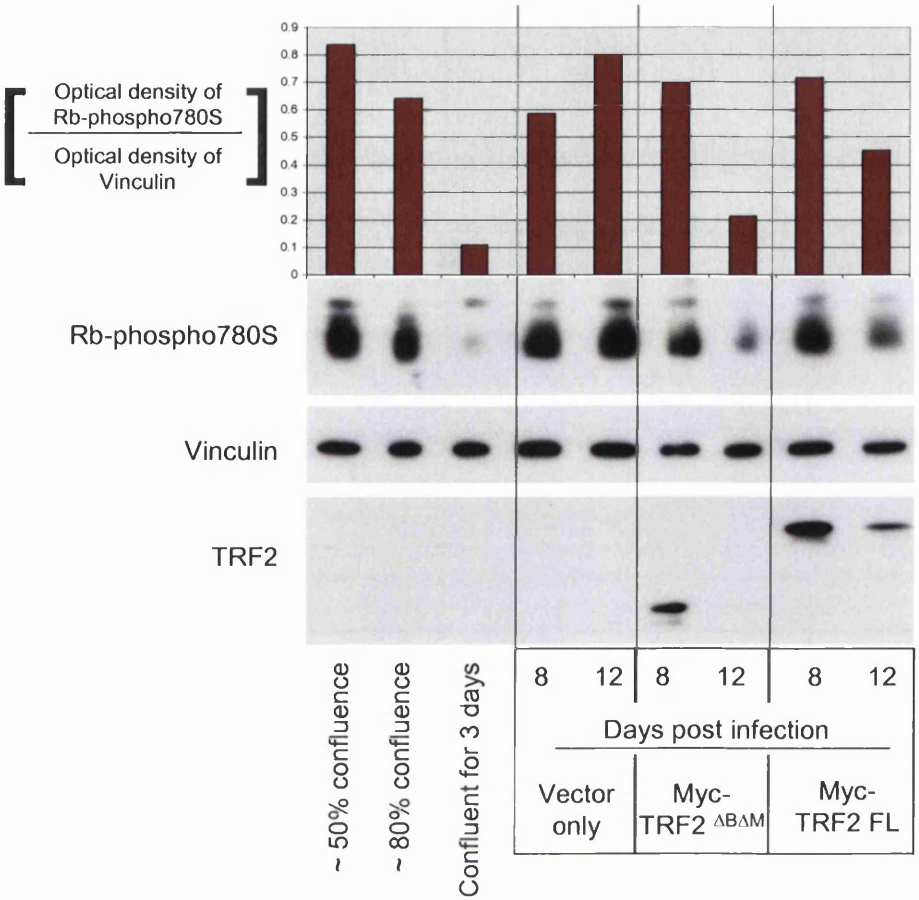

Figure 45. Phosphorylation status of Rb in NHEK expressing myc-TRF2 FL and myc-TRF2$^{\Delta B\Delta M}$ at late time points.

GFP positive cells were flow sorted 8 and 12 days after infection and harvested immediately. Compared with Vector only and myc-TRF2 FL, less Rb-phospho780S is seen in myc-TRF2$^{\Delta B\Delta M}$ cells on day 12. Myc-TRF2$^{\Delta B\Delta M}$ is not detected in day 12 and the amount of myc-TRF2 FL is reduced from day 8 to day 12.

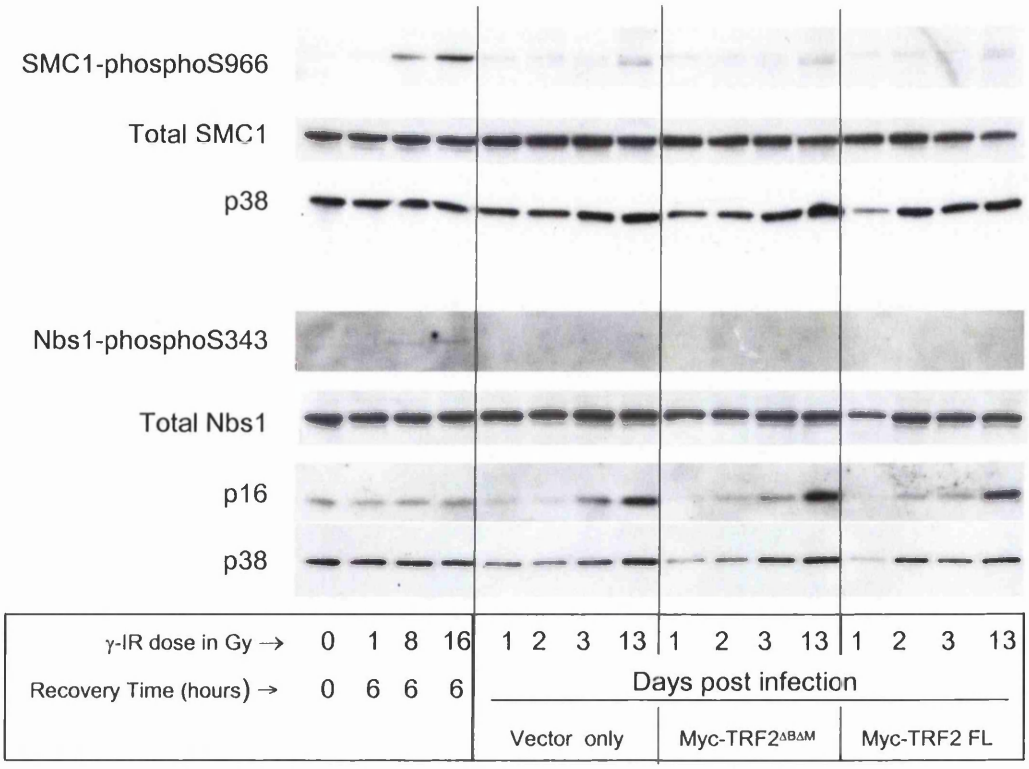

Figure 46. Markers of DNA damage other then p53-phosphoS15 in NHEK expressing myc-TRF2 FL and myc-TRF2$^{\Delta B \Delta M}$.

NHEK were harvested immediately after flow sorting on days 1, 2 and 3 whereas cells harvested on day 13 were flow sorted on day 4 and grown for 9 further days before being harvested. Control experiments show an increase in levels of SMC1-phosphoS966 and Nbs1-phosphoS343 in cells that have received IR. After allowing for slight differences in loading, no increase is seen in either NHEK expressing myc-TRF2$^{\Delta B \Delta M}$ or myc-TRF2 FL. p16 levels increase in Vector only, myc-TRF2$^{\Delta B \Delta M}$ and myc-TRF2 FL on day 13.

$p16^{INK4A}$ is a cyclin dependent kinase inhibitor that prevents Cyclin (D) Dependent Kinase (CDK) 4 or 6 from phosphorylating RB. $p16^{INK4A}$ has been shown to contribute to a delayed, p53-independent response to telomere damage in fibroblasts (Jacobs and de Lange 2004). Unlike fibroblast cell lines, mammary or keratinocyte epithelial cells require inactivation of $p16^{INK4A}$ before they become immortalised (Kiyono et al. 1998), suggesting that $p16^{INK4A}$ might have an even more important role in detecting telomere initiated senescence in epithelial cells. Normal basal levels of $p16^{INK4A}$ were found in NHEK expressing myc-TRF2 FL and myc-$TRF2^{\Delta B\Delta M}$. By day 13, elevated levels were seen in cells expressing Vector only, myc-TRF2 FL and myc-$TRF2^{\Delta B\Delta M}$. The lack of a specific increase of $p16^{INK4A}$ in the NHEK expressing myc-$TRF2^{\Delta B\Delta M}$ was surprising. The cells were not flow sorted on day 13 prior to harvest. As described in Section 5.8, it is therefore likely that the diluting effect of the NHEK that managed to down-regulate myc-$TRF2^{\Delta B\Delta M}$ would mask any genuine $p16^{INK4A}$ signal. A general increase in the level of $p16^{INK4A}$ is common in keratinocytes the longer they are cultured (Darbro et al. 2005). The increase of $p16^{INK4A}$ seen in NHEK expressing Vector only, myc-TRF2 FL and myc-$TRF2^{\Delta B\Delta M}$ from day 3 to 13 suggests that expression of the constructs is incurring a certain degree of stress on the culture.

5.11 Investigating cell death as a response in NHEK expressing myc-$TRF2^{\Delta B\Delta M}$ or myc-TRF2 FL

The clonogenicity study, (**Figure 21**) and (**Figure 22**), establish that expression of myc-$TRF2^{\Delta B\Delta M}$ and to a lesser extent myc-TRF2 FL, reduces colony formation of NHEK. Two obvious explanations for this are: (1) Although an equal number of NHEK are plated on day 2 after flow sorting, less cells expressing myc-TRF2 FL or myc-$TRF2^{\Delta B\Delta M}$ are capable of adhering to the plate. (2) Once attached, as NHEK continue to try and replicate, they incur more and more DNA damage and therefore undergo apoptosis.

Preliminary investigations were made to determine if differences in cell adherence was playing a role in the different numbers of colonies found on the plates. All cells in the medium were collected the day after plating and evaluated to determine whether there were GFP positive cells, thereby distinguishing them from any feeders that had not attached to the plate.

Between 0.0 - 0.5% of the GFP positive cells plated were found suspended in the medium and there was no obvious increase with either NHEK expressing myc-TRF2 FL or myc-TRF2$^{\Delta B\Delta M}$. However, it is possible that after 24 hours any NHEK that did not adhere to the plate may no longer be expressing GFP.

Programmed cell death, or apoptosis, is highly regulated process that can be triggered by external or internal stimuli such as DNA damage. Caspase 3 is the final cysteine Asp- specific proteases (caspases) to be cleaved in the apoptotic pathway, (**Figure 47**). Detection of cleaved caspase-3 by western blotting is an indication that apoptosis is occurring within a cell population. As a positive control for the assay, NHEK were treated with cisplatin and then analysed for caspase 3 cleavage, (**Figure 48**). Treating NHEK with 10 μM cisplatin was enough to cause a small amount of caspase 3 cleavage and treatment with 50 or 100 μM cisplatin caused large amounts of caspase 3 cleavage.

The fact that NHEK are grown with feeders considerably complicates attempts at assessing cell death. In the experiment shown in (**Figure 48**), feeders were removed 2 days prior to the day of harvest. Therefore, on the harvest day, NHEK were trypsinised and collected with any cells that might be floating in the medium. Days 8, 10 and 12 were chosen because this is the point when NHEK expressing the TRF2 constructs first show a reduced rate of proliferation compared with Vector only cells. No cleaved caspase 3 products were in fact detected in NHEK expressing myc-TRF2 FL or myc-TRF2$^{\Delta B\Delta M}$ on days 8, 10 or 12. This implies that the NHEK are not undergoing apoptosis during these specific time points, at least not at levels where cleaved caspase 3 could be detected. It remains possible that apoptosis occurs at an earlier time point or in between the harvest times examined here.

5.12 Summary of Chapter 5

Detecting co-localisation of telomeres and DNA damage in NHEK using immunofluorescence requires different protocols when imaged using a confocal microscope. Unfortunately, visualising telomeres in NHEK using a TRF1 antibody requires stringent conditions, including permeabilising the cells before fixing them. This is not compatible with staining for 53BP1, a known marker of DNA damage and therefore it was not possible to detect TIFs in NHEK expressing myc-

TRF2$^{\Delta B\Delta M}$. Some evidence was obtained for 53BP1 induction in NHEK infected with myc-TRF2$^{\Delta B\Delta M}$, however it was not representative of the entire experiment.

P53 activation is another read-out of many DNA-damage responses. Western blotting of p53-phosphoS15 in NHEK expressing TRF2 constructs revealed some evidence for p53 activation when myc-TRF2$^{\Delta B\Delta M}$ is expressed. However, no evidence was found for induction of expression of p21 or for hypo-phosphorylation of Rb, both well established downstream consequences of p53 activation. Unfortunately, complications in harvesting a pure population of myc-TRF2$^{\Delta B\Delta M}$ positive cells at later time points prevents this lack of evidence acting towards or against the evidence of a p53 response.

No selective up-regulation of p16^{INK4A} was witnessed as a consequence of expressing myc-TRF2$^{\Delta B\Delta M}$. p16^{INK4A} levels increased equally with time in NHEK expressing the Vector only, myc-TRF2 FL and myc-TRF2$^{\Delta B\Delta M}$.

Experiments were performed to determine if changes in apoptosis or cell adherence were explanations for the reduced cloning efficiency of NHEK after myc-TRF2 FL or myc-TRF2$^{\Delta B\Delta M}$ expression. However, no evidence for apoptosis as evidenced by cleaved caspase 3, nor reduced cell adherence, was obtained.

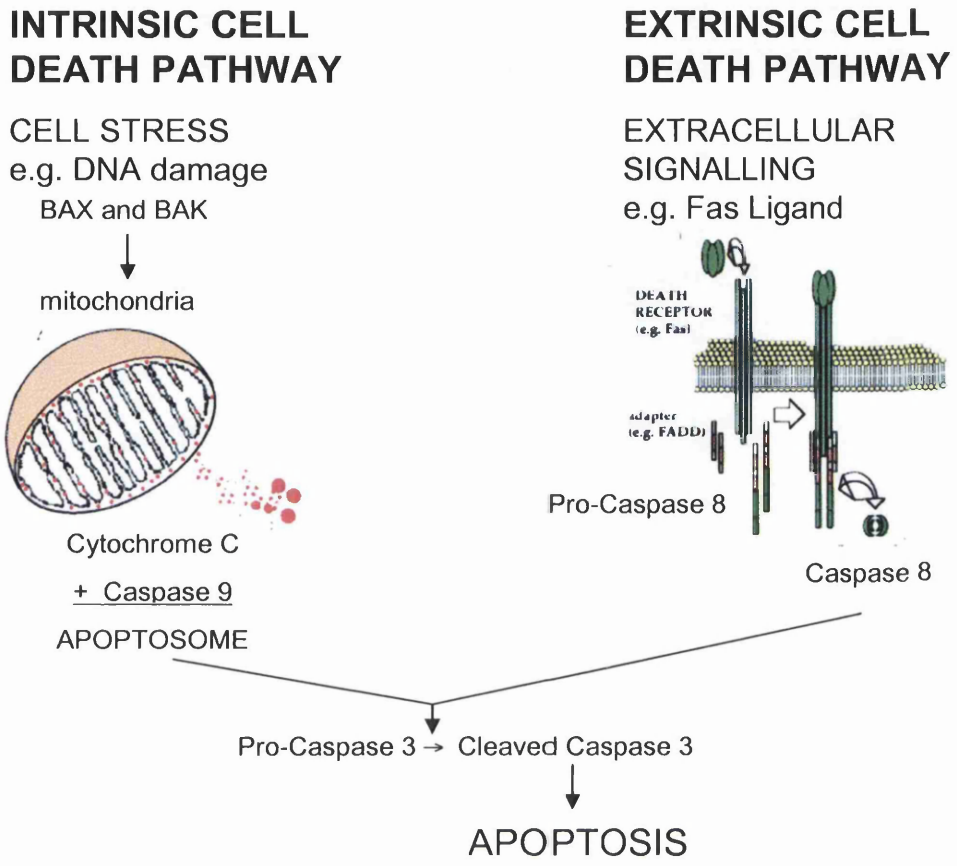

Figure 47. The role of cleaved caspase 3 in apoptosis.

This figure was copied in parts from 2 reviews:
1) Green, DR. Cell. 1998 Sep 18;94(6):695-8. Apoptotic pathways: the roads to ruin.
2) Siegel, RM. Nature Reviews Immunology. 2006 Apr;6(4):308-17. Caspases at the crossroads of immune-cell life and death.

The intrinsic apoptotic pathway is activated by internal stimuli which activate BCL-2 associated protein X protein (BAX) and /or BCL-2 antagonist/killer (BAK). Either will trigger mitochondrial permeability transition and thereby the release of factors such as cytochrome C which then triggers activation of caspase 9 in the apoptosome.

The extrinsic pathway is triggered through activation of receptors at the cell membrane that in turn activate caspase 8. Both caspase 8 (extrinsic) and the apoptosome (intrinsic) are capable of cleaving pro-caspase 3. Once cleaved, caspase 3 is active and can carry out the apoptotic execution of the cell.

Figure 48. Cleaved caspase 3 levels in NHEK expressing myc-TRF2 FL and myc-TRF2$^{\Delta B \Delta M}$.

On day 2, NHEK expressing low or high levels of GFP were plated with feeders immediately after being flow sorted. Cells were grown with the feeders until 2 days before their harvest at which point they were removed. When cells were harvested, both adherent and cells in suspension were collected and pooled. Control NHEK were treated with increasing doses of cisplatin which induced the cleavage of caspase 3. In all blots shown, the sample treated with 100 μM of cisplatin is considerably under-loaded.

There is no evidence for caspase 3 cleavage on (a) day 8, (b) day 10 and (c) day 12 of NHEK expressing either myc-TRF2$^{\Delta B \Delta M}$ or myc-TRF2 FL.

The same blots were also probed for TRF2 which was still expressed to varying degrees in all samples.

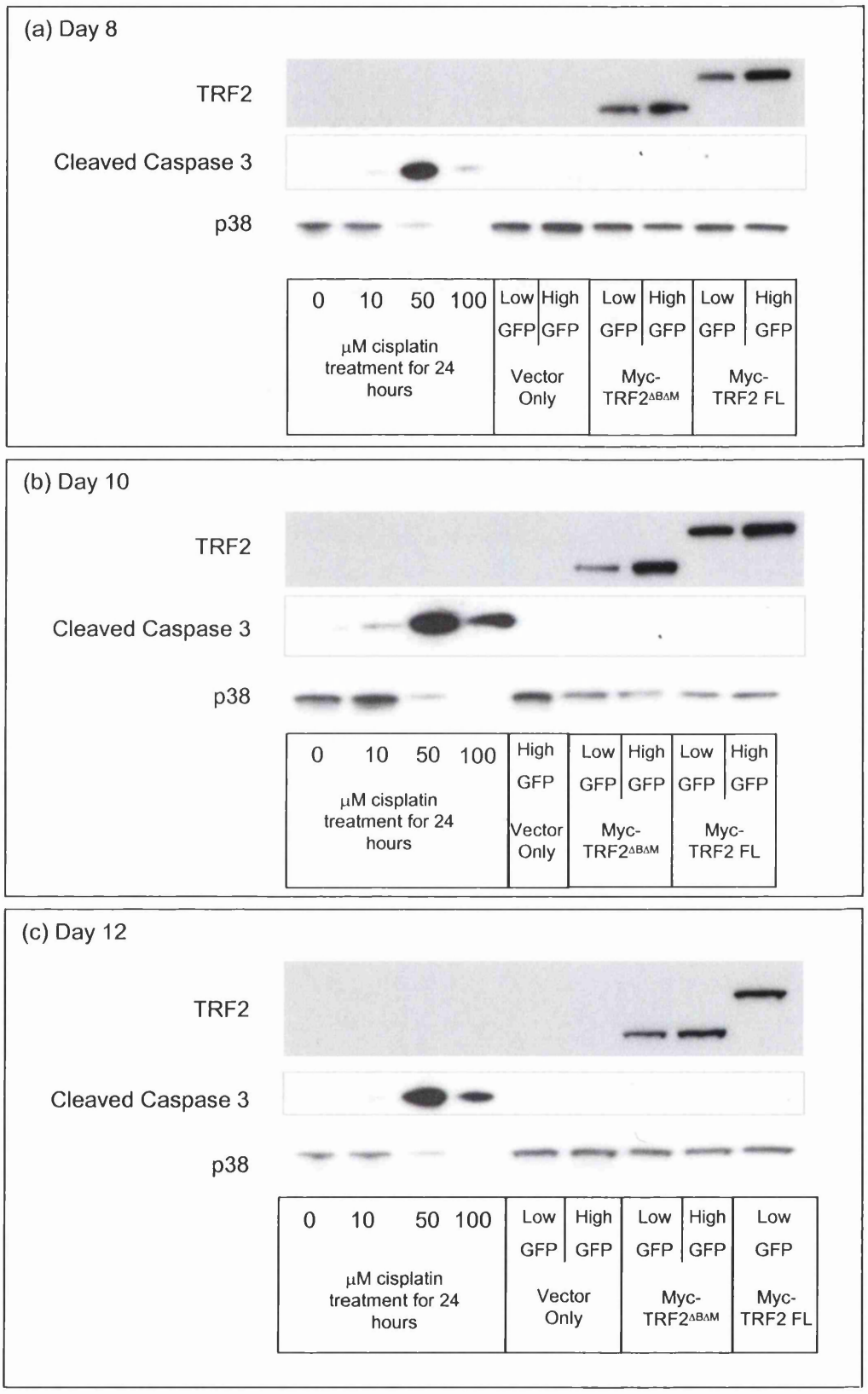

Figure 48. Cleaved caspase 3 levels in NHEK expressing myc-TRF2$^{\Delta B\Delta M}$ and myc-TRF2 FL.

Chapter 6: Discussion and Future Perspectives

6.1 Summary and Conclusions

When cells proliferate in the absence of a telomere lengthening mechanism, their telomeres shorten, a process which acts as a natural barrier to uncontrolled cell proliferation. Limitless replicative potential is one of the major hallmarks of cancer, most commonly achieved by up-regulation of telomerase which acts to lengthen telomeres (Hanahan and Weinberg 2000). TRF2 is the main protein responsible for telomere protection and keeps the telomere in what is referred to as a protected or "capped" state. An "uncapped" telomere can be created through expression of myc-TRF2$^{\Delta B\Delta M}$, a myc tagged dominant negative version of the TRF2 protein. Engineered to lack it's myb-domain, myc-TRF2$^{\Delta B\Delta M}$ works by stripping endogenous TRF2 from the telomere.

In cultured human fibroblasts (mesenchymal derived), it has been shown that p53 and p16^{INK4A} are the major regulators of uncapped telomeres (Jacobs and de Lange 2004). However, the majority of cancers originate from epithelial tissue, including the most common 3 cancers in the UK (2002): breast, lung and colorectal. To investigate if the same telomere-regulated senescence pathways used in normal fibroblasts, are activated in normal epithelium derived cells, this thesis has investigated the effects of artificially uncapping the telomeres in primary Normal Human Epidermal Keratinocytes, NHEK.

In every experiment: Vector only, myc-TRF2 FL and myc-TRF2$^{\Delta B\Delta M}$ were infected into NHEK using an optimised retroviral infection process. These IRES-GFP vectors were capable of expressing either myc-TRF2 FL or myc-TRF2$^{\Delta B\Delta M}$ and GFP as separate proteins ('Vector only' expressed GFP only.) Subsequent to infection on day -1, TRF2 and GFP expression started on day 0 and NHEK expressing the constructs could be isolated as early as day 1 or 2 using flow sorting.

NHEK flow sorted and plated on day 2, demonstrated co-localisation of the telomere binding protein TRF1 and endogenous/exogenous myc-TRF2 FL. Immunofluorescence also confirmed that, myc-TRF2$^{\Delta B\Delta M}$ stripped the endogenous TRF2 away from the telomere.

Low levels of expression of myc-TRF2 FL resulted in reduced proliferation ability and similar levels of myc-TRF2$^{\Delta B\Delta M}$ expression resulted in an even more drastic reduction in cell proliferation. Although the severity of the effect of expressing myc-TRF2 FL was unexpected, the degree of difference in proliferation between myc-TRF2 FL and myc-TRF2$^{\Delta B\Delta M}$ highlights the different effects they have at the telomere. The effect of the TRF2 constructs on proliferation of NHEK was determined by selecting and plating infected cells on day 2 and then performing cell counts at later time points.

Fewer and smaller colonies were seen in NHEK expressing myc-TRF2 FL compared with those expressing Vector only. The same effect, but even more pronounced, was seen when myc-TRF2$^{\Delta B\Delta M}$ was expressed. This provided further evidence that the uncapped telomeres severely limited replicative potential of the NHEK.

Small colonies found on plates of NHEK 10-14 days after infecting with the TRF2 constructs were no longer proliferating. Incubating the cells with Brd-U at day 12 (flow sorted and plated day 2) for 48 hours confirmed that smaller colonies, i.e. <50 cells, did not proliferate.

NHEK expressing myc-TRF2$^{\Delta B\Delta M}$ cannot grow to a colony size larger than 50 cells, whereas NHEK expressing myc-TRF2 FL are capable of developing into large colonies. Investigations using immunofluorescence on day 14 established that myc-TRF2 FL was still expressed in most colonies, small or large, although a mosaic pattern was observed in some larger colonies. In contrast, myc-TRF2$^{\Delta B\Delta M}$ was still expressed in all small colonies, but large colonies found on the same plate displayed either very little or, more commonly, no myc-TRF2$^{\Delta B\Delta M}$.

A larger number of senescent NHEK colonies were found in cultures that expressed the myc-TRF2 FL compared to Vector only as judged by Beta-galactosidase staining and colony size. Even more senescent positive cells were found in NHEK expressing myc-TRF2$^{\Delta B\Delta M}$.

FACS analysis of NHEK 10 days after infection with Vector only, myc-TRF2 FL and myc-TRF2$^{\Delta B\Delta M}$ all had the cell cycle profiles of normal NHEK. The most probable explanation is that the proliferation arrested cells were destroyed during FACS

analysis since the cells strong enough to survive the FACS analysis were no longer expressing myc-TRF2 FL or myc-TRF2$^{\Delta B \Delta M}$ and were expressing GFP only.

Telomere Induced DNA damage Foci, TIFs, were not found in NHEK expressing myc-TRF2$^{\Delta B \Delta M}$. This may have been due to incompatibility of protocols for co-localisation of TRF1 and 53BP1 and limitations in available technology made visualisation of TIFs unattainable within the timeframe of this thesis.

Activation of p53 in the form of phosphorylation at serine 15 was found in NHEK expressing myc-TRF2$^{\Delta B \Delta M}$ on day 2. Attempts to validate the activation of p53 by demonstrating a consistent up-regulation of p21 were unsuccessful. Evaluation of Rb phosphorylation status in NHEK expressing myc-TRF2$^{\Delta B \Delta M}$ provided some evidence that the Rb was hypo-phosphorylated at late time points, however it was not conclusive. It is possible that both of these known downstream targets of p53 were working to cause the proliferation arrested NHEK, but those cells could not be isolated using flow sorting due to their fragile state. p21 up-regulation was not seen in non-flow sorted cells either, however this could be an effect of the cell extract being diluted by NHEK not expressing the myc-TRF2$^{\Delta B \Delta M}$ construct.

Initial investigations to account for the differences in the number of colonies found on plates of NHEK expressing Vector only vs. myc-TRF2 FL or myc-TRF2$^{\Delta B \Delta M}$ did not provide any evidence of either less cell adhesion or apoptosis. No cleaved caspase 3 was found in preliminary experiments.

6.2 Strategy and limitations

The objective of this PhD was to characterise the effects of uncapping the telomere in a normal human epithelial cell system. NHEK cultured with Swiss 3T3 feeders was the cell system selected as it is of epithelial origin and can be grown for a limited time in tissue culture without any genetic modification (i.e. without knocking down p53, p16^{INK4A} or immortalising with telomerase). The TRF2 constructs donated to us by T. de Lange's lab were sub-cloned into the IRES-GFP vectors so that it would be possible to detect protein expression in the cells as soon as it occurred. The strategy enabled isolation of the NHEK expressing the relevant construct at early time points by flow sorting.

6.2.i Working with keratinocytes

As with all scientific endeavours, limitations occurred that complicated the interpretation of the work performed. NHEK can be grown two different ways, either using a serum-free system with collagen IV-coated plates or in medium with serum and a feeder layer, as used in this thesis. Of the two methods, culturing NHEK with feeders has been shown to provide a closer setting to the natural environment (Rheinwald and Beckett 1981) which is one reason it was selected. In addition to that, previously published retroviral infection protocols have shown high infection rates were capable of being obtained using the feeder system (Levy et al. 1998). As the myc-TRF2$^{\Delta B \Delta M}$ was expected to have detrimental effects on cell proliferation, high infection rates were made a priority. Two major drawbacks came with choosing this approach. Firstly, the time taken to prepare feeders, and even more time consuming is the time taken to remove the feeders from the tissue culture plates prior to harvest. As part of the infection process, removal of the PT67's took 15 min per 14 cm dish. In addition to limiting the number of samples that could be prepared within an experiment, this also added variability in the timing of treatment between samples within an experiment, e.g. 4 plates of Vector only might have their feeders removed, be trypsinised and sat on ice for 2 hours before the cells expressing the myc-TRF2$^{\Delta B \Delta M}$ reached the same state, or vice versa. The other major difficulty with the feeder system mentioned in the chapter 5 was trying to establish if the NHEK were failing to adhere or if they were undergoing apoptosis. It is common for a small amount of lethally irradiated feeders to detach from the tissue culture plate at a slow and constant rate. When no longer adherent to the plate it is difficult to decipher if the cells are 3T3 feeders naturally lifting from the plate or apoptotic NHEK.

Having subsequently learned [since optimising the infection process for this project] that NHEK grown in serum free systems can be infected if centrifuged with retroviral supernatant (Ken Parkinson- unpublished), with the benefit of hindsight, I would have completed the experiments using a serum and feeder free system.

6.2.ii Flow Sorting

Unexpectedly, flow sorting the cells became a major limitation within the project. Cell yields as poor as ~20% on average (of the GFP positive population) and bacterial contamination were re-occurring problems.

In addition to these struggles, the suspected loss of the proliferation arrested NHEK expressing myc-TRF2$^{\Delta B\Delta M}$ during the flow sorting process at late time points was another setback. The extent of this problem at earlier time points was difficult to ascertain, because NHEK infected with myc-TRF2$^{\Delta B\Delta M}$ and isolated using flow sorting (as late as day 5), were capable of adhering to both tissue culture plates/plastic coverslips and demonstrated the characterised lack of cell proliferation/cell localisation, appropriate to the specific vector it was expressing. It was therefore counter-intuitive to think the cells experiencing the effect of the myc-TRF2$^{\Delta B\Delta M}$ construct could not survive the flow sorting process.

A FACS profile to reveal where in cell cycle the NHEK expressing myc-TRF2$^{\Delta B\Delta M}$ had arrested was unobtainable at day 10. Levels of Brd-U incorporation remained the same, regardless of whether or not the NHEK were expressing Vector Only, myc-TRF2 FL or myc-TRF2$^{\Delta B\Delta M}$. Degradation of the proliferation arrested cells during the FACS analysis procedure seems the only likely explanation to this anomaly and is supported by increasing amounts of cell debris in the FACS profiles. It was bewildering that the profile could not be obtained as (by eye), the patterns from the Rhodamine B staining at day 10 (day 16 is shown in (**Figure 21**) suggested that the revertent colonies would not yet contain enough cells to completely dilute the growth arrested cells.

6.2.iii Over-expressing a Dominant Negative Protein

Myc-TRF2$^{\Delta B\Delta M}$ is an invaluable tool in studying the uncapped telomere. With its expression, an uncapped telomere can be created almost instantaneously compared to growing cells for long periods of time so that their telomeres naturally shorten, during which time an accumulation of genetic mutations could occur. However, there are at least 2 major drawbacks to taking this approach in studying the uncapped telomere.

Firstly, the telomere is not only deprived of TRF2, it also deprived of other telomere binding proteins which perform their own functions at the telomere and use TRF2 to anchor to the telomere during that time; Apollo (van Overbeek

and de Lange 2006), SNM1B (Freibaum and Counter 2006) and hRAP1 (Li et al. 2000) are 3 known examples. As a key member of the shelterin complex, it is more then likely that preventing TRF2 from binding at the telomere, either using TRF2$^{\Delta B\Delta M}$ or RNAi directed against TRF2, these effects will be seen.

Secondly, use of myc-TRF2$^{\Delta B\Delta M}$ to uncap the telomere may be a powerful tool for mimicking the uncapped telomere, but perhaps not be the best tool for assessing the structural changes that take place at a critically short telomere. Telomere structure has been shown to be responsible for initiating senescence in the fibroblast (Karlseder et al. 2002), and likewise SMURF2 is a protein capable of inducing senescence that is only up-regulated by critically short telomeres and not in cells expressing the TRF2$^{\Delta B\Delta M}$ (Zhang and Cohen 2004). Ultimately, any proteins suspected of inducing senescence based on experiments performed using TRF2$^{\Delta B\Delta M}$ would require confirmation in senescent cells with critically short telomeres before being proclaimed as a senescence inducing gene.

In a recent publication from the de Lange lab it was noted that "The role of TRF2 in vivo has not been tested. It is also not known whether the T-loop configuration occurs at all the telomeres and persists throughout the cell cycle." (Hockemeyer et al. 2006). It is widely believed, but still not proven, that the critically short telomere is no longer capable of folding into a T-loop structure and this is the event that leads to telomere uncapping.

6.3 How the thesis relates to the literature and future experiments

6.3.i Inability of cells with uncapped telomeres to proliferate

The most important contribution this work makes to the field of telomere biology is the establishment that uncapped telomeres in NHEK prevent the cell from further proliferating. It has been presumed that telomeres in epithelial cells would respond in the same way as fibroblasts, however until now this has remained undetermined. Proliferation curves of NHEK expressing myc-TRF2$^{\Delta B\Delta M}$ show a very slight increase just prior to 14 days in culture, as do similar proliferation curves for IMR90s published by the de Lange lab (Smogorzewska and de Lange 2002). Investigation by immunofluorescence established that at day 16, larger colonies on the myc-TRF2$^{\Delta B\Delta M}$ plates had reverted and were either: (1) no longer expressing GFP, nor myc-TRF2$^{\Delta B\Delta M}$ or (2) were still expressing GFP, but

no longer expressing myc-TRF2$^{\Delta B\Delta M}$. The NHEK were not kept under antibiotic selection pressure as the IMR90 cells were, so it is without doubt that the NHEK will have a larger amount of revertent cells. The growth of NHEK in colonies, as opposed to dispersed all over the plate, made analysis of heterogeneity within the population more obvious when examined using immunofluorescence, and emphasised the proliferation arrest seen when TRF2$^{\Delta B\Delta M}$ was still being expressed. It is likely, that the tiny escalation in proliferation also seen by the de Lange lab was also caused by revertent cells.

6.3.ii Detecting apoptosis

Using adenoviral TRF2$^{\Delta B\Delta M}$ in vivo in mouse liver, Lechel et al published that apoptosis was associated with higher expression levels of TRF2$^{\Delta B\Delta M}$, and cell senescence was associated with low levels of TRF2$^{\Delta B\Delta M}$ expression (Lechel et al. 2005). The publication used TUNEL (Terminal deoxynucleotidyl transferase-mediated dUTP-biotin Nick End-Labeling) to determine apoptotic cells. As TUNEL labels double strand breaks generated when the apoptotic cell degrades its DNA, it is possible that the uncapped telomeres are being labelled with dUTP and falsely described as apoptotic. Karlseder et al demonstrated apoptosis in HeLa cells after TRF2$^{\Delta B\Delta M}$ expression using TUNEL and a sub-G1 population in the FACS profile, but showed negative TUNEL staining and no sub-G1 staining for IMR90 cells (Karlseder et al. 1999). This would suggest that TUNEL might not be sensitive enough to detect uncapped telomeres, however an additional method to confirm the presence of apoptotic cells is preferable. Looking for cleaved caspase 3, as used in this thesis, did not provide evidence of apoptosis, nor did it manage to rule it out. Because the time window where cleaved caspase 3 is detectable during apoptosis is so short, it possible that it may have been missed. No evidence of a sub-G1 population was found in the FACS profiles for NHEK expressing myc-TRF2$^{\Delta B\Delta M}$, however it is improbable that apoptotic cells will survive both feeder removal and flow sorting.

Biroccio et al, determine the percentage of apoptotic cells using flow cytometric analysis of annexin V staining, an intracellular protein that is translocated to the external surface of the cell during apoptosis (Biroccio et al. 2006). Given the difficulties this project faced with FACS based protocols, this would also not be a suitable alternative. However, Annexin V staining can also be identified on the outside of the cell when using immunofluorescence, another future option to

identify apoptotic cells. Likewise, examining propidium iodide uptake into live cells or identifying DNA ladders typical of apoptotic cells are all other alternatives for identifying if an apoptotic population of cells is produced as a result of uncapping the telomere.

6.3.iii Lack of di-centric chromosomes

The de Lange lab has demonstrated using normal human fibroblasts that expression of TRF2$^{\Delta B\Delta M}$ results in an increase of p53 and p16^{INK4A}. They also witnessed chromosomal fusions, which were obvious in anaphase cells labelled with dapi. Conspicuous by its absence, was the lack of anaphase bridging in NHEK expressing myc-TRF2$^{\Delta B\Delta M}$ (Chapter 4). This is the first time telomere uncapping has been investigated at an early stage of growth in a primary epithelial cell system. The NHEK are derived from newborn foreskin and therefore more likely to contain the full repertoire of DNA damage response than other established cell lines that have been passaged for longer. The lack of anaphase bridging suggests that the response pathways activated following recognition of telomere damage do not allow progression through the cell cycle and therefore the end joining seen in other cell lines, e.g. IMR90 (fibroblasts) and HTC75 (fibrosarcoma) to occur. However, these points require a more thorough investigation. An important consideration is that filtering prior to flow sorting may have removed cells already experiencing the di-centric chromosomes. The dapi staining in the immunofluorescence demonstrates that after being plated as a single cell suspension, the NHEK expressing myc-TRF2$^{\Delta B\Delta M}$ were still able to form small colonies that growth arrested without any evidence of di-centric chromosome formation in anaphase. An experiment where NHEK are infected with myc-TRF2$^{\Delta B\Delta M}$ and then left for a week to develop without flow sorting is now needed to specifically investigate TRF2 construct expression correlation with the presence of di-centric chromosomes. Knockdown of Tankyrase1 in parallel cultures would serve as a nice control as this has been shown to generate mitotic arrest through telomere association in anaphase with dapi through a different mechanism (Dynek and Smith 2004).

6.3.iv P53 response in cancer

In NHEK expressing TRF2$^{\Delta B\Delta M}$, p53 was found to be phosphorylated at Serine 15 signifying its activation at an early time point. From the literature, the p53 response undoubtedly contributes to the senescent phenotype and this may have

grave implications for telomerase based therapies which intend to specifically prevent cancer cell growth by reducing telomeres to a critically short length. If cells rely on p53 (even in part) which is mutated in >50% of all tumours (Levine 1997), it is not clear what will induce senescence in these tumour cells. Using a dominant negative version of hTERT, Hahn et al demonstrated that four telomerase positive cell lines were unable to continue proliferating without their telomerase activity (Hahn et al. 1999). The lag time between when the cells started expressing the construct and either growth arrested or experienced cell death was dependent upon their telomere length. Telomere shortening and an increase in chromosomal fusions after ~20 population doublings were seen using the ovarian cancer cell line, 36M (Hahn et al. 1999). Critically, p53 was not present in two of these cell lines, yet despite the lack of p53, both cell lines contained cells with flattened morphology that had stopped proliferating and demonstrated a degree of apoptosis (as is consistent with cells in crisis). This result makes it clear that pathways other then p53 play a role in preventing further cell proliferation.

6.3.v DNA damage response and telomerase

A fairly new theme under investigation is the involvement of proteins from the field of telomere and telomerase biology in DNA damage repair. In addition to the discovery of TRF2 at non-telomeric sites of DNA damage (Bradshaw et al. 2005) there is also evidence that telomerase is involved in DNA repair. Ectopic expression of hTERT leads to transcriptional changes in a subset of genes and changes the interaction of telomeres with the nuclear matrix. These changes are associated with reduced spontaneous chromosome damage during G1, enhanced kinetics of DNA repair and an increase in nucleotide triphosphate levels (Sharma et al. 2003). Complete suppression of hTERT prevents the cellular response to DNA double strand breaks, not by altering telomere integrity, but by affecting its overall configuration of chromatin. Cells lacking hTERT exhibit increased radio sensitivity, diminished capacity for DNA repair and fragmented chromosomes, all factors which demonstrate that the loss of hTERT impairs the DNA damage response (Masutomi et al. 2005).

Given the dramatic reduction in cell proliferation that uncapped telomeres are proven to instigate, it is surprising the DNA damage response in the cells is so difficult to detect. Western blot assessment of DNA damage response proteins

published by the de Lange lab (Smogorzewska and de Lange 2002) and demonstrated in this thesis after expressing myc-TRF2$^{\Delta B \Delta M}$ appears minimal. Neither the human fibroblasts used in the Smogorzewska publication nor the NHEK used in this thesis express hTERT exogenously, as cells used to study the DNA damage response commonly do. The lack of exogenous hTERT may provide an explanation for why the DNA damage responses seen in these cells is so subdued. It is possible that expectations of the scale of the DNA damage required to generate a cell cycle arrest have been skewed by the use of cells which constitutively and unnaturally over express hTERT. Nevertheless, it is evident NHEK can induce a large DNA damage response in response to IR (Chapter 5), so perhaps double strand breaks at the telomere are effected differently by exogenous expression of hTERT. Further investigation, particularly with regard to the effect of flow sorting on DNA damage protein level assessment is required before further statements regarding this subject can be made.

Furthermore, NHEK were shown to have a low level of telomerase activity. This is most likely attributed to by cells from the basal layer, as transit amplifying cells have been shown to down-regulate their telomerase activity (Harle-Bachor and Boukamp 1996). This mosaic pattern of telomerase activity makes NHEK unique from established cell lines where all cells are likely to have some level of telomerase activity. However, it is also possible that the small amount of telomerase activity could be contributed to by even a tiny amount of 3T3 feeder contamination. A control which there was not enough time to investigate would have been to examine the telomerase activity in the same cells grown using the serum free system. This also would have served as an excellent control for the telomere length analysis.

Direct comparisons can never be made between human and mouse cells, particularly in telomere biology where the effects of uncapped telomeres are distinctly different. However, if telomerase is capable of modifying chromatin as part of the DNA damage response, this could have implications for the mTR$^{-/-}$, genetically altered mice which are usually bred for 3-4 generations to make their telomere lengths comparable with humans before being used in experiments.

6.3.vi Over-expression of myc-TRF2 FL

Each experiment in this thesis used myc-TRF2 FL as a control. Over-expression of TRF2 resulted in reduced proliferation rates compared to Vector only controls: a similar, if slightly less dramatic, effect was observed by the de Lange lab in IMR90 cells (Smogorzewska and de Lange 2002). NHEK showing low and high levels of expression of myc-TRF2 FL and myc-TRF2$^{\Delta B\Delta M}$ were examined in this thesis. Higher levels of myc-TRF2 FL expression were equally as effective at reducing cell proliferation as low expression levels myc-TRF2$^{\Delta B\Delta M}$ (specifically (**Figure 20**), Section 4.2). Although the immunofluorescence performed was not quantitative, there did not appear to be a greater level of myc-TRF2 FL bound to the telomere in NHEK expressing higher levels of the protein. This suggests that even low levels of myc-TRF2 FL expression can be saturating; thus greater levels of expression that can not bind to the telomere may in fact sequester the limited amount of other telomere binding proteins in the nucleoplasm, rather then at the telomere, thereby effectively exerting a dominant negative effect.

Mice which over-express TRF2 in the skin demonstrate a severe phenotype in response to light, consisting of premature deterioration, hyper-pigmentation and increased skin cancer, all characteristics of the human disease Xeroderma pigmentosum (Munoz et al. 2005). Their telomeres were markedly shorter, displayed loss of the G-strand overhang and increased chromosomal fusion. Over-expression of TRF2 in mice keratinocytes where XPF was deleted prevented the telomere shortening and end to end fusions (Munoz et al. 2005). The experiments from the mouse model therefore indicate that excessive amounts of TRF2 lead to increased amounts of processing at the telomere by members of the XPF/ERCC family. This could be a contributing factor in the decrease of proliferation rates in NHEK expressing myc-TRF2 FL.

6.3.vii FACS analysis to detect senescence

What remains unexplained is why the NHEK in this study were not durable enough to survive FACS analysis after being growth arrested for 10 days, when clearly the IMR90 used in the de Lange lab study were. It is possible that the IMR90s also contained revertant cells within the population that were no longer expressing the myc-TRF2$^{\Delta B\Delta M}$, but were still expressing the antibiotic resistance and therefore hardy enough for FACS analysis on day 15. The de Lange lab published the following statements regarding expression of myc-TRF2$^{\Delta B\Delta M}$ in

IMR90 cells: "FACS analysis on day 15 revealed cells with either a 2N or 4N DNA content, a profile matching that of cells undergoing replicative senescence (data not shown). It is possible that the population of cells with a 4N DNA content represents tetra-ploid cells rather then cells arrested in G2/M." (Smogorzewska and de Lange 2002). Although it is tempting to think the FACS profiles shown in this thesis might also simply be displaying NHEK arrested in G1 and G2/M, this is excluded since the NHEK in question were still proliferating as judged by incorporation of Brd-U. Immunofluorescent analysis of Brd-U incorporation over a 48 hour period revealed that only large colonies (established to be reverted in other experiments) had incorporated Brd-U. Therefore the FACS profiles seen here, demonstrating Brd-U incorporation, are dominated by revertent cells, not the proliferation arrested NHEK which were intended to be analysed.

FACS analysis of senescent cells is not prevalent in the literature, suggesting such data might be difficult to obtain. However, one publication that examines human prostatic epithelial cells, HPECs, grown from early passage to senescence, defined as those which remained sub-confluent for greater then a month. Such senescent HPECs were accompanied by a gradual loss of cells in S phase and an accumulation of cells containing 2N DNA (Sandhu et al. 2000), though similar percentages of cells in G2 were found in both growing (12%) and senescent (14%) cells. Crucially, they demonstrated that senescent cells are durable enough for FACS analysis and showed a lack of Brd-U incorporation.

γ-Ionising radiation, which induces double strand breaks, cause a G2 arrest in NHEK. It is particularly disappointing that a FACS profile could not be determined where uncapped telomeres caused proliferation arrest as it would have been of particular interest to determine if the uncapped telomere also provoked growth arrest at G2. Had time allowed, alternatives to FACs analysis could have included immunofluorescence to detect G2 specific proteins, thereby identifying such cells (e.g. CEN-PF, a protein that localises to kinetochores in late G2, remains kinetochore-bound until anaphase, and is degraded at the end of mitosis (Bomont et al. 2005)).

6.4 Future Perspectives

The goal of the research presented in this PhD was to characterise the result of uncapping telomeres in a normal primary epithelial cell system. Senescence was established as one of the cellular outcomes, most likely triggered by activated p53. Due to time restraints, it was not possible to rule out differentiation or apoptosis as other outcomes that occur as a result of telomere uncapping in NHEK or determine where in the cell cycle the NHEK had stopped proliferating. These are all important aspect of the response which should be addressed.

Examining the effect of uncapped telomeres in cancer cell cultures to further characterise the response to uncapped telomeres when various pathways such as p53 and $p16^{INK4A}$ are no longer functional is another investigation that can take place. Both apoptosis and senescence have been demonstrated as responses and better characterisation of the pathways behind these cellular decisions are required. The objective of drugs which inhibit telomerase activity is to specifically target the telomeres of cancer cells so that their critical short length induces either cell proliferation arrest or apoptosis. Use of $TRF2^{\Delta B\Delta M}$ would offer an interesting insight into what happens when the telomeres are long and uncapped vs. uncapped because they are critically short. With new found evidence that telomere binding proteins are mis-regulated in cancer cells, these studies might offer valuable insight into alternative ways the telomere can be de-regulated and contribute to cancer cell progression.

Proliferative tissues continuously progress through the cell cycle and are more exposed to carcinogens (e.g. carcinogens in food, smoke, UV light, etc.), so it is not surprising the majority of human cancers are derived from epithelial cells. It stands to reason they may have more mechanisms of preventing uncontrolled cell proliferation then fibroblasts. In a similar way to the work published by Jacobs and de Lange, it would be interesting to establish if knocking down p53 and $p16^{INK4A}$ is enough to allow NHEK to continue proliferating, despite having uncapped telomeres, as it was in human fibroblasts (Jacobs and de Lange 2004). This would serve to indicate if there are more pathways to control cell proliferation in epithelial cells as opposed to fibroblasts.

The original plan was that this telomere investigation would move on to a microarray analysis of myc-TRF2$^{\Delta B\Delta M}$ induced gene expression changes at an early time point, in between the point at which myc-TRF2$^{\Delta B\Delta M}$ is expressed (as judged by GFP expression) and the phosphorylation of p53. This might have established more as yet unknown pathways, which activate the chain of events which prevent the NHEK from further proliferating. However, in the end, time and funding was not available to pursue this option during this thesis. Identification of other possible p53 target genes as well evaluating the up-regulation of known ones (e.g. p21) would have proved interesting. Nonetheless, the Blasco lab performed a microarray investigation with Generation 3 (G3) Terc$^{-/-}$ mice in which uncapped telomeres were induced by loss of Ku86 (Ku86$^{-/-}$ mice). The different transcripts observed in double mutant G3 Terc$^{-/-}$/Ku86$^{-/-}$ cells compared with wild-type cells showed a predominance of genes involved in cell adhesion, cell-to-cell and cell-to-matrix communication, as well as increased metabolic turnover and augmented antioxidant responses (Franco et al. 2005). It would be interesting to investigate if the same genes are up-regulated in NHEK uncapped using myc-TRF2$^{\Delta B\Delta M}$.

Other techniques could be used to further evaluate the changes that occur as a result of uncapping the telomere. Activation of the DNA damage response pathway involves up-regulation of proteins such as 53BP1 and p21, but equally important processes within the pathway's activation are also phosphorylation of proteins such as p53 and NBS1. Another approach to characterising the uncapped telomere would be to compare the post-translational modifications such as phosphorylation, ubiquitination, sumoylation, and equally as importantly, looking for de-phosphorylation, de-sumoylation or de-ubiquitination of proteins that may be downstream of an uncapped telomere signal. 2-D gel electrophoresis can be used in proteomics analysis to directly quantitate differential phosphorylation patterns. It is possible to label two separate samples with different probes and run them together so that proteins that have been phosphorylated differently don't co-localise and are easily identifiable through mass spectrometry.

MicroRNA is an emerging new field of cell regulation. Naturally occurring small non-coding RNA gene products are found in diverse organisms and play key roles in regulating the translation and degradation of mRNAs (Bartel 2004). Unique

microRNA molecular profiles in lung cancer diagnosis and prognosis have recently been established (Yanaihara et al. 2006) thereby associating this new field to the general mis-regulation seen in cancer cells. MicroRNA arrays now exist for evaluating the MicroRNA status of different cells. As array evaluation is a straightforward way of detecting changes in MicroRNA, it is another technique to be considered in discovering changes that result after uncapping the telomere.

Characterisation of uncapped telomeres is important so that if drugs inhibiting telomerase activity succeed in creating critically short telomeres in tumour cells, but fail in preventing cell proliferation, the process will be well characterised and the missing components within the tumour cell readily identifiable. Ultimately, this will aid not only in devising cancer therapeutics, but also in understanding how they need to be optimised.

Appendices I

Agar Scientific, Essex, CM24 E07

Amersham, Amersham Place, Little Chalfont, Buckinghamshire, HP7 9NA

ATCC (Distributed by LGC Ltd, Middlesex, TW11 0LY)

BD PharMingen, 10975 Torreyana Road, San Diego, California 92121, USA

Becton Dickinson, Oxford, OX4 3LY

BIO-RAD, Hemel Hempstead, HP2 7TD

Cell Signalling (distributed by New England BioLabs)

DAKO Ltd., Cambridgeshire, CB7 4ET

EPICENTRE Biotechnologies, 726 Post Road, Madison, WI 53713 USA

Fisher Scientific UK Ltd, Bishop Meadow Road, Loughborough, Leicestershire LE11 5RG

Flowgen Instruments, Staffordshire, WS14 0EE

Invitrogen, Renfewshire, PA4 9RF

Jackson Immuno Research (Distributed by Stratech Scientific, Cambridgeshire, CB7 5UE)

Lorne Laboratories, Reading, RG10 9NJ

Melford Laboratories, Bildeston Road, Chelsworth, Ipswich, Suffolk, IP7 7LE

Millipore, Heretfordshire, WD1 8YW

New England Biolabs, Wilbury Way, Hichin, Hertfordshire, SG4 0TY

Perbio, Cheshire CH3 9RJ

Roche Products Limited, 6 Falcon Way, Shire Park, Welwyn Garden City, AL7 1TW

Severn Biotech Ltd, Worcestershire, DY11 6TJ

Sigma, Dorset, SP8 4XT

Upstate, Buckinghamshire, MK18 2LR

Vector Laboratories, Peterborough, PE2 6XS

List of References

Allshire, R.C., M. Dempster, and N.D. Hastie. 1989. Human telomeres contain at least three types of G-rich repeat distributed non-randomly. *Nucleic Acids Res* **17**: 4611-27.

Allsopp, R.C., E. Chang, M. Kashefi-Aazam, E.I. Rogaev, M.A. Piatyszek, J.W. Shay, and C.B. Harley. 1995. Telomere shortening is associated with cell division in vitro and in vivo. *Exp Cell Res* **220**: 194-200.

Bailey, S.M., M.N. Cornforth, A. Kurimasa, D.J. Chen, and E.H. Goodwin. 2001. Strand-specific postreplicative processing of mammalian telomeres. *Science* **293**: 2462-5.

Bakkenist, C.J., R. Drissi, J. Wu, M.B. Kastan, and J.S. Dome. 2004. Disappearance of the telomere dysfunction-induced stress response in fully senescent cells. *Cancer Res* **64**: 3748-52.

Barrandon, Y. and H. Green. 1985. Cell size as a determinant of the clone-forming ability of human keratinocytes. *Proc Natl Acad Sci U S A* **82**: 5390-4.

Barrandon, Y. and H. Green. 1987a. Cell migration is essential for sustained growth of keratinocyte colonies: the roles of transforming growth factor-alpha and epidermal growth factor. *Cell* **50**: 1131-7.

Barrandon, Y. and H. Green. 1987b. Three clonal types of keratinocyte with different capacities for multiplication. *Proc Natl Acad Sci U S A* **84**: 2302-6.

Bartel, D.P. 2004. MicroRNAs: genomics, biogenesis, mechanism, and function. *Cell* **116**: 281-97.

Bass, H.W., W.F. Marshall, J.W. Sedat, D.A. Agard, and W.Z. Cande. 1997. Telomeres cluster de novo before the initiation of synapsis: a three-dimensional spatial analysis of telomere positions before and during meiotic prophase. *J Cell Biol* **137**: 5-18.

Baus, F., V. Gire, D. Fisher, J. Piette, and V. Dulic. 2003. Permanent cell cycle exit in G2 phase after DNA damage in normal human fibroblasts. *Embo J* **22**: 3992-4002.

Bi, X., S.C. Wei, and Y.S. Rong. 2004. Telomere protection without a telomerase; the role of ATM and Mre11 in Drosophila telomere maintenance. *Curr Biol* **14**: 1348-53.

Bianchi, A. and T. de Lange. 1999. Ku binds telomeric DNA in vitro. *J Biol Chem* **274**: 21223-7.

Bianchi, A., S. Smith, L. Chong, P. Elias, and T. de Lange. 1997. TRF1 is a dimer and bends telomeric DNA. *Embo J* **16**: 1785-94.

Biroccio, A., A. Rizzo, R. Elli, C.E. Koering, A. Belleville, B. Benassi, C. Leonetti, M.F. Stevens, M. D'Incalci, G. Zupi, and E. Gilson. 2006. TRF2 inhibition triggers apoptosis and reduces tumourigenicity of human melanoma cells. *Eur J Cancer* **42**: 1881-1888.

Blackburn, E.H. 1984. The molecular structure of centromeres and telomeres. *Annu Rev Biochem* **53**: 163-94.

Blasco, M.A., H.W. Lee, M. Rizen, D. Hanahan, R. DePinho, and C.W. Greider. 1997. Mouse models for the study of telomerase. *Ciba Found Symp* **211**: 160-70; discussion 170-6.

Bodnar, A.G., M. Ouellette, M. Frolkis, S.E. Holt, C.P. Chiu, G.B. Morin, C.B. Harley, J.W. Shay, S. Lichtsteiner, and W.E. Wright. 1998. Extension of life-span by introduction of telomerase into normal human cells. *Science* **279**: 349-52.

Bomont, P., P. Maddox, J.V. Shah, A.B. Desai, and D.W. Cleveland. 2005. Unstable microtubule capture at kinetochores depleted of the centromere-associated protein CENP-F. *Embo J* **24**: 3927-39.

Bradshaw, P.S., D.J. Stavropoulos, and M.S. Meyn. 2005. Human telomeric protein TRF2 associates with genomic double-strand breaks as an early response to DNA damage. *Nat Genet* **37**: 193-7.

Braig, M., S. Lee, C. Loddenkemper, C. Rudolph, A.H. Peters, B. Schlegelberger, H. Stein, B. Dorken, T. Jenuwein, and C.A. Schmitt. 2005. Oncogene-induced senescence as an initial barrier in lymphoma development. *Nature* **436**: 660-5.

Broccoli, D., A. Smogorzewska, L. Chong, and T. de Lange. 1997. Human telomeres contain two distinct Myb-related proteins, TRF1 and TRF2. *Nat Genet* **17**: 231-5.

Brunori, M., N. Mathieu, M. Ricoul, S. Bauwens, C.E. Koering, A. Roborel de Climens, A. Belleville, Q. Wang, I. Puisieux, D. Decimo, A. Puisieux, L. Sabatier, and E. Gilson. 2006. TRF2 inhibition promotes anchorage-independent growth of telomerase-positive human fibroblasts. *Oncogene* **25**: 990-7.

Bryan, T.M., A. Englezou, J. Gupta, S. Bacchetti, and R.R. Reddel. 1995. Telomere elongation in immortal human cells without detectable telomerase activity. *Embo J* **14**: 4240-8.

Campisi, J. 2000. Cancer, aging and cellular senescence. *In Vivo* **14**: 183-8.

Carney, J.P., R.S. Maser, H. Olivares, E.M. Davis, M. Le Beau, J.R. Yates, 3rd, L. Hays, W.F. Morgan, and J.H. Petrini. 1998. The hMre11/hRad50 protein complex and Nijmegen breakage syndrome: linkage of double-strand break repair to the cellular DNA damage response. *Cell* **93**: 477-86.

Celli, G.B. and T. de Lange. 2005. DNA processing is not required for ATM-mediated telomere damage response after TRF2 deletion. *Nat Cell Biol* **7**: 712-8.

Celli, G.B., E.L. Denchi, and T. de Lange. 2006. Ku70 stimulates fusion of dysfunctional telomeres yet protects chromosome ends from homologous recombination. *Nat Cell Biol* **8**: 885-90.

Chai, W., Q. Du, J.W. Shay, and W.E. Wright. 2006a. Human telomeres have different overhang sizes at leading versus lagging strands. *Mol Cell* **21**: 427-35.

Chai, W., L.P. Ford, L. Lenertz, W.E. Wright, and J.W. Shay. 2002. Human Ku70/80 associates physically with telomerase through interaction with hTERT. *J Biol Chem* **277**: 47242-7.

Chai, W., A.J. Sfeir, H. Hoshiyama, J.W. Shay, and W.E. Wright. 2006b. The involvement of the Mre11/Rad50/Nbs1 complex in the generation of G-overhangs at human telomeres. *EMBO Rep* **7**: 225-30.

Chai, W., J.W. Shay, and W.E. Wright. 2005. Human telomeres maintain their overhang length at senescence. *Mol Cell Biol* **25**: 2158-68.

Chang, B.D., E.V. Broude, M. Dokmanovic, H. Zhu, A. Ruth, Y. Xuan, E.S. Kandel, E. Lausch, K. Christov, and I.B. Roninson. 1999. A senescence-like phenotype distinguishes tumor cells that undergo terminal proliferation arrest after exposure to anticancer agents. *Cancer Res* **59**: 3761-7.

Chang, P., M. Coughlin, and T.J. Mitchison. 2005. Tankyrase-1 polymerization of poly(ADP-ribose) is required for spindle structure and function. *Nat Cell Biol* **7**: 1133-9.

Chen, Q.M., J.C. Bartholomew, J. Campisi, M. Acosta, J.D. Reagan, and B.N. Ames. 1998. Molecular analysis of H2O2-induced senescent-like growth arrest in normal human fibroblasts: p53 and Rb control G1 arrest but not cell replication. *Biochem J* **332 (Pt 1)**: 43-50.

Chen, Z., L.C. Trotman, D. Shaffer, H.K. Lin, Z.A. Dotan, M. Niki, J.A. Koutcher, H.I. Scher, T. Ludwig, W. Gerald, C. Cordon-Cardo, and P.P. Pandolfi.

2005. Crucial role of p53-dependent cellular senescence in suppression of Pten-deficient tumorigenesis. *Nature* **436**: 725-30.

Chiang, Y.J., S.H. Kim, L. Tessarollo, J. Campisi, and R.J. Hodes. 2004. Telomere-associated protein TIN2 is essential for early embryonic development through a telomerase-independent pathway. *Mol Cell Biol* **24**: 6631-4.

Chiang, Y.J., M.L. Nguyen, S. Gurunathan, P. Kaminker, L. Tessarollo, J. Campisi, and R.J. Hodes. 2006. Generation and characterization of telomere length maintenance in tankyrase 2-deficient mice. *Mol Cell Biol* **26**: 2037-43.

Chikashige, Y., D.Q. Ding, H. Funabiki, T. Haraguchi, S. Mashiko, M. Yanagida, and Y. Hiraoka. 1994. Telomere-led premeiotic chromosome movement in fission yeast. *Science* **264**: 270-3.

Chikashige, Y., C. Tsutsumi, M. Yamane, K. Okamasa, T. Haraguchi, and Y. Hiraoka. 2006. Meiotic proteins bqt1 and bqt2 tether telomeres to form the bouquet arrangement of chromosomes. *Cell* **125**: 59-69.

Chong, L., B. van Steensel, D. Broccoli, H. Erdjument-Bromage, J. Hanish, P. Tempst, and T. de Lange. 1995. A human telomeric protein. *Science* **270**: 1663-7.

Ciapponi, L., G. Cenci, J. Ducau, C. Flores, D. Johnson-Schlitz, M.M. Gorski, W.R. Engels, and M. Gatti. 2004. The Drosophila Mre11/Rad50 complex is required to prevent both telomeric fusion and chromosome breakage. *Curr Biol* **14**: 1360-6.

Collis, S.J., T.L. DeWeese, P.A. Jeggo, and A.R. Parker. 2005. The life and death of DNA-PK. *Oncogene* **24**: 949-61.

Cook, B.D., J.N. Dynek, W. Chang, G. Shostak, and S. Smith. 2002. Role for the related poly(ADP-Ribose) polymerases tankyrase 1 and 2 at human telomeres. *Mol Cell Biol* **22**: 332-42.

Cooke, H.J. and B.A. Smith. 1986. Variability at the telomeres of the human X/Y pseudoautosomal region. *Cold Spring Harb Symp Quant Biol* **51 Pt 1**: 213-9.

Cooper, J.P., E.R. Nimmo, R.C. Allshire, and T.R. Cech. 1997. Regulation of telomere length and function by a Myb-domain protein in fission yeast. *Nature* **385**: 744-7.

Counter, C.M., A.A. Avilion, C.E. LeFeuvre, N.G. Stewart, C.W. Greider, C.B. Harley, and S. Bacchetti. 1992. Telomere shortening associated with

chromosome instability is arrested in immortal cells which express telomerase activity. *Embo J* **11**: 1921-9.

Crabbe, L., R.E. Verdun, C.I. Haggblom, and J. Karlseder. 2004. Defective telomere lagging strand synthesis in cells lacking WRN helicase activity. *Science* **306**: 1951-3.

Cristofari, G. and J. Lingner. 2006. Telomere length homeostasis requires that telomerase levels are limiting. *Embo J* **25**: 565-74.

d'Adda di Fagagna, F., M.P. Hande, W.M. Tong, D. Roth, P.M. Lansdorp, Z.Q. Wang, and S.P. Jackson. 2001. Effects of DNA nonhomologous end-joining factors on telomere length and chromosomal stability in mammalian cells. *Curr Biol* **11**: 1192-6.

d'Adda di Fagagna, F., P.M. Reaper, L. Clay-Farrace, H. Fiegler, P. Carr, T. Von Zglinicki, G. Saretzki, N.P. Carter, and S.P. Jackson. 2003. A DNA damage checkpoint response in telomere-initiated senescence. *Nature* **426**: 194-8.

Dantzer, F., M.J. Giraud-Panis, I. Jaco, J.C. Ame, I. Schultz, M. Blasco, C.E. Koering, E. Gilson, J. Menissier-de Murcia, G. de Murcia, and V. Schreiber. 2004. Functional interaction between poly(ADP-Ribose) polymerase 2 (PARP-2) and TRF2: PARP activity negatively regulates TRF2. *Mol Cell Biol* **24**: 1595-607.

Darbro, B.W., K.M. Lee, N.K. Nguyen, F.E. Domann, and A.J. Klingelhutz. 2006. Methylation of the p16(INK4a) promoter region in telomerase immortalized human keratinocytes co-cultured with feeder cells. *Oncogene*.

Darbro, B.W., G.B. Schneider, and A.J. Klingelhutz. 2005. Co-regulation of p16INK4A and migratory genes in culture conditions that lead to premature senescence in human keratinocytes. *J Invest Dermatol* **125**: 499-509.

de Lange, T. 2005. Shelterin: the protein complex that shapes and safeguards human telomeres. *Genes Dev* **19**: 2100-10.

Dimri, G.P., X. Lee, G. Basile, M. Acosta, G. Scott, C. Roskelley, E.E. Medrano, M. Linskens, I. Rubelj, O. Pereira-Smith, and et al. 1995. A biomarker that identifies senescent human cells in culture and in aging skin in vivo. *Proc Natl Acad Sci U S A* **92**: 9363-7.

Dimri, G.P., M. Nakanishi, P.Y. Desprez, J.R. Smith, and J. Campisi. 1996. Inhibition of E2F activity by the cyclin-dependent protein kinase inhibitor p21 in cells expressing or lacking a functional retinoblastoma protein. *Mol Cell Biol* **16**: 2987-97.

Dulic, V., L.F. Drullinger, E. Lees, S.I. Reed, and G.H. Stein. 1993. Altered regulation of G1 cyclins in senescent human diploid fibroblasts: accumulation of inactive cyclin E-Cdk2 and cyclin D1-Cdk2 complexes. *Proc Natl Acad Sci U S A* **90**: 11034-8.

Dynek, J.N. and S. Smith. 2004. Resolution of sister telomere association is required for progression through mitosis. *Science* **304**: 97-100.

Eller, M.S., N. Puri, I.M. Hadshiew, S.S. Venna, and B.A. Gilchrest. 2002. Induction of apoptosis by telomere 3' overhang-specific DNA. *Exp Cell Res* **276**: 185-93.

Espejel, S., S. Franco, S. Rodriguez-Perales, S.D. Bouffler, J.C. Cigudosa, and M.A. Blasco. 2002. Mammalian Ku86 mediates chromosomal fusions and apoptosis caused by critically short telomeres. *Embo J* **21**: 2207-19.

Fairall, L., L. Chapman, H. Moss, T. de Lange, and D. Rhodes. 2001. Structure of the TRFH dimerization domain of the human telomeric proteins TRF1 and TRF2. *Mol Cell* **8**: 351-61.

Franco, S., A. Canela, P. Klatt, and M.A. Blasco. 2005. Effectors of mammalian telomere dysfunction: a comparative transcriptome analysis using mouse models. *Carcinogenesis* **26**: 1613-26.

Freibaum, B.D. and C.M. Counter. 2006. hSnm1B is a novel telomere-associated protein. *J Biol Chem* **281**: 15033-6.

Galati, A., L. Rossetti, S. Pisano, L. Chapman, D. Rhodes, M. Savino, and S. Cacchione. 2006. The human telomeric protein TRF1 specifically recognizes nucleosomal binding sites and alters nucleosome structure. *J Mol Biol* **360**: 377-85.

Gazel, A., P. Ramphal, M. Rosdy, B. De Wever, C. Tornier, N. Hosein, B. Lee, M. Tomic-Canic, and M. Blumenberg. 2003. Transcriptional profiling of epidermal keratinocytes: comparison of genes expressed in skin, cultured keratinocytes, and reconstituted epidermis, using large DNA microarrays. *J Invest Dermatol* **121**: 1459-68.

Gire, V., P. Roux, D. Wynford-Thomas, J.M. Brondello, and V. Dulic. 2004. DNA damage checkpoint kinase Chk2 triggers replicative senescence. *Embo J* **23**: 2554-63.

Gire, V. and D. Wynford-Thomas. 1998. Reinitiation of DNA synthesis and cell division in senescent human fibroblasts by microinjection of anti-p53 antibodies. *Mol Cell Biol* **18**: 1611-21.

Gire, V. and D. Wynford-Thomas. 2000. RAS oncogene activation induces proliferation in normal human thyroid epithelial cells without loss of differentiation. *Oncogene* **19**: 737-44.

Gonzalo, S. and M.A. Blasco. 2005. Role of Rb family in the epigenetic definition of chromatin. *Cell Cycle* **4**: 752-5.

Gonzalo, S., I. Jaco, M.F. Fraga, T. Chen, E. Li, M. Esteller, and M.A. Blasco. 2006. DNA methyltransferases control telomere length and telomere recombination in mammalian cells. *Nat Cell Biol* **8**: 416-24.

Goto, M., R.W. Miller, Y. Ishikawa, and H. Sugano. 1996. Excess of rare cancers in Werner syndrome (adult progeria). *Cancer Epidemiol Biomarkers Prev* **5**: 239-46.

Green, H. 1978. Cyclic AMP in relation to proliferation of the epidermal cell: a new view. *Cell* **15**: 801-11.

Greider, C.W. and E.H. Blackburn. 1985. Identification of a specific telomere terminal transferase activity in Tetrahymena extracts. *Cell* **43**: 405-13.

Griffith, J.D., L. Comeau, S. Rosenfield, R.M. Stansel, A. Bianchi, H. Moss, and T. de Lange. 1999. Mammalian telomeres end in a large duplex loop. *Cell* **97**: 503-14.

Hahn, P.J. 1993. Molecular biology of double-minute chromosomes. *Bioessays* **15**: 477-84.

Hahn, W.C., S.A. Stewart, M.W. Brooks, S.G. York, E. Eaton, A. Kurachi, R.L. Beijersbergen, J.H. Knoll, M. Meyerson, and R.A. Weinberg. 1999. Inhibition of telomerase limits the growth of human cancer cells. *Nat Med* **5**: 1164-70.

Hanahan, D. and R.A. Weinberg. 2000. The hallmarks of cancer. *Cell* **100**: 57-70.

Hanish, J.P., J.L. Yanowitz, and T. de Lange. 1994. Stringent sequence requirements for the formation of human telomeres. *Proc Natl Acad Sci U S A* **91**: 8861-5.

Hao, L.Y., M. Armanios, M.A. Strong, B. Karim, D.M. Feldser, D. Huso, and C.W. Greider. 2005. Short telomeres, even in the presence of telomerase, limit tissue renewal capacity. *Cell* **123**: 1121-31.

Harle-Bachor, C. and P. Boukamp. 1996. Telomerase activity in the regenerative basal layer of the epidermis inhuman skin and in immortal and carcinoma-derived skin keratinocytes. *Proc Natl Acad Sci U S A* **93**: 6476-81.

Harley, C.B., A.B. Futcher, and C.W. Greider. 1990. Telomeres shorten during ageing of human fibroblasts. *Nature* **345**: 458-60.

Hartmann, N. and H. Scherthan. 2005. Characterization of the telomere complex, TERF1 and TERF2 genes in muntjac species with fusion karyotypes. *Exp Cell Res* **306**: 64-74.

Hastie, N.D., M. Dempster, M.G. Dunlop, A.M. Thompson, D.K. Green, and R.C. Allshire. 1990. Telomere reduction in human colorectal carcinoma and with ageing. *Nature* **346**: 866-8.

Hayflick, L. and P.S. Moorhead. 1961. The serial cultivation of human diploid cell strains. *Exp Cell Res* **25**: 585-621.

Heiss, N.S., S.W. Knight, T.J. Vulliamy, S.M. Klauck, S. Wiemann, P.J. Mason, A. Poustka, and I. Dokal. 1998. X-linked dyskeratosis congenita is caused by mutations in a highly conserved gene with putative nucleolar functions. *Nat Genet* **19**: 32-8.

Hemann, M.T., M.A. Strong, L.Y. Hao, and C.W. Greider. 2001. The shortest telomere, not average telomere length, is critical for cell viability and chromosome stability. *Cell* **107**: 67-77.

Hennings, H., K. Holbrook, P. Steinert, and S. Yuspa. 1980. Growth and differentiation of mouse epidermal cells in culture: effects of extracellular calcium. *Curr Probl Dermatol* **10**: 3-25.

Herbig, U., W.A. Jobling, B.P. Chen, D.J. Chen, and J.M. Sedivy. 2004. Telomere shortening triggers senescence of human cells through a pathway involving ATM, p53, and p21(CIP1), but not p16(INK4a). *Mol Cell* **14**: 501-13.

Hockemeyer, D., J.P. Daniels, H. Takai, and T. de Lange. 2006. Recent expansion of the telomeric complex in rodents: Two distinct POT1 proteins protect mouse telomeres. *Cell* **126**: 63-77.

Hockemeyer, D., A.J. Sfeir, J.W. Shay, W.E. Wright, and T. de Lange. 2005. POT1 protects telomeres from a transient DNA damage response and determines how human chromosomes end. *Embo J* **24**: 2667-78.

Houghtaling, B.R., L. Cuttonaro, W. Chang, and S. Smith. 2004. A dynamic molecular link between the telomere length regulator TRF1 and the chromosome end protector TRF2. *Curr Biol* **14**: 1621-31.

Hsiao, S.J., M.F. Poitras, B.D. Cook, Y. Liu, and S. Smith. 2006. Tankyrase 2 poly(ADP-ribose) polymerase domain-deleted mice exhibit growth defects but have normal telomere length and capping. *Mol Cell Biol* **26**: 2044-54.

Iwano, T., M. Tachibana, M. Reth, and Y. Shinkai. 2004. Importance of TRF1 for functional telomere structure. *J Biol Chem* **279**: 1442-8.

Jaco, I., P. Munoz, and M.A. Blasco. 2004. Role of human Ku86 in telomere length maintenance and telomere capping. *Cancer Res* **64**: 7271-8.

Jacobs, J.J. and T. de Lange. 2004. Significant role for p16INK4a in p53-independent telomere-directed senescence. *Curr Biol* **14**: 2302-8.

Karlseder, J., D. Broccoli, Y. Dai, S. Hardy, and T. de Lange. 1999. p53- and ATM-dependent apoptosis induced by telomeres lacking TRF2. *Science* **283**: 1321-5.

Karlseder, J., K. Hoke, O.K. Mirzoeva, C. Bakkenist, M.B. Kastan, J.H. Petrini, and T. de Lange. 2004. The telomeric protein TRF2 binds the ATM kinase and can inhibit the ATM-dependent DNA damage response. *PLoS Biol* **2**: E240.

Karlseder, J., L. Kachatrian, H. Takai, K. Mercer, S. Hingorani, T. Jacks, and T. de Lange. 2003. Targeted deletion reveals an essential function for the telomere length regulator Trf1. *Mol Cell Biol* **23**: 6533-41.

Karlseder, J., A. Smogorzewska, and T. de Lange. 2002. Senescence induced by altered telomere state, not telomere loss. *Science* **295**: 2446-9.

Kim, N.W., M.A. Piatyszek, K.R. Prowse, C.B. Harley, M.D. West, P.L. Ho, G.M. Coviello, W.E. Wright, S.L. Weinrich, and J.W. Shay. 1994. Specific association of human telomerase activity with immortal cells and cancer. *Science* **266**: 2011-5.

Kim, S.H., S. Han, Y.H. You, D.J. Chen, and J. Campisi. 2003. The human telomere-associated protein TIN2 stimulates interactions between telomeric DNA tracts in vitro. *EMBO Rep* **4**: 685-91.

Kim, S.H., P. Kaminker, and J. Campisi. 1999. TIN2, a new regulator of telomere length in human cells. *Nat Genet* **23**: 405-12.

Kipling, D. and H.J. Cooke. 1990. Hypervariable ultra-long telomeres in mice. *Nature* **347**: 400-2.

Kiyono, T., S.A. Foster, J.I. Koop, J.K. McDougall, D.A. Galloway, and A.J. Klingelhutz. 1998. Both Rb/p16INK4a inactivation and telomerase activity are required to immortalize human epithelial cells. *Nature* **396**: 84-8.

Knudson, M., S. Kulkarni, Z.K. Ballas, M. Bessler, and F. Goldman. 2005. Association of immune abnormalities with telomere shortening in autosomal-dominant dyskeratosis congenita. *Blood* **105**: 682-8.

Kondo, T., N. Oue, K. Yoshida, Y. Mitani, K. Naka, H. Nakayama, and W. Yasui. 2004. Expression of POT1 is associated with tumor stage and telomere length in gastric carcinoma. *Cancer Res* **64**: 523-9.

Lechel, A., A. Satyanarayana, Z. Ju, R.R. Plentz, S. Schaetzlein, C. Rudolph, L. Wilkens, S.U. Wiemann, G. Saretzki, N.P. Malek, M.P. Manns, J. Buer, and K.L. Rudolph. 2005. The cellular level of telomere dysfunction determines induction of senescence or apoptosis in vivo. *EMBO Rep* **6**: 275-81.

Lee, T.H., K. Perrem, J.W. Harper, K.P. Lu, and X.Z. Zhou. 2006. The F-box protein FBX4 targets PIN2/TRF1 for ubiquitin-mediated degradation and regulates telomere maintenance. *J Biol Chem* **281**: 759-68.

Lenain, C., S. Bauwens, S. Amiard, M. Brunori, M.J. Giraud-Panis, and E. Gilson. 2006. The Apollo 5' exonuclease functions together with TRF2 to protect telomeres from DNA repair. *Curr Biol* **16**: 1303-10.

Levine, A.J. 1997. p53, the cellular gatekeeper for growth and division. *Cell* **88**: 323-31.

Levy, L., S. Broad, A.J. Zhu, J.M. Carroll, I. Khazaal, B. Peault, and F.M. Watt. 1998. Optimised retroviral infection of human epidermal keratinocytes: long-term expression of transduced integrin gene following grafting on to SCID mice. *Gene Ther* **5**: 913-22.

Lewis, L., Y. Barrandon, H. Green, and G. Albrecht-Buehler. 1987. The reorganization of microtubules and microfilaments in differentiating keratinocytes. *Differentiation* **36**: 228-33.

Li, B. and T. de Lange. 2003. Rap1 affects the length and heterogeneity of human telomeres. *Mol Biol Cell* **14**: 5060-8.

Li, B., S. Oestreich, and T. de Lange. 2000. Identification of human Rap1: implications for telomere evolution. *Cell* **101**: 471-83.

Li, G., C. Nelsen, and E.A. Hendrickson. 2002. Ku86 is essential in human somatic cells. *Proc Natl Acad Sci U S A* **99**: 832-7.

Li, G.Z., M.S. Eller, R. Firoozabadi, and B.A. Gilchrest. 2003. Evidence that exposure of the telomere 3' overhang sequence induces senescence. *Proc Natl Acad Sci U S A* **100**: 527-31.

Lillard-Wetherell, K., A. Machwe, G.T. Langland, K.A. Combs, G.K. Behbehani, S.A. Schonberg, J. German, J.J. Turchi, D.K. Orren, and J. Groden. 2004. Association and regulation of the BLM helicase by the telomere proteins TRF1 and TRF2. *Hum Mol Genet* **13**: 1919-32.

Liu, D., M.S. O'Connor, J. Qin, and Z. Songyang. 2004. Telosome, a mammalian telomere-associated complex formed by multiple telomeric proteins. *J Biol Chem* **279**: 51338-42.

Lo, A.W., L. Sabatier, B. Fouladi, G. Pottier, M. Ricoul, and J.P. Murnane. 2002. DNA amplification by breakage/fusion/bridge cycles initiated by spontaneous telomere loss in a human cancer cell line. *Neoplasia* **4**: 531-8.

Loayza, D. and T. De Lange. 2003. POT1 as a terminal transducer of TRF1 telomere length control. *Nature* **423**: 1013-8.

Loayza, D., H. Parsons, J. Donigian, K. Hoke, and T. de Lange. 2004. DNA binding features of human POT1: a nonamer 5'-TAGGGTTAG-3' minimal binding site, sequence specificity, and internal binding to multimeric sites. *J Biol Chem* **279**: 13241-8.

Lobrich, M., S. Ikpeme, and J. Kiefer. 1994. Measurement of DNA double-strand breaks in mammalian cells by pulsed-field gel electrophoresis: a new approach using rarely cutting restriction enzymes. *Radiat Res* **138**: 186-92.

Luderus, M.E., B. van Steensel, L. Chong, O.C. Sibon, F.F. Cremers, and T. de Lange. 1996. Structure, subnuclear distribution, and nuclear matrix association of the mammalian telomeric complex. *J Cell Biol* **135**: 867-81.

Macera-Bloch, L., J. Houghton, M. Lenahan, K.K. Jha, and H.L. Ozer. 2002. Termination of lifespan of SV40-transformed human fibroblasts in crisis is due to apoptosis. *J Cell Physiol* **190**: 332-44.

Machwe, A., L. Xiao, and D.K. Orren. 2004. TRF2 recruits the Werner syndrome (WRN) exonuclease for processing of telomeric DNA. *Oncogene* **23**: 149-56.

Makarov, V.L., Y. Hirose, and J.P. Langmore. 1997. Long G tails at both ends of human chromosomes suggest a C strand degradation mechanism for telomere shortening. *Cell* **88**: 657-66.

Marrone, A., A. Walne, and I. Dokal. 2005. Dyskeratosis congenita: telomerase, telomeres and anticipation. *Curr Opin Genet Dev* **15**: 249-57.

Masutomi, K., R. Possemato, J.M. Wong, J.L. Currier, Z. Tothova, J.B. Manola, S. Ganesan, P.M. Lansdorp, K. Collins, and W.C. Hahn. 2005. The telomerase reverse transcriptase regulates chromatin state and DNA damage responses. *Proc Natl Acad Sci U S A* **102**: 8222-7.

Masutomi, K., E.Y. Yu, S. Khurts, I. Ben-Porath, J.L. Currier, G.B. Metz, M.W. Brooks, S. Kaneko, S. Murakami, J.A. DeCaprio, R.A. Weinberg, S.A. Stewart, and W.C. Hahn. 2003. Telomerase maintains telomere structure in normal human cells. *Cell* **114**: 241-53.

Mauser, A., E. Holley-Guthrie, A. Zanation, W. Yarborough, W. Kaufmann, A. Klingelhutz, W.T. Seaman, and S. Kenney. 2002. The Epstein-Barr virus immediate-early protein BZLF1 induces expression of E2F-1 and other

proteins involved in cell cycle progression in primary keratinocytes and gastric carcinoma cells. *J Virol* **76**: 12543-52.

McClintock, B. 1984. The significance of responses of the genome to challenge. *Science* **226**: 792-801.

McKnight, T.D. and D.E. Shippen. 2004. Plant telomere biology. *Plant Cell* **16**: 794-803.

Michaloglou, C., L.C. Vredeveld, M.S. Soengas, C. Denoyelle, T. Kuilman, C.M. van der Horst, D.M. Majoor, J.W. Shay, W.J. Mooi, and D.S. Peeper. 2005. BRAFE600-associated senescence-like cell cycle arrest of human naevi. *Nature* **436**: 720-4.

Miller, K.M., O. Rog, and J.P. Cooper. 2006. Semi-conservative DNA replication through telomeres requires Taz1. *Nature* **440**: 824-8.

Morris, M., P. Hepburn, and D. Wynford-Thomas. 2002. Sequential extension of proliferative lifespan in human fibroblasts induced by over-expression of CDK4 or 6 and loss of p53 function. *Oncogene* **21**: 4277-88.

Moyzis, R.K., J.M. Buckingham, L.S. Cram, M. Dani, L.L. Deaven, M.D. Jones, J. Meyne, R.L. Ratliff, and J.R. Wu. 1988. A highly conserved repetitive DNA sequence, (TTAGGG)n, present at the telomeres of human chromosomes. *Proc Natl Acad Sci U S A* **85**: 6622-6.

Munoz, P., R. Blanco, J.M. Flores, and M.A. Blasco. 2005. XPF nuclease-dependent telomere loss and increased DNA damage in mice overexpressing TRF2 result in premature aging and cancer. *Nat Genet* **37**: 1063-71.

Muntoni, A. and R.R. Reddel. 2005. The first molecular details of ALT in human tumor cells. *Hum Mol Genet* **14 Spec No. 2**: R191-6.

Myung, K., G. Ghosh, F.J. Fattah, G. Li, H. Kim, A. Dutia, E. Pak, S. Smith, and E.A. Hendrickson. 2004. Regulation of telomere length and suppression of genomic instability in human somatic cells by Ku86. *Mol Cell Biol* **24**: 5050-9.

Nakamura, T.M., G.B. Morin, K.B. Chapman, S.L. Weinrich, W.H. Andrews, J. Lingner, C.B. Harley, and T.R. Cech. 1997. Telomerase catalytic subunit homologs from fission yeast and human. *Science* **277**: 955-9.

Narita, M., S. Nunez, E. Heard, A.W. Lin, S.A. Hearn, D.L. Spector, G.J. Hannon, and S.W. Lowe. 2003. Rb-mediated heterochromatin formation and silencing of E2F target genes during cellular senescence. *Cell* **113**: 703-16.

Natarajan, E., J.D. Omobono, 2nd, Z. Guo, S. Hopkinson, A.J. Lazar, T. Brenn, J.C. Jones, and J.G. Rheinwald. 2006. A keratinocyte

hypermotility/growth-arrest response involving laminin 5 and p16INK4A activated in wound healing and senescence. *Am J Pathol* **168**: 1821-37.

Neidle, S. and G. Parkinson. 2002. Telomere maintenance as a target for anticancer drug discovery. *Nat Rev Drug Discov* **1**: 383-93.

Niemantsverdriet, M., W. Jongmans, and C. Backendorf. 2005. Radiation response and cell cycle regulation of p53 rescued malignant keratinocytes. *Exp Cell Res* **310**: 237-47.

Nijjar, T., E. Bassett, J. Garbe, Y. Takenaka, M.R. Stampfer, D. Gilley, and P. Yaswen. 2005. Accumulation and altered localization of telomere-associated protein TRF2 in immortally transformed and tumor-derived human breast cells. *Oncogene* **24**: 3369-76.

Olovnikov, A.M. 1971. [Principle of marginotomy in template synthesis of polynucleotides]. *Dokl Akad Nauk SSSR* **201**: 1496-9.

Opresko, P.L., J. Fan, S. Danzy, D.M. Wilson, 3rd, and V.A. Bohr. 2005. Oxidative damage in telomeric DNA disrupts recognition by TRF1 and TRF2. *Nucleic Acids Res* **33**: 1230-9.

Opresko, P.L., C. von Kobbe, J.P. Laine, J. Harrigan, I.D. Hickson, and V.A. Bohr. 2002. Telomere-binding protein TRF2 binds to and stimulates the Werner and Bloom syndrome helicases. *J Biol Chem* **277**: 41110-9.

O'Sullivan, J.N., M.P. Bronner, T.A. Brentnall, J.C. Finley, W.T. Shen, S. Emerson, M.J. Emond, K.A. Gollahon, A.H. Moskovitz, D.A. Crispin, J.D. Potter, and P.S. Rabinovitch. 2002. Chromosomal instability in ulcerative colitis is related to telomere shortening. *Nat Genet* **32**: 280-4.

Pardo, B. and S. Marcand. 2005. Rap1 prevents telomere fusions by nonhomologous end joining. *Embo J* **24**: 3117-27.

Parenteau, J. and R.J. Wellinger. 2002. Differential processing of leading- and lagging-strand ends at Saccharomyces cerevisiae telomeres revealed by the absence of Rad27p nuclease. *Genetics* **162**: 1583-94.

Paull, T.T. and M. Gellert. 1999. Nbs1 potentiates ATP-driven DNA unwinding and endonuclease cleavage by the Mre11/Rad50 complex. *Genes Dev* **13**: 1276-88.

Preto, A., S.K. Singhrao, M.F. Haughton, D. Kipling, D. Wynford-Thomas, and C.J. Jones. 2004. Telomere erosion triggers growth arrest but not cell death in human cancer cells retaining wild-type p53: implications for antitelomerase therapy. *Oncogene* **23**: 4136-45.

Prowse, K.R. and C.W. Greider. 1995. Developmental and tissue-specific regulation of mouse telomerase and telomere length. *Proc Natl Acad Sci U S A* **92**: 4818-22.

Purdy, A. and T.T. Su. 2004. Telomeres: not all breaks are equal. *Curr Biol* **14**: R613-4.

Qin, J.Z., V. Chaturvedi, M.F. Denning, P. Bacon, J. Panella, D. Choubey, and B.J. Nickoloff. 2002. Regulation of apoptosis by p53 in UV-irradiated human epidermis, psoriatic plaques and senescent keratinocytes. *Oncogene* **21**: 2991-3002.

Rheinwald, J.G. 1980. Serial cultivation of normal human epidermal keratinocytes. *Methods Cell Biol* **21A**: 229-54.

Rheinwald, J.G. and M.A. Beckett. 1981. Tumorigenic keratinocyte lines requiring anchorage and fibroblast support cultures from human squamous cell carcinomas. *Cancer Res* **41**: 1657-63.

Rheinwald, J.G. and H. Green. 1975. Serial cultivation of strains of human epidermal keratinocytes: the formation of keratinizing colonies from single cells. *Cell* **6**: 331-43.

Rheinwald, J.G. and H. Green. 1977. Epidermal growth factor and the multiplication of cultured human epidermal keratinocytes. *Nature* **265**: 421-4.

Sabatier, L., M. Ricoul, G. Pottier, and J.P. Murnane. 2005. The loss of a single telomere can result in instability of multiple chromosomes in a human tumor cell line. *Mol Cancer Res* **3**: 139-50.

Sandhu, C., D.M. Peehl, and J. Slingerland. 2000. p16INK4A mediates cyclin dependent kinase 4 and 6 inhibition in senescent prostatic epithelial cells. *Cancer Res* **60**: 2616-22.

Savitsky, K., A. Bar-Shira, S. Gilad, G. Rotman, Y. Ziv, L. Vanagaite, D.A. Tagle, S. Smith, T. Uziel, S. Sfez, and et al. 1995. A single ataxia telangiectasia gene with a product similar to PI-3 kinase. *Science* **268**: 1749-53.

Scherthan, H. 2001. A bouquet makes ends meet. *Nat Rev Mol Cell Biol* **2**: 621-7.

Scott, L.A., J.K. Vass, E.K. Parkinson, D.A. Gillespie, J.N. Winnie, and B.W. Ozanne. 2004. Invasion of normal human fibroblasts induced by v-Fos is independent of proliferation, immortalization, and the tumor suppressors p16INK4a and p53. *Mol Cell Biol* **24**: 1540-59.

Serrano, M., A.W. Lin, M.E. McCurrach, D. Beach, and S.W. Lowe. 1997. Oncogenic ras provokes premature cell senescence associated with accumulation of p53 and p16INK4a. *Cell* **88**: 593-602.

Sharma, G.G., A. Gupta, H. Wang, H. Scherthan, S. Dhar, V. Gandhi, G. Iliakis, J.W. Shay, C.S. Young, and T.K. Pandita. 2003. hTERT associates with human telomeres and enhances genomic stability and DNA repair. *Oncogene* **22**: 131-46.

Shay, J.W. and S. Bacchetti. 1997. A survey of telomerase activity in human cancer. *Eur J Cancer* **33**: 787-91.

Shen, M., C. Haggblom, M. Vogt, T. Hunter, and K.P. Lu. 1997. Characterization and cell cycle regulation of the related human telomeric proteins Pin2 and TRF1 suggest a role in mitosis. *Proc Natl Acad Sci U S A* **94**: 13618-23.

Simbulan-Rosenthal, C.M., V. Trabosh, A. Velarde, F.P. Chou, A. Daher, F. Tenzin, T. Tokino, and D.S. Rosenthal. 2005. Id2 protein is selectively upregulated by UVB in primary, but not in immortalized human keratinocytes and inhibits differentiation. *Oncogene* **24**: 5443-58.

Smith, S. and T. de Lange. 1999. Cell cycle dependent localization of the telomeric PARP, tankyrase, to nuclear pore complexes and centrosomes. *J Cell Sci* **112 (Pt 21)**: 3649-56.

Smith, S. and T. de Lange. 2000. Tankyrase promotes telomere elongation in human cells. *Curr Biol* **10**: 1299-302.

Smith, S., I. Giriat, A. Schmitt, and T. de Lange. 1998. Tankyrase, a poly(ADP-ribose) polymerase at human telomeres. *Science* **282**: 1484-7.

Smogorzewska, A. and T. de Lange. 2002. Different telomere damage signaling pathways in human and mouse cells. *Embo J* **21**: 4338-48.

Smogorzewska, A., J. Karlseder, H. Holtgreve-Grez, A. Jauch, and T. de Lange. 2002. DNA ligase IV-dependent NHEJ of deprotected mammalian telomeres in G1 and G2. *Curr Biol* **12**: 1635-44.

Smogorzewska, A., B. van Steensel, A. Bianchi, S. Oelmann, M.R. Schaefer, G. Schnapp, and T. de Lange. 2000. Control of human telomere length by TRF1 and TRF2. *Mol Cell Biol* **20**: 1659-68.

Stansel, R.M., T. de Lange, and J.D. Griffith. 2001. T-loop assembly in vitro involves binding of TRF2 near the 3' telomeric overhang. *Embo J* **20**: 5532-40.

Stewart, S.A., I. Ben-Porath, V.J. Carey, B.F. O'Connor, W.C. Hahn, and R.A. Weinberg. 2003. Erosion of the telomeric single-strand overhang at replicative senescence. *Nat Genet* **33**: 492-6.

Takai, H., A. Smogorzewska, and T. de Lange. 2003. DNA damage foci at dysfunctional telomeres. *Curr Biol* **13**: 1549-56.

Tanaka, H., M.S. Mendonca, P.S. Bradshaw, D.J. Hoelz, L.H. Malkas, M.S. Meyn, and D. Gilley. 2005. DNA damage-induced phosphorylation of the human telomere-associated protein TRF2. *Proc Natl Acad Sci U S A* **102**: 15539-44.

Tarsounas, M., P. Munoz, A. Claas, P.G. Smiraldo, D.L. Pittman, M.A. Blasco, and S.C. West. 2004. Telomere maintenance requires the RAD51D recombination/repair protein. *Cell* **117**: 337-47.

Tchirkov, A. and P.M. Lansdorp. 2003. Role of oxidative stress in telomere shortening in cultured fibroblasts from normal individuals and patients with ataxia-telangiectasia. *Hum Mol Genet* **12**: 227-32.

Tomita, K. and J.P. Cooper. 2006. The meiotic chromosomal bouquet: SUN collects flowers. *Cell* **125**: 19-21.

Tommerup, H., A. Dousmanis, and T. de Lange. 1994. Unusual chromatin in human telomeres. *Mol Cell Biol* **14**: 5777-85.

van Gent, D.C., J.H. Hoeijmakers, and R. Kanaar. 2001. Chromosomal stability and the DNA double-stranded break connection. *Nat Rev Genet* **2**: 196-206.

van Overbeek, M. and T. de Lange. 2006. Apollo, an Artemis-related nuclease, interacts with TRF2 and protects human telomeres in S phase. *Curr Biol* **16**: 1295-302.

van Steensel, B. and T. de Lange. 1997. Control of telomere length by the human telomeric protein TRF1. *Nature* **385**: 740-3.

van Steensel, B., A. Smogorzewska, and T. de Lange. 1998. TRF2 protects human telomeres from end-to-end fusions. *Cell* **92**: 401-13.

Verdun, R.E., L. Crabbe, C. Haggblom, and J. Karlseder. 2005. Functional human telomeres are recognized as DNA damage in G2 of the cell cycle. *Mol Cell* **20**: 551-61.

von Zglinicki, T., G. Saretzki, W. Docke, and C. Lotze. 1995. Mild hyperoxia shortens telomeres and inhibits proliferation of fibroblasts: a model for senescence? *Exp Cell Res* **220**: 186-93.

von Zglinicki, T., G. Saretzki, J. Ladhoff, F. d'Adda di Fagagna, and S.P. Jackson. 2005. Human cell senescence as a DNA damage response. *Mech Ageing Dev* **126**: 111-7.

Vulliamy, T., A. Marrone, R. Szydlo, A. Walne, P.J. Mason, and I. Dokal. 2004. Disease anticipation is associated with progressive telomere shortening in families with dyskeratosis congenita due to mutations in TERC. *Nat Genet* **36**: 447-9.

Wang, R.C., A. Smogorzewska, and T. de Lange. 2004. Homologous recombination generates T-loop-sized deletions at human telomeres. *Cell* **119**: 355-68.

Wang, W. and H. Lan. 2000. Rapid and parallel chromosomal number reductions in muntjac deer inferred from mitochondrial DNA phylogeny. *Mol Biol Evol* **17**: 1326-33.

Wu, L., A.S. Multani, H. He, W. Cosme-Blanco, Y. Deng, J.M. Deng, O. Bachilo, S. Pathak, H. Tahara, S.M. Bailey, R.R. Behringer, and S. Chang. 2006. Pot1 deficiency initiates DNA damage checkpoint activation and aberrant homologous recombination at telomeres. *Cell* **126**: 49-62.

Wynford-Thomas, D. 1999. Cellular senescence and cancer. *J Pathol* **187**: 100-11.

Yanaihara, N., N. Caplen, E. Bowman, M. Seike, K. Kumamoto, M. Yi, R.M. Stephens, A. Okamoto, J. Yokota, T. Tanaka, G.A. Calin, C.G. Liu, C.M. Croce, and C.C. Harris. 2006. Unique microRNA molecular profiles in lung cancer diagnosis and prognosis. *Cancer Cell* **9**: 189-98.

Yang, Q., Y.L. Zheng, and C.C. Harris. 2005. POT1 and TRF2 cooperate to maintain telomeric integrity. *Mol Cell Biol* **25**: 1070-80.

Ye, J.Z. and T. de Lange. 2004. TIN2 is a tankyrase 1 PARP modulator in the TRF1 telomere length control complex. *Nat Genet* **36**: 618-23.

Ye, J.Z., J.R. Donigian, M. van Overbeek, D. Loayza, Y. Luo, A.N. Krutchinsky, B.T. Chait, and T. de Lange. 2004a. TIN2 binds TRF1 and TRF2 simultaneously and stabilizes the TRF2 complex on telomeres. *J Biol Chem* **279**: 47264-71.

Ye, J.Z., D. Hockemeyer, A.N. Krutchinsky, D. Loayza, S.M. Hooper, B.T. Chait, and T. de Lange. 2004b. POT1-interacting protein PIP1: a telomere length regulator that recruits POT1 to the TIN2/TRF1 complex. *Genes Dev* **18**: 1649-54.

Yoon, K. and R.C. Smart. 2004. C/EBPalpha is a DNA damage-inducible p53-regulated mediator of the G1 checkpoint in keratinocytes. *Mol Cell Biol* **24**: 10650-60.

Zhang, H. and S.N. Cohen. 2004. Smurf2 up-regulation activates telomere-dependent senescence. *Genes Dev* **18**: 3028-40.

Zhang, H., B.S. Herbert, K.H. Pan, J.W. Shay, and S.N. Cohen. 2004. Disparate effects of telomere attrition on gene expression during replicative senescence of human mammary epithelial cells cultured under different conditions. *Oncogene* **23**: 6193-8.

Zhang, H., K.H. Pan, and S.N. Cohen. 2003. Senescence-specific gene expression fingerprints reveal cell-type-dependent physical clustering of up-regulated chromosomal loci. *Proc Natl Acad Sci U S A* **100**: 3251-6.

Zhang, P., K. Furukawa, P.L. Opresko, X. Xu, V.A. Bohr, and M.P. Mattson. 2006. TRF2 dysfunction elicits DNA damage responses associated with senescence in proliferating neural cells and differentiation of neurons. *J Neurochem* **97**: 567-81.

Zhou, X.Z. and K.P. Lu. 2001. The Pin2/TRF1-interacting protein PinX1 is a potent telomerase inhibitor. *Cell* **107**: 347-59.

Zhu, X.D., B. Kuster, M. Mann, J.H. Petrini, and T. de Lange. 2000. Cell-cycle-regulated association of RAD50/MRE11/NBS1 with TRF2 and human telomeres. *Nat Genet* **25**: 347-52.

Zhu, X.D., L. Niedernhofer, B. Kuster, M. Mann, J.H. Hoeijmakers, and T. de Lange. 2003. ERCC1/XPF removes the 3' overhang from uncapped telomeres and represses formation of telomeric DNA-containing double minute chromosomes. *Mol Cell* **12**: 1489-98.